THE ROLE OF PALMITOYLATION IN THE PATHOGENESIS OF HUNTINGTON DISEASE

by

Shaun Samantha Fancey Sanders

B.Sc., The University of British Columbia, 2007

A THESIS SUBMITTED IN PARTIAL FULFILLMENT OF THE REQUIREMENTS FOR THE DEGREE OF

DOCTOR OF PHILOSOPHY

in

THE FACULTY OF GRADUATE AND POSTDOCTORAL STUDEIS

(Neuroscience)

THE UNIVERSITY OF BRITISH COLUMBIA

(Vancouver)

December, 2014

ABSTRACT

Huntington disease (HD) is caused by a CAG expansion in *HTT* characterized by motor, cognitive, and psychiatric disturbances. Huntingtin Interacting Protein 14 (HIP14) and HIP14-like (HIP14L) are palmitoyl acyltransferases (PATs) that mediate the post-translational addition of fatty acids to proteins (palmitoylation). They palmitoylate HTT and have reduced interaction with and palmitoylation of mutant HTT (mHTT), leading to increased mHTT inclusion formation and toxicity. HTT is essential for full enzymatic activity of HIP14 and loss of either of these genes leads to HD-like phenotypes. The goal was to determine the role of palmitoylation in the pathogenesis of HD. The overall hypothesis is that disturbed HIP14- and HIP14L-HTT interaction in HD reduces PAT function leading to the under-palmitoylation and mislocalization of HTT and key HIP14 and HIP14L substrates. Multiple putative PAT binding sites in HTT were identified, one around aa224 and one around aa427, that are required for full interaction but aa1-548 are required for the structural integrity of the binding sites. Loss of both *Hip14* and *Hip14l* leads to embryonic lethality between day 10 and 11 *in utero,* due to failed placenta formation. Intriguingly, the extraembryonic tissue of *Hip14*$^{-/-}$;*Hip14l*$^{-/-}$ embryos share many features with that of *Htt*$^{-/-}$ embryos and palmitoylation of HTT was decreased by 25% in *Hip14*$^{-/-}$;*Hip14l*$^{-/-}$ mouse embryonic fibroblasts. Palmitoylation of mHTT, SNAP25, and PSD-95 was decreased in the YAC128, BACHD, and Hu97/18 mouse models of HD. The HD-like phenotype of the *Hip14*$^{-/-}$ mice is developmental and non-progressive, unlike the adult-onset, progressive phenotype of the YAC128 mice. Mice in which *Hip14* deficiency is induced in adulthood show reduced survival, motor deficits, anhedonia, increased escape response, increased forebrain weight and cortical volume, and decreased corpus callosum volume. This indicates that loss of *Hip14* from conception allows for developmental compensation that cannot occur if *Hip14* deficiency occurs in the adult.

PREFACE

Chapter 1

Portions of Chapter 1 have been published in *Progress in Neurobiology*. Young FB, Butland SL, Sanders SS, Sutton LM, and Hayden MR. (2012). Putting proteins in their place: Palmitoylation in Huntington disease and other neuropsychiatric diseases. Prog. Neurobiol *97*, 220-238.

Chapter 2

Chapter 2 has been published in *PLoS ONE*. Sanders, S.S., Mui, K.K.N., Sutton, L.M., and Hayden, M.R. (2014). Identification of binding sites in Huntingtin for the Huntingtin Interacting Proteins HIP14 and HIP14L. PLoS ONE *9*, e90669. I designed all of the experiments did all of the data analysis. Katherine KN Mui assisted with the co-immunoprecipitation experiments and Liza M Sutton assisted with the generation of the constructs.

Chapter 3

Chapter 3 has been published in *Developmental Biology* (Sanders, S.S., Hou, J., Sutton, L.M., Garside, V.C., Mui, K.K.N., Singaraja, R.R., Hayden, M.R., and Hoodless, P.A. Huntingtin interacting proteins 14 and 14-like are required for chorioallantoic fusion during early placental development. In press at the time of thesis submission). I designed or assisted with the design of all of the experiments, with the assistance of Juan Hou. Victoria Garside and Juan Hou did all of the *in situ* hybridization experiments. Juan Hou performed gross morphology experiments. I performed analysis of mendelian ratios by harvesting embryos and performing genotyping analysis, harvested embryos for H&E staining and prepped samples for Wax-it, who cut and stained the embryos, I performed all palmitoylation assays, and harvested MEFs for qPCR. Kathryn Mui performed qPCR experiments and Liza Sutton generated the mouse embryonic fibroblast cell lines. I performed all data analysis. Juan Hou and Pamela Hoodless assisted with the interpretation of the data.

Chapter 4

The BACHD and Hu97/18 analysis from Chapter 4 will be published as one figure in a manuscript describing additional characterization of the Hu97/18 mice currently titled “Delineation of novel pre-clinical endpoints in humanized Hu97/18 HD model mice” (Southwell *et al*). Although this manuscript includes a much broader set of data and thus will not be published with me as lead author, I designed all of the experiments, performed all of the palmitoylation assays, and did all of the data analysis for the data presented here in chapter 4.

Chapter 5

Chapter 5 is in preparation to be submitted. (Sanders, S.S., Parsons, M.P., Southwell A.L., Mui, K.K.N., Franciosi, S., Zhang, W., Raymond L.A., and Hayden, M.R. Loss of the Huntington disease-associated palmitoylacyltransferase HIP14 in adulthood leads to sudden unexplained death in epilepsy, motor deficits, and increased escape response). I designed all of the experiments, Amber L Southwell advised on the design of the behavior experiments. I performed all behavior testing except for rotarod and spontaneous activity, which were performed by Weining Zhang. All electrophysiology experiments were performed and analyzed by Matt Parsons. Sonia Franciosi performed the neuropathological experiments blinded to genotype. Katherine Mui performed RT-PCR experiments and assisted with the western blots and scored behavior videos blinded to genotype. All other experiments and data analysis were performed by me.

Ethics approval

The studies described in this thesis have been approved by the Animal Care Committee at the University of British Columbia. All mice were handled according to institutional guidelines. Approval certificates numbers include: A12-0063, A12-0121, A07-0106, and A07-0262.

TABLE OF CONTENTS

LIST OF TABLES

LIST OF FIGURES

LIST OF SYMBOLS AND ABBREVIATIONS

129	129S6/SvEv mouse strain
Aβ	Beta-amyloid
ABE	Acyl-biotin exchange
ACSF	Artificial cerebrospinal fluid
AD	Alzheimer disease
AKAP79/150	A kinase (PRKA) anchor protein 5
AKT	Protein kinase B
ALS	Amyotrophic lateral sclerosis
AMPAR	α–amino-3-hydroxy-5-methyl-4-isoxazolepropionic acid receptors
ANOVA	Analysis of variance
APH1	Gamma secretase subunit (*APH1A*)
APP	Amyloid precursor
APT	Acyl protein thioesterase
APT1	Acyl-protein thioesterase 1 (*LYPLA1*)
APT2	Lysophospholipase II (*LYPLA2*)
APTL1	Lysophospholipase-like I (*LYPLAL1*)
ASO	Antisense oligonucleotides
B6	C57BL/6J muse strain
BACE1	β-site amyloid precursor protein cleaving enzyme 1
BACHD	Bacterial artificial chromosome transgenic mouse model of HD carrying full-length human *HTT* with 97 CAG repeats
BMP	Bone morphogenic protein
Click	Cu(I)-catalyzed azide-alkyne cycloadditon
cKO	Conditional knockout region of *Hip14*
CoA	Coenzyme A
COS	Cell CV-1 (simian) in Origin and carrying the SV40 genetic material (COS-7)
CSP	Cysteine string protein (DNAJC5), DnaJ heat shock protein 40 homolog
DARPP-32	Dopamine- and cAMP-regulated neuronal phosphoproteins (*PPP1R1B*)
DHHC	Asp-His-His-Cys
DHHC-CR	DHHC cysteine-rich
dHIP14	*D. melanogaster* ortholog of *HIP14* (*CG6017)*
DNQX	6,7-dinitroquinoxaline-2,3-dione
DTA	Diptheria toxin A
EPM	Elevated plus maze
EPSC	Excitatory postsynaptic current
ER	Endoplasmic reticulum
FALS	Familial ALS
Flp	Flippase recombinase
FRT	Flippase recognition target site
FKBP12	FK506-binding protein 12 (*FKBP1A*)

FVB/N	FVB/NJ mouse strain, Friend virus B NIH Jackson
G418	Geneticin
$GABA_AR\gamma2$	γ2 subunit of $GABA_A$ receptor
GAD65	Glutamate decarboxylase
GAP-43	Growth associated protein 43
GLUA1	AMPA receptor subunit 1 (*GRIA1*)
GLUA2	AMPA receptor subunit 2 (*GRIA2*)
GLUN2A	NMDA receptor subunit 2A (*GRIN2A*)
GLUN2B	NMDA receptor subunit 2B (*GRIN2B*)
GM130	Cis-Golgi matrix protein 130 (*GOLGA2*)
HAM	Hydroxylamine
HD	Huntington disease
HEK293	Human embryonic kidney
HIP14	Huntingtin interacting protein 14 (*ZDHHC17*)
HIP14L	Huntingtin interacting protein 14-like (*ZDHHC13*)
HTT	Huntingtin
JNK3	c-Jun N-terminal kinase 3
LCK	Lymphocyte-specific protein tyrosine kinase
LoxP	Locus of X-over P1, 34 bp Cre recombinase sequence from P1 bacteriophage
MAP	Mitogen-activated protein
MBOAT	Membrane-bound-O-acyltransferase
mHTT	Mutant HTT, >35 polyQ's
MKK7	Mitogen-activated protein kinase kinase 7 (*MAP2K7*)
NEM	N-ethylmaleimide
MS	Mass spectrometry
MSN	Medium spiny neurons
NCL	Neuronal ceroid lipofuscinosis
NMDAR	N-methyl-D-aspartate receptors
NO	Nitric oxide
NOS	NO synthase enzymes
NT2	Human neuron-committed teratocarcinoma cell line
PAT	Palmitoyl acyltransferase
PDE10A2	Phosphodiesterase 10A isoform 2
PEN2	Presenilin enhancer 2 (*PSENEN*)
PKA	Protein kinase A
PKC	Protein kinase C
PM	Plasma membrane
PPI	Pre-pulse inhibition
PPR	Paired pulse ratio
PPT	Protein-palmitoyl thioesterase
PSD	Postsynaptic density
PSD-95	Postsynaptic density protein 95 (*DLG4*)
PS1	Presenilin 1 (*PSEN1*)
PS2	Presenilin 2 (*PSEN2*)
PTM	Post-translational modification

R6/2	Transgenic mouse model of HD carrying exon 1 of human *HTT* with 148-153 CAG repeats
SNAP25	Synaptosomal-associated protein 25
SNARE	Soluble NSF attachment protein receptor
SNP	Single nucleotide polymorphism
SOD1	Cu/Zn superoxide dismutase (*SOD1*)
Sog	Chordin, short gastrulation (*CHRD*)
STREX BK	Stress regulated exon splice variant of the calcium- and voltage-activated potassium channel
SYT1	Synaptotagmin-1
T1D	Type 1 diabetes
TM	Tamoxifen
TMD	Transmembrane domain
Wnt	Wingless-related integration site
WT	Wildtype
wtHTT	Wildtype HTT
XLMR	X-linked mental retardation
Y2H	Yeast 2-hybrid
YAC128	Yeast artificial chromosome transgenic mouse model of HD carrying full-length human *HTT* with 128 CAG repeats

ACKNOWLEDGEMENTS

There are many people to thank for their help and support throughout this journey. First, I would like to thank my supervisor, Dr. Michael Hayden, for taking me on as a graduate student, believing in me and supporting me along the way, and giving me unlimited opportunities to learn and grow as a scientist. A huge thank you to my supervisory committee: Dr. Shernaz Bamji and Drs. Lynn Raymond and Elizabeth Conibear for their support in this way and as collaborators. Thank you to all my other amazing collaborators, especially Drs. Pamela Hoodless and Juan Hou. To Dr. Elizabeth Simpson for her expert advice on transgenic generation and Dr. Tim Chen for his support and guidance.

An immense thank you to the many brilliant colleagues and friends that I have had the pleasure and opportunity to work with in the Hayden lab, many of whom will be lifelong friends and collaborators. Thank you Dr. Roshni Singaraja for being the one to initially see something in me and hire me to work with her and for being supportive of me, especially during the early part of my PhD. Thanks to Stefanie Butland for her endless passion for science and support as a team member and friend. Drs. Amber Southwell and Dagmar Ehrnhoefer it has been amazing serving as project leaders with you two. Also, to Amber thank you for helping designing my behavioral studies and being a good friend. A huge thank you to Katherine Mui for all of the amazing technical support. Thank you to everybody else who has supported me in one-way or another along the way: Safia Ladha, Dr. Liza Sutton, Mandi Schmidt, Dr. Mahmoud Pouladi, Dr. Kun Huang, Dr. Bibiana Wong, Valeria Uribe, Dr. Jeff Carroll, Crystal Doty, Chris Kay, and Dr. Niels Skotte. Those that keep the animal facility going and have assisted me by injecting my animals or by genotyping are invaluable: Mark Wang, Jason Yao, Sheng Yu, and Qingwen Xia. For support on neuropathological assessments, thank you to Sonia Franciosi and Sabine Waltl and for assistance in the behavior suite Weining Zhang. The administrative staff keeps the Hayden lab running smoothly and does so much that allows us to concentrate on the science: Dawn Ng, Seetha Kumaran, and Mahsa Amirabossi. The Hayden lab is

an amazing place largely due to the talented and hard working people; it has been a pleasure.

To my family, I love you all so much and would not be here without your support and encouragement. To my beautiful sister, your strength and drive inspire me every day. Thank you to Mom for all of your support and love; you are an inspiration. To my Uncle Dean and Aunty Tracy, thank you for your incredible support all the way, you are so generous and I am so thankful for the many skiing and sailing trips and everything else you do for me. Thank you to Aunty “K” for being one of the best aunties anybody could ask for, your endless love and support is amazing. To my grandmother, “Gran,” for everything you have done for me right from the beginning, I’m so lucky to have you. To my dad and the rest of the Sanders clan, I love you all so much and thank you for your support. Huge thanks to Uncle Wilf for taking me on in his lab as an undergraduate volunteer and inspiring me to become a scientist.

To all of my friends all over the world who have helped me get to this point in my life: Lysandra Bumstead, Dana Miller, Tareyn Rollheiser, Jenn Charlton, Cat Mills, Renee MacDermid, Tiffany Shen, and everybody else. Thank you so much for all of your love, care, and understanding.

Finally, Dale Martin your love and support have really got me through the end of this work, I could not have done it without you. Thank you for the being so understanding and taking care of me through all the late nights during the last stretch of this work. I am so thankful for you everyday and cannot wait to see what the future holds for us.

DEDICATION

TO MY BELOVED GRANDFATHER MICKEY ROCKWELL, AKA "MUFF." I WISH YOU WERE STILL HERE TO SEE ME FINISH THIS.

1 INTRODUCTION[1]

1.1 PROTEIN PALMITOYLATION: GENERAL OVERVIEW

The past decade has seen great advances toward our understanding of the post-translational modification (PTM), palmitoylation, and the enzymes that regulate this process. Palmitoylation is the most common protein lipid modification in the brain and, much like phosphorylation, palmitoylation is reversible (Fukata and Fukata, 2010). As such, palmitoylation serves as a means of dynamic regulation of neuronal substrates, often acting as a "switch" in regulating the state of the protein. This is critical not only for the neuronal proteins that control firing at the synapse, but also for proteins critical in neurodevelopmental processes and in neuronal survival. Thus, aberrant palmitoylation may result in misregulation of neuronal proteins and neuropsychiatric disease.

1.1.1 A primer on protein palmitoylation

The term palmitoylation is generally used to describe the post-translational addition of the 16-carbon fatty acid, palmitate, to a cysteine residue via a thioester bond by the family of enzymes called DHHC (Aspartic acid-Histidine-Histidine-Cysteine)-domain containing palmitoyl acyltransferases (PATs; Figure 1.1) (Greaves and Chamberlain, 2011; Linder and Deschenes, 2007). S-acylation, a broader term, refers to the attachment of fatty acids to cysteine residues. This term includes palmitoylation but may also refer to the addition of both saturated and unsaturated fatty acids of various lengths, including myristic, arachidonic, oleic, and stearic acids. Because the addition of the fatty acid palmitate is most common, S-acylation is often referred to as palmitoylation (Hallak et al., 1994; Smotrys and Linder, 2004). Less commonly, acylation may occur at an N-terminal cysteine or glycine (N-acylation) and is linked via an amide, as opposed to a thioester, bond. When involving the addition of the fatty

---

[1] Portions of this chapter have been published in *Progress in Neurobiology*. Young FB, Butland SL, Sanders SS, Sutton LM, and Hayden MR. (2012). Putting proteins in their place: Palmitoylation in Huntington disease and other neuropsychiatric diseases. Prog. Neurobiol *97*, 220-238.

acid palmitate to an N-terminal cysteine, this latter process is known as N-palmitoylation and occurs on secreted palmitoyl-proteins (Figure 1.1) (Nadolski and Linder, 2007). A small subset of PATs, the membrane-bound-O-acyltransferase (MBOAT) family, catalyzes the acylation of secreted proteins and peptide substrates (Chang and Magee, 2009). Here the term PAT refers to a member of the DHHC domain containing PAT family. While commonly referred to as DHHC PATs, the official gene names are denoted “ZDHHC” (e.g. *ZDHHC*17).

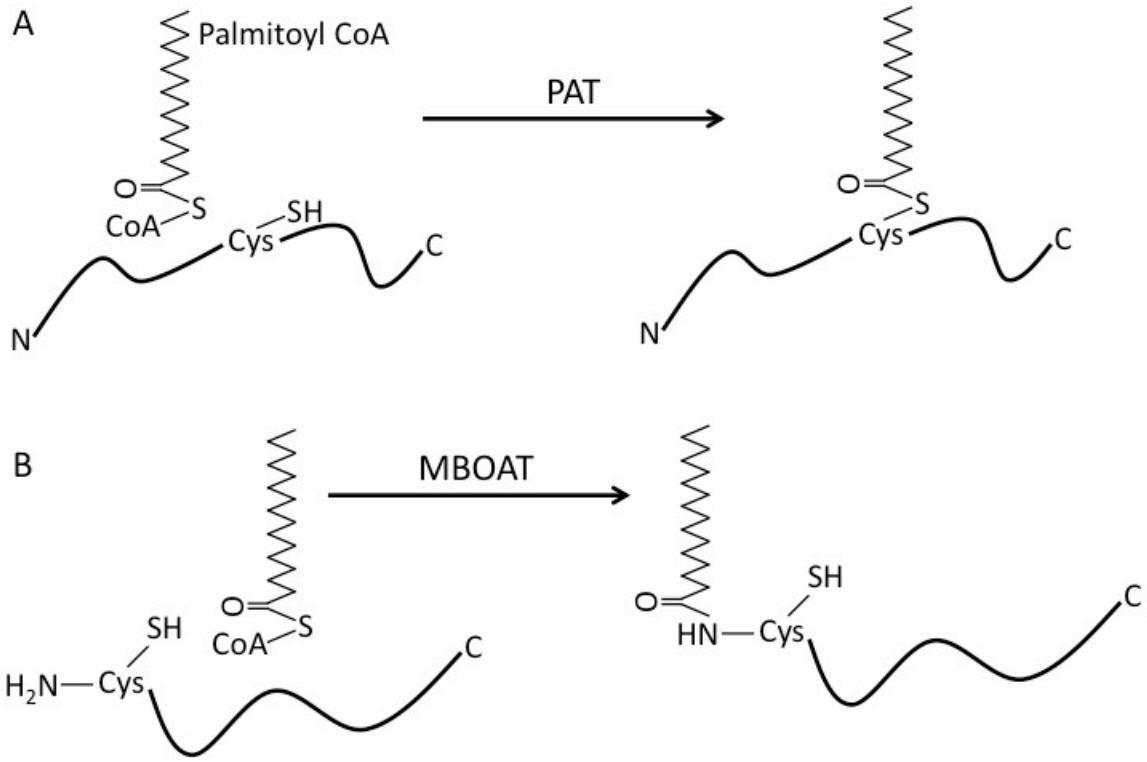

Figure 1.1: Biochemistry of palmitoylation. A) The process of S-palmitoylation. Palmitic acid is added to proteins at cysteine residues via a thioester bond by palmitoyl acyltransferases (PATs) using palmitoyl-CoA as the lipid substrate. B) The process of N-palmitoylation. Palmitic acid is added to N-terminal cysteines via an amide bond by some members of the MBOAT family using palmitoyl-CoA as the lipid substrate.

Other common lipid modifications of proteins include protein prenylation, wherein a farnesyl or geranyl-geranyl moiety is added post-translationally to a C-terminal cysteine via a stable thioether bond (Resh, 2006; Smotrys and Linder, 2004; Zhang and Casey, 1996), and myristoylation, which involves the co- or post-translational addition of myristic acid to a glycine residue via a stable amide

bond (Johnson et al., 1994; Martin et al., 2011). Notably, the relatively rare process of N-palmitoylation, by the nature of its different chemistry, is not reversible and is not involved in dynamic regulation of proteins. Similarly, prenylation and myristoylation are not reversible protein modifications. Here, the term “palmitoylation” refers specifically to the addition of palmitate to a cysteine residue via a thioester bond.

1.1.2 Functional consequences of palmitoylation

A diverse array of protein substrates are now known to undergo palmitoylation, including signaling proteins, ion channel components, scaffold proteins, membrane-associated proteins involved in vesicle trafficking, mitochondrial proteins and viral proteins (Charollais and Van Der Goot, 2009; Corvi et al., 2001; Fukata and Fukata, 2010; Kostiuk et al., 2008; Mitchell et al., 2006; Veit and Schmidt, 2006). As a consequence, palmitoylation plays a key role in many cellular processes, including tethering signaling proteins to membranes, protein trafficking, protein stability, protein-protein interactions, membrane association, and segregation of substrates to particular protein subdomains (Fukata and Fukata, 2010; Linder and Deschenes, 2007; Salaun et al., 2010).

Palmitoylation increases the hydrophobicity of a protein. Stable membrane association of cytoplasmic proteins is achieved by dual lipid modification; either via dual palmitoylation or palmitoylation with prenylation or myristoylation (El-Husseini et al., 2000a; Fukata and Fukata, 2010; Shahinian and Silvius, 1995). Often palmitoylation of membrane-associated proteins leads to their segregation into lipid rafts (membrane domains rich in cholesterol and sphingolipids) placing the substrate in proximity with other raft proteins and allowing cell signaling events to occur (Brown, 2006; Levental et al., 2010). Disturbances in lipid raft organization are implicated in some neurological diseases, such as Alzheimer disease (AD), Parkinson disease, and Huntington disease (HD) (Jacobowitz and Kallarakal, 2004; Molander-Melin et al., 2005; Valencia et al., 2010). Palmitoylation of integral membrane proteins may alter the hydrophobicity of a particular domain or induce a tilt of a transmembrane domain (TMD) within the

membrane bilayer, resulting in a conformational change and potentially enabling or inhibiting particular protein-protein interactions or function (Charollais and Van Der Goot, 2009).

A critical role for palmitoylation in the central nervous system, particularly its role in synaptic plasticity, has become evident over the last decade (El-Husseini and Bredt, 2002; Fukata and Fukata, 2010; Huang and El-Husseini, 2005). Palmitoylation reversibly regulates the assembly and compartmentalization of many neuronal proteins at specific subcellular domains, such as the presynaptic terminal and postsynaptic sites (El-Husseini and Bredt, 2002; Fukata and Fukata, 2010; Huang and El-Husseini, 2005; Prescott et al., 2009). For example, palmitoylation regulates the postsynaptic targeting of postsynaptic density-95 (PSD-95), a molecule involved in excitatory synapse development and plasticity (Craven et al., 1999; Ehrlich and Malinow, 2004; El-Husseini et al., 2000a; Kim and Sheng, 2004). At presynaptic nerve terminals, palmitoylation modulates trafficking and assembly of proteins that regulate neurotransmitter release, such as the GABA synthesizing enzyme, glutamate decarboxylase (GAD65) where loss of palmitoylation abolishes presynaptic clustering and dendritic exclusion, and synaptotagmin 1 (SYT1) (Kanaani et al., 2004; 2002; Kang, 2004). Palmitoylation also plays an important role in neuronal developmental processes, such as neurite outgrowth, axon pathfinding, filopodia formation, and spine development (Arstikaitis et al., 2008; Gauthier-Campbell et al., 2004; Kato et al., 2000; Kutzleb et al., 1998; Laux et al., 2000; Ueno, 2000). For example, palmitoylation of c-Jun N-terminal kinase 3 (JNK3) regulates axonal branching in response to Wnt signals. Wnt signaling decreases palmitoylation of JNK3, which increases axonal branching (Yang et al., 2012). Palmitoylation regulates signal transduction in neurons by modulating adhesion molecules, neurotransmitter receptors and ion channels implicated in establishing neuronal connectivity, excitability and synaptic plasticity (Fukata and Fukata, 2010; Huang and El-Husseini, 2005). Alterations in neuronal excitability and plasticity underlie many neuropsychiatric disorders (Citri and Malenka, 2008; Humeau et al., 2009; Kreitzer and Malenka, 2008; Lee and Silva, 2009).

1.1.3 Dynamic palmitoylation regulates neuronal activity

The reversibility of protein palmitoylation is afforded by the labile nature of the thioester bond (Conibear and Davis, 2010). This unique aspect of palmitoylation is a mechanism by which dynamic control of protein localization and function occurs in the central nervous system and elsewhere. Indeed, many proteins undergo dynamic cycles of palmitoylation and depalmitoylation, with important functional implications (Conibear and Davis, 2010; El-Husseini et al., 2002; Fehrenbacher et al., 2009; Rocks, 2005; Rocks et al., 2010).

A well-studied example of this dynamic cycling and its critical importance for synaptic plasticity is observed with PSD-95, a scaffold protein for α–amino-3-hydroxy-5-methyl-4-isoxazolepropionic acid receptors (AMPARs) and N-methyl-D-aspartate receptors (NMDARs) at the postsynapse (Ehrlich and Malinow, 2004; El-Husseini et al., 2000b; El-Husseini and Bredt, 2002). Palmitoylation of PSD-95 is required for its membrane scaffolding function (Craven et al., 1999; El-Husseini et al., 2000a). The dual palmitoylation of PSD-95 at Cys3 and Cys5 undergoes constitutive cycling, which is enhanced by synaptic activity (El-Husseini et al., 2000a; 2002). This reduces the amount of PSD-95 at the postsynapse and consequently reduces synaptic strength, which in turn may influence learning and memory (El-Husseini and Bredt, 2002; El-Husseini et al., 2002). Conversely, blocking synaptic activity increases PSD-95 palmitoylation and localization to the postsynaptic membrane (Noritake et al., 2009).

Recently the Fukata lab published on a single-chain variable fragment PSD-95 antibody that is specific to palmitoylated PSD-95. The antibody was found to recognize the specific conformation of palmitoylated PSD-95 and when expressed as an intrabody, it dissociated following depalmitoylation. It was found to exclusively label postsynaptic PSD-95 clusters indicating that palmitoylated PSD-95 is localized almost exclusively to the postsynaptic density (PSD) of excitatory synapses (Fukata et al., 2013). Using stimulated emission depletion super-resolution microscopy they showed that the PSD is in fact made up of several (up to four) subsynaptic clusters of palmitoylated PSD-95 facing a single

presynaptic terminal that they coined “subsynaptic nanodomains.” As there was a positive correlation between the number of nanodoamins and PSD size, it may be that the PSD is composed of a set of palmitoylated PSD-95-enriched subdomains. Indeed, AMPAR clusters were also associated with the palmitoylated PSD-95 nanodomains and these nanodomains were dynamically remodeled by synaptic-activity. The formation and dynamic nature of these palmitoylated PSD-95 nanodomains was dependent on the presence of ZDHHC2 in the PSD plasma membrane (PM) (Fukata et al., 2013).

Another good example of regulation of neuronal activity through dynamic palmitoylation involves the scaffold protein AKAP79/150 (human 70/rodent 150) (Delint-Ramirez et al., 2011; Keith et al., 2012). This protein targets protein kinase A (PKA), protein kinase C (PKC), and calcineurin to the PSD to regulate AMPAR activity and trafficking (Sanderson and Dell'Acqua, 2011). AKAP79 is palmitoylated at Cys36 and Cys129 and palmitoylation at these sites promotes association with lipid rafts but is not absolutely required for PM and spine targeting (Delint-Ramirez et al., 2011; Keith et al., 2012). Chemically induced LTD using a NMDAR agonist (cLTD) led to rapid depalmitoylation of AKAP150 and removal from dendritic spines. In contrast chemical stimulation to induce NMDAR-dependent LTP (cLTP) increased palmitoylation of AKAP150 and lead to its recruitment to spines and spine enlargement by Rab11-dependent endosomal trafficking (Keith et al., 2012). Expression of palmitoylation resistant AKAP79 led to increased basal spine size but no additional spine enlargement or recruitment of AKAP79 to spines was observed following cLTP (Keith et al., 2012). Interestingly, expression of palmitoylation resistant AKAP79 increased basal amplitude and frequency of miniature EPSCs (mEPSC) and increased the synaptic expression of the AMPAR subunit GLUA1, but not GLUA2 (Keith et al., 2012). However, following cLTP expression of palmitoylation resistant AKAP79 lead to a dramatic decrease in mEPSC frequency and in GLUA1 synaptic puncta (Keith et al., 2012). Overall it appears that palmitoylated AKAP79/150 acts as a negative regulator of endosomal recycling and GLUA1 synaptic incorporation that

is removed by cLTP and C36,129S is unable to act in this way and cannot respond to stimulation (Keith et al., 2012).

The dynamic “on/off” nature of protein palmitoylation leads to its frequent comparison to another dynamic PTM, phosphorylation, in which kinase and phosphatase enzymes regulate the addition and removal of phosphate groups from proteins with effects on nearly all aspects of cell signaling. In the less well characterized PTM, palmitoylation, the opposing actions of enzymes that add and remove palmitate can rapidly modulate membrane targeting of substrates in response to extracellular cues. The enzymes that catalyze these reactions are further described in section 1.3.

1.1.4 Interplay between palmitoylation and post-translational and transcriptional modifications

Palmitoylation at different sites in the same substrate can differentially regulate protein function as has been described for two ionotropic glutamate receptors (Hayashi et al., 2005; 2009). AMPAR subunits are palmitoylated on two domains: the second TMD and in the C-terminal region. Palmitoylation in the second TMD leads to Golgi accumulation and reduced forward trafficking, resulting in reduced expression at the PM. C-terminal palmitoylation reduces AMPAR interaction with the 4.1N scaffold protein and promotes AMPAR internalization from the PM (Hayashi et al., 2005). Palmitoylation of GRIP1b has also been shown to play a role in activity-dependent AMPAR recycling (Thomas et al., 2012). NMDAR subunits, which play a critical role in synaptic plasticity and excitotoxicity in disease processes (Fan and Raymond, 2007), display two distinct C-terminal clusters of palmitoylation (Hayashi et al., 2009). Palmitoylation in the first cluster enhances Src-kinase-mediated tyrosine phosphorylation, leading to increased stability of surface NMDAR expression and synaptic localization (Hayashi et al., 2009; Mattison et al., 2012). In contrast, palmitoylation of the second cluster reduces NMDAR surface expression and increases localization to the Golgi (Hayashi et al., 2009). Given these examples, it is likely that differential palmitoylation-mediated regulation occurs for other substrates.

Alternative splicing can also regulate protein palmitoylation status and function. For example, Cdc42, a small Rho GTPase that directs neuronal morphogenesis, is normally prenylated. Brain-specific alternative splicing serves as a “switch” to yield a variant that becomes instead palmitoylated. While both isoforms are expressed in developing neurons, the palmitoylated isoform is required for the extension of dendritic filopodia, which later develop into dendritic spines (Kang et al., 2008).

There is mounting evidence that protein palmitoylation is also influenced by other PTMs. Many instances of co-regulation by palmitoylation and phosphorylation exist (Charych et al., 2010; Dorfleutner, 2003; Hawtin et al., 2001; Ponimaskin, 2005; Soskic et al., 1999). PKA phosphorylation of the C-terminal tail of stress regulated exon splice variant of the calcium- and voltage-activated potassium (STREX BK) channels mediates inhibition of the channel (Tian, 2001; Tian et al., 2004). Palmitoylation of cysteines adjacent to the PKA site regulates PM binding of the C-terminal tail (Tian et al., 2008) and is dependent on an upstream polybasic domain (Jeffries et al., 2012). This palmitoylation-dependent PM association is disturbed upon PKA activation resulting in inhibition of the channel due to phosphorylation-induced dissociation of the palmitate groups. This was not observed when the palmitoylated cysteines were mutated to alanine or pre-treated with 2-bromopalmitate (an inhibitor of DHHC-mediated palmitoylation), suggesting that palmitoylation is required for the phospho-inhibition of the channel (Jennings et al., 2009; Tian et al., 2008). Indeed, PKA phosphorylation occurs within the polybasic domain and acts as an electrostatic switch that controls palmitoylation and PM binding of the C-terminal tail (Jeffries et al., 2012) This is in contrast to the interaction of phosphorylation and palmitoylation on the striatally-enriched, membrane bound phosphodiesterase 10A isoform 2 (PDE10A2) (Kotera et al., 2004; Xie et al., 2006). Palmitoylation of Cys11, likely by ZDHHC7 and 19, mediates PM localization. Phosphorylation at Thr16 prevents palmitoylation leading to cytosolic localization of PDE10A but, if palmitoylated, phosphorylation does not lead to loss of membrane association. These findings are of particular interest to the

neuropsychiatric disorder, schizophrenia, where excessive dopamine release in the striatum may lead to mislocalization of PDE10A2 in the striatum and, in turn, dysregulated PDE10A function (Charych et al., 2010).

Protein nitrosylation can also influence palmitoylation. Nitric oxide (NO) synthase enzymes (NOS) can generate NO from L-arginine, which can directly modify cysteine residues via S-nitrosylation (Stamler et al., 1992). Nitrosylation may alter palmitoylation either via competition for target cysteines or by direct displacement of palmitoyl moieties on palmitoylated cysteines (Baker, 2000). This was recently shown to be the case for the well-studied postsynaptic scaffolding protein, PSD-95. The sites of PSD-95 palmitoylation, Cys3 and Cys5, were shown to also undergo nitrosylation in a competitive manner. Endogenous NO inhibited PSD-95 palmitoylation resulting in decreased PSD-95 at the synapse. Conversely, a decrease in palmitoylation of PSD-95 in *Zdhhc8* knockout mice or in cells treated with 2-Bromopalmitate resulted in increased PSD-95 nitrosylation. Palmitoylation of PSD-95 results in its localization at the synapse where it coordinates NMDAR stimulation with production of NO by the neuronal NOS, therefore, the authors propose a model by which NO regulates PSD-95 localization by competition with palmitoylation at cysteine residues (Ho et al., 2011).

Palmitoylation of proteins has been reported to influence their ubiquitination status and hence their stability. Palmitoylation of the SNARE (soluble NSF attachment protein receptor) protein, Tlg1, by the yeast PAT Swf1 protects it from ubiquitination and subsequent degradation by the proteasome (Valdez Taubas and Pelham, 2005). Similarly, palmitoylation of the oncoprotein TBC1D3 also protects it from ubiquitination and degradation (Kong et al., 2013a).

1.2 METHODS TO DETECT PALMITOYLATION

1.2.1 Bioorthoginal labeling

Historically, levels of palmitoylation were assessed *in cellulo* and *in vitro* using radioactive palmitate either ^{3}H-palmitate or ^{125}I-iodopalmitate (Resh, 2006). These methods required expensive reagents and long exposure times, often up

to months, to detect palmitoylation. Recent advances including the advent of Click chemistry has led to new methods that are much cheaper and more sensitive and allow for easier proteomics style studies (Rostovtsev et al., 2002). Click chemistry palmitoylation assays involve the metabolic labeling of cells with the alkyne or azido long chain fatty acid analogues (Table 1.1) followed by the Cu(I)-catalyzed azide-alkyne cycloaddition (click) reaction with an alkyne or azido biotin, florescent, or other chemical tag (Martin and Cravatt, 2009; Yap et al., 2010). Palmitoylated proteins can then be detected by western blot, pulled down for mass spectrometry (MS) analysis, or imaged in cells (Charron et al., 2009; Gao and Hannoush, 2013; 2014; Martin and Cravatt, 2009; Yap et al., 2010).

Those proteins that are palmitoylated during the metabolic labeling incubation, i.e. those that are newly synthesized or that are undergoing dynamic cycling of palmitoylation, are labeled and detected with the click reaction. However, these assays cannot detect the total pool of palmitoylated proteins. This means that if a protein is not dynamically palmitoylated it may not label well using these methods. Increasing the labeling time will help to circumvent this issue but treating too long can also lead to β-oxidation of the fatty acid to shorter chain fatty acids and detection of myristoylation instead of palmitoylation (Yap et al., 2010). The fatty acid analogue used may also play a role in the ability to detect palmitoylation of a given protein. Traditionally 17-ODYA is used most commonly but as this is actually a stearate analogue it may not label those proteins that are preferentially palmitoylated with palmitate. Conversely, some proteins are preferentially palmitoylated with stearate, not palmitate (Wilson et al., 2011).

Table 1.1: Types of bioorthogonal labels used.

Bioorthogonal label	Synonyms	Type of analog
az-12	12-azidododecanoic acid	Myristate
13-TDYA	13-tetradecynoic acid, alk-12	Myristate
15-HDYA	15-hexadecynoic acid, alk-14	Palmitate
az-15	15-azidopentadecanoic acid	Stearate
17-ODYA	17-octadecynoic acid, alk-16	Stearate

1.2.2 Acyl-biotin exchange assay

A significance advance in the field of palmitoylation came with the invention of the acyl-biotin exchange (ABE) assay (Drisdel and Green, 2004; Wan et al., 2007). The big advantage of this assay is that it does not require live cells and as such can be used to assess palmitoylation levels in tissue samples. Another major advantage of the ABE assay is that it allows for the detection of the total palmitoylated pool. A protein sample is treated with N-ethylmaleimide (NEM) to block free cysteine residues, then with hydroxylamine (HAM) to cleave the thioester bond between cysteine and palmitate and remove the palmitate. Then the newly free cysteines are labeled with biotin to allow pull down or detection on western blot following immunoprecipitation of individual proteins (Drisdel and Green, 2004; Wan et al., 2007). This assay may lead to false positives in the two following ways: (1) it cannot differentiate between palmitoylation and other thioester modifications of cysteines, such as nitrosylation, and (2) HAM can reduce disuphide bonds between cysteines, which can then subsequently be labeled. To definitively show that a protein is palmitoylated this assay should be used in conjunction with one of the bioorthoginal labeling methods. However, it still remains the only method that allows detection of palmitoylation in tissue samples or of proteins that are stably palmitoylated and cannot be detected using bioorthoginal methods.

A variation on the ABE assay is the acyl-resin assisted capture assay. Free cysteines are also blocked with NEM and then during the HAM treatment thiol-reactive beads are added to capture the newly free cysteines allowing pull down of the total palmitoylated pool of proteins. Palmitoylated proteins can then be detected by MS or by western blot of individual proteins (Forrester et al., 2011). The original published protocol used *S*-methylmethanethiosulfonate instead of NEM to block free cysteines but this may lead to false positives as it forms a disulphide bond with the cysteine which may be subject to reduction by HAM and subsequent capture by the thiol-reactive beads.

1.2.3 Proteomics approaches

To date there have been 15 published palmitoyl proteome studies using one of the above described methods (Table 1.2). When all of the data from 14 of these studies is curated into a list of individual, non-redundant genes the resulting compendium of palmitoyl proteins reveals that there are 1840 putative palmitoyl proteins in the proteome (Sanders and Martin *et al.* In preparation for MCP). This list will be an important tool for the field, allowing people to easily check if their protein may be palmitoylated and then to follow up with low throughput methods to be sure.

Table 1.2: Published mammalian palmitoylproteomes.

Organism	Cell or Tissue Type	Cell Fraction	Detection Method	Reference
Human				
	HUVEC endothelial cells	total cell lysate	ABE-NEM	Wei ATVB 2014
	B lymphocytes	membrane lysate	ABE-NEM	Ivaldi PLoS ONE 2012
	endothelial cell line EA.hy926	total cell lysate	ABE-MMTS	Marin Circ Res 2012
	resting platelets	membrane lysate	ABE-NEM	Dowal Blood 2011
	HEK293 cells	membrane lysate	acyl-RAC-MMTS	Forrester JLR 2011
	Jurkat T cells	total cell lysate	Bioorthogonal labeling (myristic: az-12 or 13-TDYA); Bioorthogonal labeling (palmitic: 15-HDYA); Bioorthogonal labeling (stearic: az-15 or 17-ODYA)	Wilson MCP 2011
	prostate cancer cell line DU145	raft and non-raft membrane fractions	ABE-NEM	Yang MCP 2010
	Jurkat T cells	membrane lysate	Bioorthogonal labeling (stearic: 17-ODYA) + HAM	Martin Nat Methods 2009
	HeLa cells	membrane lysate	acyl-RAC-MMTS	Zhang MCP 2008
Mouse				
	brain	total cell lysate	ABE-NEM	Wan Chem & Biol 2013
	T-cell hybridoma cells	membrane lysate	Bioorthogonal labeling (stearic: 17-ODYA) + HAM	Martin Nat Methods 2012
	neuronal stem cells	membrane lysate	Bioorthogonal labeling (stearic: 17-ODYA) + HAM	Li JBC 2012
	macrophage cell line RAW 264.7 leukaemic monocytes	membrane lysate	ABE-NEM	Merrick MCP 2011
	dendritic cell line DC2.4	total cell lysate	Bioorthogonal labeling (stearic: 17-ODYA)	Yount Nat Chem Bio, 2010
Rat				
	cultured embryonic neuronal cells and whole brain	total cell lysate and brain synaptosomal fraction	ABE-NEM	Kang Nature 2008

*Note Ren et al Adipocyte 2013 not included in compendium. Supp Data file had many errors in protein identifiers leading its exclusion.

1.3 ENZYMES THAT MODIFY PROTEIN PALMITOYLATION

The first descriptions of palmitoylation (Schmidt et al., 1979) and the first studies identifying the enzymes that catalyze the process (Lobo, 2002; Roth, 2002) were separated by two decades of repeated attempts at isolating and characterizing these enzymes. During this time, the existence of such enzymes remained controversial (Dietrich and Ungermann, 2004). Spontaneous, autocatalytic palmitoylation had been observed for some proteins *in vitro*, when incubated with acyl-coenzyme A (acyl-CoA), for example, SNAP25 (Veit, 2000; Zeidman et al., 2009). However, this was not a universal process. Some proteins failed to undergo autoacylation under the same conditions and not all reactions were observed to occur at physiological pH and acyl-CoA concentrations. For example, autoacylation of GAP-43 (growth-associated protein-43) and the Fyn tyrosine kinase did not occur under the same conditions as for the G protein α subunit, $G\alpha_i1$ (Duncan and Gilman, 1996). Almost a decade after the identification of the first enzymes that catalyze palmitoylation, the process is now

believed to be enzymatically driven for the majority of proteins (Roth et al., 2006; Zeidman et al., 2009). The dynamic regulation of palmitoylation necessitates enzymes that palmitoylate and depalmitoylate substrates.

1.3.1 Palmitoyl acyltransferases (PATs)

In 2002, two landmark papers reported the discovery of two yeast PATs; Akr1 was identified as a PAT for the casein kinase isoform I Yck2 (Roth, 2002) and Erf2 and Erf4 together were identified to have *in vitro* PAT activity toward Ras2 (Lobo, 2002). Simultaneously, huntingtin interacting protein 14 (*HIP14* or *ZDHHC17*) was reported as the mammalian ortholog of *AKR1* (Singaraja et al., 2002), to be later identified as the first mammalian PAT (Huang et al., 2004). The fact that these PATs all contained a highly conserved core DHHC domain (Putilina et al., 1999) suggested that other members of the DHHC protein family may also be PATs. A series of papers describing mammalian PATs soon followed (Fukata et al., 2004; Huang et al., 2004; Keller, 2004), as well as further characterization of the PATs in yeast (Lam et al., 2006; Roth et al., 2006; Smotrys et al., 2005; Valdez Taubas and Pelham, 2005).

The PATs are multipass transmembrane proteins with four to six predicted TMDs (Figure 1.2) (Conibear and Davis, 2010; Politis, 2005). The signature DHHC cysteine-rich (DHHC-CR) domain, containing the four-amino acid DHHC motif, is a zinc finger domain most similar to the C_2H_2 zinc finger. It consists of 51 amino acids residing on the cytoplasmic face of the membrane (Mitchell et al., 2006; Politis, 2005; Putilina et al., 1999). The PAT gene family is deeply conserved in eukaryotes. The NCBI Homologene resource reports PATs in yeasts, protists, plants, insects, nematodes, fish, birds and mammals (Sayers et al., 2011). The apparent absence of genes encoding these enzymes in prokaryotes and archaea coincides with the absence of palmitoylation in these organisms (Mitchell et al., 2006; Roth, 2002). Seven genes are present in yeast, 23 in humans (*Zdhhc1-9* and *11-24*), and 24 in mice (*Zdhhc1-9* and *11-25*), and those characterized to date demonstrate distinct but overlapping substrate specificities (Fukata et al., 2004; Huang et al., 2009).

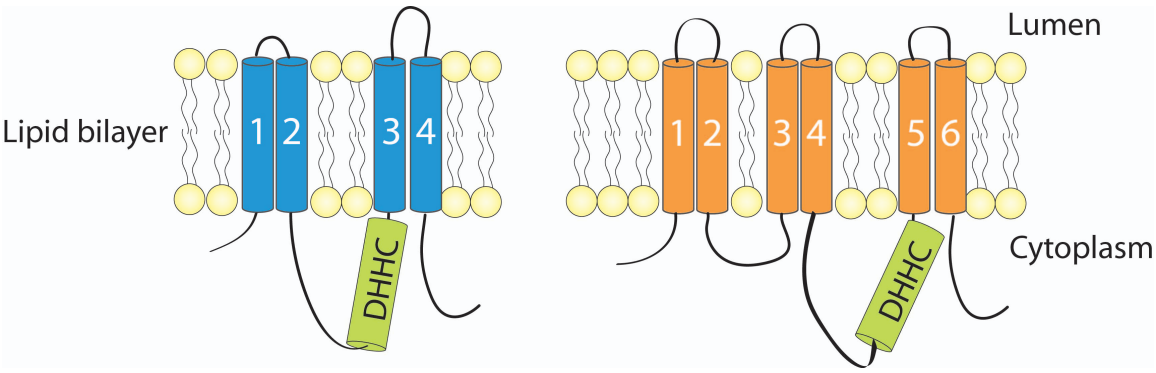

Figure 1.2: Generic PAT structure. PATs are integral membrane proteins with either 4 or 6 predicted transmembrane domains. The catalytic site resides within the DHHC-CR domain (labeled DHHC) and is located on the cytoplasmic surface.

The core DHHC motif is particularly highly conserved, and is essential for catalytic function both *in vitro* and *in vivo* (Mitchell et al., 2006). PATs have been proposed to undergo autopalmitoylation on the active site cysteine of the DHHC motif. The autopalmitoylated enzyme is thought to serve as a transient acyl-enzyme intermediate prior to transfer of palmitate to the substrate. In accordance with this mechanism, mutation of this active site cysteine abolishes palmitoylation of both the enzyme and substrate (Lobo, 2002; Mitchell et al., 2010; Roth, 2002). A two-step ping-pong mechanism involving a transient acyl enzyme intermediate was shown for ZDHHC2 and 3 where ^{3}H-palmitate was transferred from the acyl enzyme intermediate to protein substrate (Jennings and Linder, 2012). The same study also showed that ZDHHC2 and 3 have distinct lipid substrate specificities where ZDHHC2 was able to transfer fatty acids from acyl-CoA chain lengths longer than 14 carbons (14C), whereas ZDHHC3 preferred myristate (C14) and palmitate (C16) (Jennings and Linder, 2012). Indeed, 17 of the 23 human ZDHHC proteins have been shown to form acyl enzyme intermediates, ZDHHC2, 3, 5-9, 11-15, 17, 18, 20, and 21. In this study no activity was observed for ZDHHC23 or 19 and ZDHHC1, 4, 16, and 24 failed to express (Ohno et al., 2012)

Because palmitoylation occurs in a wide range of soluble and transmembrane proteins, identifying a consensus sequence for protein palmitoylation has been challenging. This lack of consensus sequence is a trend

seen in S-acylated substrates in general. However, some patterns have emerged (El-Husseini and Bredt, 2002). The number of amino acids between the target cysteine and the TMD was found to be crucial for palmitoylation in integral membrane proteins. Transmembrane proteins (e.g. SYT1) are often palmitoylated at cysteines near the final TMD (Brinke et al., 2002). The four to five residues surrounding the palmitoylated cysteine appear to be required in cytosolic proteins that are exclusively palmitoylated (e.g. PSD-95) (El-Husseini et al., 2000a; El-Husseini and Bredt, 2002). Many palmitoylated cysteines are flanked by neighboring basic amino acids or polybasic domains, a possible means to facilitate membrane association by binding to the acidic head groups of phospholipids (El-Husseini, 2001; Jeffries et al., 2012). Effective palmitoylation appears to require close proximity of the palmitoylation site to the membrane, achieved when a target cysteine is either close to or inside a TMD, adjacent to other lipid modifications, or surrounded by basic or hydrophobic amino acids. All of these features would presumably bring the substrate in close proximity to the PAT, facilitating transfer of palmitate to the target cysteine (El-Husseini and Bredt, 2002; Salaun et al., 2010). The diverse number of features influencing palmitoylation suggests that three-dimensional structure, in addition to sequence, may influence palmitoylation (Bijlmakers and Marsh, 2003).

In proteins that undergo both palmitoylation and other fatty acid modifications, their additions are sequential. Myristoylation or prenylation occurs first; the resulting weak membrane association brings the substrate in proximity with membrane-bound PATs for subsequent palmitoylation, typically on nearby cysteines, which stabilizes the membrane association (El-Husseini et al., 2000a; Fukata and Fukata, 2010; Shahinian and Silvius, 1995).

Some of the PATs appear to display an affinity for particular types of substrate. Akr1, the yeast ortholog of HIP14, appears to preferentially palmitoylate exclusively N- or C-terminally palmitoylated hydrophilic proteins. The yeast PAT, Erf2-Erf4, appears to preferentially palmitoylate heterolipidated proteins, i.e. proteins that are C-terminally prenylated and palmitoylated, N-terminally myristoylated and palmitoylated, or C-terminally prenylated and N-

terminally palmitoylated. Similarly, the yeast PAT, Swf1, showed a preference for juxta-TMD cysteines (Roth et al., 2006). Akr1 recognizes a tripartite palmitoylation signal of its substrate Yck2; this signal includes a 10-residue long, conserved C-terminal peptide containing the dual cysteine palmitoylation acceptor residues, the required central Phe-Phe motif, and the kinase domain separated by a flexible, unstructured linker domain. The DHHC-CR domain of Akr1 interacts with the conserved C-terminal peptide and the ankyrin repeat domain of Akr1 may interact with the kinase domain, with the linker domain allowing Akr1 to interact with both Yck2 domains simultaneously. There is also evidence that the HIP14 substrate SNAP25 may contain a similar tripartite palmitoylation signal (Roth et al., 2011).

The palmitoylation of some substrates appears remarkably dependent on a particular PAT (Roth et al., 2006), whereas other proteins can clearly undergo palmitoylation by multiple PATs (Fukata et al., 2004; Huang et al., 2009; Salaun et al., 2010). Thus, PATs appear to demonstrate both unique and overlapping substrate specificities, and a particular substrate may be palmitoylated by one or many PATs. Whether all of these PAT-substrate pairings occur *in vivo* is unclear.

Mammalian PATs can be found largely on Golgi, endoplasmic reticulum (ER), and endosomes but also on the PM (Ohno et al., 2006). In neurons ZDHHC5 was detected in dendrites and DHHC8 was localized to the postsynaptic compartment (Thomas et al., 2012). Their localization within the cell appears to be an important determinant of substrate specificity. However, determining the localization of PATs has yielded inconsistent findings, even within the same laboratory. The results appear to be affected by the stage of cell cycle, cell health and type, and the location of the epitope tag on the protein (Planey and Zacharias, 2009). Rocks and colleagues proposed that while depalmitoylation appears to occur throughout the cell, palmitoylation only occurs on the Golgi. Rapid depalmitoylation allows mislocalized proteins to be redirected to the Golgi, thereby serving as a means of directional sorting of peripheral membrane proteins (Rocks et al., 2010). However, Gorleku and others showed that ZDHHC4 and 6 contain dilysine-based ER targeting signals at their C-termini

and localize to the ER and that the normally Golgi localized ZDHHC3 with either ER targeting signal from ZDHHC4 or 6 appended to the C-terminus localized to the ER and was able to palmitoylate its substrates SNAP25 and CSP (Gorleku et al., 2011). ZDHHC5 was suggested to palmitoylate GRIP1b in the dendritic shaft on recycling endosomes in a highly dynamic manner (Thomas et al., 2012). These data indicate that, in fact, palmitoylation can occur on other membrane compartments other than the Golgi.

Despite the lack of a clear consensus sequence for palmitoylation, *in silico* prediction tools have been developed. CSS-Palm, which is most commonly used, generates predictions of palmitoylation sites based on a large training data set of known palmitoylated proteins using a cluster and scoring strategy (Ren et al., 2008). A caveat of such an approach is that proteins predicted to be palmitoylation substrates would tend to resemble known substrates. Therefore new tools must be developed to take into account both structure and sequence requirements for palmitoylation as new PAT substrates are identified and their elements required for palmitoylation are defined. A new tool, WAP-Palm has attempted to do so by using information from amino acid composition, sequence position, physiochemical properties, and evolutionary information to predict sites of palmitoylation (Shi et al., 2013). This tool has not been as extensively used as CSS-Palm yet as it is relatively new so it remains to be determined if it is more accurate than CSS-Palm.

1.3.2 Enzymes promoting depalmitoylation of proteins

Despite the impressive progress made in the discovery of the enzymes that catalyze palmitoylation over the past decade, progress in uncovering the enzymes that catalyze depalmitoylation has been limited. As discussed previously, palmitoylation is thought to be an enzymatic process for most proteins but autoacylation can occur. In contrast, removal of palmitate from proteins appears to be strictly an enzymatic process, and is particularly important in proteins for which palmitoylation is dynamically regulated. Furthermore, in substrates that are autoacylated, the enzymatic removal of palmitate serves as

the only means of regulation (Zeidman et al., 2009). To date, four acyl protein thioesterases (APT; commonly referred to as thioesterases) have been identified to catalyze depalmitoylation: acyl protein thioesterases, APT1, APT2, and APTL1 and the protein-palmitoyl thioesterase (PPT), PPT1 (Tomatis et al., 2010; Zeidman et al., 2009).

APT1 is a cytoplasmic thioesterase (Hirano et al., 2009). Cell-based experiments in yeast deficient in Apt1 have confirmed APT1 as a thioesterase (Duncan, 2002; Yeh et al., 1999). It is expressed in a wide range of mouse tissues (Toyoda et al., 1999), and has been shown to depalmitoylate a growing list of proteins *in vitro*, including the $G\alpha_s$ signaling molecules, H-Ras, and endothelial NOS (Duncan and Gilman, 1998; Yeh et al., 1999). The use of an inhibitor of APT1, palmostatin-B, to interrupt the dynamic palmitoylation-depalmitoylation cycle of Ras demonstrates *in vivo* that APT1 mediates the release of H/N-Ras from the PM (Dekker and Hedberg, 2011). In neurons APT1 plays an important role in synaptic function and spine morphogenesis, a process critical in long-term memory. Siegel et al. found that APT1 expression was downregulated by miRNA-138, leading to suppression of hippocampal dendritic spine enlargement, most likely through Gα13 signaling (Siegel et al., 2009).

Similar to PATs, there does not appear to be a defined substrate recognition sequence for sites of thioesterase depalmitoylation; the list of APT1 substrates contains proteins that are structurally diverse and contain different combinations of lipid modifications (Zeidman et al., 2009). Nonetheless, there are examples of proteins for which APT1 does not catalyze deacylation (Yeh et al., 1999), and the efficiency of deacylation may be highly variable from substrate to substrate (Duncan, 2002). Depalmitoylation activity is observed throughout the cell, and this has been suggested as a mechanism by which mislocalized proteins may be redirected within the cell (Rocks et al., 2010). While APT1 has no predicted TMDs (Zeidman et al., 2009), it may be palmitoylated, enabling APT1 interaction with its membrane-associated targets (Yang et al., 2010).

The crystal structure of APT1 reveals that it is a member of the alpha/beta hydrolase enzyme family and contains a catalytic triad made up of Ser114, His203, and Asp169. The alpha/beta hydrolases catalyze a two-step reaction whereby the acyl chain is removed from the substrate by nucleophilic attack by the active site serine, which itself then becomes acylated. The acyl-enzyme intermediate is then hydrolyzed to remove the acyl chain in the second step of the reaction (Devedjiev et al., 2000).

APT2 (lysophospholipase II) is an *APT1* homologue with 64% amino acid sequence identity with *APT1* and also contains the Ser-Asp-His catalytic triad (Toyoda et al., 1999). APT2 has been shown to depalmitoylate GAP-43 and H-Ras (Rusch et al., 2011; Tomatis et al., 2010).

The third known thioesterase is PPT1, which resides in the lysosome and indiscriminately cleaves fatty acids (usually palmitate) from cysteine residues as part of regular protein degradation pathways (Verkruyse and Hofmann, 1996; Zeidman et al., 2009). The lysosomal localization of PPT1 makes it unlikely to serve as a thioesterase for cytoplasmic proteins (Verkruyse and Hofmann, 1996). However, PPT1 has been reported to localize to synaptosomes and synaptic vesicles in neurons (Heinonen et al., 2000; Lehtovirta et al., 2001), where it may depalmitoylate a number of neuronal peptides (Cho et al., 2000).

Mutations in PPT1 in humans results in a form of Batten disease, known as infantile neuronal ceroid lipofuscinosis (NCL) (Vesa et al., 1995), which features an accumulation of lysosomal autofluorescent deposits (Santavuori, 1988). This is further described in section 1.3.4 below.

A *PPT1* homolog, *PPT2*, is also a lysosomal thioesterase (Soyombo and Hofmann, 1997). While mutations in *PPT2* in mice result in an NCL phenotype with slower onset and milder phenotype (Gupta et al., 2001), the smaller lipid binding groove than that of PPT1 predicted by crystal structure (Calero, 2003) together with a substrate preference for palmitoyl-CoA over palmitoylated proteins (Soyombo and Hofmann, 1997) make it unlikely that PPT2 serves as a thioesterase for palmitoylated proteins (Zeidman et al., 2009).

The search for potential thioesterases is ongoing. Other members of the alpha/beta hydrolase family may emerge as potential depalmitoylating enzymes. Indeed the APT1 homolog APT1-like (APTL1; *LYPLAL1*) was recently shown to have depalmitoylate the S0-S1 loop of the BK channel controlling its surface expression (Tian et al., 2012; Zeidman et al., 2009).

The small GTPases H- and N-Ras are palmitoylated with rapid palmitoylation/depalmitoylation cycles regulating bidirectional trafficking between the Golgi and the PM (Goodwin, 2005; Rocks et al., 2010; Swarthout, 2005). The mechanism leading to rapid depalmitoylation of Ras is presently unknown, however, *in vitro* evidence suggests that APT1 acts as the Ras APT. siRNA knockdown of APT1 reduces Ras palmitoylation in cells and recombinant rat or yeast APT1 can depalmitoylate Ras (Dekker and Hedberg, 2011; Duncan, 2002; Smotrys and Linder, 2004). APT1 and APT2 may be palmitoylated themselves and undergo dynamic palmitoylation cycles where APT1 depalmitoylates itself and APT2. The authors suggested that this dynamic palmitoylation links their cytosol-membrane trafficking with that of their substrates and maintains steady state levels of membrane localization and function (Kong et al., 2013b).

Recent findings indicate that the prolyl isomerase, FK506-binding protein 12 (FKBP12), binds to palmitoylated H-Ras and promotes depalmitoylation at Cys181 and Cys184. The ability of FKBP12 to promote depalmitoylation of H-Ras is dependent on its prolyl isomerase function and Pro179 of Ras. This suggests that the *cis-trans* isomerization about the Gly-Pro bond at this position allows hydrolysis of the thioester bond, possibly by allowing APT1 (or another thioesterase) to more efficiently perform this function (Ahearn et al., 2011). This may be a novel mechanism of protein depalmitoylation not solely dependent upon thioesterases.

1.4 INVOLVEMENT OF PALMITOYLATION IN DISEASES AFFECTING THE NERVOUS SYSTEM

In recent years, it has become clear that the enzymes that regulate protein palmitoylation play a critical role in several biological processes, which, when

disturbed, can lead to disease. To date, six PAT genes have been reported to be associated with human disease (Liu et al., 2002; Mansouri et al., 2005; Mizumaru et al., 2009; Raymond et al., 2007; Singaraja et al., 2011; Yanai et al., 2006) and other PAT genes have been associated with disease phenotypes in animal models (Table 1.3) (Li et al., 2010; Mill et al., 2009; Saleem et al., 2010). Aberrant palmitoylation, without implication of a specific PAT, has also been associated with diseases (Antinone et al., 2013; Zhu et al., 2013). Association with neurological disease and dermatological pathology appear to be major themes. However, mutations in three PATs (*ZDHHC2, 9, 11*) have been implicated in various forms of human cancer (Mansilla et al., 2007; Oyama et al., 2000; Yamamoto et al., 2007; Zhang et al., 2008) and one study reported HIP14 to be an oncogene *in vitro* and *in vivo* in mice (Ducker et al., 2004). Mutations in two PATs (huntingtin interacting protein 14-like [HIP14L or ZDHHC13] and ZDHHC21) have been shown to result in dermatological and related phenotypes in inbred mice (Mill et al., 2009; Saleem et al., 2010). In addition, mice homozygous for a hypomorphic allele of *Zdhhc5* demonstrate reduced contextual fear conditioning, suggesting defective hippocampal-dependent learning. These results suggest a previously unexplored role for ZDHHC5 in learning and memory and may implicate this PAT in neuropsychiatric diseases (Li et al., 2010).

Table 1.3: PAT and thioesterase involvement in disease processes affecting the nervous system.

Human Disease Relevance	Experimental Model	Associated Features	Enzyme	Reference
Huntington disease	*In vitro*	Weaker HTT-HIP14 interaction and reduced palmitoylation in presence of disease causing mutation in HTT.	HIP14	Singaraja *et al*. 2002, Huang *et al*. 2004
	Animal model	Reduced HTT palmitoylation in YAC128 mouse model of HD.	HIP14	Yanai *et al.* 2006
	Animal model	Phenotype in mice lacking murine Hip14 resembles mouse model of HD	HIP14	Singaraja *et al.* 2011
	Animal model	Strain 129S6/SvEv: Hair, skin, and bone abnormalities with impaired survival and global amyloidosis. Reduced HTT palmitoylation *in vitro*	HIP14L	Saleem *et al*. 2010
Alzheimer disease	*In vitro*	DHHC12 modifies APP metabolism (including Aβ production)	ZDHHC12	Mizumaru *et al*. 2009
Amyotrophic lateral sclerosis	*In vitro*	Increased palmitylation and decreased processing of familial ALS SOD1 mutatnts	--	Antinone *et al*. 2013
Schizophrenia	Human	Increased transmission of Schizophrenia-associated SNP in females with	ZDHHC8	Liu *et al.* 2002a
	Animal model	In females: Deficit in prepulse inhibition Abnormal fear-related exploratory behaviour Decreased sensitivity to NMDAR blocker Decreased density of dendritic spines Rescue by WT ZDHHC8	ZDHHC8	Mukai *et al.* 2004 Mukai *et al.* 2008
X-linked mental retardation (XLMR)	Human	Severe nonsyndromic XLMR, epileptic seizures, dysmorphic facial appearance	ZDHHC15	Mansouri *et al*. 2005
	Human	Moderate XLMR in males, developmental delay	ZDHHC9	Raymond *et al*. 2007
Infantile Neuronal Cereoid Lipofuscinosis	Human	Infantile onset blindness, neurodegeneration, autofluorescent lipopigments in neurons	PPT1	Vesa *et al.* 1995
Learning & memory	Animal model	Impaired cognition and impaired survival in a hypomorphic *Zdhhc5* mouse	ZDHHC5	Yi *et al*. 2010
Ischemic stroke	Animal model	Enhanced interaction of HIP14 with JNK3 in brains from a rat model of transient ischemic stroke, treatment before or after the ischemic insult with a peptide that inhibits this interaction reduced the infarct size by 80%	HIP14	Yang and Cynader 2011

While PPT1 does not appear to play a major role in regulated palmitoylation cycling, mutations in *PPT1* lead to a well-described neurodegenerative phenotype in infants (Vesa et al., 1995). APT1 and APT2 have not been specifically implicated in any human disease to date. As research in the field of palmitoylation progresses, further disease associations for other thioesterases may be elucidated.

Here the focus is on the evidence for involvement of aberrant palmitoylation in diseases affecting the nervous system (Table 1.3).

1.4.1 Alzheimer disease

A number of studies have explored the role of palmitoylation in AD pathogenesis. AD is a progressive neurodegenerative disorder characterized by memory loss, confusion and disorientation. The major pathogenic step in AD is the generation of neurotoxic beta-amyloid (Aβ) from amyloid precursor protein (APP) by the sequential cleavage by β-secretase (the major one being β-site amyloid precursor protein cleaving enzyme 1: BACE1) and γ-secretase enzymes (Selkoe, 2001). No genetic link has yet been found between PATs and AD but there is evidence the amyloidogenic APP-processing enzymes are palmitoylated; whether this palmitoylation is disrupted in AD is currently unclear.

ZDHHC12 has been linked to regulation of APP trafficking and metabolism (Mizumaru et al., 2009). ZDHHC12 strongly inhibited APP metabolism and Aβ generation by retaining APP in the Golgi and preventing further trafficking to the trans Golgi network and PM in neuroblastoma cells (Mizumaru et al., 2009)

BACE1, a type I transmembrane protein with a long extracellular catalytic domain and a cytoplasmic tail, is palmitoylated at four sites: three within the C-terminal cytoplasmic tail (Cys478, Cys482, Cys485) (Benjannet et al., 2001) and one on its TMD (Cys475) (Vetrivel et al., 2009). *In vitro* coexpression studies have identified five potential PATs that enhance palmitoylation of BACE1: ZDHHC3, 4, 7, 15 and 20. Palmitoylation is critical for targeting a significant pool of BACE1 to lipid rafts (Vetrivel et al., 2009).

The data to determine whether palmitoylation of BACE1 promotes or inhibits Aβ generation is contradictory. Multiple lines of evidence indicate that BACE1 cleaves APP at lipid rafts (Ehehalt, 2003) and when BACE1 is exclusively localized to rafts by a glycophosphatidylinositol anchor, Aβ production is enhanced (Cordy et al., 2003; Riddell et al., 2001). Given that palmitoylation is known to localize BACE1 to lipid rafts, BACE1 palmitoylation would be expected to promote Aβ generation. In accordance with this, disruption of lipid rafts and palmitoylation with statins (cholesterol biosynthesis inhibitors) reduced total Aβ production in Human embryonic kidney 293 (HEK293) cells (Parsons and Austen, 2007; Sidera et al., 2004). In contrast, there is evidence to suggest that BACE1 palmitoylation reduces Aβ production. BACE1 is shed from cell cultures into the medium and in order to study the amyloidogenic potential of this non-palmitoylated BACE1, a soluble form of BACE1 was generated by deletion of the TMD and cytoplasmic tail. This soluble BACE1 remains unpalmitoylated and its expression in HEK293 cells enhances amyloidogenic APP processing compared to wildtype (WT) BACE1. This indicates that shed BACE1 is capable of processing APP and that prevention of BACE1 shedding by palmitoylation is protective (Benjannet et al., 2001). These seemingly contradictory findings may arise due to methodological issues in the above studies. The study by Parsons et al., used cholesterol depletion with statins to disrupt BACE1 palmitoylation and its association with lipid raft microdomains (Parsons and Austen, 2007). Cholesterol depletion is a very crude method and has multiple effects on Golgi morphology, vesicular trafficking and membrane bulk fluidity, which may complicate the interpretation of these findings (Vetrivel et al., 2009). In Benjannet et al., the soluble BACE1 construct was overexpressed in HEK293 cells to non-physiological levels, which increased APP processing possibly due to increased BACE1 expression rather than hypopalmitoyation (Benjannet et al., 2001).

Vetrivel et al., subsequently designed an elegant study to address the role of palmitoylation in BACE1 processing of APP, avoiding a cholesterol depletion paradigm (Vetrivel et al., 2009). They mutated all four cysteine residues in BACE1 to alanines, which abrogated palmitoylation and displaced BACE1 from

lipid rafts. Protein stability and subcellular localization to the trans Golgi network or endosomes was not altered and, surprisingly, the palmitoylation-deficient BACE1 processed APP just as efficiently as WT BACE1 (Motoki et al., 2012; Vetrivel et al., 2009). Thus, in contrast to earlier studies these findings suggested that efficient cleavage of APP by BACE1 does not require palmitoylation or localization to lipid rafts. Therefore disrupted BACE1 palmitoylation is unlikely to contribute to AD.

γ-secretase acts subsequently to BACE1 to generate the toxic APP cleavage product, Aβ. γ-secretase consists of four subunits; presenilin (PS1 or PS2), PEN2, APH1, and nicastrin. The latter two are palmitoylated, nicastrin at a transmembrane site, Cys689, and APH1 at two cytosolic cysteines, Cys182 and Cys245. Lack of palmitoylation destabilizes these substrates but does not alter γ-secretase processing of APP in cells (Cheng et al., 2009). Transgenic mice coexpressing palmitoylation-deficient APH1aL and nicastrin in the forebrain do not demonstrate impaired γ-secretase assembly, enzymatic activity, or localization in dendrites and axons of cortical neurons. When crossed to mice coexpressing variants of APP and PS1, associated with familial AD, stabilization of transgenic PS1 was still observed in the brains of double transgenic mice, indicating a stable enzymatic complex was formed. The mouse model of AD expressing palmitoylation-deficient γ-secretase subunits actually showed a small but statistically significant reduction in amyloid deposition in the forebrains compared to mice overexpressing WT subunits. These data suggest that palmitoylation-deficient γ-secretase is less active towards, both WT and mutant, APP than WT γ-secretase and that reduced palmitoylation is somewhat protective in AD. The mild changes observed in amyloid deposition, however, indicate that other factors contribute to Aβ deposition (Meckler et al., 2010).

APP itself was suggested to be palmitoylated (Bhattacharyya et al., 2013). S-palmitoylation of APP was observed using the ABE assay and bioorthogonal labeling followed by Click detection of palmitoylation. As there are no cysteine residues in the cytosolic domain of APP, the sites of palmitoylation of APP were

found to be Cys186 and Cys187, which are in the N-terminal luminal copper binding domain and are involved in stabilizing the domain structure by forming disulphide bonds with Cys158 and Cys133. Mutation of these palmitoyl cysteines led to retention of APP in the ER, however it was likely that this was due to loss of disulphide bonding rather than loss of palmitoylation. Palmitoylation of APP was detected largely in lipid rafts where palmitoylated APP was preferentially cleaved by BACE1 to produce amyloidogenic cleavage products. Interestingly, palmitoylation of APP increased during normal aging of mice, suggesting a correlation between palmitoylation and Aβ production in age (Bhattacharyya et al., 2013).

Overexpression of ZDHHC7 and 21 increased palmitoylation of APP and Aβ production (Bhattacharyya et al., 2013). The idea that DHHC PATs could be mediating S-palmitoylation in the lumen is controversial. ZDHHC PATs are believed to orient in the membrane such that the DHHC active site domain faces the cytosol and as such are thought to only palmitoylate cytosolic cysteines (Fukata and Fukata, 2010; Ohno et al., 2006). The authors suggest that these enzymes reorient one or more TMDs posttranslationally such that occasionally the DHHC domain faces the lumen (Bhattacharyya et al., 2013). This is the first time that this phenomenon has been suggested to occur for ZDHHC PATs. It is also possible that ZDHHC7 and 21 increase palmitoylation of APP by regulating an MBOAT. Indeed, the authors do not show definitively that APP is S-palmitoylated. It is possible that APP is actually N-palmitoylated by MBOATs, not S-palmitoylated. APP palmitoylation was detected using bioorthogonal labeling, which can label both N- and S-palmtioylation, and using the ABE assay, which could give false positives when disulphide bonds are involved, due to reduction of the disulphide bond by HAM and subsequent labeling of previously disulphided bonded cysteines. To circumvent this issue it would be imperative to perform HAM treatment following bioorthogonal labeling to ensure that the palmitoylation detected are HAM sensitive and, thus, are S-palmitoylation events. S-palmitoylation of APP could also simply occur spontaneously.

Together these studies on AD-related proteins demonstrate the complex but prominent role that palmitoylation plays in the regulation of amyloidogenic APP processing and highlight the need for further studies to clarify the role of palmitoylation in AD.

1.4.2 Amyotrophic lateral sclerosis

Amyotrophic lateral sclerosis (ALS) is an adult onset motor neuron disease characterized by degeneration of upper and lower motor neurons, which causes progressive muscle atrophy, weakness, and spasticity. ALS is fatal with death from denervation of the respiratory muscles occurring on average five years after onset (Rothstein, 2009). Although 90-95% of cases are sporadic the remaining cases are inherited (familial ALS [FASL]) and of these FALS cases, 20% are due to mutations in the Cu/Xn superoxide dismutase (*SOD1*) gene. FALS mutations in SOD1 are believed to confer a toxic gain of function rather than loss of function (Rothstein, 2009). SOD1 was recently shown to be palmitoylated in two studies by multiple methods at Cys6 (Antinone et al., 2013; Marin et al., 2012). Antinone and colleagues found that the immature form of SOD1 that does not have a disulphide bond between Cys57 and Cys146 is predominantly palmitoylated suggesting an interplay between palmitoylation and protein maturation (Antinone et al., 2013). Interestingly, they found that three FALS-linked SOD1 mutants (A4V, G93A, and G85R) were more palmitoylated than WT SOD1 when overexpressed in HEK293 cells and in the NCS-34 motor neuron cell line. SOD1 palmitoylation was also increased in spinal cord from G93A SOD1 and G85R SOD1 transgenic mice (Antinone et al., 2013). In all these cases it was the immature, reduced form of SOD1 that was found to be palmitoylated. Increased palmitoylation of A4V SOD1 increased the membrane association of SOD1. The authors suggest that increased palmitoylation of mutant SOD1 in FALS may result in targeting to mitochondria which may contribute to the mitochondrial dysfunction in FALS (Antinone et al., 2013).

1.4.3 Schizophrenia

Microdeletions in chromosome 22q11 have been widely described and occur in one in every 6000 births (Botto et al., 2003). A large proportion of these individuals will display neurodevelopmental and neuropsychiatric symptoms, and it is estimated that 25% will develop schizophrenia in young adulthood (Murphy et al., 1999; Pulver et al., 1994). In 2002, an association was reported between the *ZDHHC8* gene located in the 22q11 microdeletion region and schizophrenia. Significant association with three single nucleotide polymorphisms (SNPs) in *ZDHHC8* was reported in US and South African populations (Liu et al., 2002). Subsequently, one of these SNPs (rs175174) was confirmed to be significantly associated with schizophrenia in American and South African patients, particularly in female patients. This SNP was found to influence alternative splicing of *ZDHHC8* by increasing retention of intron-4 leading to the introduction of a premature termination codon and increased ratios of the expression of risk allele to the non-risk allele. The subsequent reduced expression and possible dominant negative truncation product may contribute to disease pathophysiology (Mukai et al., 2004). A *Zdhhc8*-deficient mouse also displayed a sexually dimorphic effect; female mice demonstrated significant deficits in pre-pulse inhibition (PPI; a behavioral readout of sensorimotor gating) and abnormalities in fear-related measures of spontaneous activity, features that were almost absent in male mice. The changes in behavior were thought to arise at least in part from ZDHHC8 influence on glutamatergic transmission, as female *Zdhhc8*-deficient mice appeared less sensitive to an NMDAR blocker (Mukai et al., 2004). Female rats have been previously shown to have differences in glutamatergic transmission compared to males (D'Souza et al., 1999). A follow-up study by the same group demonstrated that *Zdhhc8*-deficient mice have decreased density of dendritic spines (Mukai et al., 2008).

Despite another study confirming an association between schizophrenia and *ZDHHC8* in the Han Chinese population (Chen et al., 2004), several subsequent studies failed to identify this association in other populations (Demily et al., 2007; Glaser et al., 2006; 2005; Otani et al., 2005; Saito et al., 2005; Xu et

al., 2010). However, one group recently identified *ZDHHC8* polymorphisms associated with abnormalities in smooth eye movements, a common feature in schizophrenia (Shin et al., 2010). These inconsistent findings may be partially attributed to the different ethnic origins of the various populations. It is possible that the association may be attributed to a closely linked genetic locus, and not to *ZDHHC8* itself. Nonetheless, the deficits seen in mice lacking *Zdhhc8* would seem to support its role in neuropsychiatric deficits (Mukai et al., 2004), and highlight that this protein and its relationship to neuropsychiatric disease merits further study.

1.4.4 Mental retardation

ZDHHC15 has been reported as a strong candidate for nonsyndromic X-linked mental retardation (XLMR). In the reported case of a 29-year old woman with severe nonsyndromic mental retardation, a balanced reciprocal translocation between chromosomes X and 15, 2442 to 3885 bp upstream of the *ZDHHC15* gene, resulted in an absence of *ZDHHC15* transcripts (Mansouri et al., 2005).

Mutations in *ZDHHC9*, also on the X-chromosome, were found in 4 of 250 families with XLMR. Two of these mutations were missense mutations in the DHHC-CR domain, one of which was a highly conserved residue (Mitchell et al., 2006; Raymond et al., 2007). However, this finding was not validated by an assessment of ZDHHC9 enzyme expression or functional assay.

1.4.5 Neuronal cereoid lipofuscinosis

In addition to the many PAT disease associations, mutations in enzymes regulating palmitate removal can also result in disease. Mutations in the PPT1 gene on chromosome 1p32 result in infantile NCL (Vesa et al., 1995). The NCLs are a group of genetically distinct diseases featuring an accumulation of lipofuscin (a granular autofluorescent lipopigment) and resulting in progressive blindness and neurodegeneration. Infantile NCL is a very early-onset form of NCL, featuring a striking loss of cortical neurons (Mitchison et al., 1998). After the crystal structure of PPT1 was identified, a correlation was observed between the

severity of the infantile NCL phenotype and the effect of the various mutations on the catalytic site (Bellizzi et al., 2000).

The molecular mechanism of PPT1 deficiency induced neurodegeneration may be due to activation of an apoptosis pathway. *Ppt1* deficient mice demonstrate abnormal ER morphology and an accumulation of palmitoylated GAP-43 in the ER. The authors suggest this leads to activation of unfolded protein response in the ER and subsequently activation of caspase-3 and apoptosis (Zhang et al., 2006). PPT1 may help protect against apoptosis. Reduced cell death, reduced activation of caspase-3, and increased phosphorylation of the anti-apoptotic protein AKT (protein kinase B) were observed in neuroblastoma cells overexpressing PPT1 treated with the apoptosis-inducing agent, C_2 ceramide (Cho and Dawson, 2000). Inhibition of PPT1 in the same neuroblastoma cells, either via *Ppt1* antisense RNA or a PPT1 inhibitor, resulted in enhanced apoptosis (Cho and Dawson, 2000).

In patients with an autosomal dominant form of NCL, two disease-causing mutations (Leu115Arg and Leu116del) were identified in *DNAJC5* (DnaJ heat shock protein 40 homolog), commonly known as cysteine string protein (CSP). This gene encodes a protein palmitoylated on its cysteine rich domain implicated in membrane association, trafficking, protein folding, and exocytosis with a neuroprotective role (Greaves et al., 2008). Both mutations were shown to segregate with disease and increase the proportion of unpalmitoylated CSP leading to loss of membrane localization and increased diffuse cytosolic staining in a cellular model. The Leu115Arg mutation is predicted to decrease the hydrophobicity of the cysteine-string domain that is required for the initial association with the ER membrane prior to palmitoylation and the Leu116del mutation is predicted to negatively impact the palmitoylation of the adjacent cysteines (Nosková et al., 2011). Greaves and colleagues found that both of these mutations led to loss of palmitoylation of the monomeric form of CSP and resulted in dispersed, punctate localization of CSP. They also observed the formation of high molecular weight SDS-resistant CSP aggregates that were enriched in the membrane fraction (Greaves et al., 2012). These mutant

aggregates were palmitoylated and co-expression with ZDHHC3 or 17 increased aggregation whereas treatment with HAM broke up the aggregates. The authors hypothesize that aggregation of CSP causes NCL in a dominant manner due to loss of CSP function by recruitment of WT as well as mutant CSP into the aggregate or by build up of aggregated, palmitoylated CSP that is resistant to the action of lysosomal thioesterases, a slower progressing but similar effect as in *Ppt1* deficiency. These results implicate a role for palmitoylation in the neurodegenerative disease NCL.

1.4.6 Huntington disease

Huntington disease (HD) is an autosomal dominant neurodegenerative disease that presents with cognitive, motor, and psychiatric signs and symptoms (Roos, 2010; Sturrock and Leavitt, 2010). Striatal volume loss and loss of medium spiny neurons (MSNs) of the striatum are key features of the disease (Vonsattel and DiFiglia, 1998). HD results from a mutation in the huntingtin (*HTT*) gene by expansion of a normal-length polyglutamine-encoding CAG trinucleotide repeat to greater than 35 repeats (mHTT or polyQ) (Group, 1993). The prevalence of HD in Caucasian European populations was recently estimated at 13.7 per 100,000 individuals in the general population and 17.2 per 100,00 in Caucasians, with lower prevalence in East Asian and African populations (Fisher and Hayden, 2014; Walker, 2007; Warby et al., 2011). Several lines of evidence have implicated aberrant palmitoylation by HIP14 and HIP14L in the pathogenesis of HD.

1.4.6.1 Discovery of the huntingtin interacting proteins: HIP14 and HIP14L

Prior to the identification of HIP14 as the first mammalian PAT and its implication in HD pathogenesis, the *Drosophila melanogaster* ortholog of *HIP14*, *dHIP14* (*CG6017*), was described as a gene controlling synaptogenesis and embryonic motor axon guidance (Kraut et al., 2001). Special interest in HIP14 arose later when it was identified as part of a yeast two-hybrid screen for HTT interactors (Kalchman et al., 1996; Singaraja et al., 2002). HIP14 was selected for further study, as its interaction with HTT was found to be inversely correlated with polyQ

length, suggesting a potentially important role in HD pathogenesis (Singaraja et al., 2002). Moreover, HIP14 was shown to be enriched in the brain and to be expressed in MSNs, the earliest affected cell population in HD. *HIP14L* was identified in a database search for *HIP14* homologs (Singaraja et al., 2002). HIP14L was also shown later to be enriched in the brain and to interact with HTT in a manner inversely correlated to polyQ length (Huang et al., 2011; Sutton et al., 2013).

Both HIP14 and HIP14L proteins display sequence similarity to the yeast proteins Akr1 and Akr2, the former being an essential protein for endocytosis in the yeast *Saccharomyces cerevisiae*. Expression of human HIP14 was sufficient to rescue temperature-sensitive lethality and restore defects in endocytosis in yeast cells lacking Akr1. These findings suggested a role for HIP14 in intracellular trafficking (Singaraja et al., 2002). Akr1 was described as a PAT in 2002 (Roth, 2002). The high sequence similarity of HIP14 to Akr1 and the presence of the signature DHHC-CR domain led investigators to ask whether HIP14 may also be a PAT; this was confirmed in 2004 in the laboratories of the late Alaa El-Husseini and Michael Hayden (Huang et al., 2004). HIP14 was reported to enhance palmitoylation-dependent trafficking of several proteins in neurons, and siRNA suppression of HIP14 endogenous expression in neurons reduced the synaptic clustering of PSD-95 and GAD65 (Huang et al., 2004). This study was the first of many to explore the role of HIP14 as a PAT and its importance in normal biology, as well as its potential role in human disease.

1.4.6.2 Evidence for aberrant palmitoylation in Huntington disease

Following the 2004 description of HIP14 as a PAT for HTT, Yanai *et al.* identified the major site of palmitoylation of HTT as Cys214 (Yanai et al., 2006). Mutation of this site to serine, rendering it palmitoylation-resistant, resulted in increased NMDA-induced toxicity in rat cortical neuronal cultures and increased inclusion formation in COS cells and neuronal cultures. siRNA-mediated downregulation of HIP14 in cortical neuronal cultures from the YAC128 mouse model of HD (a full-length human *HTT* transgenic mouse with 128 CAG repeats) resulted in

increased inclusion formation (Slow, 2003; Yanai et al., 2006). In contrast, overexpression of HIP14 significantly reduced inclusion formation in YAC128 cortical neurons. Finally, HTT palmitoylation is reduced in the brain of YAC128 mice. All of these findings combined suggested an important role for palmitoylation in HD (Yanai et al., 2006).

In order to assess whether HIP14 function might be impaired in HD, HIP14 expression levels were assessed in the striatum of YAC128 and R6/2 (an HD mouse model expressing exon 1 of human *HTT* with 148-153 CAG repeats (Heng et al., 2008; Mangiarini et al., 1996)) mice and found to be unaltered, confirming that HD pathology is not a result of reduced HIP14 expression (Rush et al., 2012; Singaraja et al., 2011). Like all PATs, HIP14 itself is palmitoylated (Huang et al., 2004), and this auto-palmitoylation is a conserved feature that is correlated with PAT activity (Fukata et al., 2004; Huang et al., 2004). The palmitoylation of HIP14 is reduced in brains of YAC128 and R6/2, suggesting that HIP14 activity is reduced in the presence of mutant mHTT. Similarly, HIP14 isolated from YAC128 brains demonstrated significantly reduced PAT activity toward SNAP25, confirming that HIP14 is dysfunctional in the presence of mHTT (Huang et al., 2011; Singaraja et al., 2011). Indeed, GAD65 has been shown to have dramatically reduced palmitoylation in the presence of mHTT, in N2A cells overexpressing HTT 1-68 with 103 polyQ repeats compared to cells overexpressing HTT 1-68 with 25 polyQ repeats and in the striatum of R6/2 mice (Rush et al., 2012).

There are other pieces of evidence of aberrant palmitoylation in HD. 19 proteins have been shown to have a greater than 10% decrease of palmitoylation in 12-month old YAC128 mice. This study involved determining the palmitoyl proteome in whole brain lysates from WT and YAC128 mice by stable isotope labeling of mammals and ABE MS. Interestingly, a large number of these 19 proteins are glial specific proteins, including carbonic anhydrase II, two myelin-associated oligodendrocyte proteins, the phosphodiesterase CNP and the transmembrane protein myelin oligodendrocyte glycoprotein; and three components of the astrocyte glutamate-glutamine pathway, glutamine-ammonia

ligase and two glutamate transporters GLT-1 (*SLC1A2*) and GLAST (*SLC1A3*) (Wan et al., 2013). Indeed, GLT-1 was previously shown to be less palmitoylated in the YAC128 mice. The loss of palmitoylation of GLT-1 leads to loss of glutamate uptake activity (Huang et al., 2010). These data implicate palmitoylation in the regulation of glutamate transport and metabolism, which may contribute to the glutamate toxicity in HD.

1.5 HIP14 AND HIP14L: EXPRESSION, FUNCTION, AND STRUCTURE

1.5.1 HIP14 and HIP14L are widely expressed

HIP14 is highly expressed in the adult brain, in all regions assessed at both the transcript and protein level (Singaraja et al., 2002). *HIP14* mRNA and protein has also been detected in most peripheral tissues studied (Ohno et al., 2006; Singaraja et al., 2002). Due to lack of a reliable antibody for HIP14L, only mRNA expression has been assessed; *Hip14l* mRNA expression appears ubiquitous in adult human and mouse tissue (Ohno et al., 2006; Saleem et al., 2010; Sutton et al., 2013). However, mice *Hip14l* mRNA expression was highest in the heart, muscle, brain, and kidney and within the brain was highest in the cerebellum (Sutton et al., 2013).

At the subcellular level, endogenous HIP14 localizes to Golgi and cytoplasmic vesicles according to immunogold electron microscopy of mouse cortical neurons and colocalization of HIP14 staining with that of the Golgi-specific marker GM130 in NT2 cells and rat hippocampal neurons (Huang et al., 2004; Singaraja et al., 2002). A study investigating the localization of all DHHC proteins, by expressing human constructs in HEK293 cells, confirmed Golgi localization for HIP14 and reported that HIP14L is detected in both the Golgi and ER (Ohno et al., 2006).

Whether HIP14 is localized at the presynaptic bouton is controversial because it has not been observed in an endogenous mammalian system. Exogenous expression of human HIP14-GFP in rat hippocampal neurons was localized to both the presynaptic terminals and the Golgi apparatus and, in *D. melanogaster*, the HIP14 ortholog, dHIP14, was observed at the presynapse, in

vesicles (Stowers and Isacoff, 2007) and at the PM (Ohyama et al., 2007). Moreover, human HIP14 does not colocalize with the presynaptic marker, synaptophysin, in rat hippocampal neurons (Huang et al., 2009).

1.5.2 Protein substrates for palmitoylation by HIP14

HIP14 palmitoylates a number of substrates (Table 1.4 and Figure 1.3). HIP14 appears to be predominantly a neuronal PAT and its confirmed substrates include SNAP25, GAD65, HTT, STREX-BK potassium channel, GLUA1/2 AMPA receptor subunits, and CLIP3, a modulator of AKT signaling (Fukata et al., 2004; Greaves et al., 2010; Huang et al., 2009; 2004; Ren et al., 2013; Singaraja et al., 2011; Tian et al., 2010).

Table 1.4: Reported palmitoylation substrates of HIP14.

Substrate	Human Gene Symbol	Reference
DnaJ heat shock protein 40 homolog; Cysteine string protein (CSP)	*DNAJC5*	Greaves *et al.,* 2008
65 kDa glutamate decarboxylase (GAD65)	*GAD2*	Huang *et al.*, 2004
		Huang *et al.,* 2009
AMPA-selective glutamate receptor 1 (GluA1)	*GRIA1*	Huang *et al.,* 2009
AMPA-selective glutamate receptor 2 (GluA2)	*GRIA2*	Huang *et al.,* 2009
Huntingtin (HTT)	*HTT*	Yanai *et al.,* 2006
		Huang *et al.,* 2009
		Huang *et al.,* 2011
Lymphocyte-specific protein tyrosine kinase (LCK)	*LCK*	Fukata et al., 2004
Postsynaptic density protein 95 (PSD95)	*DLG4*	Huang *et al.*, 2004
		Huang *et al.,* 2009
		Singaraja *et al.,* 2011
Synaptosomal-associated protein, 25kDa (SNAP25)	*SNAP25*	Greaves *et al.* 2010
		Fukata *et al.,* 2004
		Huang *et al.*, 2004
		Huang *et al., 2009*
		Singaraja *et al.,* 2011
Large conductance calcium- and voltage-activated potassium (STREX BK) channels	*KCNMA1*	Tian L. *et al*., 2010
Synaptotagmin I	*SYT1*	Huang *et al.*, 2004
Growth associated 43 (GAP-43)	*GAP43*	Huang *et al.*, 2004
Chordin (short gastrulation, Sog, in *D. melanogaster*)	*CHRD*	Kang *et al.,* 2010
Glycoprotein M6A (GPM6A)	*GPM6A*	Butland *et al.*, 2014
Sprouty-related, EVHI domain containing 1 (SPRED1)	*SPRED1*	Butland *et al.*, 2014
Sprouty-related, EVHI domain containing 3 (SPRED3)	*SPRED3*	Butland *et al.*, 2014
CAP-GLY domain containing linker protein 3 (CLIP3)	*CLIP3*	Ren *et al*., 2013

Note: GAP-43, LCK, CHRD, GPM6A, SPRED1, SPRED3, or CLIP3 not shown in Figure 1.3

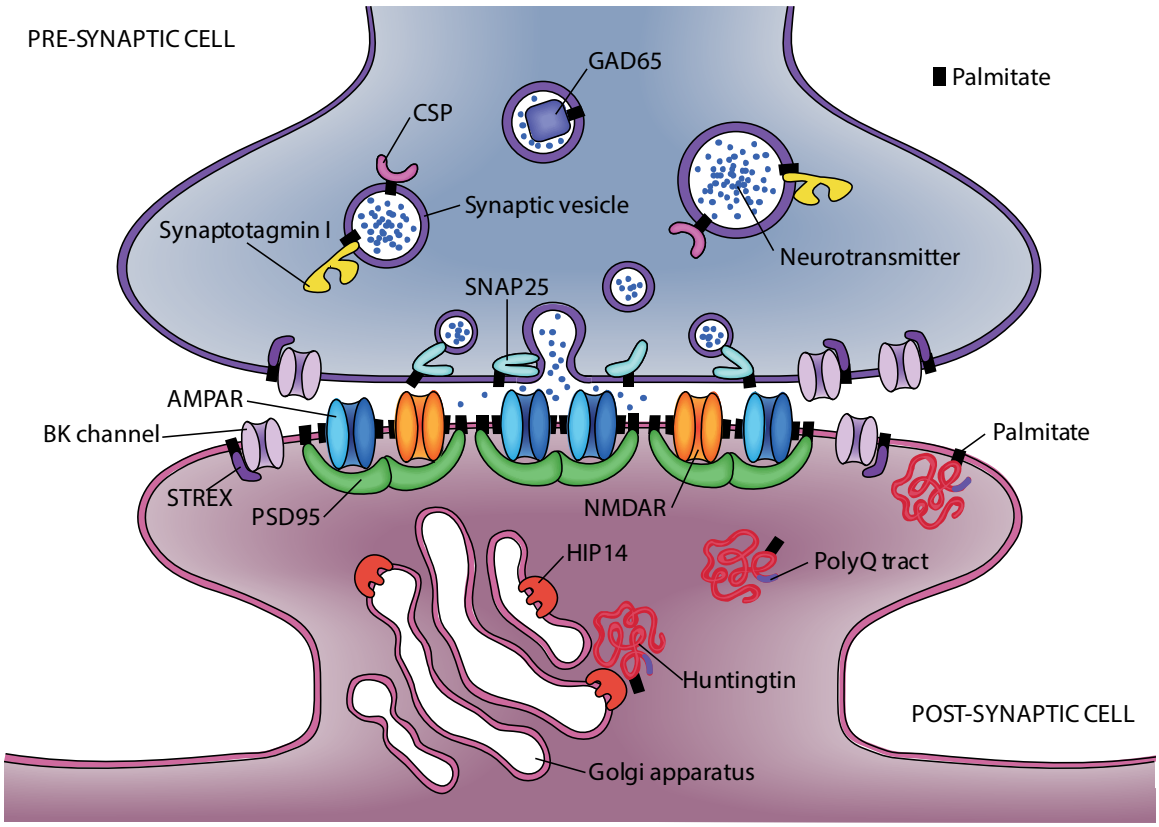

Figure 1.3: Localization of HIP14 substrates at the synapse. HIP14 palmitoylates both pre- and postsynaptic proteins (palmitate is represented by the short black bars). HIP14 substrates at the presynaptic bouton include the GABA synthesizing enzyme, GAD65, STREX BK channel and synaptic vesicle fusion machinery; cysteine string protein (CSP), synaptotagmin I and SNAP25. Postsynaptic substrates of HIP14 include AMPA receptor subunits, GLUA1 and GLUA2, HTT, STREX BK channel and PSD-95; a scaffold protein that clusters of glutamate receptors in the postsynaptic membrane.

Notably, some potential HIP14 substrates have been identified *in cellulo*, either by co-expression studies with HIP14 or *in vitro* reconstitution assays with HIP14 and ^{3}H-labeled palmitoyl-CoA, but have not been corroborated by HIP14 knockdown or knockout experiments. These include the tyrosine kinase, Lck, synaptotagmin I and CSP, a chaperone protein involved in exocytosis (Fukata et al., 2004; Greaves et al., 2008; Huang et al., 2004). CSP is palmitoylated in HEK293 cells expressing HIP14 and in *D. melanogaster* loss of CSP palmitoylation and mislocalization is observed when mutants of dHIP14 are expressed; assessment of complete loss dHIP14 was not possible because it was embryonic lethal (Ohyama et al., 2007; Stowers and Isacoff, 2007). The

Sprouty-related, EVHI domain-containing proteins SPRED1 and SPRED3 and glycoprotein M6A (GPM6A) were identified in a Yeast 2-hybrid (Y2H) screen for HIP14 interactors and were confirmed to be substrates *in cellulo* in COS cells. In fact, the HIP14 Y2H interactors were enriched for the cysteine-rich Sprouty domain, potentially indicating that any of the seven human proteins containing this domain could be substrates of HIP14 (Butland et al., 2014).

A number of HIP14 substrates remain controversial. While a number of PATs have been reported for PSD-95 (ZDHHC2, 3, 7, 8 and 15) (Fukata et al., 2004; Mukai et al., 2008), there exists some debate as to whether these include HIP14. *In vitro* reconstitution palmitoylation assays with purified HIP14 and PSD-95 and ^{3}H-labeled palmitoyl-CoA demonstrate that HIP14 is capable of palmitoylating PSD-95 (Huang et al., 2004). However, in ^{3}H-palmitate metabolic labeling of HEK293 and COS cells, expressing PSD-95 with all 23 PATs, HIP14 did not increase palmitoylation of PSD-95 (Fukata et al., 2004). It seems likely HIP14 is a PAT for PSD-95 because lentiviral shRNA-mediated knockdown of HIP14 reduced palmitoylation of PSD-95 in rat cortical neurons and COS cells (Huang et al., 2009; 2004). Similarly, GAP-43 was identified as a HIP14 substrate in *in vitro* reconstitution palmitoylation assays by Huang *et al*., but not in coexpression studies in HEK293 cells from Fukata *et al* (Fukata et al., 2004; Huang et al., 2004). These discrepancies may reflect the fact that HIP14 may not act as a PAT for PSD-95 or GAP-43 in all physiological contexts, particularly given the redundancy of PATs for these substrates. It also remains contentious whether the BMP (bone morphogenic protein) antagonist, Sog (short gastrulation; *D. melanogaster* homologue of mammalian chordin), is a substrate of dHIP14 because in the Myc western blot showing Sog palmitoylation, it is difficult to discern the Sog specific band (Kang and Bier, 2010). To definitively confirm Sog as a substrate of dHIP14, a direct effect of dHIP14 on Sog palmitoylation would need to be shown, for example by assessing Sog palmitoylation upon knockdown or overexpression of dHIP14.

A number of studies have reported on substrates that are not palmitoylated by HIP14; these include paralemmin and synaptotagmin VII

(Huang et al., 2004), the γ-2 subunit of the $GABA_A$ receptor ($GABA_AR$ γ2) (Fang et al., 2006), and $G\alpha_s$ (Fukata et al., 2004).

HIP14 and HIP14L are the two major PATs for HTT. ABE palmitoylation assays on COS cell lysates co-transfected with HTT and all 23 individual PATs revealed that HIP14 and HIP14L are the only two PATs that significantly increase HTT palmitoylation (Huang et al., 2009; 2011). In order to confirm that HTT is exclusively palmitoylated by HIP14 and HIP14L it would be important to determine if loss of PAT activity of both HIP14 and HIP14L leads to abrogation of HTT palmitoylation.

1.5.3 Protein substrates for palmitoylation by HIP14L

HTT is not the only known substrate of HIP14L, there are 6 other confirmed HIP14L substrates (Table 1.5) (Huang et al., 2009; 2011). HIP14L is a confirmed PAT for IgG kappa light chain and MT1-MMP (Saleem et al., 2010; Song et al., 2014). HIP14L was shown to be a PAT for a number of substrates *in cellulo* by co-expression studies, namely GAD65 and GP78, although not the primary PAT for either (Fairbank et al., 2012; Huang et al., 2009). Interestingly, HIP14L was shown to be a PAT for SNAP25 *in vivo* despite it not having very high activity against it *in cellulo* (Sutton et al., 2013). CLIPR-59 was shown to be a HIP14L substrate as well as a HIP14 substrate (Ren et al., 2013). The authors claim that HIP14 is a better substrate as HIP14 palmitoylated it in a dose dependent manner whereas HIP14L only palmitoylated it at high doses and HIP14 had a stronger interaction with it. However, the autopalmitoylation of HIP14 was much higher even at lower doses of HIP14 indicating that HIP14 has a much higher basal activity level, which could explain the lack of palmitoylation of CLIPR-59 by HIP14L at lower doses. Also in the coimmunoprecipitation experiments showing that HIP14 interacted a lot more with CLIPR-59 than HIP14L, HIP14L expression is much lower than that of HIP14 making it hard to make these kinds of conclusions (Ren et al., 2013).

HIP14L does not palmitoylate PSD-95, GLUA1, GLUA2, synaptotagmin VII, paralemmin I, and $GABA_AR\gamma2$ *in cellulo* (Huang et al., 2009).

Table 1.5: Reported palmitoylation substrates of HIP14L.

Substrate	Human Gene Symbol	Reference
65 kDa glutamate decarboxylase (GAD65)	*GAD2*	Huang *et al.,* 2009
Huntingtin (HTT)	*HTT*	Huang *et al.,* 2009 Huang *et al.,* 2011
Synaptosomal-associated protein, 25kDa (SNAP25)	*SNAP25*	Sutton *et al.* 2013
CAP-GLY domain containing linker protein 3 (CLIPR-59)	*CLIP3*	Ren *et al*., 2013
IgG kappa light chain		Saleem *et al.*, 2010
Autocrine motility factor receptor, E3 ubiquitin protein ligase (GP78)	*AMFR*	Fairbank *et al*., 2012
Matrix metallopeptidase 14 (MT1-MMP)	*MMP14*	Song *et al*., 2014

1.5.4 HIP14 and HIP14L are unique among PATs

HIP14 and HIP14L have identical domain structures with an ankyrin domain, comprising seven N-terminal ankyrin repeats, followed by six predicted TMDs with the signature catalytic DHHC-CR domain located between the fourth and fifth TMDs (Figure 1.4). Both the ankyrin domain and the DHHC-CR domain are predicted to reside on the cytoplasmic face of the membrane, allowing protein recognition (via the ankyrin domain) and enzyme function (mediated via the DHHC-CR domain) to occur on the same side of the membrane (Politis, 2005). HIP14 and HIP14L are the only two PATs to contain ankyrin repeats, which are tandemly repeated 30 to 34 amino acid sequences known to mediate protein-protein interactions (Li et al., 2006a; Michaely et al., 2002) and thought to play a role in substrate recognition (Huang et al., 2009). The presence of seven ankyrin repeats was determined from the crystal structure of amino acids 51-288 of human HIP14 (Gao et al., 2009) and by homology-modeling (Arnold et al., 2006) of human and mouse HIP14L on this structure and on a segment of human ankyrin protein (Michaely et al., 2002; Young et al., 2012). Prior to this, HIP14 and HIP14L have been depicted as having five ankyrin repeats. HIP14 appears to bind the N-terminal region of HTT through its ankyrin domain and this interaction is unimpaired by deletion of the DHHC-CR domain (deletion of amino acids 440 to 487) (Huang et al., 2009; 2011). The interacting regions have been mapped to amino acids 1 to 548 of HTT and amino acids 89 to 257 of HIP14 (Huang et al., 2009; 2011). Due to their shared domain structure, we expect the interaction of HIP14L with HTT to be similar to that of HIP14.

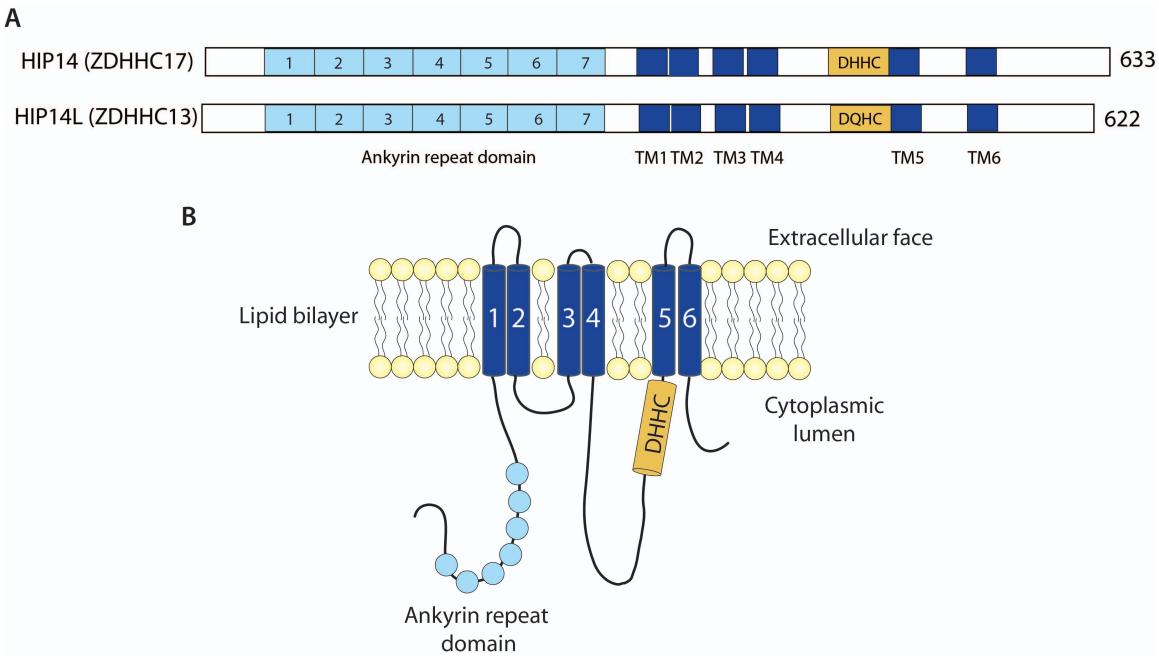

Figure 1.4: Schematic of HIP14 and HIP14L showing domain structure and membrane topology. A) Protein domain structure: HIP14 and HIP14L contain an ankyrin repeat domain (with 7 repeats), 6 transmembrane domains (TM1-6) and a catalytic DHHC-CR domain (labeled DHHC) between TM4 and TM5. HIP14L contains a DQHC motif within this domain. **B**) Membrane topology of either HIP14 or HIP14L illustrates that the ankyrin domain and DHHC-CR domain are located on the cytoplasmic surface.

1.5.5 HTT is a modulator of HIP14 function

A unique role for HTT in the function of HIP14 as a PAT has recently been identified (Huang et al., 2011). In addition to its palmitoylation at Cys214, wildtype HTT (wtHTT) appears to modulate the palmitoylation and activity of HIP14 itself. Palmitoylation of HIP14 itself was reduced in the brains of mice heterozygous for a targeted disruption of the endogenous HD gene (*Htt*$^{+/-}$), expressing half the endogenous levels of wtHTT (Nasir et al., 1995), and was further reduced in mouse cortical neurons in which wtHTT expression was knocked down by 95% via antisense oligonucleotides (ASO). Palmitoylation of HIP14 substrates was enhanced in the presence of wtHTT but not mHTT in an *in vitro* reconstituted palmitoylation assay with immunoprecipitated HTT, purified HIP14 and SNAP25, and ^{3}H-labeled palmitoyl-CoA. Palmitoylation still occurred in the absence of HTT in the *in vitro* assay, but was two-fold lower. Reduced expression of endogenous wtHTT resulted in reduced palmitoylation of HIP14

substrates in a dose-dependent manner (SNAP25 and GLUA1) when tested in brains of *Htt*$^{+/-}$ mice and in mouse cortical neurons treated with ASOs targeting HTT (Huang et al., 2011). Indeed, when wtHTT is overexpressed in the YAC18 mouse palmitoylation of the HIP14 substrate PSD-95 is increased which results in increased PSD-95 clustering at synapses in MSNs (Parsons et al., 2013). Although this was not shown to be a direct effect of increased HIP14 activity with overexpression of HTT it would be interesting to investigate this further.

Thus, wtHTT, but not mHTT, appears to enhance the palmitoylation of HIP14 itself as well as that of its substrates. In addition to serving as a palmitoylation substrate of HIP14, HTT may mediate this function as an allosteric activator of HIP14, influencing its three-dimensional structure and facilitating access to substrates. Alternatively, HTT may serve as a scaffolding protein in binding HIP14 substrates and bringing them in close proximity with HIP14 to facilitate palmitoylation. Finally, HTT may facilitate trafficking of vesicles containing HIP14 to sites where HIP14 is active (Huang et al., 2011).

The recent finding of a highly significant overlap between interactors of HIP14 and interactors of HTT further implicates the HIP14-HTT complex in the pathogenesis of HD (Butland et al., 2014). An Y2H screen for HIP14 interactors identified 214 interactors, including HTT and HIP14 itself. There was no one functional enrichment but the 214 interactors included proteins involved in trafficking, channels and transporters, proteins involved in signal transduction, translation, phosphorylation, ubiquitin-related and nuclear processes as well as 17 synaptic proteins. The surprising finding of this study was that 36 of the HIP14 interactors are also HTT interactors and seventeen of these are already implicated in HD. This high degree of overlap suggests that HIP14 is critically linked to HTT through its interactions and this warrants further investigation (Butland et al., 2014). It will be interesting to know if these shared interactors are substrates or regulators of HIP14 and to know how altered interaction with HIP14 and HTT may contribute to the pathogenesis of HD.

1.5.6 Evolutionary divergence of HIP14 and HIP14L

HIP14 is the most highly conserved of all 23 mammalian PATs, implying a particularly critical functional role throughout evolution. True homologs exist across eukaryotes including mammals, birds, fish, insects, plants and fungi (NCBI Homologene) (Sayers et al., 2011). The DHHC-CR domain of HIP14 shows striking conservation with the full 51 amino acids being identical from human to chicken and only three amino acids differing in zebrafish (Figure 1.5). While several PATs are more than 95% identical between human and mouse sequences, HIP14 is unique in the high degree of sequence identity it maintains in comparisons down to bony fishes. Human HIP14 full-length amino acid sequence is 88% identical to that in zebrafish (Table 1.6) (Needleman and Wunsch, 1970). This is 17% greater sequence identity than for ZDHHC9, the next most conserved PAT associated with a neuropsychiatric disease process and 10% greater than for ZDHHC7, which has not been linked to disease (Table 1.6). This high degree of sequence identity relative to the other PATs is consistent in comparisons between human sequence and that of other organisms not listed in Table 1.6.

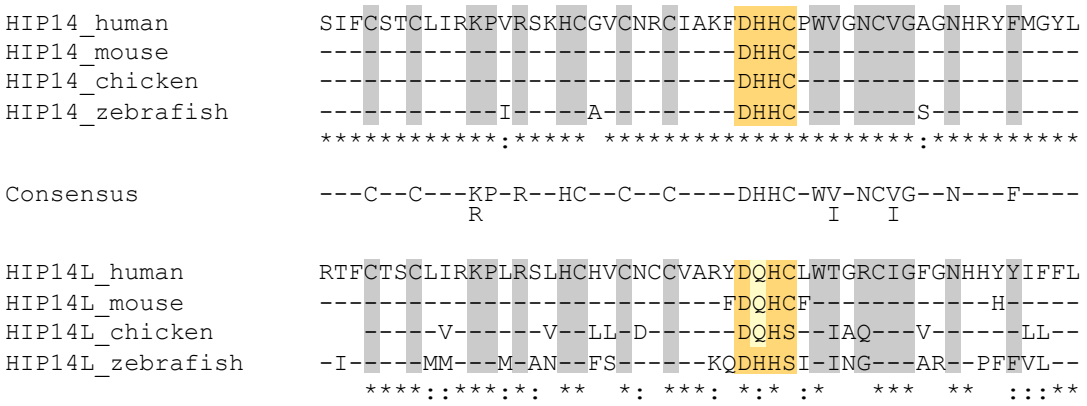

Figure 1.5: Multi-species sequence alignment of vertebrate HIP14 and HIP14L DHHC-CR domains. The HIP14 DHHC-CR domain is an exact match to the PAT consensus sequence and is marked in grey. The 4 amino acid DHHC motif is highlighted in orange. The 51-amino acid sequence in HIP14 is identical in human, mouse and chicken and differs by only three amino acids in zebrafish. Dashes mark amino acids that do not differ from the human sequence. Amino acids that differ from human sequence are specified in the other species. Asterisks mark residues that are identical within HIP14 or HIP14L; colons mark conservative amino acid differences. HIP14L diverges from the DHHC motif consensus with a Gln (Q in light yellow) in place of His (H) in the second position in human, mouse and chicken and the 51-amino acid sequence varies much more than that in HIP14. RefSeq identifiers for aligned HIP14 sequences: human (NP_056151.2); mouse (NP_766142.2); cow (NP_001192998.1); chicken (NP_001025916.1); zebrafish (NP_001121854.1). HIP14L sequences: human (NP_061901.2); mouse (NP_082307.1); cow (NP_001193070.1); chicken (NP_001026342.1); zebrafish (NP_001008650.1).

Table 1.6: Sequence conservation of PATs.

Palmitoyl acyltransferase*	Disease Relevance	human-mouse	human-zebrafish
HIP14 (ZDHHC17)	Huntington disease	99	88
ZDHHC7	-	95	78
ZDHHC2	-	95	74
ZDHHC6	-	93	74
ZDHHC9	X-linked Mental Retardation	98	71
ZDHHC3	-	97	69
ZDHHC14	-	95	67
ZDHHC15	X-linked Mental Retardation	98	66
ZDHHC21	-	98	64
ZDHHC20	-	88	62
ZDHHC8	Schizophrenia	92	56
ZDHHC12	Alzheimer disease	88	54
ZDHHC5	Learning and memory	98	50
ZDHHC18	-	93	50
HIP14L (ZDHHC13)	Huntington disease	91	49
ZDHHC16	-	99	48
ZDHHC22	-	92	46
ZDHHC23	-	83	45
ZDHHC4	-	74	45
ZDHHC24	-	88	44
ZDHHC1	-	68	40
ZDHHC11	-	42	31
ZDHHC19	-	62	n.a.

* ZDHHC10 does not exist under current PAT nomenclature. Zebrafish does not appear to have a gene encoding ZDHHC19 ("n.a."). Those PATs with no known neuropsychiatric disease relevance are indicated with a "-."

HIP14 and HIP14L are more closely related to each other than to any of the other 21 PATs (Fukata and Fukata, 2010). The HIP14 and HIP14L proteins (632aa and 622aa, respectively, in humans) share 48% amino acid identity and 57% similarity (Singaraja et al., 2002). HIP14L is intriguing in that like HIP14, it palmitoylates HTT (Huang et al., 2009; 2011) but it is far less conserved by all measures: in stark contrast to the high degree of sequence conservation of HIP14, human HIP14L full-length amino acid sequence is only 49% identical to that in zebrafish (Table 1.5); NCBI Homologene shows HIP14L homologs only in mammals, chicken and fish (while HIP14 is conserved down to yeast); and its DHHC-CR domain sequence is less conserved than that of HIP14 (Figure 1.5).

HIP14L is the only PAT to have a DQHC motif in place of the canonical DHHC (Figure 1.5) (Greaves and Chamberlain, 2011; Mitchell et al., 2006). This substitution of an amide amino acid, Gln, for the canonical His basic amino acid occurs in human, mouse (Figure 1.5) and other mammals. While changes to the DHHC motif often render a PAT inactive (Mitchell et al., 2006), catalytically active variants of the DHHC motif do occur (e.g. DHYC in yeast Akr1). In yeast Erf2, mutation of DHHC to DAHC (His to Ala) abolishes its PAT activity, however this mutant is still able to form the palmitoylated Erf2 acyl-enzyme intermediate (Lobo, 2002). The authors propose that this histidine may play a role in transfer of palmitate from the PAT to its substrate. Palmitoylation of HTT by HIP14L has been demonstrated in COS cells (Huang et al., 2009; 2011; Singaraja et al., 2011) but the effect of the DHHC to DQHC change has not specifically been assessed in the absence of other cellular factors. An *in vitro* reconstitution assay of HTT palmitoylation by HIP14L will address the effect of DQHC on PAT activity of HIP14L.

HIP14L appears to have diverged even further in the non-mammalian vertebrates. The chicken and zebrafish HIP14L sequences both have serine in place of the cysteine in the DHHC motif (DQHS and DHHS respectively). We would hypothesize that these are not catalytically active, as mutagenesis of DHHC to DHHS results in loss of palmitoylation activity of HIP14 (Ducker et al., 2004) as well as ZDHHC2, 3, 7 and 15 (Fernandez-Hernando, 2006; Fukata et al., 2004; Sharma et al., 2008). It is possible that HIP14L may have evolved to serve a specialized function in mammals.

1.5.7 Other roles for HIP14 and HIP14L

While most studies have investigated the direct roles of HIP14 and HIP14L as PATs, other roles for these proteins have been revealed by studies that were not specifically motivated by questions about palmitoylation. Both HIP14 and HIP14L have been proposed to act as Mg^{2+} transporters (Goytain et al., 2008) in a study in which HIP14 and HIP14L facilitated Mg^{2+} uptake when expressed in *Xenopus laevis* oocytes. While treatment with 2-Bromopalmitate and deletion of the HIP14

catalytic DHHC-CR domain resulted in reduced Mg^{2+} transport, the authors did not directly assess palmitoylation by HIP14. It is unclear therefore whether HIP14 and HIP14L mediate Mg^{2+} transport directly or via critical palmitoylation of another protein. The same group has since reported that ZDHHC3 mediates Ca^{2+} transport, but the role of these PATs in ion transport in a physiologically relevant system remains to be demonstrated (Hines et al., 2010). While the effects of the PATs on Ca^{2+} and Mg^{2+} transport appears not to be a direct effect of palmitoylation, Ca^{2+} homeostasis in the cell has clear implications for neuropsychiatric disease.

HIP14 has been functionally linked to Type 1 diabetes (T1D) in a "phenome-interactome analysis" of the genes contained in 11 published genome-wide T1D linkage regions. HIP14 was prioritized as a candidate based on the association of its *in silico* protein-protein interaction network with genes that were already implicated in T1D: in this case, HTT and GAD65. HIP14 was protective against apoptosis of insulin secreting beta cells of the pancreas and promoted glucose-stimulated insulin secretion (Berchtold et al., 2011). An association of HIP14 with T1D is not as surprising when considering T1D as an autoimmune disease. The immune synapse is a functional analog of the neuronal synapse with palmitoylation influencing the localization of proteins to lipid rafts and mediating key signaling pathways (Khan, 2001; Ladygina et al., 2011). HIP14 was also shown to be a PAT for CLIPR-59, which modulates AKT signaling and subsequent insulin-dependent glucose transporter type 4 (GLUT4) membrane translocation. GLUT4 mediates insulin-induced glucose disposal from the circulation. Palmitoylation of CLIPR-59 is required for its translocation to the membrane and lipid raft and for it to promote AKT PM association. HIP14 was also required for PM association of GLUT4, although the authors did not show that this was specifically mediated by CLIPR-59 palmitoylation and not also by palmitoylation of GLUT4 or AKT directly (Ren et al., 2013)

Independent lines of evidence have demonstrated a role for HIP14 in mitogen-associated protein (MAP) kinase signaling, which transduces a variety of extracellular signals like neurotrophic factors, cytokines, growth factors and

extracellular stresses to regulate many fundamental processes like apoptosis, cell proliferation and differentiation. In a large-scale characterization of the human MAP kinase interactome, HIP14 was identified as part of a functional interaction module that is not conserved in yeast, implying evolution of new roles of HIP14 (Bandyopadhyay et al., 2010). HIP14 interacts with and activates a neuronal-specific form of c-Jun N-terminal kinase, JNK3 (also known as MAPK10), as well as its upstream activator MKK7 (Map kinase kinase; MAP2K7), but does not activate the other three distinctly regulated MAP kinases p38, ERK2 or ERK5. Activation of JNK3 is independent of HIP14's PAT activity and could be blocked by a peptide specific to HIP14 ankyrin repeat-3 (Figure 1.4) (Harada et al., 2003; Yang and Cynader, 2011). In a transient ischemic stroke rat model the HIP14-JNK3 interaction was increased following ischemic insult. This was blocked by treatment with the above peptide before or after insult, reducing the infarct size by 80%. In contrast, HIP14L interacted with but did not activate MKK7 or JNK3 (Yang and Cynader, 2011).

A recent paper suggested that in Zebrafish the HIP14L regulates germ layer specification independent of its PAT function (Chen et al., 2014). HIP14L binds to and negatively regulates Smad6 thereby supporting BMP signaling and cell specification. The authors propose that it does this by increasing Smad6 ubiquitination and degradation (Chen et al., 2014).

While the role of HIP14 and HIP14L as PATs is well established, the studies summarized here have implicated them in other processes whose potential impact on the pathogenesis of neuropsychiatric disorders warrants further investigation.

1.6 ROLES FOR HIP14 AND HIP14L *IN VIVO*

A very useful means of determining the role of various proteins in disease is to study these *in vivo* through the use of mouse models. Because HIP14 and HIP14L are major PATs for HTT, and because HTT palmitoylation is thought to be protective, we predicted that *Hip14* and/or *Hip14l* null mice may recapitulate some of the phenotypes observed in human HD patients and/or mouse models of

HD. In order to better understand the role that HIP14 plays *in vivo,* we generated mice deficient for *Hip14* (*Hip14*$^{-/-}$) or for *Hip14l* (*Hip14l*$^{-/-}$) and assessed the resultant phenotypes (Singaraja et al., 2011; Sutton et al., 2013).

1.6.1 Mice lacking *Hip14* bear a resemblance to mouse models of HD

Hip14$^{-/-}$ mice were generated from a gene-trapped ES cell line on the wild type FVB/N background strain. Although gross appearance and survival appeared normal, reduced body weight was apparent as early as three months. Magnetic resonance imaging assessment of the brains of *Hip14*$^{-/-}$ mice revealed a predominant striatal volume reduction. Neuropathological assessment by stereology revealed a reduction in striatal volume and striatal neuron counts of approximately 17% appearing between embryonic days 14.5 and 17.5 and present up to 12 months. Similarly, reduced brain weight was observed by one month of age (Singaraja et al., 2011). Neurochemical assessment of the striatum revealed significant decreases in both dopamine- and cAMP-regulated neuronal phosphoproteins (DARPP-32; marking all MSNs) and enkephalin (marking dopamine D2 receptor-containing MSNs) expression, while substance P (marking dopamine D1 receptor-containing MSNs) content was normal (Singaraja et al., 2011). This pattern is highly reminiscent of HD patients wherein glutamate decarboxylase (GAD; marking all MSNs) and enkephalin are both significantly reduced even in patients with mild pathology, while substance P is reduced only later with advanced disease (Deng et al., 2004).

Assessing behavior of the *Hip14*$^{-/-}$ mice revealed deficits similar to those observed in the YAC128 (Table 1.7) (Van Raamsdonk, 2005a). *Hip14*$^{-/-}$ mice displayed deficits in motor coordination and balance, as indicated by a shorter latency to fall in both accelerating and fixed speed rotorod, as early as three months of age. Mice were found to be hyperactive in spontaneous activity measures, a finding concordant with observations in young YAC128 mice (Singaraja et al., 2011; Slow, 2003). Finally, assessment of sensorimotor gating, which is partially controlled through the cortico-striatal circuit (Graybiel, 2000) revealed significant deficits in PPI in *Hip14*$^{-/-}$ mice at 12 months (Singaraja et al.,

2011), similar to observations in YAC128 mice (Van Raamsdonk, 2005b) and in HD patients (Swerdlow et al., 1995). Taken together, these data indicate that *Hip14*$^{-/-}$ mice display HD-like behavioral deficits (Singaraja et al., 2011).

Table 1.7: Similarities and differences between YAC128, *Hip14*$^{-/-}$, and *Hip14l*$^{-/-}$ *mouse models.*

	YAC128	***Hip14*$^{-/-}$** (Singaraja *et al*. 2011)	***Hip14l*$^{-/-}$** (Sutton *et al*. 2013)
Brain weight	5% decrease at 9 months (Slow *et al.* 2003) 3% decrease in volume at 3 months by MRI (Carroll *et al.* 2011)	8% decrease at 1 month	5% decrease at 3 months
Striatal volume	5% decrease at 3 months (Carroll et al. 2011)	17% decrease at E17.5 and later ages	5% decrease at 3 months
Striatal neuronal count	15% decrease at 12 months (Slow et al. 2003)	17% decrease at 1 month 17% decrease at later ages	16% decrease at 6 months
DARPP-32 and Enkephalin staining	Decrease at 12 months in DARPP-32 (Van Raamsdonk *et al.* 2005)	Decrease at 1 month in DARPP-32 and enkephalin, substance P unchanged	Decrease at 6 months in DARPP-32 and enkephalin, substance P unchanged
Other brain regions affected	Decrease in volume of cortex, thalamus, globus pallidus, corpus callosum, hippocampus unchanged (Carroll et al. 2011)	Decrease in volume of cortex, thalamus, globus pallidus, corpus callosum, cerebellum, hippocampus	Decrease in volume of cortex, thalamus, globus pallidus, corpus callosum, *cerebellum*, hippocampus unchanged
Motor function	Accelerating and fixed rotarod deficits from 6 months. Climbing deficits at 7 months (Southwell *et al.* 2009). Hyperactivity at 3 months followed by hypoactivity at 6 month (Slow et al. 2003)	Accelerating and fixed rotarod deficits. Hyperactive at 3 month	*No accelerating rotarod deficits.* Climbing deficits at 2 months. Hypoactive from 3 months
Cognitive function	Impaired motor learning (Van Raamsdonk *et al*. 2005).	Normal motor learning (Young, unpublished)	Impaired motor learning
Palmitoylation	Decrease in HIP14, HTT and GLT-1 palmitoylation (Singaraja *et al.* 2011; Yanai *et al.* 2006; Huang *et al*. 2010)	Decrease in PSD-95 and SNAP25 palmitoylation	Decrease in SNAP25, not *PSD95*, palmitoylation

Features of HD in *Hip14*$^{-/-}$ mice could result from reduced or lost palmitoylation of key neuronal HIP14 substrates. However, despite the previous observation that polyglutamine expanded HTT displays reduced palmitoylation and mis-localization (Yanai et al., 2006), HTT palmitoylation was not altered in *Hip14*$^{-/-}$ mice (Singaraja et al., 2011). It is possible that loss of HIP14 activity in *Hip14*$^{-/-}$ mice may be compensated by other PATs that also are able to palmitoylate HTT, likely HIP14L as it robustly palmitoylates HTT *in cellulo*. Overlaps in PAT-substrate specificity as have been previously documented (Greaves and Chamberlain, 2011; Huang et al., 2009). Thus, HIP14L may compensate for the loss of HIP14-mediated palmitoylation of HTT, but not of all HIP14 substrates. Palmitoylation of two known HIP14 substrates, SNAP25 and PSD-95, was assessed in *Hip14*$^{-/-}$ brains, and was found to be decreased in the absence of HIP14 (Singaraja et al., 2011).

Striatal electrophysiological characterization of the *Hip14*$^{-/-}$ mice provides further evidence for a role for HIP14 in the pathogenesis of HD. The MSNs of *Hip14*$^{-/-}$ mice are less excitable with fewer action potentials at rheobase – the minimum current required to evoke an action potential – have decreased cell surface membrane area indicated by decreased membrane capacitance, have fewer excitatory synapses indicated by decreased spontaneous excitatory postsynaptic currents (sEPSC) and decreased evoked EPSC amplitude (eEPSC), and have lower probability of release in the remaining synapses indicated by increased paired pulse facilitation (Milnerwood et al., 2013). These MSN cellular and synaptic changes are similar to those in late-stage HD mouse models (Milnerwood et al., 2013; Raymond et al., 2011). The *Hip14*$^{-/-}$ mice also display severely impaired hippocampal LTP, completely absent without strong induction paradigms, whereas in HD models LTP is impaired early on but not absent (Milnerwood et al., 2013). *Hip14*$^{-/-}$ mice also exhibit motor inflexibility in the plus maze where they are less likely to turn and explore the perpendicular arm of a plus maze, something that occurs in HD mouse models as well (Estrada-Sánchez et al., 2013). When striatal neuronal activity is recorded while the mice explored the plus-maze, abnormal patterns of activity were observed at

the choice point. Increased firing rate and bursting activity was observed which might impact behaviors such as turning at the choice point. Neurons also tended to fire in a non-correlated way, which may also be affecting the decision-making at the choice point. Similar alterations are present in the R6/2 HD mouse model, namely increased firing rate and reduced correlated firing activity (Estrada-Sánchez et al., 2013).

In the study determining how the palmitoyl proteome is altered in YAC128 mice by stable isotope labeling of mammals and ABE MS, the authors did the same analysis in *Hip14*$^{-/-}$ brain. 19 proteins have been shown to have a greater than 10% decrease of palmitoylation in *Hip14*$^{-/-}$ brain. The palmitoyl proteomes in the YAC128 brain was compared to that in the *Hip14* deficient mice. Overall the two palmitoyl proteomes unexpectedly were not well correlated. Some proteins did show similar changes in levels of palmitoylation in the two mouse models but many did not. However, all proteins in this study that were examined further had a similar level of decrease in expression as with palmitoylation and, unfortunately, there was no way to differentiate in the MS experiment between true changes in palmitoylation and changes in the expression of palmitoylated proteins (Wan et al., 2013). It would be interesting to see what degree of overlap there is between the two palmitoyl proteomes of the two mouse models after correcting for protein expression levels. Regardless, it may be those proteins that show changes in the same direction that really contribute to the similarities in disease phenotypes (Wan et al., 2013).

Together, these observations reveal a phenotype in the *Hip14*$^{-/-}$ mice that resembles that observed in mouse models of HD and in human HD patients. As HIP14 isolated from the brains of YAC128 mice displays impaired palmitoylation activity toward itself and HIP14 substrates (Singaraja et al., 2011), this suggests that HD may be, in part, a disease of altered palmitoylation.

1.6.2 Mice lacking *Hip14l* bear a resemblance to mouse models of HD

Hip14l$^{-/-}$ mice were generated from a gene-trapped ES cell line on the wild type FVB/N background strain. *Hip14l*$^{-/-}$ mice display reduced hair growth and

alopecia around the eyes with reduced hair follicle density at post-natal day 7. Although survival appeared normal, *Hip14l*$^{-/-}$ mice displayed a progressive reduction in body weight, especially apparent at 12 months of age (Sutton et al., 2013). This is in contrast to the more dramatic reduction in body weight from three months in the *Hip14*$^{-/-}$ mice and the increased body weight in the full-length transgenic HD mouse models but is more similar to the reduced body weight observed in HD patients (Gray et al., 2008; Singaraja et al., 2011; Van Raamsdonk et al., 2006).

Neuropathological assessment by stereology revealed a progressive reduction in brain weight from three to 12 months of age in *Hip14l*$^{-/-}$ mice (Table 1.7; 4.8% to 9.1%). A non-progressive 6% reduction in cerebellar volume was observed from three months of age that was not observed at one month of age. A progressive loss of striatal and cortical volume was also observed in the *Hip14l*$^{-/-}$ mice from three to 12 months (5.7% to 9.8% in the striatum and 8.4% to 8.3% in the cortex) that were not observed at one month old. These neuropathological phenotypes are more like the progressive late onset volume losses in the cortex and striatum in the YAC128 HD mice than the non-progressive, developmental loss of striatal and cortical volume in the *Hip14*$^{-/-}$ mice (Table 1.7) (Carroll et al., 2011; Singaraja et al., 2011; Van Raamsdonk, 2005a). Neurochemical assessment of the striatum revealed significant decreases in both DARPP-32 (marking all MSNs) and enkephalin (marking dopamine D2 receptor-containing MSNs) expression, while substance P (marking dopamine D1 receptor-containing MSNs) content was normal (Sutton et al., 2013). This pattern is highly reminiscent of the *Hip14*$^{-/-}$ mice and HD patients wherein glutamate decarboxylase (GAD; marking all MSNs) and enkephalin are both significantly reduced even in patients with mild pathology, while substance P is reduced only later with advanced disease (Deng et al., 2004). Reduced volume of the globus pallidus at six months, of the thalamus at three and six months, and of the corpus callosum was also observed in the *Hip14l*$^{-/-}$ mice. The hippocampus was unchanged (Sutton et al., 2013). Again, this is more similar to the changes in

the brain of YAC128 mice than to those in the *Hip14*$^{-/-}$ mice (Table 1.7) (Carroll et al., 2011; Singaraja et al., 2011).

Assessing behavior of the *Hip14l*$^{-/-}$ mice revealed deficits similar to those observed in the YAC128 (Table 1.7) (Van Raamsdonk, 2005a). *Hip14l*$^{-/-}$ mice displayed deficits in motor learning as indicated by a shorter latency to fall on the fixed speed rotorod at three months of age and in motor coordination as indicated by reduced number of spontaneous climbing events in the climbing apparatus at two months of age (Sutton et al., 2013). Motor learning and motor coordination deficits are present in both the YAC128 and the *Hip14l*$^{-/-}$ mice (Singaraja et al., 2011; Van Raamsdonk, 2005a). Mice were found to be hypoactive in spontaneous activity measures, a finding concordant with observations in old YAC128 mice but different than the hyperactivity in the *Hip14*$^{-/-}$ mice (Singaraja et al., 2011; Slow, 2003; Sutton et al., 2013). Taken together, these data indicate that *Hip14l*$^{-/-}$ mice display HD-like behavioral deficits (Sutton et al., 2013).

Features of HD in *Hip14l*$^{-/-}$ mice could result from reduced or lost palmitoylation of key neuronal HIP14L substrates. However, despite the previous observation that polyglutamine expanded HTT displays reduced palmitoylation and mis-localization (Yanai et al., 2006), HTT palmitoylation was not altered in *Hip14l*$^{-/-}$ mice, as was the case in the *Hip14*$^{-/-}$ mice (Singaraja et al., 2011; Sutton et al., 2013). It is possible that HIP14 and HIP14L compensate for loss of each other for palmitoylation of HTT and some but not all substrates. Overlaps in PAT-substrate specificity as have been previously documented (Greaves and Chamberlain, 2011; Huang et al., 2009). Determining the substrate profiles for the two enzymes and how they overlap would provide an explanation for the similarities and differences between these two mouse models (Table 1.7).

1.6.3 Peripheral deficits in HIP14L mutant mice

A recent study described the phenotype of *Hip14l* mutant mice generated in an N-ethyl-N-nitrosurea mutagenesis screen (Saleem et al., 2010). A loss-of-function point mutation was introduced in exon-12 of *Hip14l* gene, leading to a

truncation of the enzyme just prior to the catalytic domain (*Hip14l*^{R425X}). The mouse developed a severe phenotype including failure to thrive, impaired survival, skin and hair abnormalities, osteoporosis, and generalized amyloid deposition in the entire dermis as well as most other organs examined (Saleem et al., 2010). The authors report that *Hip14l* deficient mice, generated using a gene trap strategy on a mixed 129/B6 genetic background (the same gene trap strategy used to generate the *Hip14l*$^{-/-}$ mice described above), exhibit "similar phenotypes" to *Hip14l*^{R425X} but, aside from histological abnormalities in the skin, data are not shown. Indeed, none of these severe phenotypes were observed in the *Hip14l*$^{-/-}$ mice described above on the FVB/N strain, which may explain the differences (Sutton et al., 2013). Another possibility is that the *Hip14l*^{R425X} mutation is acting in a dominant-negative manner rather than loss of function, which leads to a more severe phenotype. This mutation leads to a truncated protein that includes the ankyrin-repeat domain and the first four TMDs but does not include the DHHC catalytic domain (Saleem et al., 2010). This mutation may bind substrates and sequester them, preventing them from being palmitoylated by other PATs (Sutton et al., 2013).

The same group later reported that the *Hip14l*^{R425X} mice have growth deficits and aberrant bone mass acquisition including delayed secondary ossification center formation and disorganized growth plate structure and osteoporosis as well as reduced bone mineral density. They suggest this is due to loss of palmitoylation of MT1-MMP as mice deficient in this gene have a similar phenotype and the *Hip14l*^{R425X} mice have reduced palmitoylation of MT1-MMP. They suggest that HIP14L is a modulator of bone homeostasis (Song et al., 2014).

1.7 THESIS OBJECTIVE AND HYPOTHESIS

The primary goal of this thesis was to determine the role of palmitoylation in the pathogenesis of HD and provide further validation of palmitoylation as a potential drug target. The strongest pieces of evidence for a role of palmitoylation in HD came from the phenotypes of the *Hip14*$^{-/-}$ and *Hip14l*$^{-/-}$ mouse models both of

which have HD-like phenotypes resembling those of the YAC128 mouse model of HD (Table 1.7) (Singaraja et al., 2011; Sutton et al., 2013). The evidence that wtHTT acts as a modulator of HIP14 activity, that the relationship between these two proteins goes beyond that of just a substrate-enzyme, also suggests that disturbing this relationship will have negative consequences (Huang et al., 2011). The overall hypothesis of this thesis is that disturbed HIP14-HTT and HIP14L-HTT interaction in the presence of the HD mutation reduces HIP14 function leading to the under-palmitoylation and mislocalization of HTT and key HIP14 substrates. The work in this thesis goes towards the goal of determining the role of palmitoylation in the pathogenesis of HD thus the objectives were the following:

1. Determine the interaction domain of HTT and HIP14 and HIP14L
2. Determine the effect of loss of *Hip14* and *Hip14l in vivo* and on HTT palmitoylation
3. Determine palmitoylation levels of synaptic proteins in HD mouse models
4. Determine the role of loss of *Hip14* in the adult animal

2 IDENTIFICATION OF BINDING SITES IN HUNTINGTIN FOR THE HUNTINGTIN INTERACTING PROTEINS HIP14 AND HIP14L[2]

2.1 INTRODUCTION

HD is an autosomal dominant neurodegenerative disease characterized by motor, cognitive, and psychiatric dysfunction with onset in mid-life and death following, on average, 20 years later (Roos, 2010; Sturrock and Leavitt, 2010). The striatum is the brain region to first undergo neurodegeneration with more widespread pathology occurring at later stages of the disease (Roos, 2010; Sturrock and Leavitt, 2010). HD is caused by a CAG expansion in exon 1 of the *HTT* gene that results in a poly-Q expansion in the HTT protein (NP_002102) (Group, 1993).

One approach that has been taken to determine the functions of the HTT protein and to understand the pathogenesis of HD is to identify and characterize HTT interacting proteins and to determine how these interactions are altered in the presence of the HD mutation. HIP14 (NP_056151) was first identified as a HTT interactor in a yeast 2-hybrid screen. HIP14 was further shown to interact with HTT in mammalian systems and to interact less with mHTT (Kalchman et al., 1996; Singaraja et al., 2002). The HIP14 homolog HIP14L (NP_061901) was first identified based on its high amino acid sequence similarity to HIP14 and was later shown to also be a *bona fide* HTT interactor that also interacts less with mHTT (Singaraja et al., 2002; Sutton et al., 2013).

HIP14 and HIP14L both belong to the 23 member family of DHHC (Asp-His-His-Cys) cysteine-rich (DHHC-CR) domain-containing palmitoyl acyltransferases (PATs) (Huang et al., 2004; Ohno et al., 2006). DHHC-CR PATs

---

[2] This chapter has been published in *PLoS ONE*. Sanders, S.S., Mui, K.K.N., Sutton, L.M., and Hayden, M.R. (2014). Identification of binding sites in Huntingtin for the Huntingtin Interacting Proteins HIP14 and HIP14L. PLoS ONE *9*, e90669. All cloning, experimental design, and data analysis by SSS.

are a family of enzymes that mediate post-translational S-acylation of proteins, involving the addition of long chain fatty acids to proteins at cysteine residues via a thioester bond. S-acylation is commonly referred to as palmitoylation because palmitate is the most common long chain fatty acid in the cell (Hallak et al., 1994; Smotrys and Linder, 2004). Many proteins, including HTT, are dynamically palmitoylated and palmitoylation modulates membrane localization, function, protein-protein interactions, and other PTMs of palmitoyl-proteins (Young et al., 2012). HIP14 and HIP14L are unique among the DHHC-CR PATs as they are the only two that have six TMDs and seven ankyrin repeats (Figure 1B and C). The ankyrin repeat domain is believed to mediate the interaction between HIP14 and HTT (Huang et al., 2011; Young et al., 2012).

HIP14 and HIP14L are not only HTT interactors but they are also the primary PATs for HTT (Huang et al., 2011). These PATs show reduced interaction and palmitoylation of mHTT leading to increased mHTT inclusion formation and toxicity (Yanai et al., 2006). Interestingly, both the *Hip14*- and *Hip14l*-deficient mouse models recapitulate many HD-like phenotypes suggesting that both proteins may play a role in the pathogenesis of HD (Singaraja et al., 2011; Sutton et al., 2013). Indeed, HIP14 has been shown to be dysfunctional in the presence of the HD mutation or upon loss of wild type HTT, making it unable to effectively palmitoylate its substrates SNAP25 and GLUA1 (Huang et al., 2011; Singaraja et al., 2011). These data suggest that the interaction between HIP14 and HTT goes beyond that of only a enzyme-substrate interaction and that HTT is essential for the full enzymatic activity of HIP14 (Huang et al., 2011; Singaraja et al., 2011). HIP14L is structurally very similar to HIP14, containing all the same domains in the same orientation; thus it is possible that HTT also modulates the function of HIP14L.

It is important to further understand and characterize the interactions of HTT with HIP14 and HIP14L to guide future efforts to target and enhance this interaction to increase enzyme activity and remediate palmitoylation of HTT and their substrates. It is important to know if HIP14 and HIP14L interact with the same domain of HTT and, if so, if they compete for binding. A shared binding site

would provide further support for the hypothesis that these two PATs are able to compensate for each other in palmitoylating HTT and that HTT may also modulate the activity of HIP14L. If they were to compete for binding, this would need to be taken into consideration when taking efforts to increase the interaction between HTT and one PAT or the other at the risk of decreasing the interaction with the other PAT. HIP14 has been previously shown to interact with HTT amino acids 1-548 (HTT 1-548) (Huang et al., 2011). Here, amino (N)- and carboxy (C)-terminal deletions of HTT 1-548 were generated and their interaction with HIP14 and HIP14L was assessed to determine the location of the binding site.

2.2 MATERIALS AND METHODS

2.2.1 Plasmids and cloning

The generation of HIP14-GFP (NM_015336) and HIP14L-GFP (NM_001001483), 15Q and 128Q HTT 1-548 (15Q and 128Q 1955; NM_002111), and HTT 1-427 (1597) and HTT 1-224 (989) was described previously (Hackam et al., 1998; Huang et al., 2004; Sutton et al., 2013; Wellington et al., 1998). The C-terminal deletion mutants were generated by PCR cloning using the indicated primers in Table 2.1. The primers (Integrated DNA technologies) had EcoRI and NotI restriction enzyme sites added on the 5' and 3' sides of the PCR product respectively and the forward primers also had a start codon added. This allowed the PCR products to be digested and ligated into the EcoRI and NotI sites of pCI-neo (enzymes from New England Biolabs; pCI-neo from Promega). 15Q HTT 1-548Δ257-315 was generated by insertion of a *HTT* gBlock gene fragment into the BlpI and Bsu36I restriction enzyme sites following digestion with the same enzymes such that amino acids 257-315 were deleted. All clones were confirmed by sequencing.

Table 2.1: Cloning primers used to generate the HTT 1-548 N-terminal deletion mutants.

Primer name	Sequence
HTT N-term reverse	tcccatctgaccctgccatg**tga***gcggccgc*tactgctatg
HTT 427-548 forward	tcgtacttat*gaattc***atg**ggaggggttcctcatgcag
HTT 224-548 forward	tcgtacttatgaattc**atg**tcagtccaggagaccttggc
HTT 151-548 forward	tcgtacttat*gaattc***atg**tgcctcaacaaagttatcaa
HTT 88-548 forward	tcgtacttat*gaattc***atg**cgaccaaagaaagaactttc

*Restriction enzyme sites are in italics (EcoRI in forward primers and NotI in the reverse), the start and stop codons are in bold, and the primer binding sequence is underlined

2.2.2 Antibodies

The primary antibodies used were GFP goat polyclonal antibody (sc-5385, Santa Cruz Biotechnology, 1:50 for immunoprecipitation), HTT mouse monoclonal antibody (MAB2166, Millipore, 1:1000 for immunoblotting), HTT mouse monoclonal antibody (in-house BKP1, 1:100 for immunoblotting), and GFP rabbit polyclonal antibody (EU2, Eusera, 1:10000 for immunoblotting). Fluorescently conjugated secondary antibodies for immunoblotting used were Alexa Fluor 680 goat anti-Rabbit (A21076, Molecular Probes, 1:10000) and IRDye 800CW goat anti-Mouse (610-131-121, Rockland, 1: 2500).

2.2.3 Cell culture and transfection

Cells were cultured in DMEM with 10% fetal bovine serum, penicillin/streptomycin (1000 Units/mL Penicillin and 1000 ug/mL streptomycin), and 2 mM L-glutamine at 37°C in 5% CO_2 (Gibco). Constructs were transiently transfected in COS-7 cells (ATCC) with X-tremeGENE 9 DNA transfection reagent (Roche) according to the manufacturer's instructions. Cells were harvested after 24 h for co-immunoprecipitation experiments described below.

2.2.4 Cell lysis and co-immunoprecipitations

Cells were homogenized on ice for 5 min in one volume 1% SDS TEEN [TEEN: 1 M Tris pH 7.5, 0.5 M EDTA, 0.5 M EGTA, 3 M NaCl, 1 mM Complete protease

inhibitor cocktail (Roche), 1 mM sodium vanadate, 1 mM phenylmethylsulfonyl fluoride and 5 μM zVAD-FMK] and subsequently diluted in four volumes 1% TritonX-100 TEEN for 5 min for further homogenization. Samples were sonicated at one time at 20% power for 5 seconds to shear DNA and the insoluble material was removed by centrifugation at 14000 revolutions per minute for 15 min. Samples were immunoprecipitated overnight with Dynabeads® Protein G (Invitrogen) and antibody.

2.2.5 Western blotting analysis

Proteins in both the cell lysates and immunoprecipitates were heated at 70°C in 1 x NuPAGE LDS sample buffer (Invitrogen) with 10 mM DTT before separation by SDS-PAGE. After transfer of the proteins onto nitrocellulose membrane, immunoblots were blocked in 5% milk TBS (TBS: 50 mM Tris pH 7.5, 150 mM NaCl). Primary antibody dilutions of HTT mouse monoclonal antibody and GFP rabbit polyclonal antibody in 5%BSA PBST (Bovine Serum Albumin, Phosphate Buffered Saline with 5% Tween-20) were applied to the immunoblots at 4°C overnight. Corresponding secondary antibodies were applied in 5% BSA PBST for an hour. Fluorescence was scanned and quantified with Odyssey Infrared Imaging system (Li-COR Bioscience) and quantified using the Li-COR software. All error bars are standard error of mean.

2.3 RESULTS

2.3.1 Deletion of HTT amino acids 224-548 abolishes the interaction of HTT with HIP14 and HIP14L

HIP14 was previously shown to interact with HTT 1-548 (Singaraja et al., 2002). The domain organization of HTT 1-548 15Q and 128Q is shown in Figure 2.1.A with the poly-Q, the proline rich region, and the H1 alpha-rod domain indicated (Palidwor et al., 2009). HIP14 was previously shown in a yeast 2-hybrid experiment to have reduced interaction with HTT 1-427 compared to its interaction with HTT 1-548 and no interaction with HTT 1-224, HTT 1-151, HTT 1-88, and HTT 1-40 (Huang et al., 2011). However, as this interaction analysis was performed in yeast it was repeated here in a mammalian system using the

mammalian expression versions of the constructs used in the yeast 2-hybrid experiments (Hackam et al., 1998; Huang et al., 2011). Conveniently, these truncation constructs remove the C-terminal region upstream of the H1 alpha-rod domain (HTT 1-427) or this C-terminal region and half of the H1 alpha-rod domain (HTT 1-224) (Figure 2.2.A). HTT 1-548 and two C-terminal deletion mutants, 15Q or 128Q HTT 1-427 and 15Q or 128Q HTT 1-224 (Figure 2.2.A), were transiently co-expressed with HIP14-GFP or HIP14L-GFP expressing constructs in COS-7 cells. GFP was immunoprecipitated and resulting blots were probed with antibodies to detect GFP and HTT. As previously shown, 57% less mHTT 1-548 (128Q HTT 1-548) co-immunoprecipitated with HIP14-GFP than wtHTT 1-548 (15Q HTT 1-548), indicating reduced interaction in the presence of the HD mutation (Figure 2.2.B and C; n=3). Both 15Q and 128Q HTT 1-427 exhibited decreased, but not abolished, interaction with HIP14-GFP while both 15Q and 128Q HTT 1-224 interacted very little or not at all with HIP14-GFP (Figure 2.2.B and C; n=3). The same interaction pattern was observed with a HIP14-FLAG tagged construct and HTT 1-548 did not interact with GFP alone (data not shown). All further experiments were performed using the GFP tagged constructs as they express better in COS cells. These data indicate that HTT 1-548 is required for full interaction with HIP14 and the interaction is abolished with deletion of amino acids 224-548 in the HTT 1-224 truncation protein. No interaction between HIP14-GFP and HTT 1-151, HTT 1-88, or HTT 1-40 was observed (data not shown).

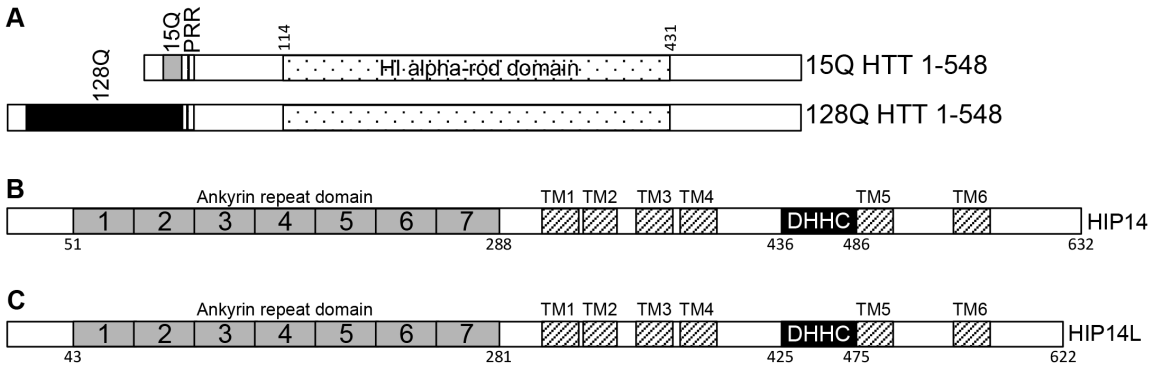

Figure 2.1: Overview schematics of the domain organization of HTT (A), HIP14 (B), and HIP14L (C). The domain organization of HTT is shown in **(A)** with the poly-glutamine domains of WT (15Q) and mutant (128Q) HTT (NP_002102) are shown in grey and black rectangles, respectively, the proline rich repeat is shown in a hatched rectangle, and the H1 alpha-rod domain is shown in a dotted rectangle with the amino acids indicated above. **(B)** The domain organization of HIP14 (NP_056151) is shown in **(B)** and of HIP14L (NP_061901) in **(C)** with the 7 ankyrin repeats making up the ankyrin repeat domain shown in numbered solid grey rectangles, the transmembrane domains shown in hatched rectangles labeled TM1-6, and the DHHC cysteine-rich domain shown in solid black rectangles labeled DHHC. The amino acids corresponding to the appropriate domains are indicated below.

As the domain of HTT that interacts with HIP14L has never been determined, the same co-immunoprecipitation experiment between HIP14L-GFP and the above-mentioned HTT C-terminal deletion mutants, 15Q or 128Q HTT 1-427 and 15Q or 128Q HTT 1-224 was performed. Similar to the results obtained with HIP14, 128Q HTT 1-548 interacted much less with HIP14L-GFP than did 15Q HTT 1-548, indicating reduced interaction with mHTT (54% decrease; Figure 2.2.D and E; n=3). However, no change in interaction of HIP14L with the 15Q and 128Q HTT 1-427 deletion mutants was observed in co-immunoprecipitation experiments (Figure 2.2.D and E; n=4). The HTT 1-224 deletion mutant did not interact with HIP14L (Figure 2.2.D and E; n=3). No interaction between HIP14L-GFP and HTT 1-151, HTT 1-88, or HTT 1-40 was observed (data not shown). These data indicate that HTT 1-427 is sufficient for interaction with HIP14L and the interaction is abolished with deletion of amino acids 224-548 in the HTT 1-224 truncation protein.

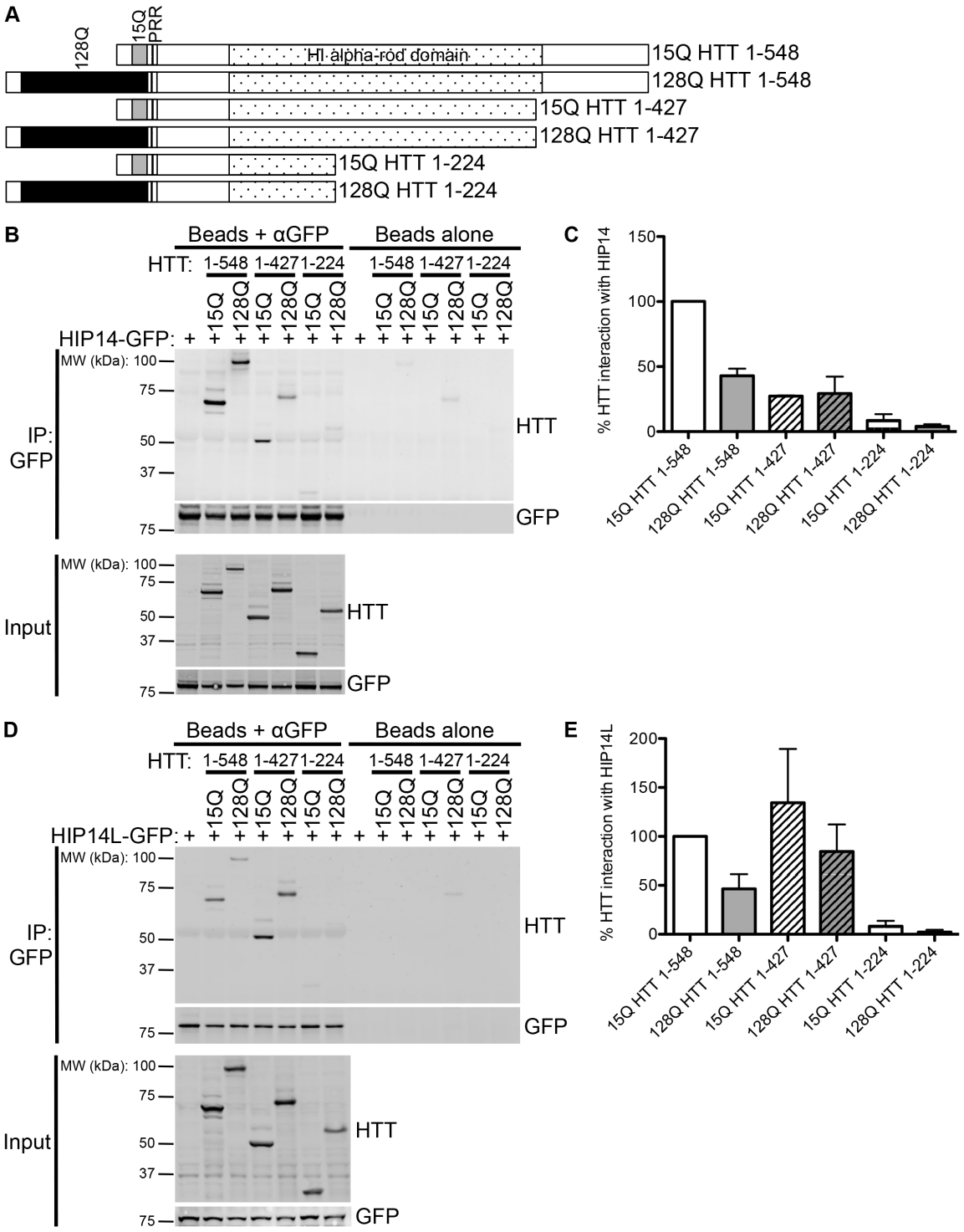

Figure 2.2: HIP14 and HIP14L interaction with C-terminal deletion mutants of HTT 1-548. (A) A schematic diagram of the HTT 1-548 C-terminal deletion mutants used in co-immunoprecipitation experiments with HIP14-GFP and HIP14L-GFP showing the 15Q or 128Q poly-Q domains, the proline rich region (PRR), and the H1 alpha-rod domain. **(B)** A representative image (top two panels) of the co-immunoprecipitation between these C-terminal deletion mutants

and HIP14-GFP where GFP was immunoprecipitated and the resulting blots were probed for HTT (top panel) and GFP (bottom panel) showing less 15Q and 128Q HTT 1-427 co-immunoprecipitated with HIP14-GFP. On the right is a beads alone (no antibody) control showing no non-specific binding of the proteins to the beads. The bottom two images show the expression of the HTT deletion mutants (top panel) and of HIP14-GFP (bottom panel). **(C)** Quantification of three independent co-immunoprecipitation experiments where the % HTT interaction with HIP14 is the indicated HTT band intensity as a percentage of the HIP14-GFP band intensity from the same sample, normalized to 15Q HTT 1-548. **(D)** A representative image (top two panels) of the co-immunoprecipitation between the HTT 1-548 C-terminal deletion mutants and HIP14L-GFP where GFP was immunoprecipitated and the resulting blots were probed for HTT (top panel) and GFP (bottom panel). Less 15Q and 128Q HTT 1-427 co-immunoprecipitated with HIP14L-GFP. On the right is a beads alone (no antibody) control showing no non-specific binding of the proteins to the beads. The bottom two panels show the expression of the HTT deletion mutants (top panel) and of HIP14L-GFP (bottom panel). **(E)** Quantification of three independent co-immunoprecipitation experiments where the % HTT interaction with HIP14L-GFP is the indicated HTT band intensity as a percentage of the HIP14L-GFP band intensity from the same sample, normalized to 15Q HTT 1-548.

2.3.2 Deletion of HTT amino acids 1-427 abolishes the interaction of HTT with HIP14 and HIP14L

To further characterize the domain of interaction of HTT with HIP14 or HIP14L, N-terminal deletion mutants complementary to the C-terminal deletion mutants were generated; HTT 88-548, HTT 151-548, HTT 224-548, and HTT 427-548 (Figure 2.3.A). These deletion mutants were transiently co-expressed with HIP14-GFP or HIP14L-GFP in COS-7 cells. Reduced interaction of HTT with HIP14-GFP was observed with HTT 88-548, HTT 151-548, and HTT 224-548 and the interaction was abolished upon the deletion of amino acids 1-427 in the HTT 427-548 deletion mutant (Figure 2.3.B and C; n=3). These data indicate that HTT amino acids 224 to 548 are sufficient for partial interaction with HIP14.

A similar effect was observed between the interaction of HIP14L and the HTT C-terminal deletion mutants as with HIP14. Reduced interaction of HTT 88-548, HTT 151-548, and HTT 224-548 with HIP14L-GFP was observed in similar co-immunoprecipitation experiments and again complete loss of interaction was observed with the HTT 427-548 deletion mutant (Figure 2.3.D and E; n=3). These data also indicate that HTT amino acids 224 to 548 are sufficient for

partial interaction with HIP14L and, along with the data discussed above, suggests that there may be a HIP14/HIP14L binding domain between amino acids 224-427 of HTT.

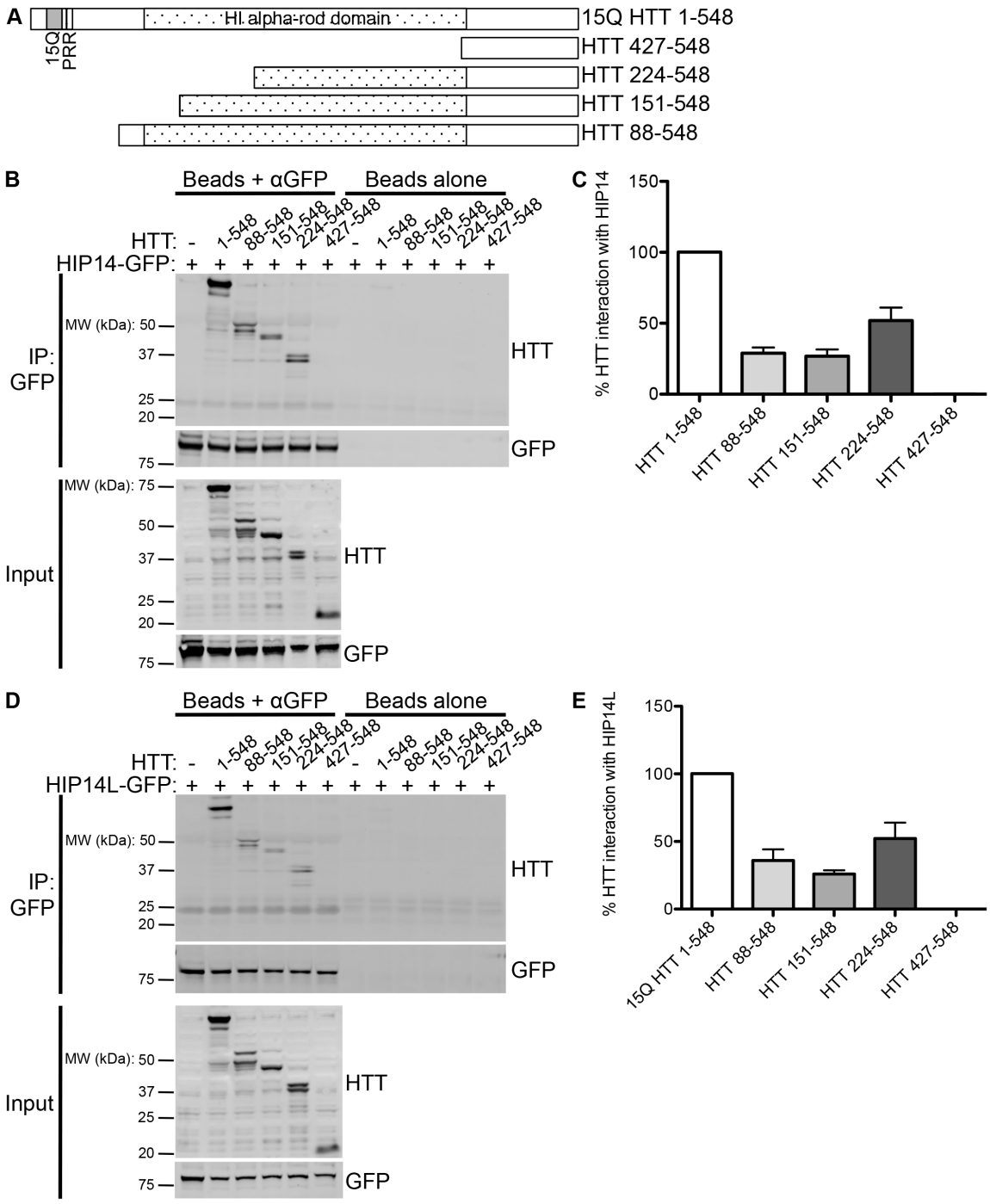

Figure 2.3: HIP14 and HIP14L interaction with N-terminal deletion mutants of HTT 1-548. (A) A diagram of the HTT 1-548 N-terminal deletion mutants used in co-immunoprecipitation experiments with HIP14-GFP and HIP14L-GFP showing the 15Q poly-Q domains, the proline rich region (PRR), and the H1 alpha-rod domain. **(B)** A representative image (top two panels) of the co-immunoprecipitation between these N-terminal deletion mutants and HIP14-GFP where GFP was immunoprecipitated and the resulting blots were probed for HTT

(top panel) and GFP (bottom panel) showing less HTT 88-548, HTT 151-548, and HTT 224-548 co-immunoprecipitated with HIP14-GFP and no HTT 427-548 was co-immunoprecipitated with HIP14. On the right is a beads alone control showing no non-specific binding of the proteins to the beads. The bottom two images show the expression of the HTT deletion mutants (top panel) and of HIP14-GFP (bottom panel). **(C)** Quantification of three co-immunoprecipitation experiments where the % HTT interaction with HIP14 is the indicated HTT band intensity as a percentage of the HIP14-GFP band intensity from the same sample, normalized to 15Q HTT 1-548. **(D)** A representative image (top two panels) of the co-immunoprecipitation between the HTT 1-548 N-terminal deletion mutants and HIP14L-GFP where GFP was immunoprecipitated and the resulting blots were probed for HTT (top panel) and GFP (bottom panel). Less HTT 88-548, HTT 151-548, and HTT 224-548 and no HTT 427-548 was co-immunoprecipitated with HIP14L-GFP. On the right is a beads alone control showing no non-specific binding of the proteins to the beads. The bottom two panels show the expression of the HTT deletion mutants (top panel) and of HIP14L-GFP (bottom panel). **(E)** Quantification of three co-immunoprecipitation experiments where the % HTT interaction with HIP14L-GFP is the indicated HTT band intensity as a percentage of the HIP14L-GFP band intensity from the same sample, normalized to 15Q HTT 1-548.

2.3.3 Deletion of amino acids 257-315 of HTT does not abolish the interaction with HIP14 and HIP14L

One potential mechanism of binding of HIP14 and HIP14L to HTT within amino acids 224-427 is a putatively methylated lysine at K262 within a LKS motif (in human HTT NP_002102). Gao *et al* determined the crystal structure of the HIP14 ankyrin repeat domain and found that it forms a surface aromatic cage that may bind methylated lysines, much like the ankyrin repeat domains of the G9a and G9a-like protein histone lysine methyltransferases (Gao et al., 2009). The K262 of the LKS motif within residues 224-427 of HTT is the only lysine in this region that contains an adjacent serine or threonine like that of the methylated lysine of the histone H3 tail sequence, making it a potential site of methylation (Gao et al., 2009). To determine if this is a potential binding domain, a HTT deletion protein with amino acids 257-315 deleted, including the LKS motif, was generated (Figure 2.4.A). This deletion mutant was transiently co-expressed with HIP14-GFP or HIP14L-GFP in COS-7 cells. Reduced but not abolished interaction of 15Q HTT 1-548Δ257-315 with HIP14-GFP and HIP14L-GFP was observed

(Figure 2.4.B and C for HIP14 and D and E for HIP14L; n=3). These data indicate that the HIP14/HIP14L binding domain in HTT is not within these amino acids.

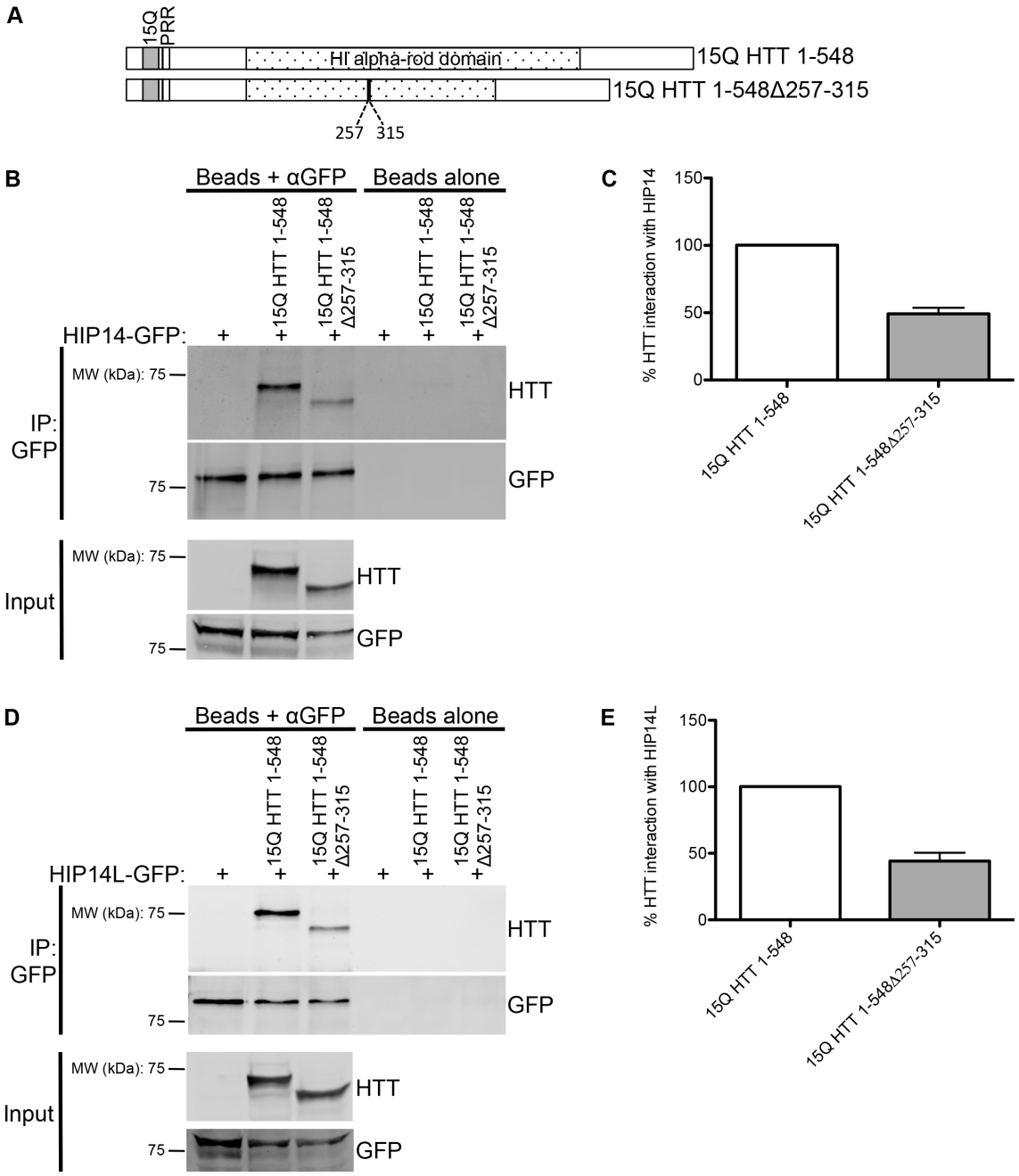

Figure 2.4: HIP14 and HIP14L interaction with 15Q HTT 1-548Δ257-315. (A) A diagram of the 15Q HTT 1-548Δ257-315 deletion mutant used in co-immunoprecipitation experiments with HIP14-GFP and HIP14L-GFP showing the 15Q poly-Q domains, the proline rich region (PRR), and the H1 alpha-rod domain. **(B)** A representative image (top two panels) of the co-immunoprecipitation between 15Q HTT 1-548Δ257-315 deletion mutant and HIP14-GFP where GFP was immunoprecipitated and the resulting blots were

probed for HTT (top panel) and GFP (bottom panel) showing less of the 15Q HTT 1-548Δ257-315 deletion mutant co-immunoprecipitated with HIP14-GFP and compared to 15Q HTT 1-548. On the right is a beads alone (no antibody) control showing no non-specific binding of the proteins to the beads. The bottom two images show the expression of the 15Q HTT 1-548Δ257-315 deletion mutant (top panel) and of HIP14-GFP (bottom panel). **(C)** Quantification of three independent co-immunoprecipitation experiments where the % HTT interaction with HIP14 is the indicated HTT band intensity as a percentage of the HIP14-GFP band intensity from the same sample, normalized to 15Q HTT 1-548. **(D)** A representative image (top two panels) of the co-immunoprecipitation between the 15Q HTT 1-548Δ257-315 deletion mutant and HIP14L-GFP where GFP was immunoprecipitated and the resulting blots were probed for HTT (top panel) and GFP (bottom panel). Less 15Q HTT 1-548Δ257-315 deletion mutant was co-immunoprecipitated with HIP14L-GFP. On the right is a beads alone (no antibody) control showing no non-specific binding of the proteins to the beads. The bottom two panels show the expression of the 15Q HTT 1-548Δ257-315 deletion mutant (top panel) and of HIP14L-GFP (bottom panel). **(E)** Quantification of three independent co-immunoprecipitation experiments where the % HTT interaction with HIP14L-GFP is the indicated HTT band intensity as a percentage of the HIP14L-GFP band intensity from the same sample, normalized to 15Q HTT 1-548.

2.4 DISCUSSION

HIP14 and HIP14L are HTT interacting and palmitoylating proteins and their interaction and palmitoylation of HTT are decreased in the presence of mHTT (Singaraja et al., 2002; Sutton et al., 2013; Yanai et al., 2006). Interestingly, it appears that the interaction between HIP14 and HTT goes beyond that of only an enzyme-substrate interaction and that HTT actually modulates the enzymatic activity of HIP14 (Huang et al., 2011; Singaraja et al., 2011). To further understand and characterize the interactions of HTT with HIP14 and HIP14L it is important to identify the domains of interaction to guide future efforts to target and enhance this interaction to increase enzyme activity and remediate palmitoylation of HTT and their substrates. It is necessary to know if HIP14 and HIP14L interact with the same domain of HTT and, if so, if they compete for binding.

HIP14 was previously shown to interact with HTT 1-548 (Huang et al., 2011). Here the interaction between HIP14 and HIP14L with N- and C-terminal HTT 1-548 deletion mutants was characterized. HTT amino acids 1-548 are

sufficient for the full interaction of HTT with HIP14 and partial interaction is achieved with amino acids 1-427 and 224-548. Full interaction between HTT and HIP14L was achieved with HTT amino acids 1-548 and 1-427 and partial interaction with 224-427. Amino acids 1-224 or 427-548 of HTT were not sufficient for interaction with HIP14 and HIP14L, indicating that a binding domain is likely to exist between amino acids 224-427. To further characterize this binding region a HTT deletion protein with amino acids 257-315 deleted was generated. Reduced but not abolished interaction of 15Q HTT 1-548Δ257-315 with HIP14-GFP and HIP14L-GFP was observed. These data indicate that the HIP14/HIP14L binding domain in HTT is not within these amino acids but that these amino acids are required for the structural integrity of the actual binding domain.

A larger region of HTT, amino acids 1-548, is required to achieve full interaction, possibly to achieve correct folding and structural stability of the binding domain or because other sequences outside of this region also contribute to the interaction. The full 1-548 amino acids are required for structural integrity and the correct interaction conformation of HTT likely requires interactions between 1-548 N- and C-terminal parts of HTT to form a compact structure. Based on these data, it is possible that there is one or two binding sites, one around amino acid 224 and/or another around amino acid 427, and that the biding site(s) are required for full interaction and all of the amino acids from 1-548 are required for the structural integrity and conformation of these binding sites (Figure 2.5; dashed lines).

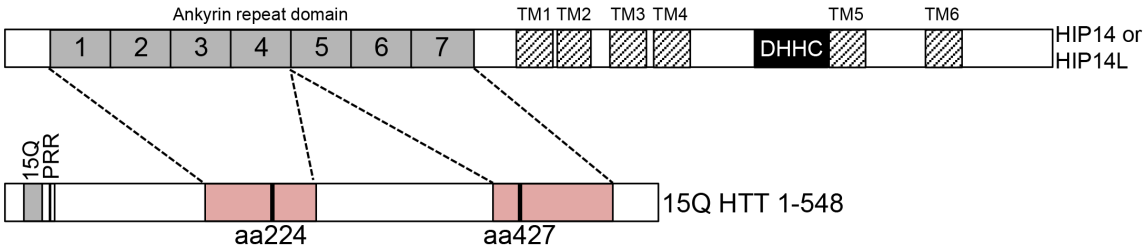

Figure 2.5: A schematic diagram of the two hypothetical binding scenarios of HTT with HIP14 or HIP14L. In both **(A)** and **(B)** for HIP14 or HIP14L the numbered, solid grey boxes are the seven ankyrin repeats that make up the ankyrin repeat domain, the six TMDs are in hatched boxes labeled TM1-TM6, and the DHHC-CR domain is a black box labeled DHHC. **(A)** In this first scenario, the HIP14 and HIP14L HTT binding site (solid pink box) is between amino acids 224-427 and this binding site interacts with the ankyrin repeat domain of HIP14 or HIP14L. **(B)** In an alternate scenario there are two binding sites (solid pink boxes), one between amino acids 1-427 and the other between amino acids 224-548, that both interact with the ankyrin repeat domain.

Interestingly, in the hypothetical 3D structure of HTT proposed by Palidwor *et al*, HTT has 3 alpha-rod domains (H1-3) that fold back on and interact with each other and interact with HTT interacting proteins (Figure 2.1.A) (Palidwor et al., 2009). The two potential binding domains around residues 224 and 427 are contained within a single structural element of HTT, the H1 alpha-rod domain (resides within amino acids 114-431; Figure 2.1.A). It would be logical that the PAT binding domain would be contained within a single structural element such as the H1 domain thus favoring our model that the PAT binding domains are fully contained within this structural element (Figure 2.5) (Palidwor et al., 2009). This is consistent with the data presented here where the full 1-548 HTT protein is required for the correct confirmation of this large structural domain and of the two binding sites contained within.

This study identified two potential binding domains around residues 224 and 427 for the PAT enzymes HIP14 and HIP14L. Further characterization of the interactions of HTT with HIP14 and HIP14L is important, as this interaction is believed to go beyond that of a simple enzyme-substrate interaction where HTT actually modulates their function and facilitates palmitoylation of HIP14 substrates.

A common binding domain in HTT for HIP14 and HIP14L along with the fact that HIP14L's domain structure is virtually identical to HIP14, with all the same domains in the same orientation suggests that HTT may also modulate the enzymatic activity of HIP14L (Young et al., 2012). HTT may modulate the function of these enzymes in several ways. First, HTT is an α–solenoid protein made up of HEAT (Huntingtin, Elongation factor 3, protein phosphatase 2A, TOR1) repeats suitable for its function as a scaffolding protein with many protein-protein interactions (Huang et al., 2011; Li et al., 2006b; Palidwor et al., 2009; Seong et al., 2010; Takano and Gusella, 2002). It is possible that HTT may act as a scaffolding protein to bring substrates into close proximity with HIP14 and HIP14L, acting as an essential linker between PATs and their other substrates. Second, HTT may act as an allosteric activator of HIP14 by affecting the conformational structure of HIP14 thereby allowing substrates to access the DHHC active site (Huang et al., 2011). Third, as HTT has been shown to be involved in trafficking of organelles along the cytoskeleton, interacting with multiple motor and motor-associated proteins, HTT may be important for trafficking HIP14 and/or HIP14L to particular subcellular locations allowing it to interact with and palmitoylate its substrates (Caviston and Holzbaur, 2009; Huang et al., 2011).

As the interactions between HTT and HIP14 or HIP14L are reduced in HD and these PATs are implicated in the pathogenesis of HD, understanding the nature of their interactions with HTT may guide future efforts to target and enhance this interaction to increase enzyme activity and remediate palmitoylation of HTT and its substrates. These data indicate that HIP14 and HIP14L share a binding site, providing evidence that these two PATs may compensate for each other in palmitoylating HTT and may compete for binding to HTT and other substrates. This needs to be considered when taking efforts to increase the interaction between HTT and HIP14 at the risk of decreasing the interaction with the other, which may have detrimental effects. If HTT acts as an allosteric activator of HIP14 and HIP14L, binding of a small HTT peptide, including the two binding sites, may enhance HIP14 and HIP14L activity in the disease state,

which would likely have a beneficial effect by restoring palmitoylation of HTT and other proteins. This would not be possible without knowing which motifs of HTT bind HIP14 and HIP14L and this study brings us much closer to this goal.

3 HUNTINGTIN INTERACTING PROTEINS 14 AND 14-LIKE ARE REQUIRED FOR CHORIOALLANTOIC FUSION DURING EARLY PLACENTAL DEVELOPMENT[3]

3.1 INTRODUCTION

Huntington disease (HD) is an adult-onset, autosomal dominant neurodegenerative disease characterized by motor, cognitive, and psychiatric symptoms. In HD early degeneration of the striatum occurs followed by more widespread degeneration in the later stages of the disease (Roos, 2010; Sturrock and Leavitt, 2010). Most patients with HD have an onset in midlife with death following, on average, 20 years later (Roos, 2010; Sturrock and Leavitt, 2010). HD is caused by a CAG (coding for glutamine, Q) expansion in the first exon of the *HTT* gene, leading to an N-terminal poly-Q expansion in the Huntingtin (HTT) protein (Group, 1993).

The HTT protein undergoes many PTMs, including phosphorylation, SUMOylation, ubiquitination, acetylation, proteolytic cleavage, and palmitoylation. These PTMs modulate the functions of HTT and influence toxicity of mHTT (reviewed in (Ehrnhoefer et al., 2011)). Palmitoylation is the commonly used term for S-acylation, the reversible post-translational addition of long-chain saturated fatty acids to proteins at cysteine residues via a thioester bond. S-acylation is often referred to as palmitoylation because the most abundant lipid substrate in the cell is the 16-carbon fatty acid palmitate (Hallak et al., 1994; Smotrys and Linder, 2004). Palmitoylation is mediated by a family of enzymes called the

---

[3] This chapter has been accepted for publication in *Developmental Biology* (in press at the time of thesis submission). Sanders, S.S., Hou, J., Sutton, L.M., Garside, V.C., Mui, K.K.N., Singaraja, R.R., Hayden, M.R., and Hoodless, P.A. Huntingtin interacting proteins 14 and 14-like are required for chorioallantoic fusion during early placental development. Experimental design, assessments of Mendelian ratios, some imaging of histological staining, palmitoylation assays, and all data analysis by SSS.

DHHC-domain containing palmitoylacyl transferases (DHHC PATs) of which humans have 23 (*ZDHHC1-9* and *11-24*) and mice have 24 (*Zdhhc1-9* and *11-25*) (Ohno et al., 2006). The palmitoylation of HTT and of many other proteins serves to dynamically regulate membrane localization, function, protein-protein interactions, and other PTMs of palmitoyl-proteins (reviewed in (Young et al., 2012)).

Palmitoylation of HTT and other proteins has been previously implicated in the pathogenesis of HD and other neuropsychiatric disorders including AD, schizophrenia, mental retardation, and neuronal cereoid lipofuscinosis (reviewed in (Young et al., 2012)). Palmitoylation of HTT is reduced in the presence of the polyglutamine expansion and further reduction of palmitoylation of mHTT, mediated by a reduction in activity of its PATs, accelerates its aggregation and increases cellular toxicity, whereas increased palmitoylation reduces aggregation (Yanai et al., 2006). HTT interacts with and is palmitoylated primarily by two PATs: the huntingtin interacting proteins 14 and 14-like (HIP14 and HIP14L or ZDHHC17 and 13 respectively) (Huang et al., 2011; Singaraja et al., 2002; Sutton et al., 2013). These two PATs are unique in that they are the only two PATs that have an ankyrin repeat domain. It is this domain that mediates the interaction between HIP14 and HTT (Huang et al., 2011; Ohno et al., 2006). In fact, wtHTT is a modulator of HIP14 activity such that loss of wtHTT or the presence of mHTT leads to decreased HIP14 auto-palmitoylation and reduced palmitoylation of HIP14 substrates (Huang et al., 2011; Wan et al., 2013). Interestingly, mouse models deficient in either *Hip14* (*Hip14*$^{-/-}$) or *Hip14l* (*Hip14l*$^{-/-}$) develop HD-like phenotypes, including predominant striatal degeneration and motor dysfunction, but do not exhibit changes in the palmitoylation of HTT itself (Singaraja et al., 2011; Sutton et al., 2013). It has been suggested that the phenotypes of these two mouse models result from the aberrant palmitoylation of other neuronal substrates rather than of HTT itself (Singaraja et al., 2011; Sutton et al., 2013).

The biological function of HTT palmitoylation and exactly what role the loss of HTT palmitoylation plays in the pathogenesis of HD are unknown. To

answer these questions and to determine if HIP14 and HIP14L are in fact the only two PATs for HTT, the *Hip14*$^{-/-}$ and *Hip14l*$^{-/-}$ mouse models were intercrossed to generate mice deficient for both *Hip14* and *Hip14l* genes. Here we provide the first description of a double PAT deficient mouse model and show that loss of a PAT or multiple PATs results in embryonic lethality in mammals, demonstrating that palmitoylation is a critical factor in early embryonic development.

3.2 MATERIALS AND METHODS

3.2.1 Mouse breeding and embryo dissection

FVB/N *Hip14* gene-trapped mice (*Hip14*$^{-/-}$*;* previously described (Singaraja et al., 2011)), were crossed to FVB/N *Hip14l* gene-trapped mice (*Hip14l*$^{-/-}$*;* previously described (Sutton et al., 2013)) to generate *Hip14*$^{+/-}$*;Hip14l*$^{-/-}$ mice, which were intercrossed to generate all embryos in this study. The University of British Columbia Committee on Animal Care approved all procedures. Previously described FVB/N *Htt*$^{preex1/+}$ mice were intercrossed to generate *Htt*$^{preex1/preex1}$ (*Htt*$^{-/-}$) embryos (Zeitlin et al., 1995).

Timed pregnancies were set up and female mice were examined for plugs every morning for 5 days. Noon of the day the plug was found was considered embryonic day 0.5 (E0.5). Embryos were either fully dissected or left within the yolk sac or within the decidua at various gestational ages (E8.5-12.5) and either immediately imaged and genotyped or fixed for in situ hybridization or histology.

3.2.2 Genotyping

Embryos harvested to determine the stage of embryonic lethality, for gross morphology, for in situ hybridization, or to establish MEFs were genotyped by PCR following quick lysis of the yolk sac, a piece of the yolk sac, or the embryo in the yolk sac. Quick lysis is performed by overnight digestion at 55° with Proteinase K (Life Technologies, Carlsbad, CA, USA) in 40 mM Tris, 50 mM KCl, and 1% Tween-20 followed by inactivation of Proteinase K at 95° for 15 minutes. Breeding mice and cell pellets from mouse embryonic fibroblast (MEF) cell lines

were genotyped as previously described at the *Hip14l* locus to confirm homozygosity (Sutton et al., 2013). All embryos and cell pellets were genotyped by PCR at the *Hip14* locus as previously described (Singaraja et al., 2011). Embryos from $Htt^{+/-}$ intercrosses were genotypes at the Htt^{Preex1} locus as previously described (Zeitlin et al., 1995). All primer sequences are in Table 3.1.

Table 3.1: Sequences of qPCR and genotyping primers and *in situ* hybridization probes.

qPCR primers:		qPCR primers:	
m*Hip14* rt2f_F	TGGTGTGTCTCTTACTGGGG	*Zdhhc9*_R	CTGCTTCATCTGGTAGTGCTC
m*Hip14* rt2f_R	CATCCACGGGGAGCATGTG	*Zdhhc12*_F2	TCGGCTGAGGAAGAGGAAG
*Hip14l*_qPCR_F	TGGGTGGTGACCTAAATTCAACT	*Zdhhc12*_R2	CTCTGGCTTTTAGGCACAAC
*HIP14l*_qPCR_R	GCACCGTGCTGGAGCAATA	*Zdhhc15*_F2	ATCTAATCAAGCCAGACCGC
*Zdhhc1*_F	CTGCAACAAACCCTCCAACAA	*Zdhhc15*_R2	CATGGGCAGTGATGGTCC
*Zdhhc1*_R	ATCACCGCGAAGAAGAGGTAG	*Zdhhc16*_F	TGGCGTTATGGCAAGGTTTG
*Zdhhc2*_F	TCCCGGTGGTGTTCATCAG	*Zdhhc16*_R	CAGCGGATCACATTGTCCAC
*Zdhhc2*_R	TGGCGTAGGCGTAGTAGGAC	*Zdhhc18*_F2	GCCCTGGAGAAGCAGATC
*Zdhhc3*_F	CGGGAGCCATGTGGTTTATCC	*Zdhhc18*_R2	CGGTATGTGGAGCTGCCTGTGTTAT
*Zdhhc3*_R	ACTCCGCATAGAGGACCAGAA	*Zdhhc20*_F2	GTGGCTGCAACAGTTTTAGAG
*Zdhhc4*_F	GTGTTGTCCTGATCTGCATCTT	*Zdhhc20*_R2	AAAAGGAACAGTACGTGGAACT
*Zdhhc4*_R	ACTGCGGGATTACCCTGGA	*Zdhhc21*_F2	TCCCTACCACTTTGCCAATC
*Zdhhc5*_F	CAAACCCAGCAAGTATGTACCG	*Zdhhc21*_R2	CTGTAACGCATTTCCAGCATG
*Zdhhc5*_R	CTGGACACGTAAAGGCAAAGA	*Zdhhc24*_F2	CTTTGCCTGGAGATGGGATC
*Zdhhc6*_F3	GACCAGTACAGCCTCACAATAG	*Zdhhc24*_R2	CCTGTTCAGTTCTGGCTCTAC
*Zdhhc6*_R3	GCAGGCACCATTGTAATCTTC	*Actb*_F	ACGGCCAGGTCATCACTATTG
*Zdhhc7*_F2	AGGGTGTTTCAGGGAATCATG	*Actb*_R	CAAGAAGGAAGGCTGGAAAAGA
*Zdhhc7*_R2	AGGATGCTGAGTCGTAATTGTC	*Rpl13a*_F	GGAGGAGAAACGGAAGGAAAAG
*Zdhhc8*_F2	ATGTATAAGTTCCGGCCAGC	*Rpl13a*_R	CCGTAACCTCAAGATCTGCTTCTT
*Zdhhc8*_R2	TGCCAGAGTAAGGGAGTCAG	*Hprt1*_F	CGTCGTGATTAGCGATGATGA
*Zdhhc9*_F	TTCTTTGCCTTCGAGTGTCG	*Hprt1*_R	TCCAAATCCTCGGCATAATGA
Hip14l genotyping primers:		*Hip14* genotyping primers:	
*Hip14l*_F	CTCCCAGTCTTGGTCTTCACTAC	*Hip14* Int5_F	CCGTCTTAGTGCCATTTGTTCGTC
Hip14l pGT01xr_R	GAACTTCCCTAGGCCTATCAC	*Hip14* βGeo5_R	GGTGCCGGAAACCAGGCAAAG
*Hip14l*_R	GAGCAAGCGCATCATCAGGATC	*Hip14* Int5_R	CATGTGTCGGGATGGCTGTGAAAAG
Hdhpreex1 genotyping primers:		*Hdhpreex1* genotyping primers:	
Htt^{Preex1}_F	CATTCATTGCCTTGCTGCTAAG	Htt^{Preex1} Neo_F	GATCGGCCATTGAACAAGATG
Htt^{Preex1}_R	CTGAAACGACTTGAGCGACTC	Htt^{Preex1} Neo_R	AGAGCAGCCGATTGTCTGTTG
Primers for generation of *In situ* hybridization probes:			
*Hip14*_F XhoI	GTGCTATGCTCGAGACTTGGCTGCTCAGTTCGGACATA		
*Hip14*_R EcoRI	GTGCTATGGAATTCTGGCTTCCGAATCAAGCAGGTACT		
*Hip14l*_F XhoI	GTGCTATGCTCGAGGCCTCTTAAAGCAAAGCAGGCACA		
*Hip14l*_R EcoRI	GTGCTATGGAATTCAACAGGCCATCTTTCTGGGTCTGA		
*Vcam1*_F XhoI	GTGCTATGCTCGAGACATCCCTCCACAAGGCTTCAAGA		
*Vcam1*_R EcoRI	GTGCTATGGAATTCTCACTTGAGCAGGTCAGGTTCACA		
*Itga4*_F XhoI	GTGCTATGCTCGAGATAGGGAAGCAAACAGGGAAGGCT		
*Itga4*_R EcoRI	GTGCTATGGAATTCACCAGGCAGGAAAGGTGGTTAAGA		

DNA was extracted from paraffin embedded embryos as previously described (Gilbert et al., 2007). Briefly, the remaining piece of embryos following paraffin embedding and sectioning were cut out of the paraffin block, warmed at 55° until the paraffin melted, left in xylene for 24 hours, washed two times with xylene, washed 3 times with 100% ethanol; sequentially rehydrated with 95%,

70% and 50% ethanol, and then carefully dissected out of the decidua. DNA was extracted from embryonic tissue using the QIAamp DNA Micro Kit (Qiagen, Limburg, Netherlands) according to the protocol with the following additions: a 15 minute 98° incubation in buffer ATL, prior to adding Proteinase K, to reverse cross-linking of proteins to nucleic acids and a 96 hour digestion at 55° with Proteinase K.

3.2.3 Histology and *in situ* hybridization (ISH)

Embryos in decidua were paraffin embedded, sectioned at 5 uM, and stained with hematoxylin and eosin (H&E) by Wax-it Histology Services (Vancouver, BC, Canada; www.waxitinc.com).

Whole mount ISH, cryo-sectioning after whole mount ISH, section ISH, and probe labeling were performed according to standard protocols that were previously described (McKnight et al., 2007). Probe templates were generated by RT-PCR amplification from total RNA isolated from E8.5 mouse embryos, with an average size of 400-800 bp, followed by sequence verification. All PCR products were digested with XhoI and EcoRI and ligated into pBluescriptII digested with the same enzymes. The subsequent probe labeling was performed as previously described (McKnight et al., 2007). At least three embryos were examined for each probe at each time point. The primer sequences for generating the ISH probes are included in Table 3.1.

3.2.4 Generation of mouse embryonic fibroblasts

Mouse embryonic fibroblasts (MEFs) were generated from E9.5 embryos as previously described (Shiota et al., 2006). Briefly, embryos were washed with PBS and the heads were removed. The rest of the embryo was disaggregated by passage slowly once through a 28-gauge needle into DMEM with 10% fetal bovine serum, penicillin/streptomycin (1000 Units/mL Penicillin and 1000 ug/mL streptomycin), non-essential amino acids, 1 mM sodium pyruvate, 10 uM β-mercaptoethanol, and 2 mM L-glutamine in a single well of a 48-well plate (all media and additives from Life Technologies, Carlsbad, CA, USA; β-mercaptoethanol from Sigma-Aldrich, St. Louis, MO, USA). Cells were

maintained until confluent (1-2 days) at 37° in 5% CO_2 at which point they were passaged by trypsinization and replated into a 24-well plate (passage one). At passage three cells were immortalized by transfection with pSV3-neo (SV40 immortalization construct; ATCC) using X-tremeGENE 9 DNA transfection reagent (Roche, Basel, Switzerland) according to the manufacturer's instructions. 48 hours later cells were passaged and 1 mg/mL G418 (Thermo Fisher Scientific, Waltham, MA, USA) was added to the culture media to select for SV40 immortalization.

3.2.5 Acyl-biotin exchange palmitoylation assay and western blotting analysis

ABE palmitoylation assays were performed on frozen cell pellets from WT and *Hip14*$^{-/-}$*;Hip14l*$^{-/-}$ MEFs as previously described (Drisdel and Green, 2004; Huang et al., 2009). Briefly, cell pellets from three wild type and two *Hip14*$^{-/-}$*;Hip14l*$^{-/-}$ cell lines from three separate passage numbers were harvested and immediately frozen and stored at -80° until genotyping results were obtained. Frozen cell pellets were then homogenized on ice in 500 uL lysis buffer (150 mM NaCl, 50 mM Tris, 5 mM ethylenediaminetetraacetic acid, 0.1% SDS, 1% triton X-100, pH 7.4) with 100 mM NEM (Sigma-Aldrich, St. Louis, MO, USA). Cell homogenates were sonicated for 5 seconds at 20% power to shear DNA and the insoluble material was removed by centrifugation at 14000 revolutions per minute for 15 minutes. HTT was immunoprecipitated from cell lysates by overnight incubation with Protein G Dynabeads® (Life Technologies, Carlsbad, CA, USA) and in-house anti-HTT antibody (BKP1). Beads were then washed and split into two and treated with neutral pH hydroxylamine (HAM+; Sigma-Aldrich, St. Louis, MO, USA) in lysis buffer or just lysis buffer (HAM-) for two hours at room temperature. Following HAM treatment beads were washed and treated with 2.5 uM EZ-Link BMCC-Biotin (Thermo Fisher Scientific, Waltham, MA, USA) in pH 6.2 lysis buffer for one hour at 4°. At the end of the BMCC-Biotin treatment beads were washed and then heated at 70° with 1X NuPAGE LDS Sample Buffer (Life Technologies, Carlsbad, CA, USA) and 50 uM fresh dithiothreitol (Sigma-Aldrich, St. Louis, MO, USA) to elute HTT protein.

Supernatants were run on NuPAGE® Novex® 3-8% Tris-Acetate gels (Life Technologies, Carlsbad, CA, USA), transferred to nitrocellulose, and blocked with 5% bovine serum albumin (BSA; Sigma-Aldrich, St. Louis, MO, USA) in Phosphate Buffered Saline (PBS). Primary antibody dilutions of HTT mouse monoclonal antibody (MAB2166, EMD Millipore, Billerica, MA, USA) in 5%BSA PBST (5% Tween-20) were applied to the immunoblots at 4°C overnight. Dilutions of IRDye 800CW goat anti-Mouse (610-131-121; Rockland, Boyertown, PA USA; 1: 2500) secondary antibody and Alexa Fluor® 680 conjugated streptavidin (S-32358, Molecular Probes, Life Technologies, Carlsbad, CA, USA; 1:10000) were applied in 5% BSA PBST for an hour. Fluorescence was scanned and quantified with Odyssey Infrared Imaging system (Li-COR Bioscience; Lincoln, NE, USA) and quantified using the Li-COR software. Palmitoylation of HTT in *Hip14*$^{-/-}$*;Hip14l*$^{-/-}$ MEFs was analyzed as a ratio of HAM+ palmitoylation signal to total immunoprecipitated HTT protein signal and normalized to the wild type cells control condition. Data were analyzed using the Student's t-test. Error bars are in standard error of mean.

3.2.6 Quantitative real time PCR

Total RNA was isolated from -80ºC frozen WT and *Hip14*$^{-/-}$*;Hip14l*$^{-/-}$ MEFs cell pellets using the RNeasy mini kit (Qiagen, Venio, Limburg, Netherlands). RNA was treated with DNAse I (Life Technologies, Carlsbad, CA, USA) to remove residual genomic DNA. cDNA was prepared from 1 µg total RNA using SuperScript® III First-Strand Synthesis System (Life Technologies, Carlsbad, CA, USA). Quantitative RT-PCR (qPCR) on the mouse *Zdhhc* genes (*Hip14, Hip14l* and *Zdhhc1-9*, *12, 15, 16, 18, 20, 21,* and *24*) was performed using Power SYBR Green PCR master mix (Applied Biosystems, Life Technologies, Carlsbad, CA, USA) in ABI 7500 Fast Real-Time PCR system (Applied Biosystems, Life Technologies, Carlsbad, CA, USA) under default condition. Each sample was run in triplicate. Expression levels for mRNA were normalized to a normalization factor calculated from the geometric average of endogenous levels of three reference genes: beta-actin (*Actb*), hypoxanthine phsphoribosyl-transferase 1 (*Hprt1*)*,* and 60S ribosomal protein L13a (*Rpl13a*). All primer sequences are

shown in Table 3.1. Data were analyzed using the Student's t-test. Error bars are in standard error of mean.

3.3 RESULTS

3.3.1 Loss of both *Hip14* and *Hip14l* leads to early embryonic lethality

To generate mice deficient for both *Hip14* and *Hip14l, Hip14*$^{-/-}$ mice were crossed with *Hip14l*$^{-/-}$ mice to generate *Hip14*$^{+/-}$*;Hip14l*$^{-/-}$ mice, which were intercrossed to generate all embryos in this study (*Hip14*$^{+/-}$*;Hip14l*$^{-/-}$ x *Hip14*$^{+/-}$*;Hip14l*$^{-/-}$) (Singaraja et al., 2011; Sutton et al., 2013). No *Hip14*$^{-/-}$*;Hip14l*$^{-/-}$ were observed upon genotyping mice of weaning age (Table 3.2; p=3.90E^{-17}; N=218). These data indicate that the mice of this genotype were dying during embryogenesis or shortly following birth.

Table 3.2: Genotypes of offspring from *Hip14*$^{+/-}$;*Hip14l*$^{-/-}$ intercrosses.

		Hip14$^{+/+}$; *Hip14l*$^{-/-}$	*Hip14*$^{+/-}$; *Hip14*$^{-/-}$	*Hip14*$^{-/-}$; *Hip14l*$^{-/-}$	Total (alive)	$\chi 2$ *p* value
E8.5	Observed	30	61	33	124	0.92
	Expected	31	62	31		
E9.5	Observed	52	109	57	218	0.88
	Expected	55	108	55		
E10.5	Observed	16	40	6	62	0.01
	Expected	16	30	16		
E11.5	Observed	20 (1)	27 (3)	0 (8)	47	1.22E-04
	Expected	12	23	12		
E12.5	Observed	17	26	0 (10)	43	4.39E-04
	Expected	11	21	11		
Weaning	Observed	65	153	0	218	3.90E-17
	Expected	55	108	55		

*The number of progeny is shown with dead or reabsorbing embryos in brackets

To determine when the *Hip14*$^{-/-}$;*Hip14l*$^{-/-}$ mice were dying, embryos from at least three litters per time point were harvested from embryonic days 8.5 to 12.5 *in utero* (E8.5 to E12.5) timed pregnancies. No changes in the expected Mendelian ratios of genotypes were observed at E8.5 or E9.5 (Table 3.2; p=0.92 and 0.88, respectively; N= 124 and 218, respectively). However, at E10.5 there was a significant decrease in the number of *Hip14*$^{-/-}$;*Hip14l*$^{-/-}$ embryos recovered (Table 3.2; p=0.01; N=62). At E11.5 no live embryos were recovered and eight dead or reabsorbing *Hip14*$^{-/-}$;*Hip14l*$^{-/-}$ embryos were recovered (Table 3.2; p=1.22E^{-04}; N=47). Again at E12.5 only dead or reabsorbing *Hip14*$^{-/-}$;*Hip14l*$^{-/-}$ embryos were recovered (Table 3.2; p=4.39E^{-04}; N=43). These data indicate that the stage of embryonic lethality in the *Hip14*$^{-/-}$;*Hip14l*$^{-/-}$ embryos is between E10 and E11 *in utero*.

3.3.2 *Hip14* and *Hip14l* are widely expressed during embryonic development

Since *Hip14*$^{-/-}$;*Hip14l*$^{-/-}$ mice are embryonic lethal between days E10-11, we sought to determine the expression pattern of *Hip14* and *Hip14l* just prior to this time point. *In situ* hybridizations (ISH) using probes against *Hip14* or *Hip14l* mRNA in whole mount embryos were performed using WT embryos at E7.5, E8.5, and E9.5. With the exception of a slightly lower level of expression of *Hip14* in the heart at E9.5 (asterisk in Figure 3.1F) both genes were expressed in the entire embryo at all three time points tested as observed in whole mount embryos and in the indicated sections (Figure 3.1). To determine the pattern of expression of *Hip14* and *Hip14l* in the placenta, ISH was performed using the probes mentioned above in sectioned E8.5 decidua. *Hip14* and *Hip14l* are expressed in the chorion (arrow) and allantois (arrowhead) of the E8.5 developing placenta (Figure 3.1 G and O, respectively).

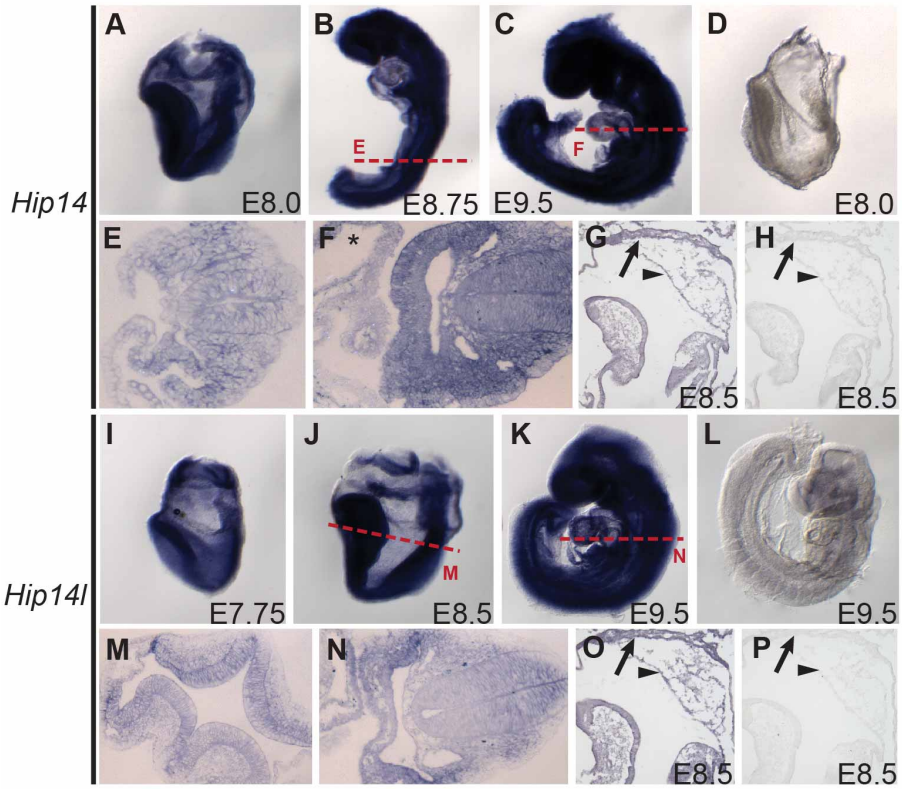

Figure 3.1: Expression of *Hip14* and *Hip14l* mRNA in the whole embryo at E8.0, E8.5, and E9.5. Expression of *Hip14* in E8.0 (**A**), E8.75 (**B**), E9.5 (**C**) whole mount embryos by *in situ* hybridization using an antisense probe against *Hip14* mRNA. The indicated sections (red dotted lines) through the E8.75 and E9.5 embryos are shown in **E** and **F**, respectively. Expression of *Hip14* in the placenta at E8.5 is shown in **G**, where desidua were embedded and sectioned prior *in situ* hybridization, with the chorion indicated by an arrow and the allantois indicated by an arrowhead. The negative control staining using the sense version of the *Hip14* probe is shown in **D** and **H**. *Hip14l* mRNA expression in E7.75 (**I**), E8.5 (**J**), E9.5 (**K**) embryos by *in situ* hybridization is shown. The indicated sections (red dotted lines) through the E8.5 and E9.5 embryos are shown in **M** and **N**, respectively. Expression of *Hip14l* in the placenta at E8.5 is shown in **G**, where desidua were embedded and sectioned prior *in situ* hybridization, with the chorion indicated by an arrow and the allantois indicated by an arrowhead. *Hip14l* sense probe negative control staining is shown in **L** and **P**.

3.3.3 Chorioallantoic fusion is abrogated in *Hip14$^{-/-}$;Hip14l$^{-/-}$* embryos

To determine the cause of embryonic lethality in the *Hip14$^{-/-}$;Hip14l$^{-/-}$* embryos, the gross morphology was examined in embryos from five E8.5-E9.5 litters. A total of 16 *Hip14$^{-/-}$;Hip14l$^{-/-}$* embryos were obtained from these five litters. In 11 of the 16 (69%) *Hip14$^{-/-}$;Hip14l$^{-/-}$* embryos chorioallantoic fusion was observed to have completely failed (Figure 3.2F, G and H) and in the remaining incomplete chorioallantoic fusion was evident (Figure 3.2D, E, and I). Chorioallantoic fusion occurs at E8.5 when the allantoic mesoderm attaches to the chorionic mesothelium to ultimately form the placenta (Cross et al., 2003; Inman and Downs, 2007). In the former case, where chorioallantoic fusion had failed, the allantois had grown in size appropriately but failed to make contact with the chorionic mesothelium and formed a balloon-like structure (Figure 3.2F, G, and H). In addition, the allantois was observed to ectopically fuse to the yolk sac in some embryos such as in Figure 3.2G and H (arrow in H). In embryos in which incomplete chorioallantoic fusion occurred, the allantois appeared to make contact with the chorionic mesothelium but did not form the appropriate funnel shape as in the control embryos. Although the allantois in these mutants suggests that cavitation is occurring, it formed a balloon-like shape, indicating incomplete fusion (Figure 3.2C versus 2I). This incomplete or failed chorioallantoic fusion in the *Hip14$^{-/-}$;Hip14l$^{-/-}$* embryos is likely the cause of the embryonic lethality observed as the placenta, in turn, fails to develop and the embryo fails to receive sufficient nutrition. In embryos past this stage of development, the development of the embryo was delayed.

Two variations on the phenotype of the embryo were also observed: a severe and a mild phenotype (Figure 3.2D-F and G-I, respectively). In the severe phenotype the embryos exhibit growth retardation as early as E8.5, do not turn properly, and are disorganized (Figure 3.2D-F). This phenotype was observed in 14 out of 16 (87.5%) *Hip14$^{-/-}$;Hip14l$^{-/-}$* embryos and 10 of these had failed chorioallantoic fusion. In those *Hip14$^{-/-}$;Hip14l$^{-/-}$* embryos with a severe phenotype, the amniotic membrane was small and tight possibly restricting the growth of the embryo along the anterior-posterior axis to the point that by E10.5

the embryos were severely contorted (Figure 3.2D-F). The mild phenotype was observed in two of the 16 *Hip14*$^{-/-}$;*Hip14l*$^{-/-}$ embryos (12.5%; Fig. G-I), in which, the growth of the embryo was not significantly delayed. In one, the chorioallantoic fusion failed (Figure 3.2G-H) and in the other there was incomplete chorioallantoic fusion (Figure 3.2I).

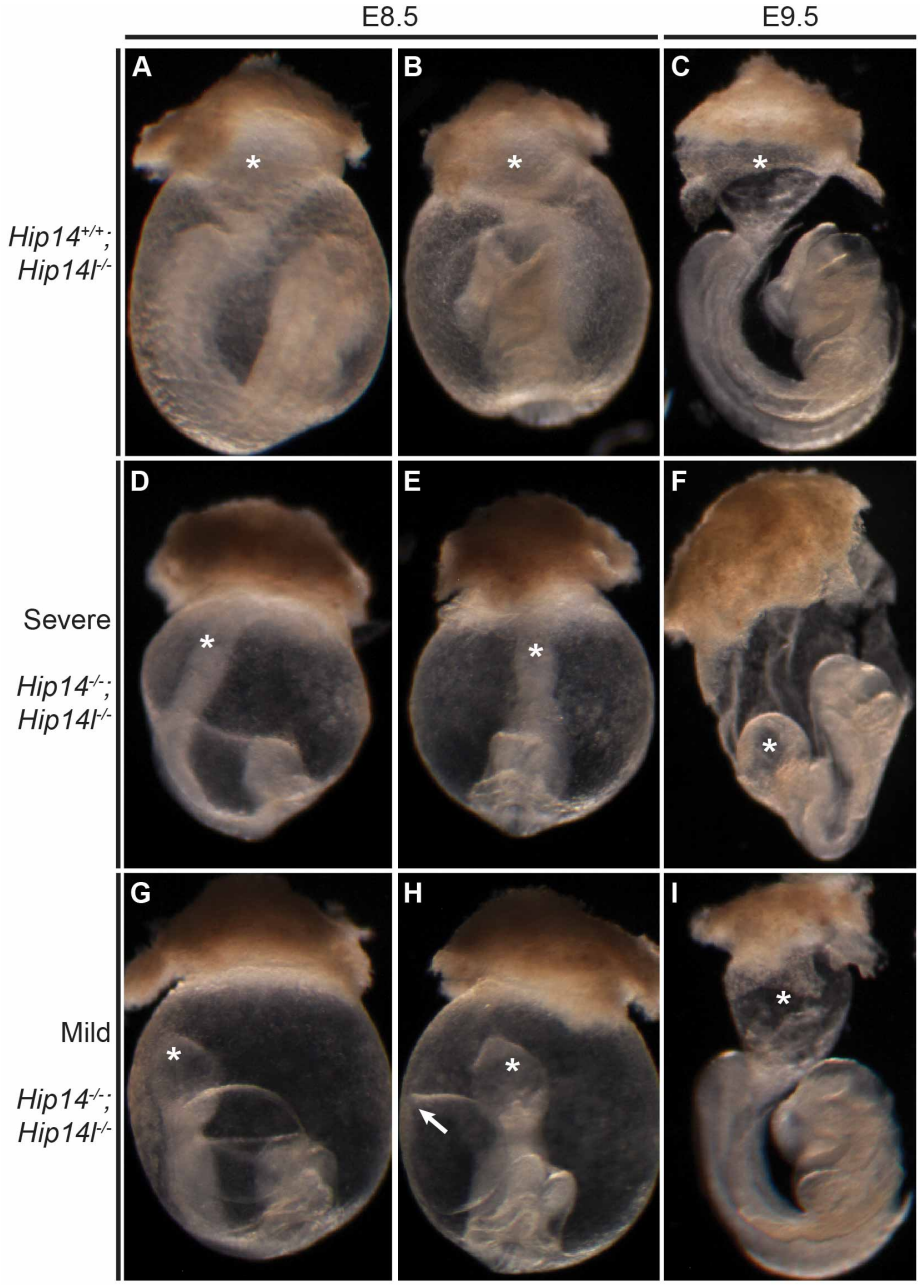

Figure 3.2: Gross morphology of *Hip14*$^{-/-}$;*Hip14l*$^{-/-}$ embryos. Images of control *Hip14*$^{+/+}$;*Hip14l*$^{-/-}$ embryos at E8.5 (**A** and **B**) within the yolk sac and E9.5 (**C**) removed from the yolk sac with the allantois and chorion still attached are shown with the allantois indicated by an asterisk (***** denotes allantois in all images of fig). The lateral view of the E8.5 embryo is shown in (**A**) and the front view is shown in (**B**). The severe phenotype of the *Hip14*$^{-/-}$;*Hip14l*$^{-/-}$ embryos is shown in the middle three panels with the lateral and front views of the E8.5 embryo in (**D**) and (**E**), respectively, and the E9.5 embryo without yolk sac in (**F**). The mild phenotype of the E8.5 *Hip14*$^{-/-}$;*Hip14l*$^{-/-}$ embryos is shown in (**G**) and (**H**), lateral and front views respectively and the E9.5 embryo is shown in (**I**).

More detailed examination of the gross morphology of the *Hip14*$^{-/-}$;*Hip14l*$^{-/-}$ embryos was performed by H&E staining of paraffin embedded and sectioned embryos. Embryos at E9.5 were sectioned within the yolk sac with the chorion still attached and embryos at E8.5 were dissected and sectioned within the decidua in order to maintain structural integrity of the embryo and extraembryonic tissues. In the control embryos at E8.5, the allantois (indicated by arrowheads) fused normally to the chorion (indicated by an arrow in the inset) and the chorionic mesothelium had appropriately formed a bilayer (Figure 3.2A and B). However, in the *Hip14*$^{-/-}$;*Hip14l*$^{-/-}$ embryos, the allantois (arrowhead and inset) had grown towards the chorion (arrow and inset) but did not fuse with the chorionic mesothelium (Figure 3.2D-F). The chorionic mesothelium in the *Hip14*$^{-/-}$;*Hip14l*$^{-/-}$ embryo was also thickened and disorganized and did not form the appropriate cell bilayer (Figure 3.2E).

An example of a severe phenotype of the *Hip14*$^{-/-}$;*Hip14l*$^{-/-}$ embryos at E9.5 was sectioned and H&E stained (Figure 3.2G-I). An image of the embryo pre-sectioning is shown in Figure 3.2G wherein the balloon-like shape of the allantois and the ectopic fusion of the allantois to the yolk sac can be observed. The embryo was distorted and disorganized (Figure 3.2H) and the ectopic fusion of the allantois (arrowhead) to the yolk sac can clearly be seen (Figure 3.2H and the inset I). In addition, abnormal folding of the yolk sac visceral endoderm was also observed (Figure 3.2H).

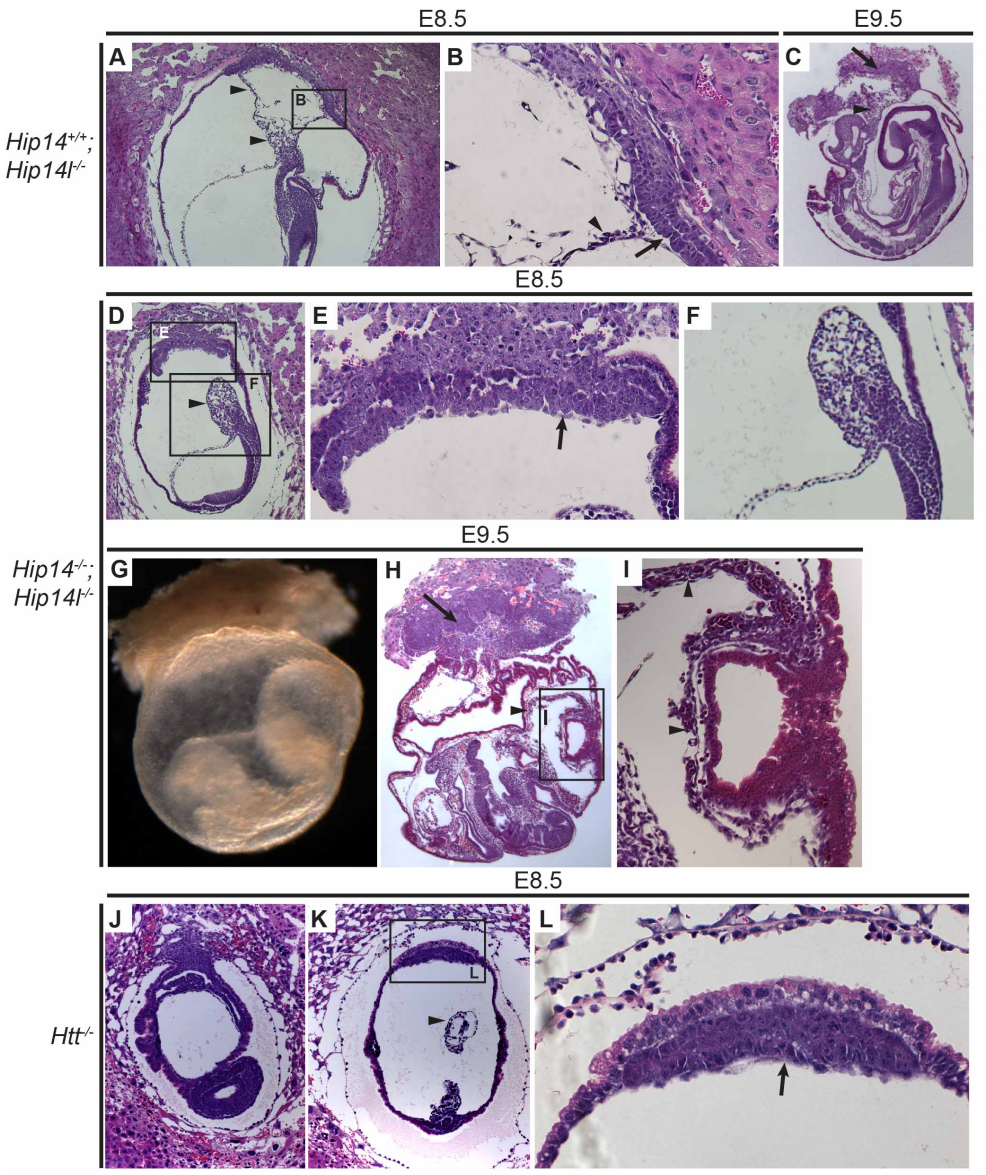

Figure 3.3: Histology of *Hip14*$^{-/-}$;*Hip14l*$^{-/-}$ and *Htt*$^{-/-}$ embryos. An H&E stained section of a control E8.5 embryo (*Hip14*$^{+/+}$;*Hip14l*$^{-/-}$) is shown in (**A**) with the inset in (**B**) and an E9.5 embryo in (**C**). Arrowheads indicate the allantois and arrows indicate the chorion. An H&E stained section of an E8.5 *Hip14*$^{-/-}$;*Hip14l*$^{-/-}$ embryo is shown in (**D**) with the inset in (**E**) and an E9.5 embryo in (**F**), the inset in G, and the pre-sectioning whole mount of the same embryo in H. H&E stained sections of two different E8.5 *Htt*$^{-/-}$ embryos are shown in (**I**) and (**J**), with the inset of (**J**) shown in (**K**).

3.3.4 No change in expression of cell adhesion molecules in *Hip14*$^{-/-}$ *;Hip14l*$^{-/-}$ embryos

The receptor ligand complex between the adhesion molecules, VCAM1 and α4-integrin (ITGA4) mediate the union of the allantois and the chorion and embryos deficient in either of these genes partially phenocopy the *Hip14*$^{-/-}$*;Hip14l*$^{-/-}$ embryos (Cross et al., 2003; Inman and Downs, 2007). *Itga4* is normally expressed on the basal surface of the chorion (Yang et al., 1995), while *Vcam1* is expressed in the allantois (Gurtner et al., 1995; Kwee et al., 1995). To determine the molecular basis of the chorioallantoic fusion defect in the *Hip14*$^{-/-}$*;Hip14l*$^{-/-}$ embryos, the expression of cell adhesion molecules, required for chorioallantoic fusion, was assessed by *in situ* hybridization in control (*Hip14*$^{+/+}$*;Hip14l*$^{-/-}$) and *Hip14*$^{-/-}$*;Hip14l*$^{-/-}$ embryos. There was no change in expression of either of these genes in the *Hip14*$^{-/-}$*;Hip14l*$^{-/-}$ embryos compared to control embryos (Figure 3.4). *Itg4a* is appropriately expressed on the basal surface of the chorion (arrows in Figure 3.4A and E) and *Vcam1* is still expressed in the allantois (arrowheads of Figure 3.4B and F and sections in Figure 3.4C and G). These data indicate that the defect is not due to altered expression of either of these two genes. In addition, the mRNA expression of the hedgehog signaling genes *Shh*, *Foxa2*, *Ptch1*, and *Isl1*, and the left/right patterning gene *Pitx2* were unchanged in *Hip14*$^{-/-}$*;Hip14l*$^{-/-}$ embryos compared to control embryos suggesting that the embryo proper is appropriately patterned (data not shown).

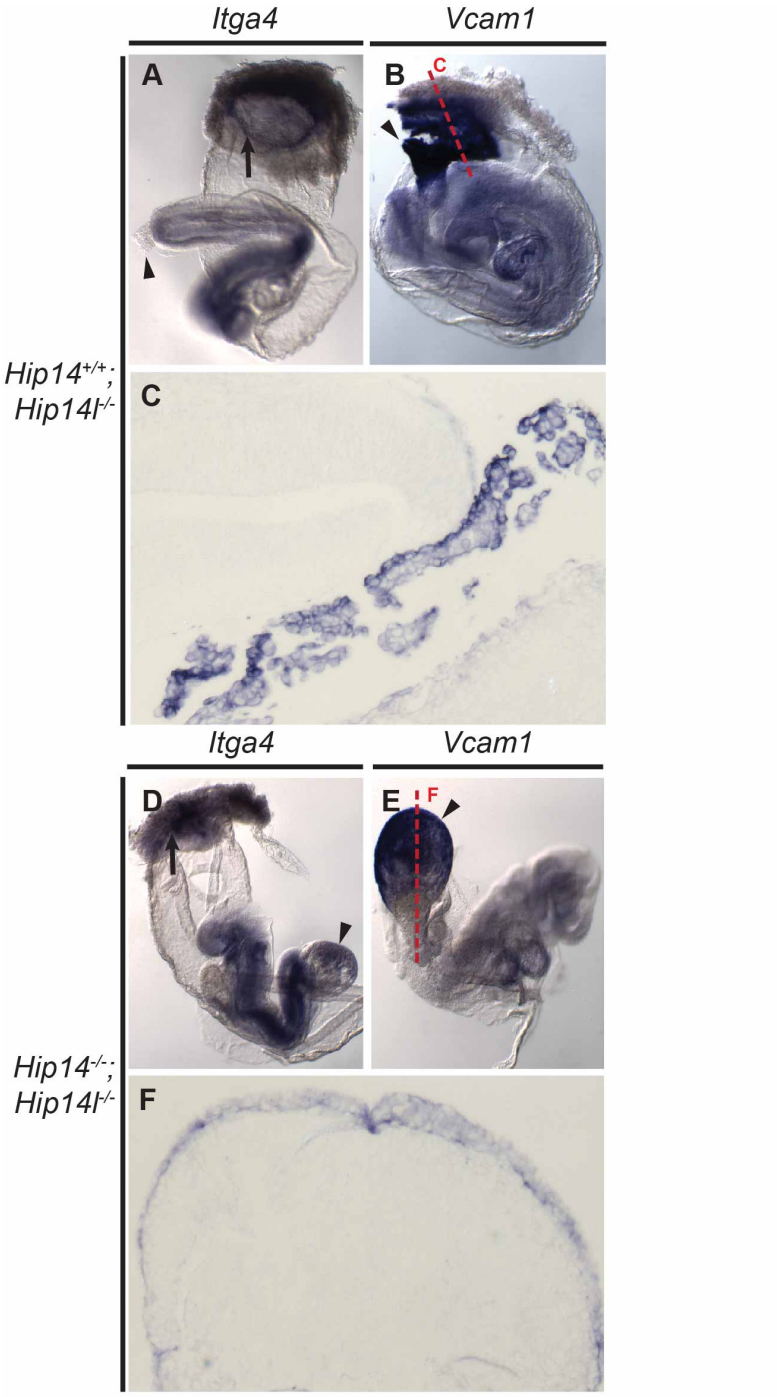

Figure. 4.4: Expression of *Itga4* and *Vcam1* in *Hip14*$^{-/-}$;*Hip14l*$^{-/-}$ whole embryos. Expression of *Itga4* is shown in a control embryo (*Hip14*$^{+/+}$;*Hip14l*$^{-/-}$) in (**A**) and an *Hip14*$^{-/-}$;*Hip14l*$^{-/-}$ in (**D**) with the allantois indicated by an arrowhead and the chorion indicated by an arrow. Expression of *Vcam1* is shown in a control embryo (*Hip14*$^{+/+}$;*Hip14l*$^{-/-}$) in (**B**) and an *Hip14*$^{-/-}$;*Hip14l*$^{-/-}$ in (**E**) with the indicated section (red dotted line) shown in (**C**) and (**F**), respectively.

3.3.5 *Hip14*$^{-/-}$;*Hip14l*$^{-/-}$ embryos have morphological similarities to embryonic lethal *Htt* deficient embryos

The phenotype of the *Hip14*$^{-/-}$;*Hip14l*$^{-/-}$ embryos was reminiscent of that of the three *Htt* deficient mouse lines (Table 3.3) that are also embryonic lethal (Duyao et al., 1995; Nasir et al., 1995; Zeitlin et al., 1995). These three lines primarily vary in their targeting strategy and also have subtle differences in phenotypes. The phenotype of the *Hip14*$^{-/-}$;*Hip14l*$^{-/-}$ embryos were particularly reminiscent of the *Htt*^{Preex1} (*Htt*$^{-/-}$) mice, which have a targeted deletion of the *Htt* promotor and exon 1. These mice are embryonic lethal between E8.5-10, slightly later than the other two *Htt* deficient lines, and have folded and disorganized extraembryonic membranes (Zeitlin et al., 1995), similar to that observed in the *Hip14*$^{-/-}$;*Hip14l*$^{-/-}$ embryos. The similarity in phenotypes between the *Hip14*$^{-/-}$;*Hip14l*$^{-/-}$ and the *Htt*$^{-/-}$ embryos (Zeitlin et al., 1995) and the fact that HIP14 and HIP14L are the two primary PATs for HTT (Huang et al., 2011) suggests that the lethality may have a common origin. Consequently, the morphology of the *Htt*^{Preex1} deficient embryos was examined by histology and compared to that of the *Hip14*$^{-/-}$;*Hip14l*$^{-/-}$ embryos (Figure 3.2 J-L).

Table 3.3: Comparison of the phenotype of *Hip14*$^{-/-}$;*Hip14l*$^{-/-}$ embryos to that of *Hdh*$^{-/-}$ embryos.

	Hdh^{ex5} (Nasir et al., 1995)	*Hdh*$^{ex4-5}$ (Duyao et al., 1995)	*Hdh*^{Preex1} (Zeitlin et al., 1995)	*Hip14-/-;Hip14l-/-*
Stage of lethality	E7.5-8.5	E7.5-8.5	E8.5-10.5	E10-11
Extraembryonic membranes	Present but reduced in size	Reduced in size but grossly normal	Folded and disorganized	Failed A-C union, folded and disorganized

Two phenotypes of *Htt*$^{-/-}$ embryos were observed. The first closely resembled embryos previously described by Zeitlin *et al* in which gastrulation had occurred but the embryo did not develop normally along the distal-proximal axis (Zeitlin et al., 1995) (Figure 3.2J). In these embryos, folding of the yolk sac visceral endoderm and a bulb shaped allantois was also observed (Figure 3.2I

and data not shown). In the second phenotype of the *Htt*$^{-/-}$ embryos (shown in Figure 3.2K and L) the germ layers had formed but no organs or other structures had developed. In these embryos, a bulb shaped allantois and a thickened and disorganized chorionic mesothelium was also observed (Figure 3.2K and L). The folding of the yolk sac visceral endoderm, the bulb shaped allantois, and the thickened and disorganized chorionic mesothelium observed in the *Htt*$^{-/-}$ embryos are reminiscent of the defect observed in the *Hip14*$^{-/-}$*;Hip14l*$^{-/-}$ embryos. However, the developmental defects of the *Htt*$^{-/-}$ embryo are more pronounced than those in the *Hip14*$^{-/-}$*;Hip14l*$^{-/-}$ embryos. These data indicate that the *Hip14*$^{-/-}$*;Hip14l*$^{-/-}$ embryos at least partially phenocopy the *Htt*$^{-/-}$ embryos.

3.3.6 Palmitoylation of HTT is significantly decreased in *Hip14*$^{-/-}$*;Hip14l*$^{-/-}$ mouse embryonic fibroblasts

Since HIP14 and HIP14L are the primary PATs for palmitoylation of HTT and *Hip14*$^{-/-}$*;Hip14l*$^{-/-}$ embryos partially phenocopy the *Htt*$^{-/-}$ embryos, we hypothesized that the defects in the extraembryonic tissues in the *Hip14*$^{-/-}$*;Hip14l*$^{-/-}$ might be due to loss of HTT function as a result of loss of HTT palmitoylation. To address this question, ideally HTT palmitoylation levels would have been assessed in the extraembryonic tissues of *Hip14*$^{-/-}$*;Hip14l*$^{-/-}$ embryos, however, even when pooling theses tissues among embryos of the same genotype within a litter the small amount of tissue was not sufficient for immunoprecipitation of HTT. Therefor, MEF cell lines were generated from three WT and two *Hip14*$^{-/-}$*;Hip14l*$^{-/-}$ E9.5 embryos and ABE assays were performed to compare the levels of HTT palmitoylation. Cell pellets were lysed and HTT was immunoprecipitated in the presence of N-ethylmaleimide to block unmodified cysteine residues and immunoprecipitated HTT was then subjected to the following subsequent chemical treatments: incubation in neutral hydroxylamine to cleave the thioester bond between palmitate and cysteine residues and incubation in 2.5 uM biotin-BMCC to label newly free cysteines with biotin. HTT was then eluted from the beads and run on western blot and probed with streptavidin to detect palmitoylation and with an antibody against HTT to detect total immunoprecipitated HTT. A significant decrease in HTT palmitoylation of 25%

was observed in the *Hip14*$^{-/-}$;*Hip14l*$^{-/-}$ cells compared to the WT control cells with no signal observed as expected in the negative control HAM- lanes (Fig. 5). In agreement with previously published reports, no change in HTT palmitoylation was observed in the *Hip14*$^{-/-}$ or *Hip14l*$^{-/-}$ MEF cell lines (data not shown) (Singaraja et al., 2011; Sutton et al., 2013).

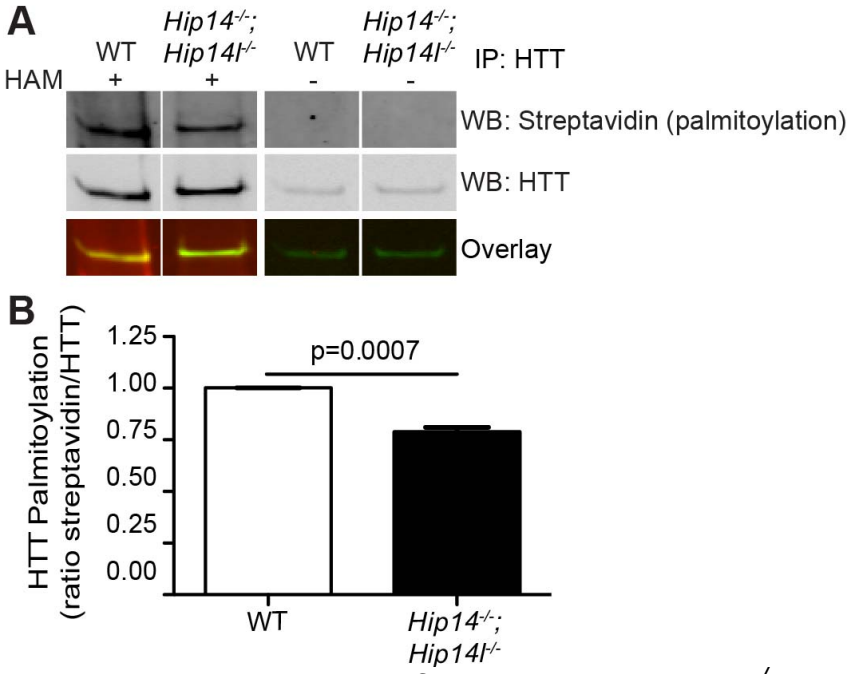

Figure 3.5: Palmitoylation of HTT in WT and *Hip14*$^{-/-}$;*Hip14l*$^{-/-}$ MEFs. HTT acyl-biotin exchange assay were performed to assess HTT palmitoylation levels in WT and *Hip14*$^{-/-}$;*Hip14l*$^{-/-}$ MEFs. MEF pellets were lysed and HTT was immunoprecipitated in the presence of N-ethylmaleimide to block unmodified cysteine residues. Immunoprecipitated HTT was then split in half and half was treated with hydroxylamine (HAM) to cleave the thioester bond between palmitate and cysteine residues (HAM+) and the other half was treated with buffer alone (HAM-). Samples were then treated with biotin-BMCC to label newly free cysteines with biotin. The HAM- negative control was included to show that the streptavidin signal is specific to the ABE treatment. HTT was then run on western blot and probed with streptavidin to detect biotin (palmitoylation) and an antibody against HTT to detect total immunoprecipitated HTT. The images are a composite of individual wells from the same Western blot image from one individual experiment. The quantification of an N of 3 independent experiments of 3 WT and 2 *Hip14*$^{-/-}$;*Hip14l*$^{-/-}$ MEF cells lines is shown in (**B**). HTT palmitoylation is calculated as ratio of streptavidin (palmitoylation) signal to total immunoprecipitated HTT signal. The error bars represent standard error of the mean and p=0.0007 by Student's t-test.

Although HTT palmitoylation in the *Hip14*$^{-/-}$*;Hip14l*$^{-/-}$ cells was significantly decreased, the change was fairly modest. This may suggest that other PATs are involved/responsible for the palmitoylation of HTT and are compensating for loss of HIP14 and HIP14L. Therefore, the level of mRNA expression of all 24 murine DHHC PATs was determined in WT and *Hip14*$^{-/-}$*;Hip14l*$^{-/-}$ MEFs to determine if there is upregulation of expression of any of these genes that may provide partial compensation and palmitoylation of HTT. No expression of *Zdhhc11, 14, 19, 22, 23,* or *25* was detected using 3 sets of primers each. Figure 3.6 shows mRNA expression of *Hip14, Hip14l,* and *Zdhhc1-9, 12, 15, 16, 18, 20, 21,* and *24.* As expected, a significant decrease in expression of *Hip14* and *Hip14l* was observed in the *Hip14*$^{-/-}$*;Hip14l*$^{-/-}$ cells. No other significant changes in mRNA expression of any of the other DHHC PAT genes were observed. These data indicate that none of the other DHHC PATs are compensating for loss of *Hip14* and *Hip14l* by up-regulation of expression at the mRNA level (Figure 3.6).

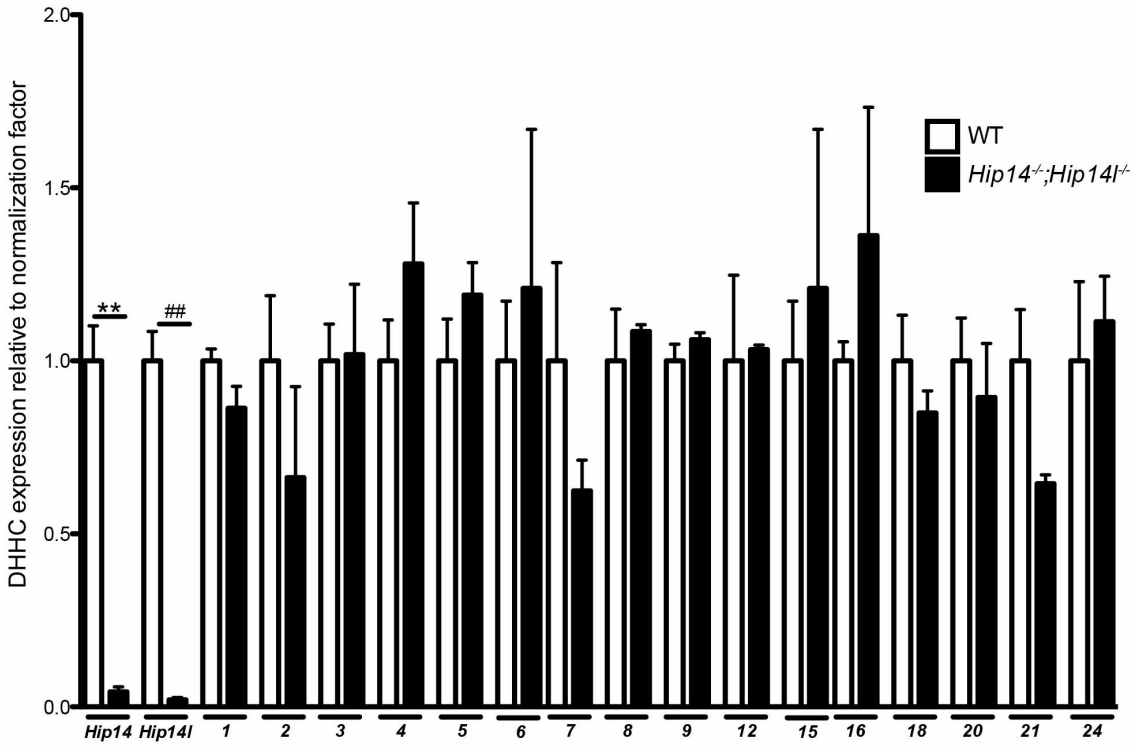

Figure 3.6. Expression of *Hip14, Hip14l, zDhhc1-9, 12, 15, 16, 18, 20, 21,* and *24* mRNA in WT and *Hip14*$^{-/-}$*;Hip14l*$^{-/-}$ MEFs by qPCR. Expression is shown relative to a normalization factor of combined expression of *Actb*, *Hprt1*, and *Rpl13a*. Error bars represent standard error of the mean. ** p=0.005 and ## p=0.003.

3.4 DISCUSSION

We present here a description of a double PAT deficient mouse model and provide the first report of embryonic lethality in mammals related to the absence of any DHHC PAT or PATs. The most striking finding of this study is that mice deficient in both *Hip14* and *Hip14l* phenocopy *Htt* deficient mice.

Loss of both *Hip14* and *Hip14l* leads to embryonic lethality between E10 and E11 *in utero*. We identified failed chorioallantoic fusion leading to failure in placental formation as the cause of this lethality. The defect appears to be in the chorion where the chorionic mesothelium, which mediates the initial contact with the allantoic mesoderm (Cross et al., 2003), is thickened and disorganized. In contrast, the allantois appears to form and extend properly but is unable to fuse normally, or at all, with the chorionic mesothelium. Subsequently, the allantois forms a balloon-like shape indicating incomplete or failed chorioallantoic fusion and occasionally it is found ectopically fused to the yolk sac. Besides these defects in placental formation, two distinct phenotypes are observed in the embryos themselves, one a severe phenotype and the other a more mild phenotype (Figure 3.2). In embryos displaying the severe phenotype, which occurred in 87.5% of *Hip14*$^{-/-}$;*Hip14l*$^{-/-}$ embryos, early growth retardation occurs along with a small, tight amniotic membrane that restricts the growth along the anterior-posterior axis causing the embryo to become disorganized and distorted. The mild phenotype is observed in 12.5% of *Hip14*$^{-/-}$;*Hip14l*$^{-/-}$ embryos and the growth of the embryo is not significantly delayed. The factors that influence the variation in phenotypes are presently unknown but may be due to variation in the levels of palmitoylation of the various HIP14 and HIP14L substrates.

Palmitoylation of proteins can affect their function or localization. Thus, the *Hip14*$^{-/-}$;*Hip14l*$^{-/-}$ phenotype is likely due to a functional disruption of a protein target or targets. One potential target is HTT. HIP14 and HIP14L are the two primary DHHC PATs that palmitoylate HTT, and mouse models deficient in either of these genes develop HD-like phenotypes, despite there being no change in HTT palmitoylation in the brains from these mice (Huang et al., 2011; Singaraja

et al., 2011; Sutton et al., 2013). The HD-like phenotypes of the *Hip14*$^{-/-}$ and *Hip14l*$^{-/-}$ mouse models likely result from deficient palmitoylation of other neuronal substrates (Singaraja et al., 2011; Sutton et al., 2013). wtHTT enhances the enzyme activity of HIP14 towards its substrates in a dose dependent manner, whereas mHTT does not. Thus, in HD, loss of HIP14 activity leads to the underpalmitoylation of neuronal HIP14 and HIP14L substrates, including HTT, which may contribute to the pathogenesis of HD (Huang et al., 2011; Singaraja et al., 2011). The biological function of HTT palmitoylation and the consequences of loss of HTT palmitoylation are currently unknown.

Interestingly, the *Hip14*$^{-/-}$;*Hip14l*$^{-/-}$ embryos share many features with the *Htt*$^{-/-}$ embryos, including folding of the yolk sac visceral endoderm, bulb shaped allantois, and thickened and disorganized chorionic mesothelium. There are two possible mechanisms underlying the observed similarity in phenotypes between *Hip14*$^{-/-}$;*Hip14l*$^{-/-}$ and *Htt*$^{-/-}$ mice: loss of HIP14/HIP14L function leading to decreased substrate palmitoylation or loss of HTT palmitoylation. The first possibility is that wtHTT regulates HIP14 and, potentially, HIP14L function, thus, in the absence of wtHTT or in the absence of HIP14 and HIP14L there would be aberrant palmitoylation of yet to be determined HIP14 and HIP14L substrates.

There are many other examples of mice deficient in genes that exhibit failed chorioallantoic fusion and embryonic lethality, for example mice lacking brachyury (*T*), α-4 integrin (*Itga4*), *Vcam1*, fibroblast growth factor receptor 2 (*Fgfr2*), and the Hsp40 homolog *Dnajb6* (Mrj) all have failed chorioallantoic fusion, like the *Hip14*$^{-/-}$;*Hip14l*$^{-/-}$ embryos (Cross et al., 2003; Hunter et al., 1999; Inman and Downs, 2007; Xu et al., 1998). Since palmitoylation of proteins can affect their function or localization, the *Hip14*$^{-/-}$;*Hip14l*$^{-/-}$ phenotype is likely due to a functional disruption of a protein target. These proteins, or others, could be potential HIP14 and HIP14L substrates and loss of palmitoylation of any of these may contribute to the *Hip14*$^{-/-}$;*Hip14l*$^{-/-}$ phenotype. Although, there was no change in the mRNA expression of *T* (data not shown), *Itga4,* and *Vcam1* in the *Hip14*$^{-/-}$;*Hip14l*$^{-/-}$ embryos their palmitoylation and localization or function could still be altered by the loss of *Hip14* and *Hip14l.* Currently, palmitoylation of these

proteins has not been explored. If that were the case, they would be expected to be less palmitoylated in *Hip14*$^{-/-}$;*Hip14l*$^{-/-}$ and *Htt*$^{-/-}$ embryos. Indeed, any of the proteins mentioned above or others could be substrates of HIP14 and HIP14L and could be contributing to the phenotype.

The second possible mechanism underlying the observed similarity in phenotypes between the *Hip14*$^{-/-}$;*Hip14l*$^{-/-}$ and *Htt*$^{-/-}$ embryos is that reduced HTT palmitoylation causes the phenotype. This is possible since HIP14 and HIP14L are the two primary PATs for HTT (Huang et al., 2011). In MEF cells generated from *Hip14*$^{-/-}$;*Hip14l*$^{-/-}$ embryos, a 25% decrease in HTT palmitoylation was observed compared to WT MEF cells (Figure 3.5). HTT palmitoylation is significantly decreased but not completely abolished in this system, which may be due to compensation by another DHHC PAT in the *Hip14*$^{-/-}$;*Hip14l*$^{-/-}$ MEF cells that does not occur in the extraembryonic tissues of the developing *Hip14*$^{-/-}$;*Hip14l*$^{-/-}$ embryos. Although there was no change in mRNA expression of any other *Zdhhc* genes in the *Hip14*$^{-/-}$;*Hip14l*$^{-/-}$ MEFs, there may be compensation occurring at the protein expression level or at the PAT activity level that cannot be detected using current techniques.

It is likely that in the *Hip14*$^{-/-}$;*Hip14l*$^{-/-}$ MEF cell lines compensation occurs following loss of both *Hip14* and *Hip14l* that does not occur in the extraembryonic tissues of the developing embryo. Different cell types express different *Zdhhc* genes at different levels. For example, Zd*hhc2*, *-3*, *-6*, *-15*, *-19*, and *-23* are not expressed in human placental tissue despite being expressed at varying levels in most other tissues tested (Ohno et al., 2006). Interestingly, ZDHHC2, -3, and -23 are among those DHHC PATs that have been shown to have a low level of palmitoylation activity towards HTT when overexpressed in COS cells with HTT (120-150% increase in palmitoylation versus the 225-250% increase in palmitoylation observed with overexpression of HIP14 or HIP14L with HTT) (Huang et al., 2011). *Zdhhc23* was not expressed in the *Hip14*$^{-/-}$;*Hip14l*$^{-/-}$ MEFs making it an unlikely candidate for a compensatory PAT but *Zdhhc2* and *3* are expressed in these cell lines but not in human placental tissue (Ohno et al., 2006). ZDHHC3 is an especially good candidate as a compensatory PAT for loss

of *Hip14* and *Hip14l* in the *Hip14*$^{-/-}$;*Hip14l*$^{-/-}$ MEFs, as it is a promiscuous PAT that has been shown to have many overlapping substrates and has a low level of palmitoylation activity towards HTT and is Golgi localized, as are HIP14 and HIP14L (Huang et al., 2009; Ohno et al., 2006).

Ideally, the levels of HTT palmitoylation would be compared between the *Hip14*$^{-/-}$;*Hip14l*$^{-/-}$ MEF cell lines and the extraembryonic tissues of *Hip14*$^{-/-}$;*Hip14l*$^{-/-}$ embryos to determine if there is a greater decrease in HTT palmitoylation in the extraembryonic tissues. Unfortunately, the methods currently available are not sensitive enough to detect HTT palmitoylation in such a small amount of tissue. If in the future this is possible, it would provide more evidence for the hypothesis that decreased HTT palmitoylation contributes to the similar phenotypes in the extraembryonic tissues of the *Hip14*$^{-/-}$;*Hip14l*$^{-/-}$ and the *Htt*$^{-/-}$ embryos.

In fact, these two mechanism may not be mutually exclusive and both may be contributing to the observed similarity in phenotypes between *Hip14*$^{-/-}$;*Hip14l*$^{-/-}$ and *Htt*$^{-/-}$ embryos. In the *Hip14*$^{-/-}$;*Hip14l*$^{-/-}$ embryos there is decreased HTT palmitoylation, which leads to reduced HTT function, as well of loss of the two PATs, which would lead to decreased palmitoylation of other putative substrates. Since HIP14 function is impaired following loss of wtHTT (Huang et al., 2011), in the *Htt*$^{-/-}$ embryos not only is HTT function completely lost but there would also be decreased HIP14, and potentially HIP14L, function. It is possible that less compensation by other PATs occurs in the *Htt*$^{-/-}$ embryos since HIP14 and HIP14L are still expressed at their normal levels. This would mean that in the *Htt*$^{-/-}$ embryos there is actually a greater decrease in palmitoylation of other HIP14 and HIP14L substrates compared to that in the *Hip14*$^{-/-}$;*Hip14l*$^{-/-}$ embryos. This along with a complete loss of HTT function would explain why the *Htt*$^{-/-}$ phenotype is more severe than the *Hip14*$^{-/-}$;*Hip14l*$^{-/-}$ phenotype.

This is the first description of embryonic lethality in a mouse model deficient in a DHHC PAT(s) deficient mouse model, demonstrating the physiological importance of palmitoylation during embryogenesis. The most compelling finding of this study is the phenotypic overlap with the *Htt*$^{-/-}$ mice and

the evidence that HIP14 and HIP14L are important for development of the extraembryonic membranes and the placenta.

4 ABERRANT PALMITOYLATION IN HD MOUSE MODELS[4]

4.1 INTRODUCTION

HD is an autosomal dominant adult onset neurodegenerative disease caused by an expansion of a normally occurring CAG repeat in the N-terminus of the *HTT* gene resulting in a poly-Q expansion in the HTT protein of more than 35 repeats (Group, 1993; Roos, 2010; Sturrock and Leavitt, 2010). HD is characterized by the progressive degeneration of the striatum with more widespread degeneration occurring at later stages and by motor, cognitive, and psychiatric symptoms (Roos, 2010; Sturrock and Leavitt, 2010). The average age of onset is 50 years of age with death occurring on average 15-20 years after onset (Roos, 2010; Sturrock and Leavitt, 2010).

HTT was shown to be palmitoylated in 2006 and mHTT in the YAC128 mouse model of HD was shown to be less palmitoylated (Yanai et al., 2006). Palmitoylation is the post-translational addition of a long chain saturated fatty acid, usually the 16-carbon palmitate, to proteins on cysteine residues via a reversible thioester bond (Hallak et al., 1994; Smotrys and Linder, 2004). Palmitoylation modulates membrane localization, function, protein-protein interactions, and other PTMs of palmitoyl-proteins and many proteins, including HTT, are dynamically palmitoylated and (Young et al., 2012). HTT was later shown the be palmitoylated by and to interact with the PAT HIP14 (Huang et al., 2011; 2004; Singaraja et al., 2002). HIP14 was particularly interesting for further study as it interacts less with mHTT (Singaraja et al., 2002). At the same time the HIP14 homolog HIP14L was identified based on its high amino acid sequence similarity to HIP14 and was later shown to also be a *bona fide* HTT interactor that also interacts less with mHTT (Singaraja et al., 2002; Sutton et al., 2013). HIP14

---

[4] The BACHD and Hu97/18 analysis from this chapter is being prepared for publication in a manuscript describing additional characterization of the Hu97/18 mice currently titled “Delineation of novel pre-clinical endpoints in humanized Hu97/18 HD model mice.” All experimental design, palmitoylation assays, and data analysis by SSS.

and HIP14L were shown to be the two primary PATs for HTT *in cellulo* (Huang et al., 2011). These PATs are unique among the large family of DHHC-domain containing PATs in that they are the only two of 23 that have six TMDs and seven ankyrin repeats, which mediate the interaction with HTT (Huang et al., 2011; Ohno et al., 2006; Young et al., 2012).

Subsequently mice deficient in these genes were generated, namely the *Hip14*$^{-/-}$ and *Hip14l*$^{-/-}$ mice (Singaraja et al., 2011; Sutton et al., 2013). Interestingly, both of these mouse models develop HD-like phenotypes that are reminiscent of the YAC128 phenotypes, including motor coordination deficits and selective striatal volume loss. Surprisingly, HTT palmitoylation was not affected in either of these mouse models, suggesting that these enzymes are able to compensate for loss of each other to palmitoylate HTT. It is believed that the similarities between these the *Hip14*$^{-/-}$ and *Hip14l*$^{-/-}$ mice and the YAC128 mice are due to altered palmitoylation of substrates other than HTT (Singaraja et al., 2011; Sutton et al., 2013). Indeed, HIP14 has been shown to be dysfunctional in the presence of the HD mutation towards its other substrates and as HIP14L is structurally identical, it may be as well (Huang et al., 2011).

Thus loss of interaction with HTT results in dysfunction of HIP14, and possible HIP14L as well, in the presence of the HD mutation in the YAC128 mouse model, which may lead to aberrant palmitoylation of HTT itself and of other HIP14 and HIP14L substrates. Indeed, in a proteomics study comparing the palmitoyl proteomes of WT and YAC128 mice, YAC128 mice were found to have fairly widespread alterations in the levels of palmitoylated proteins (Wan et al., 2013). Also, GAD65 was shown to be less palmitoylated in the R6/2 mouse model of HD that expresses expanded mutant exon one of *HTT* (Rush et al., 2012) and the glutamate transporter GLT1 was shown to be less palmitoylated in the YAC128 mouse model (Huang et al., 2010).

Here the palmitoylation of HTT, of the HIP14 and HIP14L substrates SNAP25 and GAD65, and of the HIP14 substrate PSD-95 is assessed in a low throughput, high confidence manner in the YAC128 mouse model of HD to

confirm that palmitoylation is altered in HD. This is further confirmed in the following two other HD mouse models: the BACHD mouse that contains full-length human *HTT* on a bacterial artificial chromosome with 97 CAG repeats and the Hu97/18 humanized mouse that contains human WT *HTT* with 18 CAGs on a yeast artificial chromosome (the YAC18), the BACHD transgene, and no mouse *Htt* (Gray et al., 2008; Southwell et al., 2013).

4.2 MATERIALS AND METHODS

4.2.1 Mice and genotyping

All mice in this study were on the FVB/N strain. The YAC128 mice used were eight month old males and were genotyped as previously described (Hodgson et al., 1996; Slow, 2003). The BACHD, Hu18/18, and Hu97/18 mice used were six month old males and were bred and genotyped as previously described (Gray et al., 2008; Southwell et al., 2013). The University of British Columbia Committee on Animal Care approved all procedures.

4.2.2 Antibodies

The primary antibodies used were HTT mouse monoclonal antibody (MAB2166, Millipore, 1:1000 for immunoblotting), HTT rabbit polyclonal antibody (in-house rabbit BKP1 for immunoprecipitation), human specific HTT mouse monoclonal antibody (in-house HD650 for immunoprecipitation), SNAP25 monoclonal antibody (SMI81, Covance for immunoprecipitation), SNAP25 polyclonal antibody (111 002, Synaptic Systems, 1:1000 for immunoblotting), PSD-95 monoclonal antibody (MA1-046, Thermo Scientific, 1:1000 for immunoblotting), PSD-95 polyclonal antibody (in-house for immunoprecipitation), GAD65 polyclonal antibody (ABN101, Millipore, for immunoprecipitation or 1:1000 for immunoblotting), and GAD65 monoclonal antibody (GAD-6, Developmental Studies Hybridoma Bank for immunoprecipitation or 1:1000 for immunoblotting). Fluorescently conjugated secondary antibodies for immunoblotting used were IRDye 800CW goat anti-Mouse (610-131-121, Rockland, 1: 5000) and IRDye 800CW goat anti-Rabbit (610-131-002, Rockland, 1: 5000). Alexa Fluor 680

conjugated to streptavidin (S-32358, Life Technologies, 1:10000) was used to detect biotin.

4.2.3 Acyl-biotin exchange palmitoylation assay and western blotting analysis

ABE palmitoylation assays were performed on frozen whole brain samples from WT, YAC128, BACHD, and Hu97/18 male mice as previously described (Drisdel and Green, 2004; Huang et al., 2009). Briefly, brains were harvested and immediately frozen and stored at -80°. Frozen brains were then homogenized on ice in 8 mL lysis buffer (150 mM NaCl, 50 mM Tris, 5 mM ethylenediaminetetraacetic acid, 0.1% SDS, 1% triton X-100, pH 7.4) with 100 mM (Sigma-Aldrich, St. Louis, MO, USA). Homogenates were sonicated for 7 seconds at 30% power to shear DNA and the insoluble material was removed by centrifugation at 14000 revolutions per minute for 15 minutes. HTT, PSD-95, and GAD65 were immunoprecipitated from brain lysates by overnight incubation with Protein G Dynabeads® (Life Technologies, Carlsbad, CA, USA) and antibodies for immunoprecipitation (BKP1, polyclonal anti-PSD-95, and monoclonal anti-GAD65, respectively). SNAP25 was immunoprecipitated from brain lysates by overnight incubation with Protein G PureProteome™ magnetic beads (Millipore, Damstadt, Germany) and SMI81 anti-SNAP25 antibody. Beads were then washed and split into two and treated with neutral pH hydroxylamine (HAM+; Sigma-Aldrich, St. Louis, MO, USA) in lysis buffer or just lysis buffer (HAM-) for two hours for HTT and one hour for the other three proteins at room temperature. Following HAM treatment beads were washed and treated with 2.5 uM EZ-Link BMCC-Biotin (Thermo Fisher Scientific, Waltham, MA, USA) in pH 6.2 lysis buffer for one hour at 4°. At the end of the BMCC-Biotin treatment beads were washed and then heated at 70° with 1X NuPAGE LDS Sample Buffer (Life Technologies, Carlsbad, CA, USA) and 100 mM fresh dithiothreitol (Sigma-Aldrich, St. Louis, MO, USA) to elute the protein.

Supernatants from HTT assays were run on NuPAGE® Novex® 3-8% Tris-Acetate gels (Life Technologies, Carlsbad, CA, USA) and supernatants from

the other three proteins were run on homemade gels, transferred to nitrocellulose, and blocked with 5% milk in Phosphate Buffered Saline (PBS). Primary antibody dilutions of HTT MAB2166, SNAP25 polyclonal, PSD-95 monoclonal, and GAD65 polyclonal in 5%BSA PBST (5% Tween-20) were applied to the immunoblots at room temperature for one hour. The appropriate secondary antibodies and and Alexa Fluor® 680 conjugated streptavidin were applied in 5% BSA PBST for an hour. Fluorescence was scanned and quantified with Odyssey Infrared Imaging system (Li-COR Bioscience; Lincoln, NE, USA) and quantified using the Li-COR software. Palmitoylation was analyzed as a ratio of HAM+ palmitoylation signal to total immunoprecipitated protein signal and normalized to the wild type control condition. Data were analyzed using the Student's t-test or One-Way ANOVA (Analysis of Variance). Error bars are in standard error of mean.

4.3 RESULTS

4.3.1 Mutant HTT palmitoylation is decreased in the YAC128, BACHD, and Hu97/18 HD mouse models

Since methods to assess palmitoylation levels have become more sensitive and because palmitoylation of wtHTT in YAC128 mice has never been assessed, palmitoylation of WT and mHTT in the YAC128 HD was model was determined (Yanai et al., 2006). Palmitoylation of Q7 endogenous wtHTT in the YAC128 mice was decreased by 18% compared to Q7 HTT in WT mice (Figure 4.1). As expected palmitoylation of Q128 mHTT in the YAC128 mice was decreased by 69% compared to Q7 HTT from WT mice (Figure 4.1).

To validate the results from the YAC128 mice in another HD mouse model, palmitoylation of HTT was assessed in another full-length HD mouse model the BACHD mice. Palmitoylation of Q7 HTT in the BACHD mice was unchanged compared to Q7 HTT in the WT mice but palmitoylation of Q97 mHTT was decreased by 68% (Figure 4.1). These data were further validated in a third HD mouse model, the humanized Hu97/18 mice. As in the BACHD mice palmitoylation of Q18 HTT in the Hu97/18 mice was unchanged compared to that

of the Hu18/18 mice but palmitoylation of Q97 mHTT in the Hu97/18 mice was decreased by 43% compared to Hu18/18 mice (Figure 4.1).

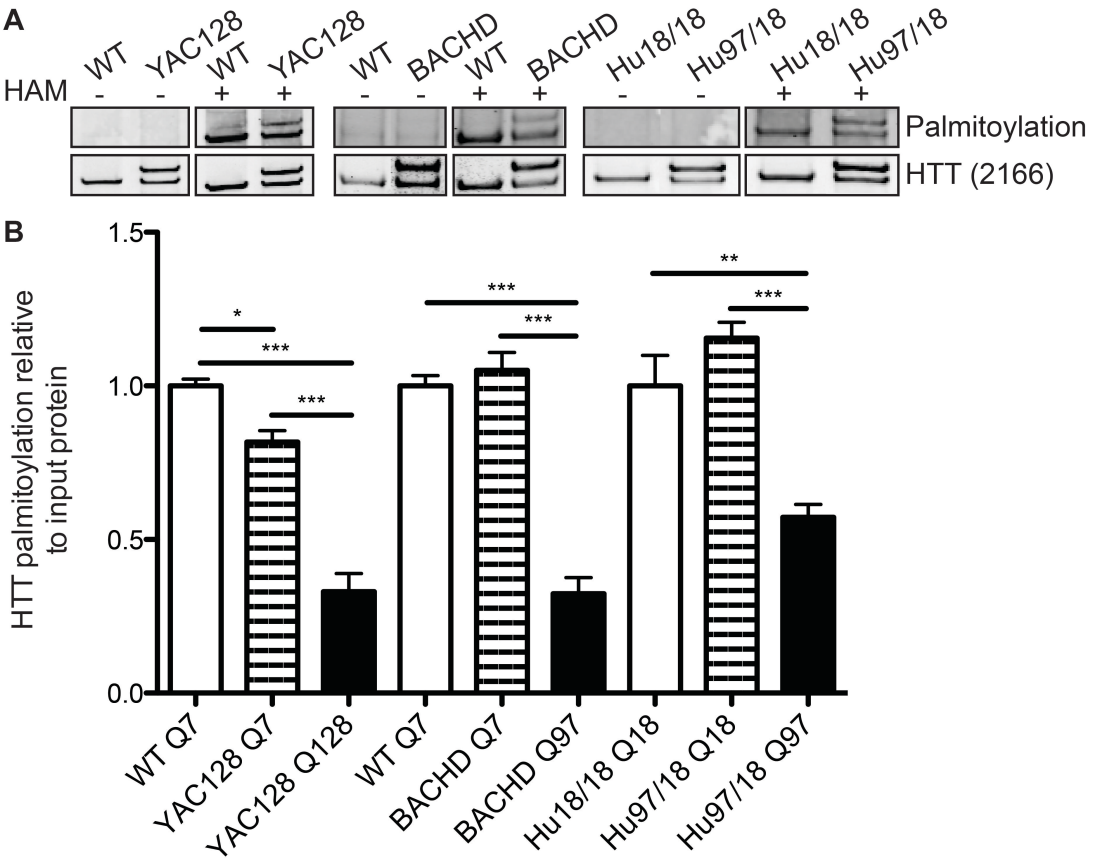

Figure 4.1: Mutant HTT palmitoylation is decreased in the YAC128, BACHD, and Hu97/18 mouse models of HD. Total brain lysates from eight month old WT and YAC128 and six month old WT, BACHD, Hu18/18, and Hu97/18 mice were subjected to the ABE assay and ran on allele separating gels to separate WT and mHTT. The palmitoylation signal of one representative image is shown in the top panel of each set of genotypes and the total HTT immunoprecipitated is shown in the bottom panel (**A**). The negative control hydroxylamine minus treatment is shown on the left of each set of blots. wtHTT is the lower band and mHTT is the upper band in each set. The quantification of four to five individual mice of all genotypes is shown in and was calculated as a ratio of palmitoylation signal over total protein. (**B**). MHTT was quantified separately from wtHTT and is represented by black bars and wtHTT by notched bars in the same mice. wtHTT in the YAC128 mice was decreased compared to HTT in WT mice and mHTT was even further decreased (ANOVA $F(2,12)=66.36$, $p<0.0001$; N=5). MHTT in the BACHD mice was decreased compared to wtHTT from WT or BACHD mice (ANOVA $F(2,12)=71.27$, $p<0.0001$; N=4-5). MHTT in the humanized Hu97/18 mice was also decreased compared to WT humanized mice or wtHTT from the Hu97/18 mice (ANOVA $F(2,12)=19.36$, $p=0.0002$; N=5). * $p<0.05$, ** $p<0.01$. *** $p<0.0001$. All images are composites from the same blot.

4.3.2 SNAP25 palmitoylation is decreased in the YAC128, BACHD, and Hu97/18 HD mouse models

Since SNAP25 is a HIP14 and a HIP14L substrate and its palmitoylation was previously shown to be decreased in both the *Hip14*$^{-/-}$ and *Hip14l*$^{-/-}$ mice, its palmitoylation was assessed in all three HD mouse models (Singaraja et al., 2011; Sutton et al., 2013). Palmitoylation of SNAP25 was decreased in the YAC128 mice compared to WT mice by 29% (Figure 4.2). To validate the results from the YAC128 mice in another HD mouse model, palmitoylation of SNAP25 was assessed the BACHD mice. SNAP25 palmitoylation was decreased by 40% in the BACHD mice compared to WT mice (Figure 4.2). These data were further validated in a third HD mouse model, the humanized Hu97/18 mice. As in both the BACHD and YAC128 mice palmitoylation of SNAP25 was decreased by 45% compared to Hu18/18 mice (Figure 4.2).

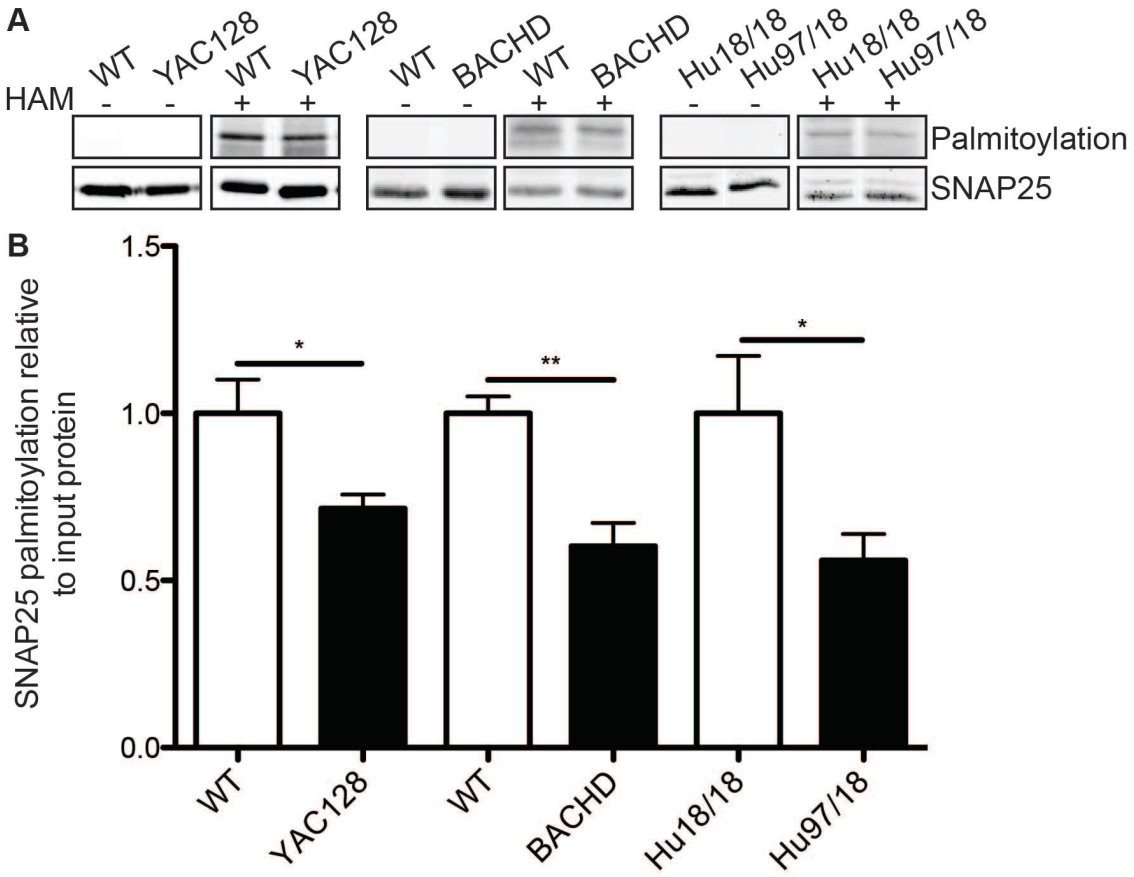

Figure 4.2: SNAP25 palmitoylation is decreased in the YAC128, BACHD, and Hu97/18 mouse models of HD. Total brain lysates from eight month old WT and YAC128 and six month old WT, BACHD, Hu18/18, and Hu97/18 mice were subjected to the ABE assay. The palmitoylation signal of one representative image is shown in the top panel of each set of genotypes and the total SNAP25 immunoprecipitated is shown in the bottom panel (**A**). The negative control hydroxylamine minus treatment is shown on the left of each set of blots. The quantification of four to five individual mice of all genotypes is shown and was calculated as a ratio of palmitoylation signal over total protein (**B**). Palmitoylation of SNAP25 in the YAC128 mice was decreased compared to that in WT mice (Student's t-test, p=0.031, N=5). SNAP25 palmitoylation was also decreased in the BACHD mice compared to WT mice (Student's t-test, p=0.0017, N=5). In the humanized Hu97/18 mice SNAP25 palmitoylation was decreased as well compared to that in WT humanized Hu18/18 mice (Student's t-test, p=0.041, N=4-5). * p<0.05, ** p<0.01. *** p<0.0001. All images are composites from the same blot.

4.3.3 PSD-95 palmitoylation is decreased in the YAC128, BACHD, and Hu97/18 HD mouse models

Since PSD-95 is a HIP14 substrate and its palmitoylation was previously shown to be decreased in the *Hip14*$^{-/-}$ mice, its palmitoylation was assessed in all three HD mouse models (Singaraja et al., 2011). Palmitoylation of PSD-95 was decreased in the YAC128 mice compared to WT mice by 33% (Figure 4.3). To validate the results from the YAC128 mice in another HD mouse model, palmitoylation of PSD-95 was assessed in the BACHD mice and was found to be decreased by 24% in the BACHD mice compared to WT mice (Figure 4.3). These data were further validated in the humanized Hu97/18 mice. As in both the BACHD and YAC128 mice palmitoylation of PSD-95 was decreased by 23% in the Hu97/18 mice compared to that in the Hu18/18 mice (Figure 4.3).

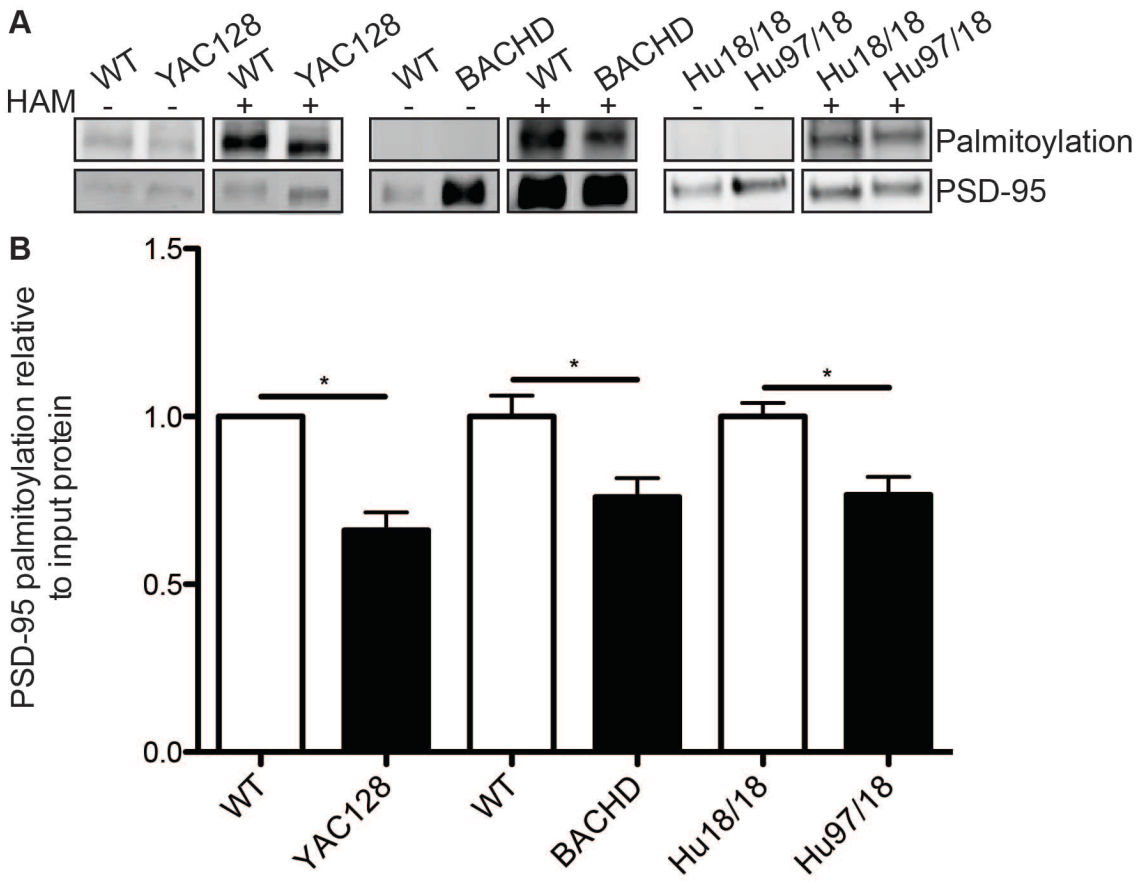

Figure 4.3: PSD-95 palmitoylation is decreased in the YAC128, BACHD, and Hu97/18 mouse models of HD. Total brain lysates from eight month old WT and YAC128 and six month old WT, BACHD, Hu18/18, and Hu97/18 mice were subjected to the ABE assay. The palmitoylation signal of one representative image is shown in the top panel of each set of genotypes and the total PSD-95 immunoprecipitated is shown in the bottom panel (**A**). The negative control hydroxylamine minus treatment is shown on the left of each set of blots. The quantification of five to six individual mice of all genotypes is shown and was calculated as a ratio of palmitoylation signal over total protein (**B**). Palmitoylation of PSD-95 in the YAC128 mice was decreased compared to that in WT mice (Wilcoxon signed rank test, p=0.031, N=6). PSD-95 palmitoylation was also decreased in the BACHD mice compared to WT mice (Student's t-test, p=0.020, N=5). In the humanized Hu97/18 mice PSD-95 palmitoylation was decreased as well compared to that in WT humanized Hu18/18 mice (Student's t-test, p=0.013, N=4-5). * p<0.05, ** p<0.01. *** p<0.0001. All images are composites from the same blot.

4.3.4 GAD65 palmitoylation is not changed in the YAC128, BACHD, and Hu97/18 HD mouse models

Since GAD65 is a HIP14 and a HIP14L substrate and its palmitoylation was previously shown to be decreased in the R6/2 HD mouse model, its

palmitoylation was assessed in all three HD mouse models (Huang et al., 2009; Rush et al., 2012). Palmitoylation of GAD65 unchanged in the YAC128, BACHD, and Hu97/18 mice compared to WT (Figure 4.4). There appeared to be two palmitoylated GAD65 bands in the BACHD and Hu97/18 mice, possibly representing monoacylated and diacylated forms of GAD65 (Figure 4.4).

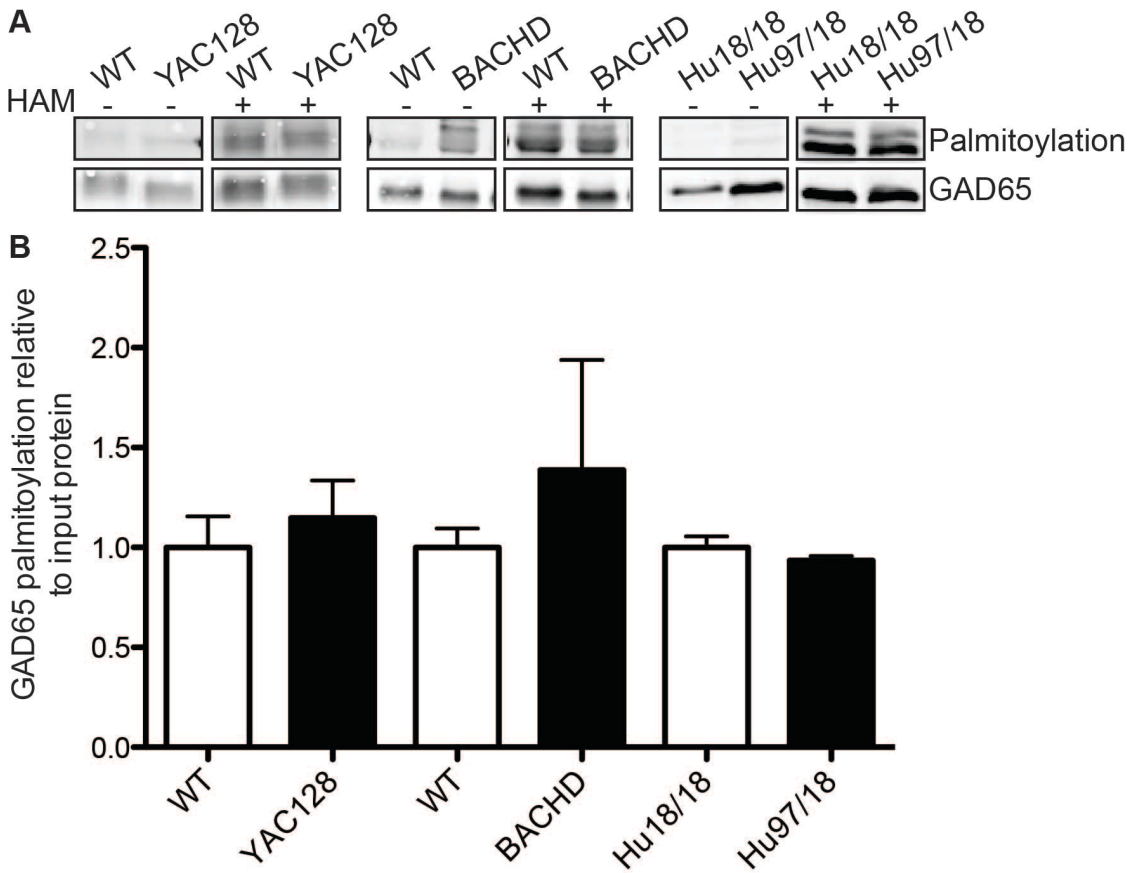

Figure 4.4: GAD65 palmitoylation is unchanged in the YAC128, BACHD, and Hu97/18 mouse models of HD. Total brain lysates from eight month old WT and YAC128 and six month old WT, BACHD, Hu18/18, and Hu97/18 mice were subjected to the ABE assay. The palmitoylation signal of one representative image is shown in the top panel of each set of genotypes and the total PSD-95 immunoprecipitated is shown in the bottom panel (**A**). The negative control hydroxylamine minus treatment is shown on the left of each set of blots. The quantification of five individual mice of all genotypes is shown and was calculated as a ratio of palmitoylation signal over total protein (**B**). Palmitoylation of GAD65 was unchanged in the YAC128, BACHD, and Hu97/18 mice compared to that in WT mice (Student's t-test; p=0.56, p=0.53, and p=0.31, respectively; N=3-5). All images are composites from the same blot.

4.4 DISCUSSION

HTT is palmitoylated and mHTT in the YAC128 mouse model of HD was previously shown to be less palmitoylated compared to human wtHTT from the YAC18 mice (Yanai et al., 2006). It is believed that the similarities between the *Hip14*$^{-/-}$ and *Hip14l*$^{-/-}$ mice and the YAC128 mice are due to altered palmitoylation of substrates other than HTT but that loss of palmitoylation of HTT also plays a role in HD (Singaraja et al., 2011; Sutton et al., 2013). Indeed, the YAC128 mice

were found to have fairly widespread alterations in the levels of palmitoylated proteins, including SNAP25, PSD-95, GAD65, and GLT1 (Huang et al., 2010; Rush et al., 2012; Wan et al., 2013). Here the palmitoylation of HTT and of the HIP14 and/or HIP14L substrates SNAP25, PSD-95 and GAD65 was assessed in a low throughput, high confidence manner in the YAC128, BACHD, and Hu97/18 mouse models of HD.

As expected, in all three mouse models of HD mHTT palmitoylation was decreased both compared to littermate control mice and compared to the WT allele within the same mouse. Only in the YAC128 mouse was palmitoylation of the WT allele decreased in the presence of the HD mutation, i.e. in the same mouse, and even then it was only by 18%. This is in contrast to the 43-68% decrease in mHTT palmitoylation compared to WT mice. This may be because it is not until very high CAG repeats that palmitoylation of the WT allele is affected by loss of HIP14 and possibly HIP14L function and may reflect the collective remaining PAT activities of the two enzymes. Alternatively, an additional PAT may also be compensating to palmitoylate wtHTT.

A confounding factor in the YAC128 and BACHD mouse models is the presence of two alleles of wtHTT in addition to the one allele of mHTT. It would be very interesting to know what occurs in the human situation, i.e. where there is one allele of WT and one allele of mHTT, or in a YAC128 or BACHD mouse with only one copy of wtHTT. Would palmitoylation of wtHTT be further decreased in these situations? What about palmitoylation of mHTT? The Hu97/18 mouse is the most like the human situation. When HTT protein levels are assessed the total HTT levels are similar to WT mice; however, the Hu18/18 mice are haploinsufficient as they express less WT human HTT than a mouse expresses murine HTT (Southwell et al., 2013). It would also be interesting to assess palmitoylation of HTT in Hu97/18 mice compared to WT mice instead of compared to Hu18/18 mice, as was done here.

The effect on wtHTT palmitoylation may also be due to aggregate formation. The YAC128 mice form aggregates whereas the BACHD do not (Pouladi et al.,

2012). If wtHTT and potentially HIP14 and HIP14L are being pulled into the HTT aggregate via interaction with mHTT this may explain why there is a decrease in wtHTT palmitoylation in the YAC128 mice but not in the BACHD mice.

The palmitoylation of SNAP25 was decreased in all three mouse models, as expected. As SNAP25 is a substrate of both HIP14 and HIP14L and the function of HIP14, and possibly HIP14L, is decreased in the presence of the HD mutation it is expected that its palmitoylation would be decreased in HD mouse models (Fukata et al., 2004; Huang et al., 2011; 2004; Sutton et al., 2013). Palmitoylation is not abolished, which is also not unexpected given that SNAP25 is palmitoylated by other PATs. It is possible that palmitoylation of SNAP25 is more dependent on HIP14 and HIP14L in certain cell types or at certain subcellular localizations.

Palmitoylation of PSD-95 was also decreased in all three mouse models of HD. This is also expected as PSD-95 is a HIP14 substrate and it was previously shown that its palmitoylation is decreased in the YAC128 mice in the palmitoyl proteomics study (Wan et al., 2013). Again, palmitoylation was not abolished which is not unexpected given that PSD-95 is palmitoylated by other PATs. Again, as with SNAP25, it is possible that palmitoylation of PSD-95 is more dependent on HIP14 in certain cell types or at certain subcellular localizations.

GAD65 palmitoylation was not changed in any of the three mouse models. This is slightly unexpected as in the R6/2 HD mouse model GAD65 palmitoylation was decreased. However, the R6/2 mouse model is a HTT fragment mouse model that expresses mutant exon1 of HTT and as a result it has a much more severe phenotype. In this mouse autopalmitoylation of HIP14 was almost completely abolished suggesting much more severe HIP14 dysfunction which may explain why there is a much greater affect on GAD65 palmitoylation. The data presented here is agreement with the data from the palmitoyl proteomics study in YAC128 mice where there was no change in palmitoylation of GAD65.

This study provides further support for aberrant palmitoylation in HD mouse models and is the first study to examine palmitoylation of wtHTT in the presence of mHTT. It will be interesting to apply these findings to a human situation to determine if palmitoylation is also disturbed in human HD samples.

5 LOSS OF THE HUNTINGTON DISEASE-ASSOCIATED PALMITOYLACYLTRANSFERASE HIP14 IN ADULTHOOD LEADS TO SUDDEN UNEXPLAINED DEATH IN EPILEPSY, MOTOR DEFICITS, AND INCREASED ESCAPE RESPONSE[5]

5.1 INTRODUCTION

HD is an autosomal dominant neurodegenerative disease characterized by the selective degeneration of the striatum and motor, cognitive, and psychiatric disturbances (Roos, 2010; Sturrock and Leavitt, 2010). HD is fatal with death occurring 15-20 years after onset, on average, at 50 years of age. There are currently no disease modifying therapies, only those directed at symptom management (Roos, 2010; Sturrock and Leavitt, 2010). The prevalence of HD has recently been estimated at 13.7 per 100,000 with 81.6 per 100,000 at a 25% to 50% risk in the general population (Fisher and Hayden, 2014). Thus identifying and validating new potential drug targets for the treatment of HD is very important.

HD is caused by a CAG repeat expansion mutation in the *HTT* gene that results in a poly-Q expansion in the HTT protein (Group, 1993). wtHTT is post-translationally modified in many different ways, including phosphorylation, acetylation, palmitoylation, SUMOylation, ubiquitination, and proteolytic cleavage (Ehrnhoefer et al., 2011). For many of these PTMs, the mutation in HTT alters them in some way leading to loss of function or a toxic gain of function of the HTT protein (Ehrnhoefer et al., 2011). Palmitoylation is the reversible S-acylation of proteins at cysteine residues by long chain fatty acids. It is often called

---

[5] This chapter is being prepared for publication. Sanders, S.S., Parsons, M.P., Southwell A.L., Mui, K.K.N., Franciosi, S., Raymond L.A., and Hayden, M.R. All experimental design, western blots; behavior testing, except rotarod, spontaneous activity, and climbing, western blots, and all data analysis, except of electrophysiology data, by SSS.

palmitoylation due to the fact that palmitate, the 16-C fatty acid, is the most common fatty acid in the cell (Hallak et al., 1994; Smotrys and Linder, 2004). HTT is palmitoylated at Cys214 and mHTT is less palmitoylated. Further reducing palmitoylation increases toxicity and aggregation of mHTT (Yanai et al., 2006).

S-palmitoylation is mediated by a family of DHHC-domain containing PATs that palmitoylated proteins at cysteine residues via a thioester bond (Huang et al., 2004; Ohno et al., 2006). HTT is palmitoylated by huntingtin interacting protein 14 (HIP14) and HIP14-like (HIP14L) (Huang et al., 2011; 2004). When HTT is mutated it interacts less with both enzymes and wtHTT but not mHTT was found to modulate the activity of HIP14 (Huang et al., 2011; Singaraja et al., 2002; Sutton et al., 2013). Interestingly, the constitutive *Hip14* deficient mouse model (*Hip14*$^{-/-}$) has an HD-like phenotype similar to that of the YAC128 mouse model of HD, including selective degeneration of the striatum and motor deficits (Singaraja et al., 2011). The YAC128 mouse model is a transgenic mouse that expresses the full human *HTT* gene with 128 CAG repeats and accurately recapitulates many features of HD (Ehrnhoefer et al., 2009; Slow, 2003; Van Raamsdonk, 2005b).

Although the *Hip14*$^{-/-}$ mouse has an HD-like phenotype, it is developmental and non-progressive unlike the adult-onset, progressive phenotype of the YAC128 mice (Singaraja et al., 2011; Slow, 2003; Van Raamsdonk, 2005b). In fact, the selective degeneration of the striatum occurs during development, before the mouse is born, where increased cell death was observed at day 14.5 *in utero* in the developing striatum and decreased striatal volume was observed at day 17.5 *in utero* (Singaraja et al., 2011). Since altered HIP14 function will occur throughout the animal's life in the presence of the HD mutation rather than just during development, we sought to determine the consequences of loss of *Hip14* in the adult animal. An inducible *Hip14* deficient mouse model was generated and *Hip14* deletion was induced in the young adult mouse.

5.2 MATERIALS AND METHODS

5.2.1 Generation of *Hip14* inducible knockout mice

Xenogen Bioscienes (now Taconic) generated the *Hip14* "floxed" mice (*Hip14*^{F}) on the FVB/N background strain. The 5' and 3' homology arms and the conditional knockout region (cKO) region were amplified from bacterial artificial chromosome DNA and inserted into the targeting vector at the indicated restriction enzyme sites such that the cKO region was flanked by loxP sites (Figure 5.1A). A positive selection Neo cassette was included and flanked by flippase (Flp) recognition target (FRT) sites and a negative selection cassette diphtheria toxin A (DTA) was also included to select against random insertion (Figure 5.1A). Male FVB/N embryonic stem cells were electroporated with the targeting vector and selected using G418 resistance and screened for homologous recombination at the 5' and 3' homology arms with the WT allele (Figure 5.1B) by restriction enzyme digest and southern blot and PCR. The neo cassette was then removed in positive clones by electroporation with Flp recombinase to mediate recombination between the FRT sites and generate the recombined *Hip14*^{F} allele (Figure 5.1C). Neo cassette deletion was confirmed by G418 sensitivity and PCR. *Hip14*^{F} embryonic stem cells were then injected into C57BL/6J blastocysts to generate male chimeras that were bred with FVB/N females. Resulting white coat progeny indicated germline transmission and those mice were genotyped using the following primers: the forward primer in the 5' homology arm in intron 1 (5'-GGAGAATGGTTAGGAAAAGCTCGTACC-3') and the reverse primer in the cKO region in intron 1 upstream of the first loxP site (5'-GAGGAAAGCATGCAAGAGCACTTCTC-3').

The *Hip14*$^{F/F}$ mice were then crossed to a ubiquitous tamoxifen (TM) inducible Cre expressing line, the Cre-ER^{T2} line (Ruzankina et al., 2007), to generate mice in which *Hip14* can be deleted at any time point (*Hip14*$^{F/F}$;Cre-ER^{T2}). The primers used to genotype at the Cre-ER^{T2} transgene were as follows: 5'-GCGGTCTGGCAGTAAAAACTATC-3' and 5'-GTGAAACAGCATTGCTGTCACTT-3'. Gene deletion was induced using a five-

day TM treatment paradigm. Mice were given a single intraperitoneal injection once a day for five days at a dose of 0.2 mg TM/g body weight in 98% corn oil with 2% ethanol (*iHip14*$^{F/F}$ and *iHip14*$^{\Delta/\Delta}$ mice) or vehicle alone (WT VEH mice, 98% corn oil with 2% ethanol) as previously described (Ruzankina et al., 2007). Mice were treated with TM at 6-weeks of age. The University of British Columbia Committee on Animal Care approved all procedures.

5.2.2 Quantitative real time PCR

Total RNA was isolated from -80ºC frozen tissues using the RNeasy mini kit (Qiagen, Venio, Limburg, Netherlands). RNA was treated with DNAse I (Life Technologies, Carlsbad, CA, USA) to remove residual genomic DNA. cDNA was prepared from 1 µg total RNA using SuperScript® III First-Strand Synthesis System (Life Technologies, Carlsbad, CA, USA). Quantitative RT-PCR (qPCR) on the mouse *Hip14* gene using primers spanning exons 1 and 2 (5'-ACCCGGAGGAAATCAAACCACAGA-3' and 5'-TACATCGTAACCCGCTTCCACCAA3') was performed using Power SYBR Green PCR master mix (Applied Biosystems, Life Technologies, Carlsbad, CA, USA) in ABI 7500 Fast Real-Time PCR system (Applied Biosystems, Life Technologies, Carlsbad, CA, USA) under default conditions. Each sample was run in triplicate. Expression levels for mRNA were normalized to beta-actin.

5.2.3 Antibodies

The primary antibodies used were HIP14 polyclonal antibody (in house, 1:400 for immunoblotting), β-tubulin monoclonal antibody (T8328, Sigma, 1:5000 for immunoblotting), and NeuN antibody (Millipore, 1:1000 for immunohistochemistry). Biotinylated anti-mouse antibody (Vector Laboratories, 1:1000 for immunohistochemistry) was used as a secondary antibody for immunohistochemistry. Fluorescently conjugated secondary antibodies for immunoblotting used were Alexa Fluor 680 goat anti-Rabbit (A21076, Molecular Probes, 1:10000) and IRDye 800CW goat anti-Mouse (610-131-121, Rockland, 1: 2500).

5.2.3.1 Tissue lysis, and western blotting analysis

Tissues were homogenized on ice for 5 min in one volume 1% SDS TEEN [TEEN: 50 mM Tris pH 7.5, 1 mM EDTA, 1 mM EGTA, 150 mM NaCl, and 1X complete protease inhibitor cocktail (Roche)] and subsequently diluted in four volumes 1% TritonX-100 TEEN for 5 min for further homogenization. Samples were sonicated at one time at 20% power for 5 seconds to shear DNA and the insoluble material was removed by centrifugation at 14000 revolutions per minute for 15 min.

Proteins in both the cell lysates were heated at 70°C in 1 x NuPAGE LDS sample buffer (Invitrogen) with 10 mM DTT before separation by SDS-PAGE. After transfer of the proteins onto nitrocellulose membrane, immunoblots were blocked in 5% milk TBS (TBS: 50 mM Tris pH 7.5, 150 mM NaCl). Primary antibody dilutions of HIP14 polyclonal antibody and β-tubulin monoclonal antibody in 5%BSA PBST (Bovine Serum Albumin, Phosphate Buffered Saline with 5% Tween-20) were applied to the immunoblots at 4°C overnight. Corresponding secondary antibodies were applied in 5% BSA PBST for an hour. Fluorescence was scanned and quantified with Odyssey Infrared Imaging system (Li-COR Bioscience) and quantified using the Li-COR software. All error bars are standard error of mean.

5.2.4 Behaviour

All behavioral testing was performed with the tester blind to genotypes. All mice were only given a particular test once at three months of age (six weeks post TM injection). All of the apparatuses were cleaned between individual mice using ethanol.

5.2.4.1 Med Associates spontaneous activity

Spontaneous activity in the dark was measured using the Med Associates activity monitoring system (Med Associates Inc., St Albans, VT, USA) as previously described (Slow, 2003). Briefly, no later than one hour after the beginning of the dark cycle following one hour of acclimatization to the room, mice were placed in

the center of the testing chamber and allowed to freely move about and explore for half an hour. A number of automated readouts were recorded. Ambulatory time is the total time the mouse spent moving and ambulatory episodes are the number of times the mouse begins ambulating from a resting position.

5.2.4.2 Rotarod and climbing

Fixed and accelerating rotarod was used to assess motor coordination (UGO Basile, Comerio, Italy) as previously described (Slow, 2003). Mice were trained once a day for three days on the fixed speed 18-rpm rotarod for 120 s and the number of falls and latency to the first fall was recorded. On the fourth day mice are tested on the accelerating rotarod that accelerates from 5 to 40 rpm over 300 s and latency to fall is recorded. The average of three trials is reported

Motor coordination was also tested on the climbing apparatus as previously described (Southwell et al., 2009). Mice were placed inside closed top wire mesh cylinder (10x15 cm) on the tabletop and were allowed to freely explore the apparatus for 300 s while being video recorded. A climbing event was recorded when all four paws were lifted off the surface of the tabletop and a rearing event was recorded when the two front paws came off the surface of the tabletop. Climbing time was recorded as the total time from when the fourth paw left the tabletop to when the first paw touched back down.

5.2.4.3 Pre-pulse inhibition

Acoustic startle and PPI were performed using the Startle Response System (Sand Diego Instruments) as previously described (Van Raamsdonk, 2005b). Mice are placed in a startle chamber and allowed to acclimatize to the chamber with background noise for five minutes. Mice are then exposed to six trials of a 40 ms, 120 dB startle pulse to test the acoustic startle response. Mice are then exposed to eight blocks of six (48 trials in total) pseudorandomized trials of (1) no stimulus, (2) the 40 ms 120 dB startle pulse alone, or (3-6) the 40 ms 120 dB startle pulse preceded 100 ms by a 20 ms pre-pulse of two, four, eight, or 16 dB above background. An extra 40 ms 120 dB pulse was given in four of the eight blocks. Finally, the mice are then exposed to another six trials of the 40 ms 120

dB startle pulse. The intertrial interval was between eight and 23 s and was randomized between trials. PPI is the percentage of decrease in the startle response when a pre-pulse is given prior to the startle pulse and was calculated as the average of six trials per pre-pulse as follows: PPI=[(startle pulse-alone startle) - (pre-pulse + startle pulse startle)]/pulse-alone startle.

5.2.4.4 Porsolt forced swim test

The porsolt forced swim was used to test for depressive-like behaviors and was performed as previously described (Cryan et al., 2002; Porsolt et al., 1977a; 1977b; Pouladi et al., 2008). Briefly, mice were placed in individual cylinders (25 cm tall x 19 cm wide) filled with room temperature water to a depth of 15 cm and allowed to swim for six minutes while their behavior was recorded with a video camera placed directly above the cylinders. The first minute the mice were allowed to acclimatize and for the full last five minutes of the video the behavior was recorded. The time spent immobile was recorded as any time the mouse spent not swimming.

5.2.4.5 Open field

Open field spontaneous activity was used as a test for anxiety-like behaviors as previously described (Southwell et al., 2009). Mice were placed into the lower left corner of a 50 x 50 cm open black Plexiglas box with 16 cm sides in a brightly lit room. They were allowed to explore the box and spontaneous activity was recorded with a ceiling mounted camera for 10 minutes. Videos were simultaneously scored by Ethovision XT 7 animal tracking software (Noldus) and the distance travelled, average velocity, time spent in the center, and center entries were recorded.

5.2.4.6 Elevated plus maze

Elevated plus maze (EPM) was also used as a test of anxiety-like behaviors as previously described (Southwell et al., 2013). Briefly, mice were placed in the center of an elevated plus maze 50 cm off the ground with 30 x 10 cm arms two of which are closed in with 20 cm walls. Mice were allowed to freely explore the

maze for five minutes while a ceiling mounted camera recorded their spontaneous activity and Ethovision XT 7 animal tracking software (Noldus) simultaneously scored the videos. Distance travelled and average velocity (data not shown) were used to assess exploratory activity. The time spent in the open arms (open arm duration) and head dips of the edges of the open arms were used as measures of anxiety.

5.2.4.7 Light-dark box

The light-dark box was used to test for anxiety in an environment where there are no ways to escape, i.e. a completely enclosed environment. The Gemini Avoidance System (San Diego Instruments) was used for this purpose with no cues or shocks used. The door between the two chambers was kept open so mice could freely explore both sides of the box and on one side a light was shone through the transparent door to create a brightly lit light box. The door on the other side was blacked out to create a dark box. Mice were allowed to freely explore the apparatus and their activity was recorded using a video camera through the light box side. The total time spent in the light box was used as a measure of anxiety.

5.2.4.8 Sucrose preference

Sucrose preference was used to test for anhedonia, or the loss of pleasure seeking behaviors, a symptom of depression, as previously described (Pouladi et al., 2008; Strekalova et al., 2004). Mice were single housed in a full size cage and were given *ad libitum* access to food and to two water bottles. Mice were allowed to acclimatize to the bottles for one week. On day seven the water in one of the bottles was replaced with 2% sucrose solution and the mice and both bottles were weighed. 24 hours later the bottles were weighed again and total fluid and sucrose intake were calculated as g/kg of body weight. Sucrose preference was calculated as follows: sucrose preference=(sucrose intake/total fluid intake)x100.

5.2.5 Neuropathology

All neuropathological studies were conducted as previously described (Singaraja et al., 2011; Southwell et al., 2013). To determine brain, cerebellum, and forebrain weight and all volumetric measurements mice were anesthetized by intraperitoneal injection of 2.5% avertin and then intracardially perfused with ice-cold 4% paraformaldehyde. The brains were harvested and post-fixed in 4% paraformaldehyde for 24 hours at 4°, and then cryopreserved in 30% sucrose in PBS. To determine the brain weight the olfactory bulbs and brain stem were removed prior to weighing. The cerebellum was then removed and weighed on its own. Forebrain weight was calculated as brain weight minus the cerebellum weight. The forebrain was then flash frozen on dry ice, mounted with Tissue-TEK O.C.T. compound (Sakura), and sectioned coronally on the cryostat (Microm HM 500 M) into 25 uM free-floating sections. Sections were stored until immunohistochemical processing in PBS with 0.08% sodium azide.

A series of 25 uM sections spaced 200 uM apart spanning the striatum were processed for stereological volumetric assessments by staining with NeuN antibody overnight at room temperature to stain all neurons. Sections were then stained with biotinylated anti-mouse antibody and the signal was amplified using the ABC Elite kit (Vector Laboratories) and was detected with diaminobenzidine (Thermo Scientific). The StereoInvestigator software (Microbrightfield) was used to determine striatal, cortical, and corpus callosum volumes by tracing the perimeter of the desired structures and volumes were determined using the Cavalieri principle.

5.2.6 Electrophysiology

Mice were transferred to UBC's Animal Research Unit approximately 4-5 weeks following the TM injections and all electrophysiological experiments were carried out on mice that were approximately three months old. Briefly, mice were anesthetized with isofluorane and brains were quickly removed and immediately placed in an ice-cold cutting solution that contained (mM): 125 NaCl, 2.5 KCl, 25 $NaHCO_3$, 1.25 NaH_2PO4, 2.5 $MgCl_2$, 0.5 $CaCl_2$, and 10 glucose. Coronal blocks

containing the striatum or horizontal blocks containing the hippocampus were then cut on a vibratome (Leica VT1200S) at 400 μm. The striatal sections were transferred to artificial cerebrospinal fluid (ACSF), which was the same as the cutting solution with the exception of 1 mM $MgCl_2$ and 2 mM $CaCl_2$, and were heated to approximately 32°C for 30-45 minutes. For the hippocampus, sections were initially transferred to a recovery solution immediately following sectioning. The recovery solution consisted of (mM): 120 N-methyl-D-glucamine, 2.5 KCl, 1.2 NaH_2PO_4, 25 $NaHCO_3$, 1 $CaCl_2$, 7 $MgCl_2$, 2.4 sodium pyruvate, 1.3 sodium ascorbate, 2 Glucose (Rungta et al., 2013; Zhao et al., 2011). After 10 minutes at 32°C, hippocampal sections were then transferred to room temperature ACSF and allowed an additional 60 minutes to recover. We found that this 10 minute incubation in the recovery solution dramatically improved cell health and longevity in the CA1 region.

Following recovery, slices were transferred to a recording chamber with ACSF perfused at a rate of 2-3 ml/min. In striatal sections, spiny projection neurons in the dorsal striatum were targeted for recording (Milnerwood et al., 2013). In hippocampal sections, pyramidal neurons in CA1 were targeted based on their distinct morphological appearance. For miniature excitatory postsynaptic current (mEPSC) recordings, picrotoxin (50 μM) and tetrodotoxin (0.5 mM) were added to the ACSF. For miniature inhibitory postsynaptic currents (mIPSC) recordings, 6,7-dinitroquinoxaline-2,3-dione (DNQX; 10 μM) and tetrodotoxin (0.5 mM) were added to the ACSF. Glass pipettes (3-6 MΩ) were filled with a potassium gluconate (KGlu) internal solution for mEPSC recordings (Parsons et al., 2013). Liquid junction potential (theoretical = -15.6 mV) was left uncorrected. The internal solution used for mIPSC recording consisted of (mM): 145 CsCl, 1 $MgCl_2$, 10 HEPES, 1 EGTA, 2 MgATP, 0.5 Na_2GTP. Voltage clamp recordings were performed at a holding potential of -70 mV and both mEPSCs and mIPSCs were filtered at 1kHz and digitized at 20kHz. For EPSC recordings in the striatum, TTX was omitted as we have previously shown that the large majority of EPSCs in our coronal slice preparation are action potential-independent (Kolodziejczyk et al., 2014). Though, while largely action-potential independent,

these are referred to as spontaneous EPSCs (sEPSCs) in the manuscript to indicate the lack of TTX. Where applicable, glutamate release was evoked by an ACSF-filled glass pipette (1 MΩ) placed 200-250 μm dorsal to the recorded cell. Paired pulse ratios (PPR) were obtained at a -70 mV holding voltage and various inter-pulse intervals were applied with a stimulus intensity known to generate a response approximately 30-40% of the maximal response. Basic membrane properties were obtained within 60 seconds following break-in by monitoring the current response to a 10 mV voltage step applied in the membrane test feature in Clampex 10. All electrophysiological recordings were acquired and analyzed using the pClamp 10 software bundle.

5.2.7 Statistics

Data were analyzed by the Student's t-test, one-way ANOVA, or 2-way ANOVA as indicated using Prism 5 software. Error bars are in standard error of the mean.

5.3 RESULTS

5.3.1 Generation of post-development *Hip14* deficient mice

To generate *Hip14* "conditional knockout" mice exon 2 was selected as the conditional deletion region (Figure 5.1), as deletion of this region leads to a frameshift mutation and multiple premature stop codons (Figure 5.1E). A gene targeting strategy was used to generate $Hip14^{F/F}$ mice that could be crossed to any Cre recombinase expressing mice to delete *Hip14* in a tissue or temporal specific way (Figure 5.1).

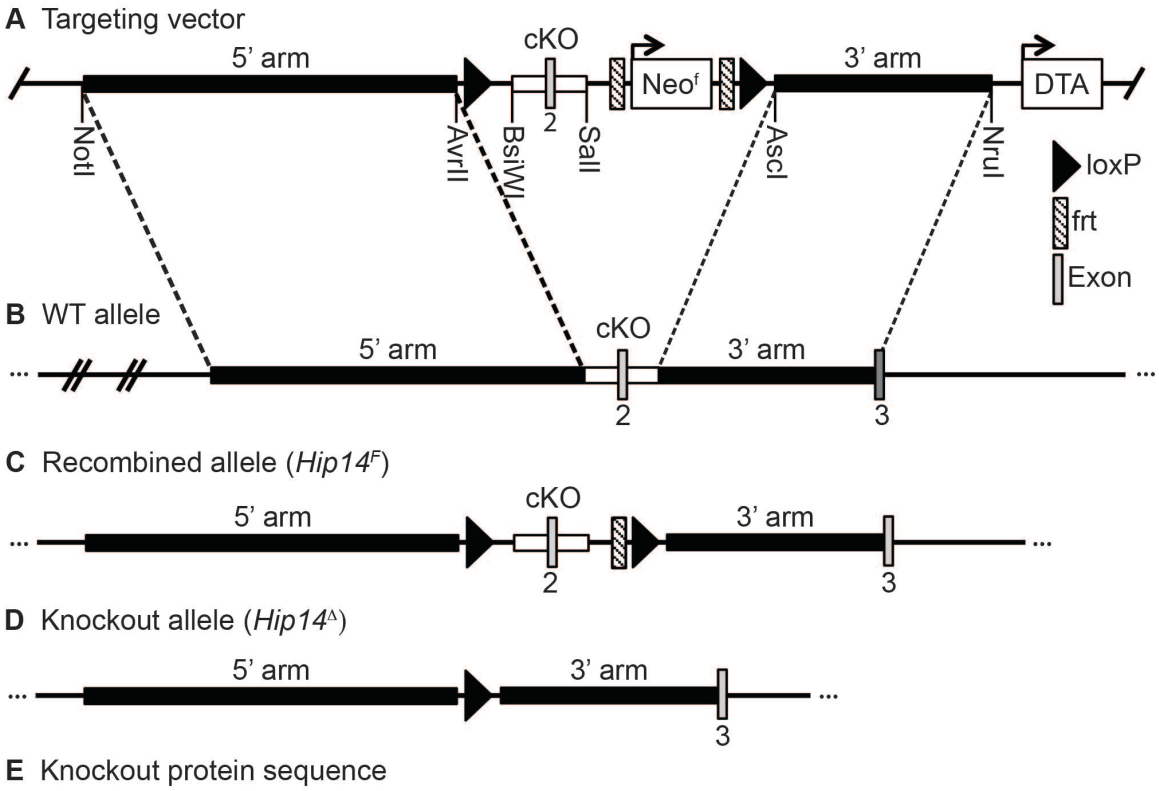

Figure 5.1: Generation of *Hip14* conditional knockout mice. The targeting vector that was used is shown in **A**. It was generated using PCR cloning of the 5' and 3' homolgy arms (5.5 and 3.2 kbp, respectively) and the deletion region (cKO) with the indicated restriction enzyme sites added by PCR and used for cloning into the targeting vector, such that loxP sites are oriented in the same direction up and downstream of the cKO region. The deletion region, in grey, includes exon 2 and upsteam and downstream intronic sequence to a total of 1.1 kbp. The targeting vector also includes a positive neomycin (Neo) selection cassette flanked by frt sites and a negative diptheria toxin A (DTA) selection cassette outside of the homolgy arms. The WT allele is showin in **B** with the 5' and 3' homolgy arms and the cKO region indicated. The recombined allele (*Hip14*^{F}) is shown in **C**. The Neo cassette was removed during embyronic cell culture after targeting by electroporation with flp recombinase and negative selection with G418. The knockout allele following expression of Cre recombinase is shown in **D** where recombination between the loxP sites occurs by the action of Cre leading to deletion of the cKO region, including exon 2, which leads to a frameshift mutaion (in orange) and multiple premature stop codons shown in **E**.

Hip14$^{F/F}$ mice were crossed to mice expressing Cre-ER^{T2} under the human ubiquitin ligase C promotor, a promotor that will result in ubiquitous Cre expression in all cell types (Ruzankina et al., 2007). The Cre-ER^{T2} transgene expresses Cre recombinase fused to a mutated form of the estrogen receptor that is not activated by estrogen but is activated by the estrogen analogue TM (Ruzankina et al., 2007). *Hip14* deletion was induced in *Hip14*$^{F/F}$;Cre+ mice at six weeks of age by TM treatment (*iHip14*$^{\Delta/\Delta}$ from here on). This time point was after any developmental peaks in HIP14 expression (data not shown) and allowed enough time for the mice to recover from any TM toxicity prior to behavior testing at three months of age.

mRNA and protein levels were assessed at 10-days post and six weeks post induction to assess deletion efficiency compared to the *Hip14*$^{F/F}$;Cre- TM control (*iHip14*$^{F/F}$ from here on). *Hip14* mRNA expression was decreased by >90% 10-days post TM treatment in the brain regions tested – the striatum, hippocampus, cortex, and cerebellum – and in the peripheral tissues tested – the spleen, liver, kidney and heart (Figure 5.2A). >90% loss of HIP14 protein was observed in the striatum, hippocampus, cerebellum, and cortex at 10-days post induction and >95% loss of HIP14 in the whole brain at six weeks post TM treatment (Figure 5.2B). These data indicate that deletion of HIP14 in *iHip14*$^{\Delta/\Delta}$ mice is >90% effective.

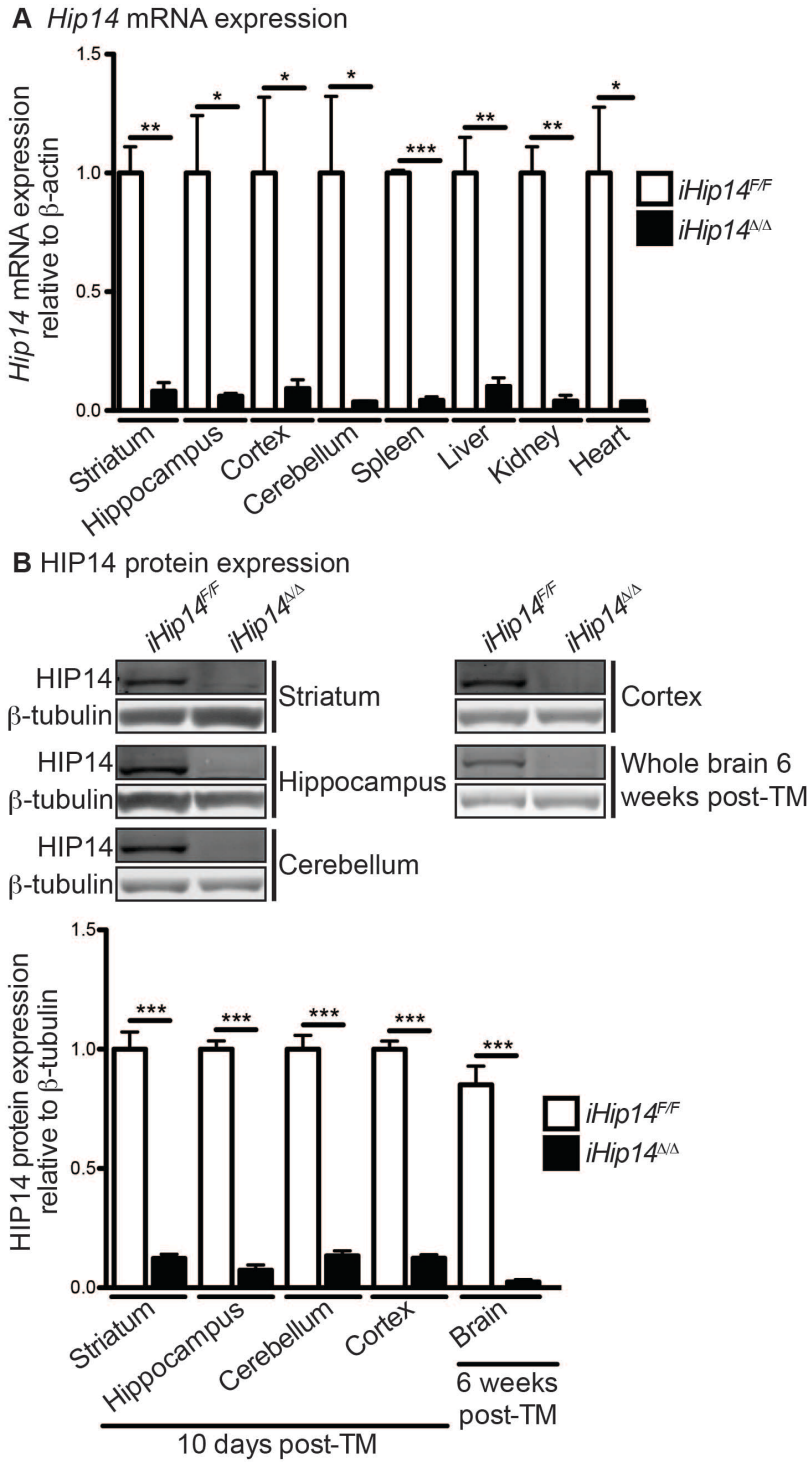

Figure 5.2: *Hip14* mRNA and protein expression is significantly reduced in *iHip14*$^{\Delta/\Delta}$ mice. The expression of *Hip14* mRNA in the striatum, hippocampus, cortex, cerebellum, spleen, liver, kidney, and heart *iHip14*$^{\Delta/\Delta}$ mice and in *iHip14*$^{F/F}$ control mice relative to β-actin is shown in **A** (N=3). There was a 90 percent or greater decrease in *Hip14* mRNA in *iHip14*$^{\Delta/\Delta}$ mice compared to control mice. (**B**) HIP14 protein expression in the striatum, hippocampus, cerebellum, and cortex from *iHip14*$^{\Delta/\Delta}$ and *iHip14*$^{F/F}$ mice, where the tissues were collected 10 days post-

TM treatment, is shown. Also shown is whole brain collected 6 weeks post-TM treatment from *iHip14*$^{\Delta/\Delta}$ and *iHip14*$^{F/F}$ mice. Whole cell lysate was run on western blot and probed with anti-HIP14 and anti-β-tubulin antibodies. The HIP14 immunoblot is the top panel in each set of images and the β-tubulin is in the bottom panel. The amount of HIP14 protein expressed is quantified in the graph relative to β-tubulin expression (N=2-10). A 90 percent or greater decrease in HIP14 was observed *iHip14*$^{\Delta/\Delta}$ mice. Data were analyzed using the Student's t-test. * p<0.05, ** p<0.01, *** p<0.0001.

5.3.2 Reduced survival, low body weight, and hyperactivity in *iHip14*$^{\Delta/\Delta}$ mice

To first assess the overall health of *iHip14*$^{\Delta/\Delta}$ mice, female and male mice were weighed at three months of age. Both female and male *iHip14*$^{\Delta/\Delta}$ mice are about 10% smaller than WT VEH and *iHip14*$^{F/F}$ control mice (Figure 5.3A and B, respectively).

As mice were being aged for longitudinal behavior studies, a dramatic decrease in survival of *iHip14*$^{\Delta/\Delta}$ mice beginning at about 16 weeks of age or 10 weeks post-*Hip14* deletion was observed (Figure 5.3C, dotted line). The same effect was observed when *Hip14* deletion was induced at six months of age instead of at six weeks of age (data not shown). Most of the time the mice appeared relatively healthy; i.e. not noticeably smaller than their littermate controls or with any signs of sickness, such as piloerection or hunched posture, and were suddenly found dead in their cage. A small number of mice (four or five) were found in the home cage with hind limb paralysis that in one case got progressively worse until the mouse was later found dead but, unfortunately, in this case constant monitoring was not possible.

Serendipitously, one *iHip14*$^{\Delta/\Delta}$ mouse was found in its cage almost completely paralyzed and was video monitored for a few minutes until had a seizure and died. Post-mortem examination of the bodies of *iHip14*$^{\Delta/\Delta}$ mice revealed signs of seizure including blood in the nostrils, hind legs sprawled behind the body, and clenched and bloody front paws. These data indicate that *iHip14*$^{\Delta/\Delta}$ mice have dramatically reduced survival due to a seizure disorder. A small proportion of *iHip14*$^{\Delta/\Delta}$ mice, 5-10%, survive past 20 weeks of age (2 in

total). One of these mice reached a humane endpoint at 43 weeks of age and had to be euthanized. At this time it weighed 30% less than its *iHip14*$^{F/F}$ littermate control. HIP14 protein levels in the brain were assessed to ensure sufficient gene deletion and almost no HIP14 protein was detected (data not shown).

In addition to the reduced body weight and survival, the *iHip14*$^{\Delta/\Delta}$ mice were hyper and reactive to handling. To begin to characterize this phenotype, spontaneous activity was assessed in the Med Associates spontaneous activity apparatus during the dark phase. *iHip14*$^{\Delta/\Delta}$ mice had increased distance travelled, ambulatory time, and ambulatory episodes (Figure 5.3D, E, and F, respectively). This increase in activity of *iHip14*$^{\Delta/\Delta}$ mice may explain the modest decrease in body weight observed in these mice.

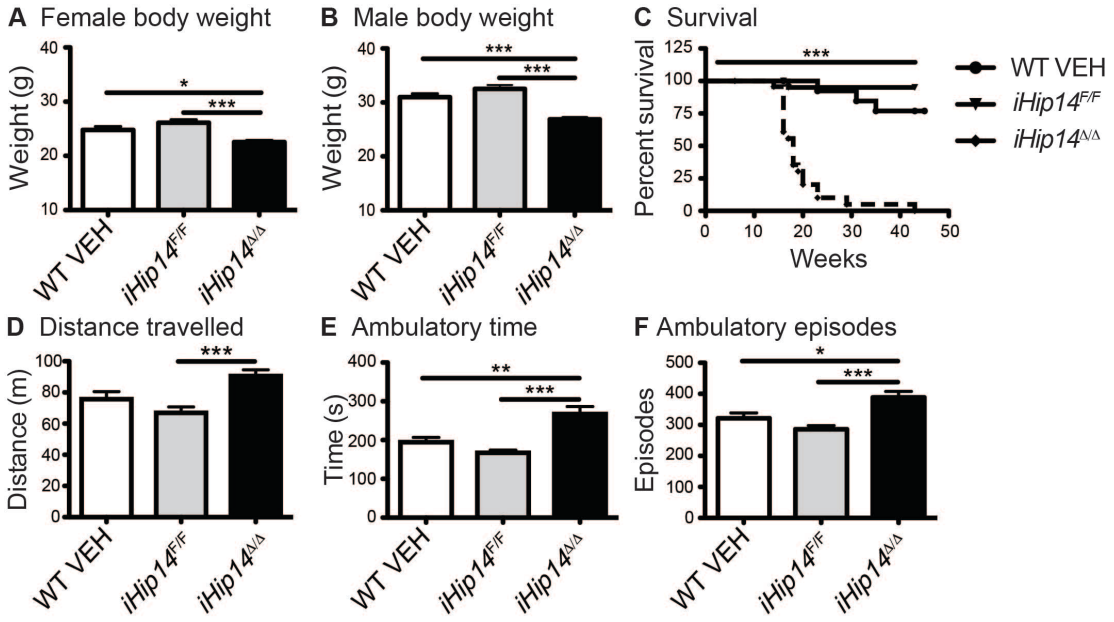

Figure 5.3: Decreased body weight and survival and hyperactivity in *iHip14*$^{\Delta/\Delta}$ mice. A 10% decrease in the body weight of three month old female (**A**) and male (**B**) *iHip14*$^{\Delta/\Delta}$ mice compared to WT VEH and *iHip14*$^{F/F}$ mice was observed (Females ANOVA: $F(2,55)=12.22$, $p<0.0001$; Males ANOVA: $F(2,59)=20.07$, $p<0.0001$; N=16-24). A dramatic reduction in survival (Log-rank test: $X^2(4)=93.76$; N=11-24) was observed in the *iHip14*$^{\Delta/\Delta}$ mice compared to WT VEH and *iHip14*$^{F/F}$ control mice (**C**). Spontaneous activity was assessed by infrared beam breaks during a 30 minute exploration at three months of age. Distance travelled (**D**), ambulatory time (**E**), and ambulatory episodes (**F**) were assessed. On all three measures the *iHip14*$^{\Delta/\Delta}$ mice were hyperactive compared to both controls (Distance travelled ANOVA: $F(2,45)=9.112$, $p=0.0005$; Ambulatory time ANOVA: $F(2,45)=13.50$, $p=<0.0001$; Ambulatory episodes ANOVA $F(2,45)=10.95$, $p=0.0001$; N=13-18). * $p<0.05$, *** $p<0.0001$.

5.3.3 Motor coordination and sensorimotor gating deficits in *iHip14*$^{\Delta/\Delta}$ mice

As both *Hip14*$^{-/-}$ and YAC128 mice have motor deficits, the motor coordination of *iHip14*$^{\Delta/\Delta}$ mice was tested on rotarod and climbing (Singaraja et al., 2011; Slow, 2003). During rotarod training at a fixed speed, *iHip14*$^{\Delta/\Delta}$ mice fell off the rotatod more and fell off sooner than control WT VEH and *iHip14*$^{F/F}$ mice (Figure 5.4A and B, respectively). On the fourth day mice were tested on the accelerating rotarod and latency to fall was measured. Compared to control mice, *iHip14*$^{\Delta/\Delta}$ mice fell off sooner (Figure 5.4B).

As rotarod is a trained test where mice learn to stay on the rotarod, it is less sensitive to basal ganglia motor dysfunction than the spontaneous test of

motor coordination, climbing (Hickey et al., 2008; Southwell et al., 2009). As YAC128 mice have a climbing deficit (Southwell and Patterson, 2011), *iHip14*$^{\Delta/\Delta}$ mice were tested on climbing. There was a dramatic reduction in the number of climbing events in these mice (Figure 5.4C) but there was no change in the number of rearing events, which is indicative of motivation to explore the apparatus (Figure 5.4D).

PPI is a test of sensorimotor gating and does not involve learning. When a quieter tone (the pre-pulse) is played prior to a loud stimulus (the startle pulse) mice will startle less than they would to the loud startle stimulus alone (Van Raamsdonk, 2005b) and thus PPI tests motor inhibition or sensorimotor gating, which is thought to be mediated by the striatum (Mink, 1996; Slow, 2003). As YAC128 mice and *Hip14*$^{-/-}$ mice have PPI deficits, the *iHip14*$^{\Delta/\Delta}$ mice were tested as well (Singaraja et al., 2011; Van Raamsdonk, 2005b). PPI deficits were observed in the *iHip14*$^{\Delta/\Delta}$ mice at all pre-pulse levels indicating a sensorimotor gating deficit (Figure 5.4E).

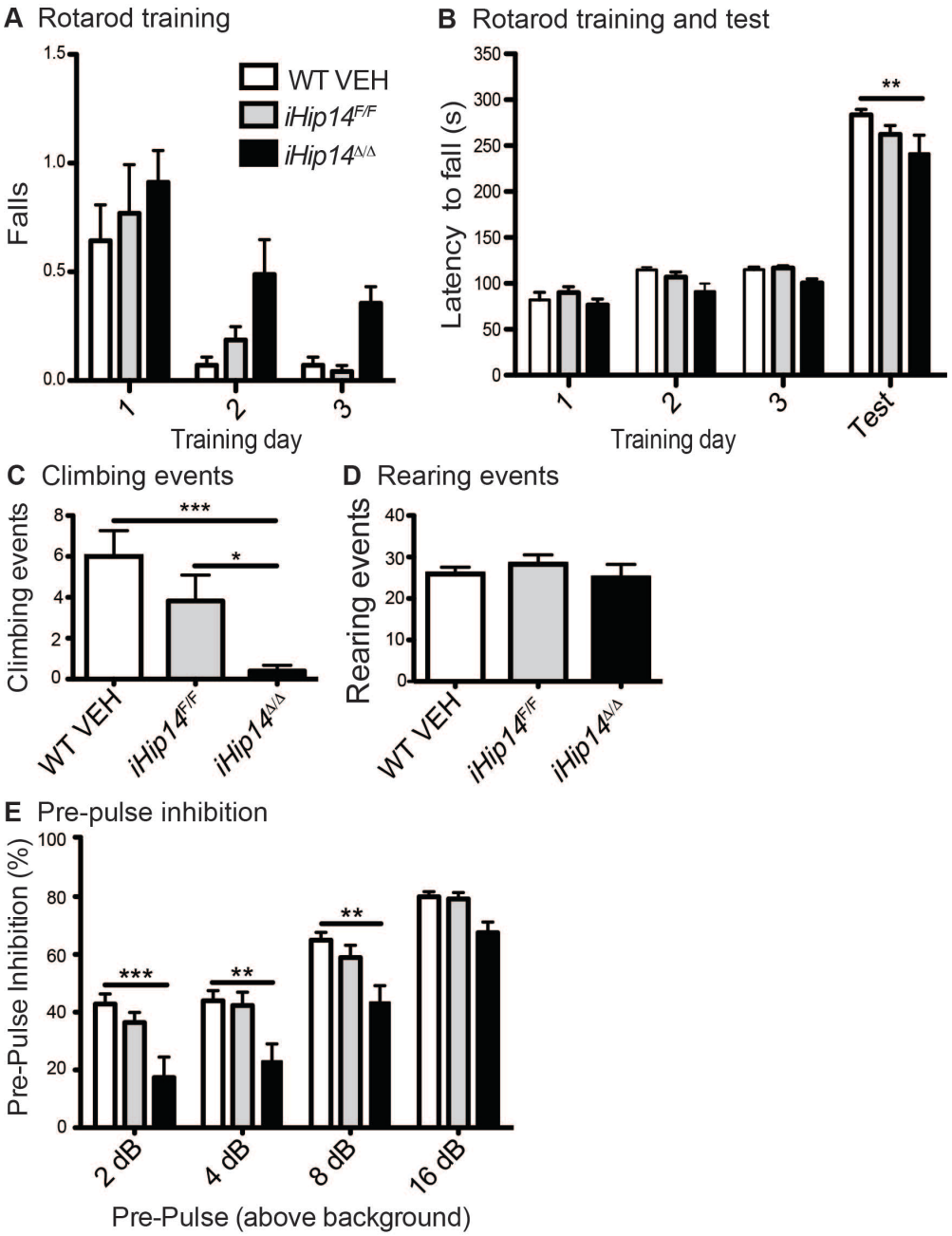

Figure 5.4: Motor coordination and sensorimotor gating deficits in *iHip14*$^{\Delta/\Delta}$ mice. Over three consecutive days three month old mice were trained on a fixed speed rotarod and tested on an accelerating rotarod on the fourth day. The number of falls (**A**) and the latency to the first fall (**B**) were recorded. *iHip14*$^{\Delta/\Delta}$ mice fell off the rotarod more (**A**; 2-way ANOVA: genotype $F(2)=5.46$, $p=0.0053$; training day $F(2)=21.26$, $p<0.0001$; interaction $F(4)=0.2534$, $p=0.9071$; N=14-16) and sooner (**B**; 2-way ANOVA: genotype $F(2)=7.32$, $p=0.0009$; training day $F(3)=299.4$, $p<0.0001$, interaction $F(6)=0.9541$, $p=0.4581$; N=14-16) both during training and during testing. Three month old mice were allowed to freely explore and climb a wire mesh container for five minutes and the number of times the mouse climbed (**C**) and reared (**D**) were recorded. *iHip14*$^{\Delta/\Delta}$ mice climbed fewer

times (**C**; ANOVA: $F(2,45)=8.130$, $p=0.001$; N=13-18) but did not rear less (**D**; ANOVA: $F(2,45)=0.43$, $p=0.65$; N=13-18) compared to control mice. Pre-pule inhibition (PPI) was measured as the percentage of decrease in the amount of startle with a prepulse compared to the amount of startle without a prepulse. Three month old *iHip14*$^{\Delta/\Delta}$ mice had a PPI deficit compared to controls (**E**; 2-way ANOVA: genotype $F(2)=24.77$, $p<0.0001$; pre-pulse $F(3)=67.70$, $p<0.0001$; N=15-18). * $p<0.05$, ** $p<0.01$, *** $p<0.0001$.

5.3.4 *iHip14*$^{\Delta/\Delta}$ mice display increased escape response and anhedonia

Since YAC128 mice and patients have anxiety and depression and the *iHip14*$^{\Delta/\Delta}$ mice are hyper and reactive to handling, psychiatric endpoints were assessed (Pouladi et al., 2008; Southwell et al., 2009). Anxiety-like behavior was assessed in the open field where mice are placed in a large, brightly lit box. A more anxious mouse will spend less time in the center of the open field (Southwell et al., 2009). Although *iHip14*$^{\Delta/\Delta}$ mice explored the open field apparatus to the same extent as the WT VEH and *iHip14*$^{F/F}$ control mice as measured by distance travelled (Figure 5.5A) they made fewer entries into the center of the open field (Figure 5.5B). This suggests anxiety-like behavior in *iHip14*$^{\Delta/\Delta}$ mice.

To confirm that the *iHip14*$^{\Delta/\Delta}$ mice indeed have anxiety, the mice were also tested on the EPM test of anxiety. In this test mice are placed in the center of a plus maze that is high off the ground and has two open arms and two closed arms. A more anxious mouse will spend less time in the open arms of the EPM (Kordasiewicz et al., 2012; Southwell et al., 2013). Surprisingly, the *iHip14*$^{\Delta/\Delta}$ mice spent more in the open arms of the EPM and dipped their heads off the edge of the open arms more than the control WT VEH and *iHip14*$^{F/F}$ mice (Figure 5.5D and E, respectively. The *iHip14*$^{\Delta/\Delta}$ mice did not explore the EPM as much as the control mice (Figure 5.5C), likely due to the fact that they spend more of their time dipping their head off the edge of the open arms of the maze. These data contradict the open field activity data described above and indicate an anxiolytic phenotype instead of anxiety-like phenotype. The other possible interpretation of this phenotype is that in both cases the *iHip14*$^{\Delta/\Delta}$ mice are trying to escape the apparatus and are in fact not anxious at all, i.e. they are spending more time exploring the edges of the open field box trying to find a way out and

on the EPM they are dipping their heads off the open arms trying to escape the maze. This explanation would also be consistent with their reactivity to handling.

To determine if the *iHip14*$^{\Delta/\Delta}$ mice have an anxiety-like phenotype, a modified light-dark box test was designed that completely removed any possibility of escape. Mice were placed in a completely enclosed apparatus where one side was dark and the other side was brightly lit. Mice were able to move freely between the two sides through a small door. If a mouse is anxious it will spend less time on the light side (light box) and more time in the dark. The *iHip14*$^{\Delta/\Delta}$ mice spent the same amount of time in the light box as the control WT VEH and *iHip14*$^{F/F}$ mice (Figure 5.5F). These data indicate that the *iHip14*$^{\Delta/\Delta}$ mice are not anxious and suggest that their behavior in the open field and EPM is indeed an increase in escape response-like behavior.

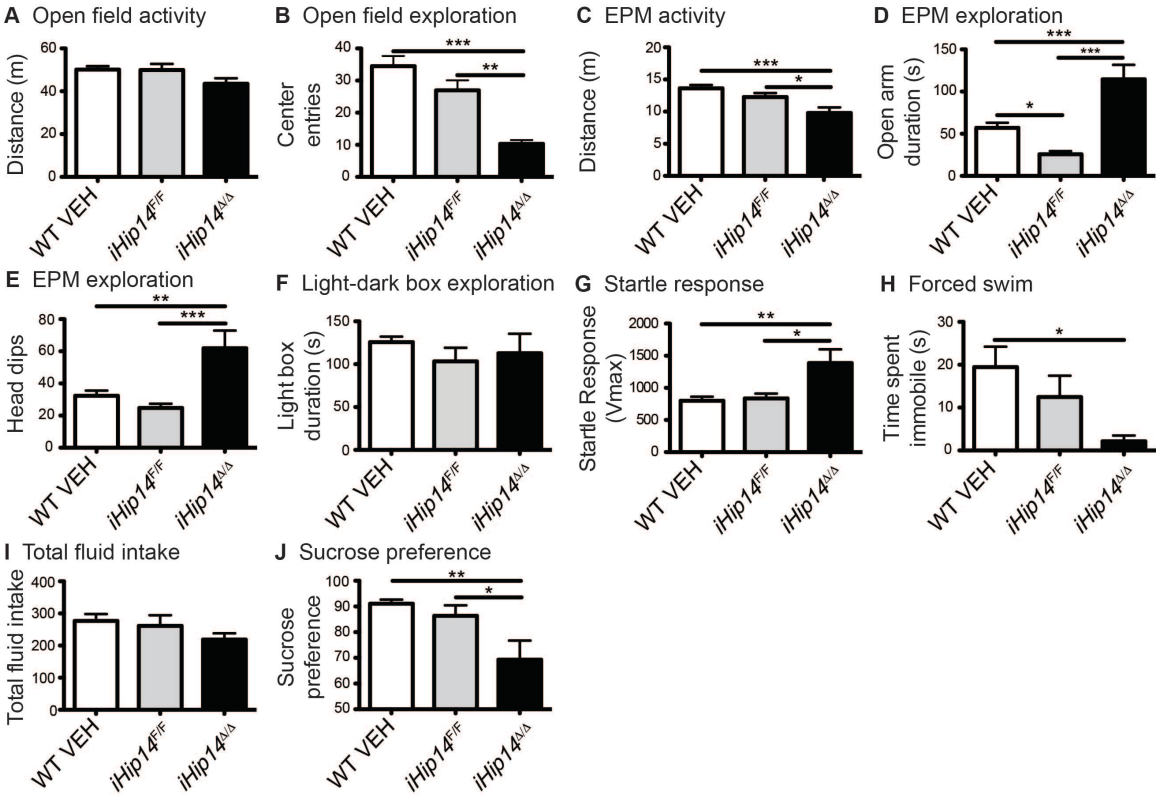

Figure 5.5: Three month old *iHip14*$^{\Delta/\Delta}$ mice have increased escape response and display anhedonic-like behavior. Mice were placed in an open field under bright lighting for 10 minutes and allowed to freely explore. Exploration was recorded by a ceiling-mounted video camera and the animal's movement was scored by Ethovision XT7 software. *iHip14*$^{\Delta/\Delta}$ mice explored the field to the same extent as the control mice as measured by distance travelled (**A**; ANOVA: $F(2,47)=2.607$, $p=0.0844$; N=24-25) but made fewer entries into the center of the open field (**B**; ANOVA: $F(2,47)=11.81$, $p<0.0001$; N=24-25). *iHip14*$^{\Delta/\Delta}$ mice explored the elevated plus maze less than controls over a five minute exploration, where mice were allowed to freely explore the maze and were tracked by Ethovision XT7 software (**C**; ANOVA: $F(2,86)=7.911$, $p=0.0007$; N=25-34). *iHip14*$^{\Delta/\Delta}$ mice also spent more time in the open arms of the maze (**D**; ANOVA: $F(2,86)=22.23$, $p<0.0001$; N=25-34) and more time dipping their heads of the edge of the open arms (**E**; $F(2,84)=10.09$, $p=0.0001$; N=25-34). Mice were placed in a box with a brightly lit side and a dark side and allowed to freely explore for five minutes and time spent in the light side of the light-dark box was measured. *iHip14*$^{\Delta/\Delta}$ mice spent the same amount of the time in the light box as the control mice (**F**; ANOVA: $F(2,39)=0.56$, $p=0.58$; N=13-16)**.** Mice were subjected to a 40 ms 120 dB stimulus and startle response was measured as the average Vmax over six trials. *iHip14*$^{\Delta/\Delta}$ mice startled significantly more than control mice did (**G**; ANOVA: $F(2,47)=6.52$, $p=0.0032$; N=15-18). *iHip14*$^{\Delta/\Delta}$ mice spent significant less time immobile in the forced swim test where mice were placed in a beaker of water for six minutes and the time spent immobile was recorded during the last five minutes (**H**; ANOVA: $F(2,48)=3.889$, $p=0.0272$; N=15-19). Mice were allowed free access to a 2% sucrose solution and water over a 24-hour period and the

total fluid consumption (g/kg of body weight; **I**) and sucrose preference (**J**), measured as the percentage of sucrose intake of the total fluid consumption (per kg of body weight), were measured. *iHip14*$^{\Delta/\Delta}$ mice had no change in total fluid intake (ANOVA: $F(2,42)=1.37$, $p=0.27$; N=14-16) but had decreased preference for the sucrose solution (ANOVA: $F(2,42)=5.68$, $p=0.0066$; N=14-16). * $p<0.05$, ** $p<0.01$, *** $p<0.0001$.

To quantify the hyper, reactive phenotype of the *iHip14*$^{\Delta/\Delta}$ mice, their startle response was assessed. Mice were placed in a startle chamber and subjected to a startle stimulus of 120 dB and their response was measured. Indeed, *iHip14*$^{\Delta/\Delta}$ mice startled to a much greater extent, about twice as much, as the control WT VEH and *iHip14*$^{F/F}$ mice (Figure 5.5G). This is consistent with these mice being more reactive to handling and testing.

Since YAC128 mice exhibit depressive-like phenotypes, the *iHip14*$^{\Delta/\Delta}$ mice were tested on the Porsolt forced swim test of depression (Porsolt et al., 1977a; 1977b; Pouladi et al., 2008). In this test mice are placed in a beaker of water and the time spent immobile is assessed as a measure of depressive-like behavior. A depressed mouse will spend more time immobile and reversal of this endpoint is highly correlated with antidepressant affects of drugs in humans (Porsolt et al., 1977a; 1977b). Interestingly, *iHip14*$^{\Delta/\Delta}$ mice spend dramatically less time immobile on the forced swim test (Figure 5.5H). This response is likely due to the mice continually trying to escape the maze, as in the open field and on the EPM, rather than an anti-depressant affect.

To separate out escape response and depressive-like behavior, the *iHip14*$^{\Delta/\Delta}$ mice were tested on sucrose preference test. This is a test of anhedonia-like behaviors (the inability to experience pleasure) and anhedonia is a major symptom of depression (Willner et al., 1987). Indeed, the YAC128 mice also display anhedonia (Pouladi et al., 2008). This test is done in the home cage where the exposure to an experimenter and novel testing apparatus are removed, which should eliminate any escape-response. The mice are given *ad libitum* access to water and a 2% sucrose solution and the amount of water and sucrose consumed is measured after 24 hours. The *iHip14*$^{\Delta/\Delta}$ mice consumed the same total fluid as control mice (Figure 5.5I) but had a decreased preference for

sucrose than control mice (Figure 5.5J). These data indicate that the *iHip14*$^{\Delta/\Delta}$ mice have anhedonia, suggesting a depressive-like phenotype.

5.3.5 Increased forebrain weight, increased cortical volume, and decreased corpus callosum volume in *iHip14*$^{\Delta/\Delta}$ mice

Since both *Hip14*$^{-/-}$ and YAC128 mice have selective striatal and cortical atrophy and loss of white matter (Carroll et al., 2011; Singaraja et al., 2011; Slow, 2003; Van Raamsdonk, 2005b), similar neuropathological endpoints were assessed in the *iHip14*$^{\Delta/\Delta}$ mice. In contrast, increased brain and forebrain weight and no change in cerebellar weight were observed in the *iHip14*$^{\Delta/\Delta}$ mice (Figure 5.6A, C, and B, respectively). Also unexpectedly, there was no change in striatal volume in the *iHip14*$^{\Delta/\Delta}$ mice compared to WT VEH and *iHip14*$^{F/F}$ controls (Figure 5.6D) but there was an increase in cortical volume in *iHip14*$^{\Delta/\Delta}$ mice (Figure 5.6E). As in the YAC128 mice and the *Hip14*$^{-/-}$ mice, *iHip14*$^{\Delta/\Delta}$ mice had a loss of white matter, indicated by decreased corpus callosum volume (Figure 5.6F).

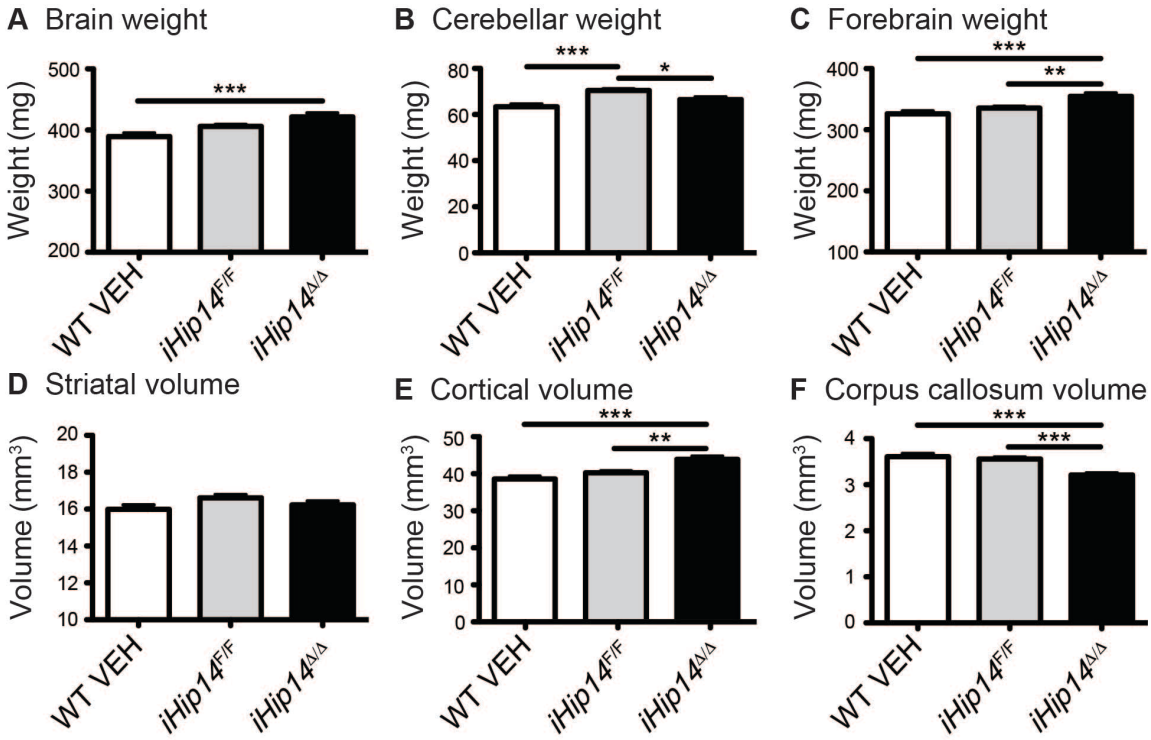

Figure 5.6: Three month old *iHip14*$^{\Delta/\Delta}$ mice have increased brain and forebrain weight, increased cortical volume, and decreased corpus callosum volume. Mice were cardiac perfused with 4% paraformaldehyde and the brains were removed and weighed. *iHip14*$^{\Delta/\Delta}$ mice have increased brain weight compared to control mice (**A**; ANOVA: $F(2,44)=9.38$, $p=0.0004$; N=13-18), unchanged cerebellum weight (**B**; ANOVA: $F(4,64)=10.13$, $p<0.0001$; N=12-18), and larger forebrain weight (**C**; ANOVA: $F(2,44)=10.46$, $p=0.0002$; N=13-18). Brains were then sectioned and stained with NeuN to stain neurons and striatal (**D**), cortical (**E**), and corpus callosum (**F**) volume was determined. No change in striatal volume was observed (**D**; ANOVA: $F(2,59)=0.86$, $p=0.43$; N=18-23) in *iHip14*$^{\Delta/\Delta}$ mice but there was a significant increase in cortical volume (**E**; ANOVA: $F(2,44)=12.55$, $p<0.0001$; N=13-18) and decrease in corpus callosum volume (**F**; ANOVA: $F(2,44)=13.56$, $p<0.0001$; N=13-18). * $p<0.05$, ** $p<0.01$, *** $p<0.0001$.

5.3.6 *iHip14*$^{\Delta/\Delta}$ MSNs have increased paired pulse ratios and reduced frequency but increased amplitude of spontaneous excitatory transmission to MSNs

Since striatal physiology is altered in the YAC128 and *Hip14*$^{-/-}$ mice, the synaptic properties of MSNs in the striatum, the most vulnerable cell type in HD, were examined (Milnerwood and Raymond, 2010; Milnerwood et al., 2013; 2010; Raymond et al., 2011). Current- and voltage-clamp recordings were performed on MSNs in the dorsal striatum to measure basic membrane properties and synaptic currents. There was no significant effect of loss of *Hip14* on membrane

capacitance, suggesting no change in the surface area of individual MSNs and consistent with the lack of gross volume changes in the striatum (Figure 5.6D). Similarly, we observed no significant effect on the amount of injected current required to initiate action potential firing (rheobase) or the resting membrane potential in *iHip14*$^{\Delta/\Delta}$ MSNs (Figure 5.7B, C, and D, respectively). These data indicate that there is no change in membrane excitability or surface area in *iHip14*$^{\Delta/\Delta}$ MSNs.

To assay excitatory synaptic function, AMPAR-mediated spontaneous postsynaptic currents (sEPSCs) were recorded from MSNs held at -70 mV in the presence of picrotoxin, a $GABA_A$ antagonist. There was a significant decrease in sEPSC frequency in *iHip14*$^{\Delta/\Delta}$ MSNs (Figure 5.7H) as well as a significant increase in sEPSC amplitude (Figure 5.7I) compared to MSNs from both WT VEH and *iHip14*$^{F/F}$ mice. These data demonstrate a significant synaptic dysfunction in *iHip14*$^{\Delta/\Delta}$ mice and suggest a reduction in the number of excitatory synapses and/or a reduction in transmitter release probability. Despite this reduction on frequency, the observed sEPSC amplitude was increased, suggesting additional AMPARs at these synapses.

To assess transmitter release probability from cortical afferents onto MSNs in the striatum, a stimulating electrode was placed 200-250 um dorsal to the recorded cell and various inter-pulse intervals were applied and the PPR was calculated by dividing the peak current of the second response to that of the first. MSNs from *iHip14*$^{\Delta/\Delta}$ mice had increased PPRs compared to MSNs from WT VEH or *iHip14*$^{F/F}$ mice (Figure 5.7F). These data are indicative of a lower probability of transmitter release and are consistent with the reduction in sEPSC frequency.

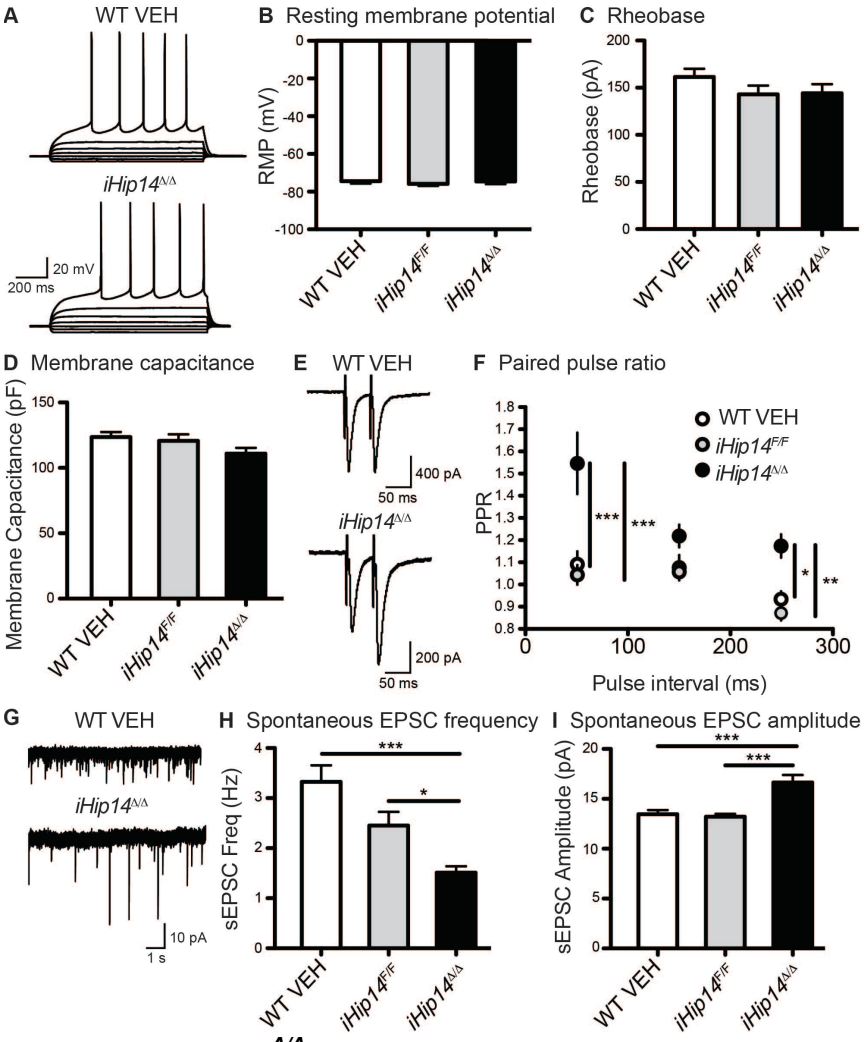

Figure 5.7: *iHip14*$^{\Delta/\Delta}$ MSNs have impaired paired pulse ratios and decreased frequency and increased amplitude of sEPSCs. MSNs in the central dorsal striatum were whole-cell patch clamped in acute coronal slices from three month old mice. A representative trace of current-clamp membrane potential responses to a series of current injections (from -100 pA to 200 pA in 50 pA increments) is shown in (**A**). *iHip14*$^{\Delta/\Delta}$ MSNs had the same resting membrane potential (RMP) (**B**: ANOVA: $F(2,66)=0.39$, $p=0.68$; N=21-25), fired at same rheobase current (**C**; ANOVA: $F(2,65)=1.216$, $p=0.30$; N=21-25), and had the same membrane capacitance (**D**; ANOVA: $F(2,107)=2.41$, $p=0.094$; N=31-43). *iHip14*$^{\Delta/\Delta}$ mice had increased paired pulse ratios (**F**; 2-way ANOVA: genotype $F(2)=12.94$, $p=0.0001$; pulse interval $F(2)=20.51$, $p<0.0001$; interaction $F(4)=4.276$, $p=0.0047$; N=8-10), representative traces are shown in (**E**). *iHip14*$^{\Delta/\Delta}$ mice had decreased frequency (**H**; ANOVA: $F(2,60)=13.50$, $p<0.0001$; N=19-23) but increased amplitude (**I**; ANOVA: $F(2,60)= 12.79$, $p<0.0001$; N=19-23) of spontaneous excitatory postsynaptic currents (sEPSCs), representative traces are shown in (**G**). * $p<0.05$, ** $p<0.01$, *** $p<0.0001$.

5.3.7 *iHip14*$^{\Delta/\Delta}$ CA1 hippocampal neurons have increased amplitude of miniature excitatory transmission

As a reduction in excitatory transmitter release is not consistent with the epileptic phenotype, we then asked whether these same synaptic abnormalities can be observed in the hippocampus, an area of the brain highly associated with the underlying neurobiology of epilepsy (Ben-Ari and Cossart, 2000). As with MSNs, current- and voltage-clamp recordings were performed on CA1 pyramidal neurons. Despite a trend of a depolarized resting membrane potential in CA1 neurons from *iHip14*$^{\Delta/\Delta}$ mice, this was not significant in the one-way ANOVA (Figure 5.8B). Similarly, there was no significant difference in the current-voltage (I-V) relationship (Figure 5.8C), membrane capacitance, or resistance in *iHip14*$^{\Delta/\Delta}$ CA1 pyramidal neurons (data not shown). Thus, the basic membrane properties of CA1 pyramidal neurons are largely normal in *iHip14*$^{\Delta/\Delta}$ mice.

To assay excitatory and inhibitory synaptic function of CA1 pyramidal neurons, AMPAR-mediated miniature postsynaptic currents (mEPSCs) in the presence of picrotoxin and tetrodotoxin were recorded (Figure 5.8D). GABAR-dependent miniature inhibitory postsynaptic currents in the presence of tetrodotoxin and DNQX, an AMPAR and kainite receptor antagonist, were also recorded (Figure 5.8G). As we saw with the striatum, there was a significant increase in the amplitude of mEPSCs recorded from CA1 pyramidal neurons in *iHip14*$^{\Delta/\Delta}$ mice (Figure 5.8F). Interestingly, the decreased frequency of EPSCs observed in the striatum was not evident in the hippocampus; rather, the mean mEPSC frequency was highest in CA1 pyramidal neurons from *iHip14*$^{\Delta/\Delta}$ mice, although this did not reach significance (Figure 5.8E). There was no change in either frequency or amplitude of mIPSCs in *iHip14*$^{\Delta/\Delta}$ CA1 pyramidal neurons (Figure 5.8H and I, respectively), although there was a general trend towards a lower frequency of inhibitory events in *iHip14*$^{\Delta/\Delta}$ animals. Together, these data suggest an imbalance between excitatory and inhibitory input to CA1 pyramidal neurons as a result of loss of *Hip14* in adulthood.

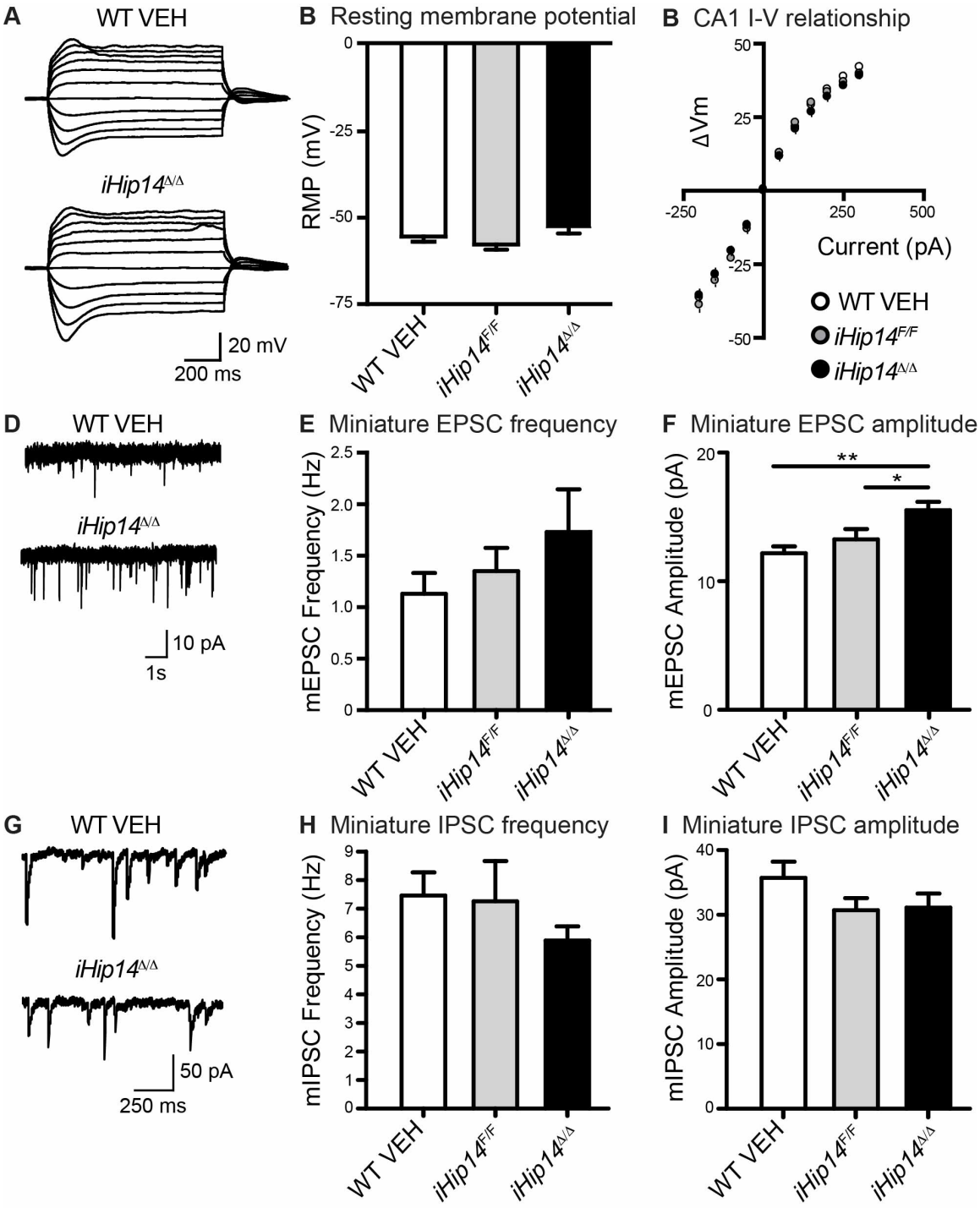

Figure 5.8: *iHip14*$^{\Delta/\Delta}$ CA1 pyramidal neurons have increased amplitude of mEPSCs. CA1 pyramindal neurons in the hippocampus were whole-cell patch clamped in acute coronal slices from three month old mice. A representative trace of current-clamp membrane potential responses to 50 pA current injection steps (from 200 pA to 300 pA) is shown in (**A**). *iHip14*$^{\Delta/\Delta}$ CA1 pyramidal neurons had the same resting membrane potential (RMP) (**B**: ANOVA: $F(2,46)=2.40$, $p=0.10$; N=15-17) and the same I-V relationship (**C**). *iHip14*$^{\Delta/\Delta}$ CA1 pyramidal neurons had the same frequency (**E**: ANOVA: $F(2,44)=0.96$, $p=0.39$; N=15-16)

but increased amplitude (**F**: ANOVA: $F(2,44)=6.47$, $p=0.0034$; N=15-16) of miniature excitatory postsynaptic currents (mEPSCs), representative traces are shown in (**D**). There was no significant change in miniature IPSC frequency (**H**: ANOVA: $F(2,34)=0.96$, $p=0.39$; N=10-15) or amplitude (**I**: ANOVA: $F(2,34)=1.64$, $p=0.21$; N=10-15) in *iHip14*$^{\Delta/\Delta}$ CA1 pyramidal neurons, representative traces are shown in (**G**). * $p<0.05$, ** $p<0.01$, *** $p<0.0001$.

5.4 DISCUSSION

The constitutive *Hip14* deficient mouse model has an HD-like phenotype but it is developmental and non-progressive unlike the adult-onset, progressive phenotype of the YAC128 mice (Singaraja et al., 2011; Slow, 2003; Van Raamsdonk, 2005b). Since altered HIP14 function will occur throughout the life of the animal in the presence of the HD mutation rather than just during development, we sought to determine the consequences of loss of *Hip14* in the adult animal. An inducible *Hip14* deficient mouse model was generated and *Hip14* deletion was induced in the young adult mouse. This is the first example of a "conditional knockout" of a DHHC PAT and the first evidence implicating PATs in a seizure disorder.

The *iHip14*$^{\Delta/\Delta}$ mice have a phenotype surprisingly different than that of the *Hip14*$^{-/-}$ mice (Table 5.1). These mice were expected to develop a progressive HD-like phenotype similar to the YAC128 mice. The most surprising phenotype is the progressive hind limb paralysis and seizure disorder resulting in dramatically reduced survival of the *iHip14*$^{\Delta/\Delta}$ mice. This was highly unexpected as there is no change in survival of the *Hip14*$^{-/-}$ mice or the YAC128 mice. The R6/2 mice have reduced survival but death due to a seizures was only reported to occur in a small subset of the mice that die (Mangiarini et al., 1996; Stack et al., 2005). HIP14 was shown to be dramatically less autopalmitoylated in the R6/2 mice (Rush et al., 2012) indicating that it is much less active. Thus, there may be some overlap in the survival phenotype of the *iHip14*$^{\Delta/\Delta}$ and the R6/2 mice.

The *iHip14*$^{\Delta/\Delta}$ mice have motor coordination deficits similar to HD mouse models and *Hip14*$^{-/-}$ mice on rotarod and climbing (Table 5.1). The deficits are pretty dramatic, particularily on the climbing test, and the limited time frame between induction of loss of *Hip14* and the onset of the seizure disorder

precluded longitudinal studies to determine if the motor coordination deficits would get progressively worse. Also similar to HD mouse models and the *Hip14*$^{-/-}$ mice (Singaraja et al., 2011; Van Raamsdonk, 2005b), *iHip14*$^{\Delta/\Delta}$ mice have sensoriomotor gating impairments (Table 5.1). As PPI tests the ability to inhibit an unwanted motor response to a stimulus and it is believed to be mediated by the striatum (Mink, 1996), impairment on this test suggests striatal pathology in the *iHip14*$^{\Delta/\Delta}$ mice.

The psychiatric phenotype of the *iHip14*$^{\Delta/\Delta}$ mice is not similar to HD mouse models but may also in fact suggest striatal dysfunction (Table 5.1). The psychiatric phenotype of the *Hip14*$^{-/-}$ mice was never studied (Singaraja et al., 2011). The YAC128 mouse model displays anxiety- and depressive-like behaviors (Pouladi et al., 2008; Southwell et al., 2009). The *iHip14*$^{\Delta/\Delta}$ mice are anhedonic as are the YAC128 mice (Pouladi et al., 2008), which is a symptom of depression, but when tested on the forced swim test of depression, the *iHip14*$^{\Delta/\Delta}$ mice appeared to have an anti-depressant like phenotype. When the anxiety phenotype of *iHip14*$^{\Delta/\Delta}$ mice was examined, contradictory results were obtained from the open field and EPM tests. The mice display an anxiety-like phenotype in the open field but an anxiolytic phenotype on the EPM. However, when these results are considered along with the forced swim results, the simplest interpretation is that all of these behaviors are due to an increase in escape response, ie the mice never stop trying to escape the forced swim and do not stop swimming, they continually search for an escape route in the open field by staying at the edges, and they try to find a way off the EPM by searching the open arms. Indeed, when tested in a modified light-dark box test that eliminated any avenues for escape the *iHip14*$^{\Delta/\Delta}$ mice did not show anxiety-like behaviors. Interestingly, rodents with striatal lesions display impaired escape response behavior (Kirkby and Kimble, 1968). Thus, these data may suggest striatal dysfunction.

The interpretation of these results as increased escape response behavior is not without precedence. When approached by a predator or put in a new environment wild rodents will exhibit a range of responses including

flight/escape, freezing, and defensive attack. Through domestication and inbreeding, laboratory rodents display significantly less intense defensive and escape responses when compared to wild mice (Holmes et al., 2000). Indeed, multiple studies have described an explosive response to testing situations in wild mice. In a study of wild mice on the EPM compared to inbred laboratory strains, wild mice displayed behavior very similar to the *iHip14*$^{\Delta/\Delta}$ mice, including increased time spent in the open arms (Holmes et al., 2000), that the authors described as a “high level of behavioral reactivity directed towards rapid escape from the apparatus” (Holmes et al., 2000).

Table 5.1: Similarities and differences between YAC128, *Hip14*$^{-/-}$, and *iHip14*$^{\Delta/\Delta}$ *mouse models.*

	HD models	***Hip14*$^{-/-}$** (Singaraja *et al*. 2011)	***iHip14*$^{\Delta/\Delta}$**
Survival	No change in YAC128, reduced survival in R6/2 (Slow et al. 2003; Mangiarini et al. 2006)	No change	90% reduced survival at 4 months of age
Motor function	Accelerating and fixed rotarod deficits from 6 months. Climbing deficits at 7 months (Southwell *et al.* 2009). Hyperactivity at 3 months followed by hypoactivity at 6 month (Slow et al. 2003)	Accelerating and fixed rotarod deficits Hyperactive at 3 months	Accelerating and fixed rotarod and climbing deficits at 3 months Hyperactive at 3 months
Sensorimotor gating	PPI deficits at 12 months (Van Raamsdonk et al. 2005)	PPI deficits	PPI deficits at 3 months
Psychiatric function	Anxiety and depression (Southwell et al. 2009; Pouladi et al. 2008)	---	Increased escape-response Anhedonia
Brain weight	5% decrease at 9 months (Slow *et al.* 2003)	8% decrease at 1 month	12% increase in brain and 13% increase in forebrain weight at 3 months
Striatal volume	3% decrease in volume at 3 months by MRI (Carroll *et al.* 2011)	17% decrease at E17.5 and later ages	No change
Other brain regions affected	Decrease in volume of cortex, thalamus, globus pallidus, corpus callosum, hippocampus unchanged (Carroll et al. 2011)	Decrease in volume of cortex, thalamus, globus pallidus, corpus callosum, cerebellum, hippocampus	Increase in volume of cortex and decrease in volume of corpus callosum, cerebellum unchanged

The *iHip14*$^{\Delta/\Delta}$ mice have increased brain and forebrain weights, which is in contrast to the decreased brain weight in the YAC128 and the *Hip14*$^{-/-}$ mice (Singaraja et al., 2011; Van Raamsdonk, 2005a) (Table 5.1). Also, although there is clear striatal dysfunction in *iHip14*$^{\Delta/\Delta}$ mice, there was no change in striatal volume, unlike the atrophy observed in the YAC128 and *Hip14*$^{-/-}$ mice (Carroll et al., 2011; Singaraja et al., 2011). This is likely because there is not enough time from loss of *Hip14* to seizure-induced death for striatal neuron death to occur. There was, however, a decrease in corpus callosum volume suggesting a decrease in white matter. This may indicate that some axonal degeneration is occurring, which may precede neuron death. Decreased corpus callosum volume occurs in both the YAC128 mice and the *Hip14*$^{-/-}$ mice (Carroll et al., 2011; Singaraja et al., 2011). In contrast, there is an increase in cortical volume in *iHip14*$^{\Delta/\Delta}$ mice, potentially due to a reactive gliosis response to neural injury.

Further evidence for striatal dysfunction was apparent in the physiology of MSNs. Although there is no change in membrane excitability or surface area in *iHip14*$^{\Delta/\Delta}$ MSNs, there was reduced frequency and increased amplitude of sEPSC amplitude and increased PPRs. These data are indicative of a lower probability of transmitter release and/or fewer synapses but, potentially, more AMPARs at the remaining synapses. These data demonstrate a significant synaptic dysfunction. The increase in sEPSC amplitude may instead suggest more glutamate released per vesicle to the same number of AMPARs. The striatal physiology in *iHip14*$^{\Delta/\Delta}$ MSNs is not the same as that in *Hip14*$^{-/-}$ and in HD mice. The *Hip14*$^{-/-}$ mice are very similar to HD mice in their striatal physiology (Milnerwood and Raymond, 2010; Milnerwood et al., 2013; Raymond et al., 2011). MSNs from HD mice have increased resting membrane potential and *Hip14*$^{-/-}$ and HD MSNs have decreased capacitance and increased rheobase (Milnerwood and Raymond, 2010; Milnerwood et al., 2013; Raymond et al., 2011) whereas there is no change in any of these parameters in the *iHip14*$^{\Delta/\Delta}$ MSNs. There is a decrease in sEPSC frequency in MSNs from all three mouse lines but sEPSC amplitude is decreased in HD and *Hip14*$^{-/-}$ MSNs (Milnerwood and Raymond, 2010; Milnerwood et al., 2013; Raymond et al., 2011) whereas it

is increased in *iHip14*$^{\Delta/\Delta}$ MSNs. Also, MSNs from all three mouse models display reduced release probability (Milnerwood and Raymond, 2010; Milnerwood et al., 2013; Raymond et al., 2011).

As a reduction in excitatory transmitter release is not consistent with the epileptic phenotype, synaptic function was assessed in the hippocampus. There was a trend of a depolarized resting membrane potential in CA1 neurons from *iHip14*$^{\Delta/\Delta}$ mice, which may suggest a hyperexcitability. There was also a significant increase in the amplitude of mEPSCs recorded from CA1 pyramidal neurons in *iHip14*$^{\Delta/\Delta}$ mice as with the MSNs but, interestingly, the decreased frequency of EPSCs observed in the striatum was not evident in the hippocampus. Instead there was a trend to an increase in the mean mEPSC frequency. There was also a general trend towards a lower frequency of inhibitory events in *iHip14*$^{\Delta/\Delta}$ animals. Together, these data suggest an imbalance between excitatory and inhibitory input to CA1 pyramidal neurons as a result of loss of *Hip14* in adulthood. Whether these alterations of synaptic function in the hippocampus contribute to the seizure phenotype remains to be seen.

The seizure disorder in *iHip14*$^{\Delta/\Delta}$ mice may be due, in part, to increased surface trafficking of AMPARs. Indeed, the physiology data suggests that there are more AMPARs at synapses. AMPAR subunits are palmitoylated at two sites, one in the TMD 2 site and the other in the C-terminal site. Loss of palmitoylation at either site will lead to increased synaptic expression of AMPARs (Hayashi et al., 2005). Thus if HIP14 palmitoylates the AMPAR subunits at either of these sites, loss of HIP14 would lead to increased synaptic AMPAR. Indeed, HIP14 is a PAT for GLUA1 and GLUA2 (Huang et al., 2009). *Glua2* mRNA is post-transcriptionally edited rendering GLUA2-containing receptors calcium impermeable. Interestingly, post-transtranscriptional editing deficient *GluA2* mice that express GLUA2 that is permeable to calcium develop progressively agitated states and eventually have multiple seizures and die (Brusa et al., 1995). Thus, the seizure disorder could be caused by an increase in synaptic AMPARs.

This is the first example of a “conditional knockout” of a DHHC PAT. This study implicates HIP14 as an essential gene for the maintenance of the adult mouse, which is not surprising considering that *Hip14* is the most highly conserved of all 23 human PATs (Young et al., 2012). This is also the first example of a PAT being implicated in a seizure disorder. The consequences of loss of *Hip14* in the adult mouse are very different than the consequences of loss of *Hip14* from conception. This suggests that there is a compensatory mechanism that occurs during development when *Hip14* is lost from conception that cannot occur when it is lost in the adult animal. This study does not rule out the possibility that HIP14 plays a role in the pathogenesis of HD, despite the fact that this mouse model does not develop an HD-like phenotype. In fact, this study shows that HIP14 is important for striatal function and is an essential gene that if dysfunctional in HD could have hugely detrimental consequences.

6 DISCUSSION AND CONCLUSIONS

6.1 OVERVIEW OF MAJOR FINDINGS

The overall goal of this thesis was to determine the role of palmitoylation in the pathogenesis of HD and provide further validation of palmitoylation as a potential drug target. The *Hip14*$^{-/-}$ and *Hip14l*$^{-/-}$ mouse models both of which have HD-like phenotypes resembling those of the YAC128 mouse model of HD provide the strongest evidence for a role of palmitoylation in HD (Singaraja et al., 2011; Sutton et al., 2013). The fact that wtHTT acts as a modulator of HIP14 activity and that the relationship between these two proteins goes beyond that of just enzyme-substrate provides suggests that this relationship may be very important (Huang et al., 2011). The overall hypothesis is that disturbed HIP14-HTT and HIP14L-HTT interaction in the presence of the HD mutation reduces HIP14, and potentially HIP14L, function leading to the under-palmitoylation and mislocalization of HTT and key HIP14 substrates.

The first specific aim of this thesis was to determine the interaction domain of HTT and HIP14 and HIP14L. This is important to guide future efforts to target and enhance this interaction to increase enzyme activity and remediate palmitoylation of HTT and their substrates. It is important to know if HIP14 and HIP14L interact with the same domain of HTT and, if so, if they compete for binding. A shared binding site would provide further support for the hypothesis that these two PATs are able to compensate for each other in palmitoylating HTT and that HTT may also modulate the activity of HIP14L. If they were to compete for binding, this would need to be taken into consideration when taking efforts to increase the interaction between HTT and one PAT or the other at the risk of decreasing the interaction with the other PAT. HIP14 has been previously shown to interact with HTT 1-548 (Huang et al., 2011). Here, amino (N)- and carboxy (C)-terminal deletions of HTT 1-548 were generated and their interaction with HIP14 and HIP14L was assessed to determine the location of the binding site. Putative multiple PAT binding sites were identified in HTT, one around amino acid 224 and another around amino acid 427, that are both required for full

interaction and all of the amino acids from 1-548 are required for the structural integrity and conformation of these binding sites. A common binding domain in HTT for HIP14 and HIP14L along with the fact that HIP14L's domain structure is virtually identical to HIP14, with all the same domains in the same orientation, suggests that HTT may also modulate the enzymatic activity of HIP14L (Young et al., 2012). These data provide evidence that these two PATs may compensate for each other in palmitoylating HTT and may compete for binding to HTT and other substrates.

The second specific aim of this thesis was to determine the effect of loss of *Hip14* and *Hip14l in vivo* and on HTT palmitoylation. The biological function of HTT palmitoylation and exactly what role loss of HTT palmitoylation plays in the pathogenesis of HD are unknown. To answer these questions and to determine if HIP14 and HIP14L are in fact the only two PATs for HTT, the *Hip14*$^{-/-}$ and *Hip14l*$^{-/-}$ mouse models were intercrossed to generate mice deficient for both *Hip14* and *Hip14l* genes. Loss of both *Hip14* and *Hip14l* leads to embryonic lethality between E10 and E11 *in utero* due to failed chorioallantoic fusion leading to failure in placental formation. Intriguingly, the extraembryonic tissue of the *Hip14*$^{-/-}$;*Hip14l*$^{-/-}$ embryos share many features with that of the *Htt*$^{-/-}$ embryos. There are two possible mechanisms underlying the observed similarity in phenotypes between *Hip14*$^{-/-}$;*Hip14l*$^{-/-}$ and *Htt*$^{-/-}$ mice: loss of HIP14/HIP14L function leading to decreased substrate palmitoylation or loss of HTT palmitoylation. Indeed, there was a 25% decrease in HTT palmitoylation in *Hip14*$^{-/-}$;*Hip14l*$^{-/-}$ MEFs. HTT palmitoylation is significantly decreased but not completely abolished in this system, which may be due to compensation by another DHHC PAT in *Hip14*$^{-/-}$;*Hip14l*$^{-/-}$ MEFs that does not occur in the extraembryonic tissues of the developing *Hip14*$^{-/-}$;*Hip14l*$^{-/-}$ embryos. Different cell types express different *Zdhhc* genes at different levels. Interestingly, ZDHHC2, -3, and -23 are among those DHHC PATs that have been shown to have a low level of palmitoylation activity towards HTT when overexpressed in COS cells with HTT and that are not expressed in human placental tissue (Huang et al., 2011; Ohno et al., 2006). In the *Hip14*$^{-/-}$;*Hip14l*$^{-/-}$ embryos there is decreased HTT palmitoylation, which leads

to reduced HTT function, as well of loss of the two PATs, which would lead to decreased palmitoylation of other putative substrates.

The third specific aim of this thesis was to determine palmitoylation levels of synaptic proteins in HD mouse models. mHTT in the YAC128 mouse model of HD was decreased compared to palmitoylation of human wtHTT in the YAC18 mouse model (Yanai et al., 2006). Surprisingly, HTT palmitoylation was not affected in the *Hip14*$^{-/-}$ and *Hip14l*$^{-/-}$ mouse models, suggesting that these enzymes compensate for loss of each other to palmitoylate HTT and that the phenotypic overlap between these two mouse models and the YAC128 mice may be due to loss of palmitoylation of other substrates (Singaraja et al., 2011; Sutton et al., 2013). Indeed, the YAC128 mice were found to have fairly widespread alterations in the levels of palmitoylated proteins (Wan et al., 2013). Here, the palmitoylation of HTT and of the HIP14 and/or HIP14L substrates SNAP25, PSD-95 and GAD65 was assessed in a low throughput, high confidence manner in the YAC128, BACHD, and Hu97/18 mouse models of HD. mHTT palmitoylation was decreased in all three mouse models both compared to littermate control mice and compared to the WT allele within the same mouse. Only in the YAC128 mouse was palmitoylation of the WT allele decreased in the presence of the HD mutation. The palmitoylation of SNAP25 and PSD-95 was also decreased in all mouse models. There was no change in GAD65 palmitoylation in any of the mouse models. This is slightly unexpected as GAD65 palmitoylation was decreased in the R6/2 HD mouse model. The fact that HIP14 autopalmitoylation was almost completely abolished in the R6/2 mice suggests (Rush et al., 2012) much more severe HIP14 dysfunction than in the YAC128 mice where HIP14 palmitoylation was only decreased by about 25%, which may explain these results. This is a strange finding given that HTT does not interact with HIP14 in exon1 (Sanders et al., 2014). It is possible that exon1 overexpression in the R6/2 mice sequesters wild type endogenous HTT into the aggregate to a greater extent than in the YAC138 mice, resulting in a loss of wtHTT and HIP14 dysfunction.

The fourth specific goal of this thesis was to determine the role of loss of *Hip14* in the adult animal. The constitutive *Hip14* deficient mouse model has an HD-like phenotype but it is developmental and non-progressive unlike the adult-onset, progressive phenotype of the YAC128 mice (Singaraja et al., 2011; Slow, 2003; Van Raamsdonk, 2005b). An inducible *Hip14* deficient mouse model was generated and *Hip14* deletion was induced in the young adult mouse. The *iHip14*$^{\Delta/\Delta}$ mice have a phenotype surprisingly different than that of the *Hip14*$^{-/-}$ mice. The most surprising phenotype is the progressive hind limb paralysis and seizure disorder resulting in dramatically reduced survival of the *iHip14*$^{\Delta/\Delta}$ mice. This was highly unexpected as there is no change in survival of the *Hip14*$^{-/-}$ mice or the YAC128 mice. The *iHip14*$^{\Delta/\Delta}$ mice have motor coordination deficits and sensorimotor gating deficits similar to HD mouse models and *Hip14*$^{-/-}$ mice on rotarod and climbing. These data, along with the MSN physiology data, suggests profound striatal dysfunction. The psychiatric phenotype of the *iHip14*$^{\Delta/\Delta}$ mice is not like that of HD mouse models. The *iHip14*$^{\Delta/\Delta}$ mice are anhedonic and display increased escape response. The *iHip14*$^{\Delta/\Delta}$ mice have increased brain and forebrain weights and increased cortical volume, which is in contrast to the decreased brain weight and cortical volume in the YAC128 and the *Hip14*$^{-/-}$ mice (Singaraja et al., 2011; Van Raamsdonk, 2005a). Also, there was no change in striatal volume, unlike the striatal atrophy observed in the YAC128 and *Hip14*$^{-/-}$ mice (Carroll et al., 2011; Singaraja et al., 2011), but there was, however, a decrease in corpus callosum volume suggesting a decrease in white matter, which occurs in both the YAC128 mice and the *Hip14*$^{-/-}$ mice (Carroll et al., 2011; Singaraja et al., 2011). In the hippocampus there potentially was an imbalance between excitatory and inhibitory input to CA1 pyramidal neurons as a result of loss of *Hip14* in adulthood. Whether these alterations of synaptic function in the hippocampus contribute to the seizure phenotype remains to be seen.

This is the first example of a “conditional knockout” of a DHHC PAT. This study implicates HIP14 as an essential gene for the maintenance of the adult mouse, which is not surprising considering that *Hip14* is the most highly conserved of all 23 human PATs (Young et al., 2012). These data suggest that

there is a compensatory mechanism that occurs during development when *Hip14* is lost from conception that cannot occur when it is lost in the adult animal. This study does not rule out the possibility that HIP14 plays a role in the pathogenesis of HD, despite the fact that this mouse model does not develop an HD-like phenotype. In fact, this study shows that HIP14 is important for striatal function and is an essential gene that if dysfunctional in HD could have hugely detrimental consequences.

6.2 FUTURE DIRECTIONS

6.2.1 Potential novel function of wild type HTT: Modulator of palmitoylation

6.2.1.1 Do wild type HTT levels modulate palmitoylation of mutant HTT?

A confounding factor in the studies presented here in the YAC128 and BACHD mouse models is the presence of two alleles of wtHTT in addition to the one allele of mHTT. It would be very interesting to know what occurs in the human situation, i.e. where there is one allele of WT and one allele of mHTT, or in a YAC128 or BACHD mouse with only one copy of WT murine HTT. Would palmitoylation of wtHTT be further decreased in these situations? What about palmitoylation of mHTT? The Hu97/18 mouse is the most like the human situation. When HTT protein levels are assessed the total HTT levels are similar to WT mice; however, the Hu18/18 mice are haploinsufficient as they express less WT human HTT than a mouse expresses murine HTT (Southwell et al., 2013). It would also be interesting to assess palmitoylation of HTT in Hu97/18 mice compared to WT mice instead of compared to Hu18/18 mice, as was done here. Also, what happens to palmitoylation in the YAC128 or BACHD mice with no murine HTT? It would also be interesting to apply these findings to a human situation to determine if palmitoylation is also disturbed in human HD samples.

6.2.1.2 Does wild type HTT modulate HIP14L activity?

A major missing piece of information that would have implications for many of these and future studies is whether or not HIP14L is also dysfunctional in the

presence of the HD mutation as is HIP14 and if WT HTT also modulates HIP14L PAT function. Given the structural similarities of HIP14L to HIP14, and the fact that they are both HTT PATs, it is likely that HIP14L is also dysfunctional in HD. Unfortunately, the lack of a good antibody against HIP14L and the fact that it does not express well in bacteria or mammalian systems to allow immunoprecipitation or purification of enzyme has hindered this line of research. However, the optimization of a HIP14L expression and purification system would advance this line of research. Indeed, the relationships between HIP14, HIP14L, HTT are interesting for further research. Do HIP14 and HIP14L form homo and heterodimers? What would their function be as a heterodimer? What about as a homodimer? What is the consequence of the DQHC as opposed to the canonical DHHC motif in HIP14L? It is the only PAT of the 23 human PATs to have a DHHC motif that differs in any way.

6.2.1.3 How does HTT modulate activity of HIP14?

HTT may modulate the function of HIP14 in several ways. First, HTT is an α–solenoid protein made up of HEAT (Huntingtin, Elongation factor 3, protein phosphatase 2A, TOR1) repeats suitable for its function as a scaffolding protein with many protein-protein interactions (Huang et al., 2011; Li et al., 2006b; Palidwor et al., 2009; Seong et al., 2010; Takano and Gusella, 2002). It is possible that HTT may act as a scaffolding protein to bring substrates into close proximity with HIP14 and HIP14L, acting as an essential linker between PATs and their other substrates. Second, HTT may act as an allosteric activator of HIP14 by affecting the conformational structure of HIP14 thereby allowing substrates to access the DHHC active site (Huang et al., 2011). Third, as HTT has been shown to be involved in trafficking of organelles along the cytoskeleton, interacting with multiple motor and motor-associated proteins, HTT may be important for trafficking HIP14 and/or HIP14L to particular subcellular locations allowing it to interact with and palmitoylate its substrates (Caviston and Holzbaur, 2009; Huang et al., 2011). Firstly, characterization of the mechanism of modulation of PAT enzyme function by HTT would greatly advance our understanding of the role HIP14 may play in HD.

If HTT acts as an allosteric activator of HIP14, and potentially HIP14L, binding of a small HTT peptide, including the two binding sites, may enhance HIP14 and HIP14L activity in the disease state, which would likely have a beneficial effect by restoring palmitoylation of HTT and other proteins. This would not be possible without knowing which exact motifs of HTT bind HIP14 and HIP14L and this study brings us much closer to this goal.

6.2.2 The role of palmitoylation in the pathogenesis of HD

6.2.2.1 What is the normal and pathogenic role of palmitoylation of HTT?

Loss of both *Hip14* and *Hip14l* leads to a 25% decrease in palmitoylation of HTT in *Hip14*$^{-/-}$;*Hip14l*$^{-/-}$ MEF cells. Ideally, the levels of HTT palmitoylation would be compared between the *Hip14*$^{-/-}$;*Hip14l*$^{-/-}$ MEF cell lines and the extraembryonic tissues of *Hip14*$^{-/-}$;*Hip14l*$^{-/-}$ embryos to determine if there is a greater decrease in HTT palmitoylation in the extraembryonic tissues. Unfortunately, the methods currently available are not sensitive enough to detect HTT palmitoylation in such a small amount of tissue. If in the future this is possible, it would provide more evidence for the hypothesis that decreased HTT palmitoylation contributes to the similar phenotypes in the extraembryonic tissues of the *Hip14*$^{-/-}$;*Hip14l*$^{-/-}$ and the *Htt*$^{-/-}$ embryos. Clearly though, another PAT is able to compensate for loss of HIP14 and HIP14L to palmitoylate HTT. It would be interesting to know which other PAT(s) are involved. There was no change in mRNA expression of any of the other 22 murine DHHC PATs in the *Hip14*$^{-/-}$;*Hip14l*$^{-/-}$ MEFs but there still may be an increase in protein expression or in activity. At this time there are not functional antibodies available for most of the other DHHC PATs. The precise biological role of palmitoylation of HTT in normal mouse development and in the pathogenesis of HD has yet to be determined. It appears that palmitoylation of HTT may be essential for embryonic development but to provide definitive evidence for this a palmitoylation resistant HTT expressing mouse would need to be generated. At this point, Cys214 appears to be a site of HTT palmitoylation but it is not the only one (data not shown). The other sites of palmitoylation would need to be determined in order to answer these questions.

6.2.3 Ways to restore aberrant palmitoylation in HD

6.2.3.1 Can HD phenotypes in the YAC128 mice be ameliorated by overexpression of HIP14 or HIP14L?

Downregulation of HIP14 results in increased cell death and inclusion formation, whereas overexpression of HIP14 when co-transfected with mHTT decreases the percentage of cells with inclusions (Yanai et al., 2006). HIP14 or HIP14L can be overexpressed in YAC128 neuronal cell culture or in the CNS of YAC128 mice by AAV-mediated delivery to determine if levels of palmitoylation are restored and if HD phenotypes are ameliorated.

6.2.3.2 Does inhibiting the JNK3-HIP14 interaction ameliorate HD-like phenotypes?

Recent investigations have shown increased activation of the c-Jun N-terminal kinase (JNK) pathway in both cellular and animal models of HD (Morfini et al., 2009). JNK3 interaction with HIP14 is enhanced under pathological stress, promoting increased toxicity and cell death. The NIMoE peptide was designed to specifically disrupt this interaction. NIMoE protects against NMDA induced toxicity in neuronal cell culture and decreases infarct size and improves behavior in a rat stroke model (Yang and Cynader, 2011). If when bound to JNK3 HIP14 is unable to palmitoylate HTT, NIMoE may free HIP14 from the JNK3 complex making it available to palmitoylate HTT. NIMoE could be used in neuronal culture to determine if it protects against toxicity in the YAC128 model and if it restores palmitoylation of HTT and HIP14 substrates by freeing HIP14 from the JNK3 complex. Ultimately, this peptide could also be used in the YAC128 mice to determine if disruption of this complex is protective *in vivo*.

6.2.3.3 Is *Hip14* gene expression negatively regulated by microRNAs and could inhibiting these microRNAs increase HIP14 expression and restore palmitoylation levels in the YAC128 mice?

Six different sites in the HIP14 3'UTR are predicted to be targeted by microRNA (miRNA) families that are broadly conserved among vertebrates (Table 6.1). The

expression of these miRNAs could be determined in human and mouse striatum and cortex by absolute quantitative qRT-PCR. Those expressed at the highest level in these tissues would then be tested for activity against HIP14 expression *in vitro* and *in vivo*. Ultimately an antisense oligonucleotide inhibitor against the target miRNA could be developed to increase expression of HIP14. It could then be tested for amelioration of the HD phenotype in the YAC128 mice.

Table 6.1. Conserved mammalian miRNA regulatory target sites for conserved miRNA families in the 3' UTR regions of HIP14 in human and mouse.

UCSC Browser track TargetScan Release 5.1 (Dec. 2010):		
miRNA families	Score – human	Score - mouse
miR-34a/34b-5p/34c/34c-5p/449/449abc/699	99	97
miR-148/152	90	97
miR-30a/30a-5p/30b/30b-5p/30cde/384-5p	69	91
miR-200bc/429	48	nd
miR-204/211	84	nd
miR-96/1271	91	nd
TargetScan Release 6.1 (June 2012) website:		
miR-34ac/34bc-5p/449abc/449c-5p	99	97
miR-148ab-3p/152	78	64
miR-96/507/1271	93	91
miR-200bc/429/548a	44	nd
miR-204/204b/211	61	67
miR-30abcdef/30abe-5p/384-5p	27	16

6.2.3.4 Does APT1, APT2, or some other unidentified APT mediate depalmitoylation of HTT and HIP14 substrates?

Significant progress has been made in the discovery of PATs and in their enzymatic mechanism, but regulation of protein depalmitoylation is not as well understood. Dynamic regulation of palmitoylation has been shown for a number of proteins, but only four acyl protein thioesterases have been shown to have APT activity (APT1, APT2, APTL1 and PPT1) (Rusch et al., 2011; Tian et al., 2012; Tomatis et al., 2010; Verkruyse and Hofmann, 1996; Zeidman et al., 2009). The list of known substrates of APT1, APT2, and APTL1 is still quite small so it is still not clear whether they also depalmitoylates other neuronal proteins, such as

HTT and PSD-95, that have rapid palmitate turnover rates. It is possible that a yet-to-be-discovered APT(s) regulates protein depalmitoylation in the brain. APTs will represent an important class of drug targets in HD and other disorders, including schizophrenia, mental retardation, hypercholesterolemia and cancer, in which prominent roles for palmitoylation have been implicated (Young et al., 2012).

To increase HIP14/HIP14L substrate palmitoylation, one can either increase production or decrease palmitate turnover. Developing therapeutics to increase PAT activity is technically difficult. In contrast, inhibiting the thioesterases that catalyze palmitate removal is a highly feasible therapeutic approach to achieving this outcome. Thus determining which known or yet-to-be-discovered APTs play a role in HD will be instrumental to targeting palmitoylation in HD.

6.2.3.5 Does FKBP12 facilitate depalmitoylation and/or regulate HIP14 activity?

The prolyl isomerase FKBP12 facilitates depalmitoylation of Ras by isomerization of a proline residue near the palmitoylated cysteine. FK506, an FDA-approved drug, inhibits this isomerase activity, restoring Ras palmitoylation (Ahearn et al., 2011). Some of the therapeutic benefit of FK506 in models of HD (2006) might be attributable to restored palmitoylation. HTT has several conserved proline residues near its palmitoylated cysteine making it a good candidate for depalmitoylation by FKBP12. HIP14 itself may be regulated by FKBP12 as it has a conserved proline next to the palmitoylated cysteine of its DHHC active site. FKBP12 may, therefore, be targeted to increase levels of palmitoylation of HTT and HIP14 and the subsequent activity of HIP14 on its substrates. The effects of inhibition, overexpression or knockdown of FKBP12 on palmitoylation of HTT, HIP14 and its substrates could be determined.

6.2.4 The role of HIP14 in seizure-induced death

Firstly, it would be important to confirm via continuous EEG and EKG monitoring that the *iHip14*$^{\Delta/\Delta}$ mice do in fact die from seizures. If true, the seizure disorder in

iHip14$^{\Delta/\Delta}$ mice may be due, in part, to increased surface trafficking of AMPARs. Indeed, the physiology data suggests that there are more AMPARs at synapses. Loss of palmitoylation at either site of palmitoylation will lead to increased synaptic expression of AMPARs (Hayashi et al., 2005). Thus if HIP14 palmitoylates the AMPAR subunits at either of these sites, loss of HIP14 would lead to increased synaptic AMPAR. Indeed, HIP14 is a PAT for GLUA1 and GLUA2 (Huang et al., 2009). It would be prudent to determine the levels of palmitoylation of GLUA1 and GLUA2 and to determine the synaptic expression of these proteins in the *iHip14*$^{\Delta/\Delta}$ mice to provide further evidence for this hypothesis. There are other proteins whose palmitoylation also regulates synaptic expression of AMPAR subunits, such as AKAP79/150 and JNK3 (Keith et al., 2012; Yang et al., 2013). Assessing their palmitoylation status and synaptic localization in the *iHip14*$^{\Delta/\Delta}$ mice would also be very interesting.

6.3 CONCLUSIONS

Aberrant palmitoylation has been implicated in the pathogenesis of HD by the observations that some features of the disease are recapitulated in *Hip14*- and *Hip14l*-deficient mice and that HIP14 is dysfunctional in the presence of mHTT. Not only is HIP14 a PAT for HTT, it appears that wtHTT but not mHTT enhances HIP14 activity in part due to reduced interaction between HIP14 and mHTT. This may be the mechanism of HIP14 dysfunction in HD, which would be much more pronounced in HD than with loss of wtHTT. The replication of some features of HD in *Hip14*-deficient mice may not be due wholly to its dysfunctional PAT activity; other roles of HIP14 that are not a direct effect of palmitoylation may also contribute. These other roles should be considered when determining how to target HIP14 therapeutically.

Given the evidence presented here for aberrant palmitoylation in HD, one therapeutic approach could involve restoring levels of palmitoylation. This would be achieved either globally by targeting the relevant PATs, i.e. HIP14 and HIP14L, or thioesterase enzymes or by targeting specific substrates. We have just begun to understand the complex relationships between PATs,

thioesterases, and their substrates and we know little about the specific drivers that regulate this dynamic PTM. In order to appropriately target and predict potential side effects, a much better understanding of these processes is required. Given the interplay of palmitoylation with other PTMs, targeting these PTMs, for example the more easily druggable kinases and phosphatases, may also be a viable approach for therapy.

REFERENCES

Ahearn, I.M., Tsai, F.D., Court, H., Zhou, M., Jennings, B.C., Ahmed, M., Fehrenbacher, N., Linder, M.E., and Philips, M.R. (2011). FKBP12 Binds to Acylated H-Ras and Promotes Depalmitoylation. Molecular Cell *41*, 173–185.

Antinone, S.E., Ghadge, G.D., Lam, T.T., Wang, L., Roos, R.P., and Green, W.N. (2013). Palmitoylation of superoxide dismutase 1 (SOD1) is increased for familial amyotrophic lateral sclerosis-linked SOD1 mutants. Journal of Biological Chemistry *288*, 21606–21617.

Arnold, K., Bordoli, L., Kopp, J., and Schwede, T. (2006). The SWISS-MODEL workspace: a web-based environment for protein structure homology modelling. Bioinformatics *22*, 195–201.

Arstikaitis, P., Gauthier-Campbell, C., Carolina Gutierrez Herrera, R., Huang, K., Levinson, J.N., Murphy, T.H., Kilimann, M.W., Sala, C., Colicos, M.A., and El-Husseini, A. (2008). Paralemmin-1, a modulator of filopodia induction is required for spine maturation. Mol. Biol. Cell *19*, 2026–2038.

Baker, T.L. (2000). S-Nitrosocysteine Increases Palmitate Turnover on Ha-Ras in NIH 3T3 Cells. Journal of Biological Chemistry *275*, 22037–22047.

Bandyopadhyay, S., Chiang, C.-Y., Srivastava, J., Gersten, M., White, S., Bell, R., Kurschner, C., Martin, C.H., Smoot, M., Sahasrabudhe, S., et al. (2010). A human MAP kinase interactome. Nat Meth *7*, 801–805.

Bellizzi, J.J., Widom, J., Kemp, C., Lu, J.Y., Das, A.K., Hofmann, S.L., and Clardy, J. (2000). The crystal structure of palmitoyl protein thioesterase 1 and the molecular basis of infantile neuronal ceroid lipofuscinosis. Proc. Natl. Acad. Sci. U.S.a. *97*, 4573–4578.

Ben-Ari, Y., and Cossart, R. (2000). Kainate, a double agent that generates seizures: two decades of progress. Trends in Neurosciences *23*, 580–587.

Benjannet, S., Elagoz, A., Wickham, L., Mamarbachi, M., Munzer, J.S., Basak, A., Lazure, C., Cromlish, J.A., Sisodia, S., Checler, F., et al. (2001). Post-translational Processing of beta -Secretase (beta -Amyloid-converting Enzyme) and Its Ectodomain Shedding. J. Biol. Chem. *276*, 10879–10887.

Berchtold, L.A., Størling, Z.M., Ortis, F., Lage, K., Bang-Berthelsen, C., Bergholdt, R., Hald, J., Brorsson, C.A., Eizirik, D.L., Pociot, F., et al. (2011). Huntingtin-interacting protein 14 is a type 1 diabetes candidate protein regulating insulin secretion and beta-cell apoptosis. Proceedings of the National Academy of Sciences *108*, E681–E688.

Bhattacharyya, R., Barren, C., and Kovacs, D.M. (2013). Palmitoylation of

amyloid precursor protein regulates amyloidogenic processing in lipid rafts. Journal of Neuroscience *33*, 11169–11183.

Bijlmakers, M.-J., and Marsh, M. (2003). The on-off story of protein palmitoylation. Trends in Cell Biology *13*, 32–42.

Botto, L.D., May, K., Fernhoff, P.M., Correa, A., Coleman, K., Rasmussen, S.A., Merritt, R.K., O'Leary, L.A., Wong, L.-Y., Elixson, E.M., et al. (2003). A population-based study of the 22q11.2 deletion: phenotype, incidence, and contribution to major birth defects in the population. Pediatrics *112*, 101–107.

Brinke, ten, A., Vaandrager, A.B., Haagsman, H.P., Ridder, A.N.J.A., van Golde, L.M.G., and Batenburg, J.J. (2002). Structural requirements for palmitoylation of surfactant protein C precursor. Biochem. J. *361*, 663–671.

Brown, D.A. (2006). Lipid Rafts, Detergent-Resistant Membranes, and Raft Targeting Signals. Physiology *21*, 430–439.

Brusa, R., Zimmermann, F., Koh, D.S., Feldmeyer, D., Gass, P., Seeburg, P.H., and Sprengel, R. (1995). Early-onset epilepsy and postnatal lethality associated with an editing-deficient GluR-B allele in mice. Science *270*, 1677–1680.

Butland, S.L., Sanders, S.S., Schmidt, M.E., Riechers, S.-P., Lin, D.T.S., Martin, D.D.O., Vaid, K., Graham, R.K., Singaraja, R.R., Wanker, E.E., et al. (2014). The palmitoyl acyltransferase HIP14 shares a high proportion of interactors with huntingtin: implications for a role in the pathogenesis of Huntington's disease. Human Molecular Genetics *23*, 4142–4160.

Calero, G. (2003). The Crystal Structure of Palmitoyl Protein Thioesterase-2 (PPT2) Reveals the Basis for Divergent Substrate Specificities of the Two Lysosomal Thioesterases, PPT1 and PPT2. Journal of Biological Chemistry *278*, 37957–37964.

Carroll, J.B., Lerch, J.P., Franciosi, S., Spreeuw, A., Bissada, N., Henkelman, R.M., and Hayden, M.R. (2011). Natural history of disease in the YAC128 mouse reveals a discrete signature of pathology in Huntington disease. Neurobiology of Disease *43*, 257–265.

Caviston, J.P., and Holzbaur, E.L.F. (2009). Huntingtin as an essential integrator of intracellular vesicular trafficking. Trends in Cell Biology *19*, 147–155.

Chang, S.-C., and Magee, A.I. (2009). Acyltransferases for secreted signalling proteins (Review). Mol Membr Biol *26*, 104–113.

Charollais, J., and Van Der Goot, F.G. (2009). Palmitoylation of membrane proteins (Review). Mol Membr Biol *26*, 55–66.

Charron, G., Zhang, M.M., Yount, J.S., Wilson, J., Raghavan, A.S., Shamir, E.,

and Hang, H.C. (2009). Robust fluorescent detection of protein fatty-acylation with chemical reporters. J. Am. Chem. Soc. *131*, 4967–4975.

Charych, E.I., Jiang, L.-X., Lo, F., Sullivan, K., and Brandon, N.J. (2010). Interplay of palmitoylation and phosphorylation in the trafficking and localization of phosphodiesterase 10A: implications for the treatment of schizophrenia. Journal of Neuroscience *30*, 9027–9037.

Chen, W.-Y., Shi, Y.-Y., Zheng, Y.-L., Zhao, X.-Z., Zhang, G.-J., Chen, S.-Q., Yang, P.-D., and He, L. (2004). Case-control study and transmission disequilibrium test provide consistent evidence for association between schizophrenia and genetic variation in the 22q11 gene ZDHHC8. Human Molecular Genetics *13*, 2991–2995.

Chen, X., Shi, W., Wang, F., Du, Z., Yang, Y., Gao, M., Yao, Y., He, K., Wang, C., and Hao, A. (2014). Zinc finger DHHC-type containing 13 regulates fate specification of ectoderm and mesoderm cell lineages by modulating Smad6 activity. Stem Cells Dev. *23*, 1899–1909.

Cheng, H., Vetrivel, K.S., Drisdel, R.C., Meckler, X., Gong, P., Leem, J.Y., Li, T., Carter, M., Chen, Y., Nguyen, P., et al. (2009). S-palmitoylation of gamma-secretase subunits nicastrin and APH-1. J. Biol. Chem. *284*, 1373–1384.

Cho, S., and Dawson, G. (2000). Palmitoyl protein thioesterase 1 protects against apoptosis mediated by Ras-Akt-caspase pathway in neuroblastoma cells. J Neurochem *74*, 1478–1488.

Cho, S., Dawson, P.E., and Dawson, G. (2000). Antisense palmitoyl protein thioesterase 1 (PPT1) treatment inhibits PPT1 activity and increases cell death in LA-N-5 neuroblastoma cells. J. Neurosci. Res. *62*, 234–240.

Citri, A., and Malenka, R.C. (2008). Synaptic plasticity: multiple forms, functions, and mechanisms. Neuropsychopharmacology *33*, 18–41.

Conibear, E., and Davis, N.G. (2010). Palmitoylation and depalmitoylation dynamics at a glance. Journal of Cell Science *123*, 4007–4010.

Cordy, J.M., Hussain, I., Dingwall, C., Hooper, N.M., and Turner, A.J. (2003). Exclusively targeting beta-secretase to lipid rafts by GPI-anchor addition up-regulates beta-site processing of the amyloid precursor protein. Proc. Natl. Acad. Sci. U.S.a. *100*, 11735–11740.

Corvi, M.M., Soltys, C.L., and Berthiaume, L.G. (2001). Regulation of mitochondrial carbamoyl-phosphate synthetase 1 activity by active site fatty acylation. J. Biol. Chem. *276*, 45704–45712.

Craven, S.E., El-Husseini, A.E., and Bredt, D.S. (1999). Synaptic targeting of the postsynaptic density protein PSD-95 mediated by lipid and protein motifs. Neuron

22, 497–509.

Cross, J.C., Simmons, D.G., and Watson, E.D. (2003). Chorioallantoic morphogenesis and formation of the placental villous tree. Ann. N. Y. Acad. Sci. *995*, 84–93.

Cryan, J.F., Markou, A., and Lucki, I. (2002). Assessing antidepressant activity in rodents: recent developments and future needs. Trends Pharmacol. Sci. *23*, 238–245.

D'Souza, D.N., Harlan, R.E., and Garcia, M.M. (1999). Sexual dimorphism in the response to N-methyl-D-aspartate receptor antagonists and morphine on behavior and c-Fos induction in the rat brain. Neuroscience *93*, 1539–1547.

Dekker, F.J., and Hedberg, C. (2011). Small molecule inhibition of protein depalmitoylation as a new approach towards downregulation of oncogenic Ras signalling. Bioorganic & Medicinal Chemistry *19*, 1376–1380.

Delint-Ramirez, I., Willoughby, D., Hammond, G.V.R., Ayling, L.J., and Cooper, D.M.F. (2011). Palmitoylation Targets AKAP79 Protein to Lipid Rafts and Promotes Its Regulation of Calcium-sensitive Adenylyl Cyclase Type 8. Journal of Biological Chemistry *286*, 32962–32975.

Demily, C., Legallic, S., Bou, J., Houy-Durand, E., Van Amelsvoort, T., Zinkstok, J., Manouvrier-Hanue, S., Vogels, A., Drouin-Garraud, V., Philip, N., et al. (2007). ZDHHC8 single nucleotide polymorphism rs175174 is not associated with psychiatric features of the 22q11 deletion syndrome or schizophrenia. Psychiatr. Genet. *17*, 311–312.

Deng, Y.P., Albin, R.L., Penney, J.B., Young, A.B., Anderson, K.D., and Reiner, A. (2004). Differential loss of striatal projection systems in Huntington's disease: a quantitative immunohistochemical study. Journal of Chemical Neuroanatomy *27*, 143–164.

Devedjiev, Y., Dauter, Z., Kuznetsov, S.R., Jones, T.L., and Derewenda, Z.S. (2000). Crystal structure of the human acyl protein thioesterase I from a single X-ray data set to 1.5 A. Structure *8*, 1137–1146.

Dietrich, L.E.P., and Ungermann, C. (2004). On the mechanism of protein palmitoylation. EMBO Reports *5*, 1053–1057.

Dorfleutner, A. (2003). Regulation of tissue factor cytoplasmic domain phosphorylation by palmitoylation. Blood *102*, 3998–4005.

Drisdel, R.C., and Green, W.N. (2004). Labeling and quantifying sites of protein palmitoylation. BioTechniques *36*, 276–285.

Ducker, C.E., Stettler, E.M., French, K.J., Upson, J.J., and Smith, C.D. (2004).

Huntingtin interacting protein 14 is an oncogenic human protein: palmitoyl acyltransferase. Oncogene *23*, 9230–9237.

Duncan, J.A. (2002). Characterization of Saccharomyces cerevisiae Acyl-protein Thioesterase 1, the Enzyme Responsible for G Protein alpha Subunit Deacylation in Vivo. Journal of Biological Chemistry *277*, 31740–31752.

Duncan, J.A., and Gilman, A.G. (1996). Autoacylation of G protein alpha subunits. J. Biol. Chem. *271*, 23594–23600.

Duncan, J.A., and Gilman, A.G. (1998). A cytoplasmic acyl-protein thioesterase that removes palmitate from G protein alpha subunits and p21(RAS). J. Biol. Chem. *273*, 15830–15837.

Duyao, M.P., Auerbach, A.B., Ryan, A., Persichetti, F., Barnes, G.T., McNeil, S.M., Ge, P., Vonsattel, J.P., Gusella, J.F., and Joyner, A.L. (1995). Inactivation of the mouse Huntington's disease gene homolog Hdh. Science *269*, 407–410.

Ehehalt, R. (2003). Amyloidogenic processing of the Alzheimer beta-amyloid precursor protein depends on lipid rafts. The Journal of Cell Biology *160*, 113–123.

Ehrlich, I., and Malinow, R. (2004). Postsynaptic density 95 controls AMPA receptor incorporation during long-term potentiation and experience-driven synaptic plasticity. Journal of Neuroscience *24*, 916–927.

Ehrnhoefer, D.E., Butland, S.L., Pouladi, M.A., and Hayden, M.R. (2009). Mouse models of Huntington disease: variations on a theme. Disease Models and Mechanisms *2*, 123–129.

Ehrnhoefer, D.E., Sutton, L., and Hayden, M.R. (2011). Small Changes, Big Impact: Posttranslational Modifications and Function of Huntingtin in Huntington Disease. Neuroscientist *17*, 475–492.

El-Husseini, A.E.D. (2001). Polarized Targeting of Peripheral Membrane Proteins in Neurons. Journal of Biological Chemistry *276*, 44984–44992.

El-Husseini, A.E., Craven, S.E., Chetkovich, D.M., Firestein, B.L., Schnell, E., Aoki, C., and Bredt, D.S. (2000a). Dual palmitoylation of PSD-95 mediates its vesiculotubular sorting, postsynaptic targeting, and ion channel clustering. The Journal of Cell Biology *148*, 159–172.

El-Husseini, A.E., Schnell, E., Chetkovich, D.M., Nicoll, R.A., and Bredt, D.S. (2000b). PSD-95 involvement in maturation of excitatory synapses. Science *290*, 1364–1368.

El-Husseini, A.E.-D., and Bredt, D.S. (2002). Protein palmitoylation: a regulator of neuronal development and function. Nat Rev Neurosci *3*, 791–802.

El-Husseini, A.E.-D., Schnell, E., Dakoji, S., Sweeney, N., Zhou, Q., Prange, O., Gauthier-Campbell, C., Aguilera-Moreno, A., Nicoll, R.A., and Bredt, D.S. (2002). Synaptic strength regulated by palmitate cycling on PSD-95. Cell *108*, 849–863.

Estrada-Sánchez, A.M., Barton, S.J., Burroughs, C.L., Doyle, A.R., and Rebec, G.V. (2013). Dysregulated Striatal Neuronal Processing and Impaired Motor Behavior in Mice Lacking Huntingtin Interacting Protein 14 (HIP14). PLoS ONE *8*, e84537.

Fairbank, M., Huang, K., El-Husseini, A., and Nabi, I.R. (2012). RING finger palmitoylation of the endoplasmic reticulum Gp78 E3 ubiquitin ligase. FEBS Lett. *586*, 2488–2493.

Fan, M.M.Y., and Raymond, L.A. (2007). N-methyl-D-aspartate (NMDA) receptor function and excitotoxicity in Huntington's disease. Progress in Neurobiology *81*, 272–293.

Fang, C., Deng, L., Keller, C.A., Fukata, M., Fukata, Y., Chen, G., and Lüscher, B. (2006). GODZ-mediated palmitoylation of GABA(A) receptors is required for normal assembly and function of GABAergic inhibitory synapses. Journal of Neuroscience *26*, 12758–12768.

Fehrenbacher, N., Bar-Sagi, D., and Philips, M. (2009). Ras/MAPK signaling from endomembranes. Molecular Oncology *3*, 297–307.

Fernandez-Hernando, C. (2006). Identification of Golgi-localized acyl transferases that palmitoylate and regulate endothelial nitric oxide synthase. The Journal of Cell Biology *174*, 369–377.

Fisher, E.R., and Hayden, M.R. (2014). Multisource ascertainment of Huntington disease in Canada: prevalence and population at risk. Mov. Disord. *29*, 105–114.

Forrester, M.T., Hess, D.T., Thompson, J.W., Hultman, R., Moseley, M.A., Stamler, J.S., and Casey, P.J. (2011). Site-specific analysis of protein S-acylation by resin-assisted capture. The Journal of Lipid Research *52*, 393–398.

Fukata, M., Fukata, Y., Adesnik, H., Nicoll, R.A., and Bredt, D.S. (2004). Identification of PSD-95 palmitoylating enzymes. Neuron *44*, 987–996.

Fukata, Y., and Fukata, M. (2010). Protein palmitoylation in neuronal development and synaptic plasticity. Nat Rev Neurosci *11*, 161–175.

Fukata, Y., Dimitrov, A., Boncompain, G., Vielemeyer, O., Perez, F., and Fukata, M. (2013). Local palmitoylation cycles define activity-regulated postsynaptic subdomains. The Journal of Cell Biology *202*, 145–161.

Gao, T., Collins, R.E., Horton, J.R., Zhang, X., Zhang, R., Dhayalan, A., Tamas, R., Jeltsch, A., and Cheng, X. (2009). The ankyrin repeat domain of Huntingtin

interacting protein 14 contains a surface aromatic cage, a potential site for methyl-lysine binding. Proteins *76*, 772–777.

Gao, X., and Hannoush, R.N. (2013). Single-cell imaging of Wnt palmitoylation by the acyltransferase porcupine. Nat. Chem. Biol.

Gao, X., and Hannoush, R.N. (2014). A method for cellular imaging of palmitoylated proteins with clickable probes and proximity ligation applied to Hedgehog, tubulin and Ras. J. Am. Chem. Soc.

Gauthier-Campbell, C., Bredt, D.S., Murphy, T.H., and El-Husseini, A.E.-D. (2004). Regulation of dendritic branching and filopodia formation in hippocampal neurons by specific acylated protein motifs. Mol. Biol. Cell *15*, 2205–2217.

Gilbert, M.T.P., Haselkorn, T., Bunce, M., Sanchez, J.J., Lucas, S.B., Jewell, L.D., Marck, E.V., and Worobey, M. (2007). The Isolation of Nucleic Acids from Fixed, Paraffin-Embedded Tissues–Which Methods Are Useful When? PLoS ONE *2*, e537.

Glaser, B., Moskvina, V., Kirov, G., Murphy, K.C., Williams, H., Williams, N., Owen, M.J., and O'Donovan, M.C. (2006). Analysis of ProDH, COMT and ZDHHC8 risk variants does not support individual or interactive effects on schizophrenia susceptibility. Schizophrenia Research *87*, 21–27.

Glaser, B., Schumacher, J., Williams, H.J., Jamra, R.A., Ianakiev, N., Milev, R., Ohlraun, S., Schulze, T.G., Czerski, P.M., Hauser, J., et al. (2005). No Association Between the Putative Functional ZDHHC8 Single Nucleotide Polymorphism rs175174 and Schizophrenia in Large European Samples. Biological Psychiatry *58*, 78–80.

Goodwin, J.S. (2005). Depalmitoylated Ras traffics to and from the Golgi complex via a nonvesicular pathway. The Journal of Cell Biology *170*, 261–272.

Gorleku, O.A., Barns, A.-M., Prescott, G.R., Greaves, J., and Chamberlain, L.H. (2011). Endoplasmic reticulum localization of DHHC palmitoyltransferases mediated by lysine-based sorting signals. Journal of Biological Chemistry *286*, 39573–39584.

Goytain, A., Hines, R.M., and Quamme, G.A. (2008). Huntingtin-interacting proteins, HIP14 and HIP14L, mediate dual functions, palmitoyl acyltransferase and Mg2+ transport. J. Biol. Chem. *283*, 33365–33374.

Gray, M., Shirasaki, D.I., Cepeda, C., Andre, V.M., Wilburn, B., Lu, X.H., Tao, J., Yamazaki, I., Li, S.H., Sun, Y.E., et al. (2008). Full-length human mutant huntingtin with a stable polyglutamine repeat can elicit progressive and selective neuropathogenesis in BACHD mice. *28*, 6182–6195.

Graybiel, A.M. (2000). The basal ganglia. Curr. Biol. *10*, R509–R511.

Greaves, J., Gorleku, O.A., Salaun, C., and Chamberlain, L.H. (2010). Palmitoylation of the SNAP25 Protein Family: Specificity and Regulation of by DHHC Palmitoyl Transferases. Journal of Biological Chemistry *285*, 24629–24638.

Greaves, J., and Chamberlain, L.H. (2011). DHHC palmitoyl transferases: substrate interactions and (patho)physiology. Trends in Biochemical Sciences *36*, 245–253.

Greaves, J., Lemonidis, K., Gorleku, O.A., Cruchaga, C., Grefen, C., and Chamberlain, L.H. (2012). Palmitoylation-induced aggregation of cysteine-string protein mutants that cause neuronal ceroid lipofuscinosis. Journal of Biological Chemistry *287*, 37330–37339.

Greaves, J., Salaun, C., Fukata, Y., Fukata, M., and Chamberlain, L.H. (2008). Palmitoylation and membrane interactions of the neuroprotective chaperone cysteine-string protein. J. Biol. Chem. *283*, 25014–25026.

Gupta, P., Soyombo, A.A., Atashband, A., Wisniewski, K.E., Shelton, J.M., Richardson, J.A., Hammer, R.E., and Hofmann, S.L. (2001). Disruption of PPT1 or PPT2 causes neuronal ceroid lipofuscinosis in knockout mice. Proc. Natl. Acad. Sci. U.S.a. *98*, 13566–13571.

Gurtner, G.C., Davis, V., Li, H., McCoy, M.J., Sharpe, A., and Cybulsky, M.I. (1995). Targeted disruption of the murine VCAM1 gene: essential role of VCAM-1 in chorioallantoic fusion and placentation. Genes & Development *9*, 1–14.

Hackam, A.S., Singaraja, R., Wellington, C.L., Metzler, M., McCutcheon, K., Zhang, T., Kalchman, M., and Hayden, M.R. (1998). The influence of huntingtin protein size on nuclear localization and cellular toxicity. The Journal of Cell Biology *141*, 1097–1105.

Hallak, H., Muszbek, L., Laposata, M., Belmonte, E., Brass, L.F., and Manning, D.R. (1994). Covalent binding of arachidonate to G protein alpha subunits of human platelets. J. Biol. Chem. *269*, 4713–4716.

Harada, T., Matsuzaki, O., Hayashi, H., Sugano, S., Matsuda, A., and Nishida, E. (2003). AKRL1 and AKRL2 activate the JNK pathway. Genes Cells *8*, 493–500.

Hawtin, S.R., Tobin, A.B., Patel, S., and Wheatley, M. (2001). Palmitoylation of the vasopressin V1a receptor reveals different conformational requirements for signaling, agonist-induced receptor phosphorylation, and sequestration. J. Biol. Chem. *276*, 38139–38146.

Hayashi, T., Rumbaugh, G., and Huganir, R.L. (2005). Differential Regulation of AMPA Receptor Subunit Trafficking by Palmitoylation of Two Distinct Sites. Neuron *47*, 709–723.

Hayashi, T., Thomas, G.M., and Huganir, R.L. (2009). Dual Palmitoylation of NR2 Subunits Regulates NMDA Receptor Trafficking. Neuron *64*, 213–226.

Heinonen, O., Kyttälä, A., Lehmus, E., Paunio, T., Peltonen, L., and Jalanko, A. (2000). Expression of Palmitoyl Protein Thioesterase in Neurons. Molecular Genetics and Metabolism *69*, 123–129.

Heng, M.Y., Detloff, P.J., and Albin, R.L. (2008). Rodent genetic models of Huntington disease. Neurobiology of Disease *32*, 1–9.

Hickey, M.A., Kosmalska, A., Enayati, J., Cohen, R., Zeitlin, S., Levine, M.S., and Chesselet, M.-F. (2008). Extensive early motor and non-motor behavioral deficits are followed by striatal neuronal loss in knock-in Huntington's disease mice. Neuroscience *157*, 280–295.

Hines, R.M., Kang, R., Goytain, A., and Quamme, G.A. (2010). Golgi-specific DHHC Zinc Finger Protein GODZ Mediates Membrane Ca2+ Transport. Journal of Biological Chemistry *285*, 4621–4628.

Hirano, T., Kishi, M., Sugimoto, H., Taguchi, R., Obinata, H., Ohshima, N., Tatei, K., and Izumi, T. (2009). Thioesterase activity and subcellular localization of acylprotein thioesterase 1/lysophospholipase 1. BBA - Molecular and Cell Biology of Lipids *1791*, 797–805.

Ho, G.P.H., Selvakumar, B., Mukai, J., Hester, L.D., Wang, Y., Gogos, J.A., and Snyder, S.H. (2011). S-nitrosylation and S-palmitoylation reciprocally regulate synaptic targeting of PSD-95. Neuron *71*, 131–141.

Hodgson, J.G., Smith, D.J., McCutcheon, K., Koide, H.B., Nishiyama, K., Dinulos, M.B., Stevens, M.E., Bissada, N., Nasir, J., Kanazawa, I., et al. (1996). Human huntingtin derived from YAC transgenes compensates for loss of murine huntingtin by rescue of the embryonic lethal phenotype. Human Molecular Genetics *5*, 1875–1885.

Holmes, A., Parmigiani, S., Ferrari, P.F., Palanza, P., and Rodgers, R.J. (2000). Behavioral profile of wild mice in the elevated plus-maze test for anxiety. Physiol. Behav. *71*, 509–516.

Huang, K., Sanders, S.S., Kang, R., Carroll, J.B., Sutton, L., Wan, J., Singaraja, R., Young, F.B., Liu, L., El-Husseini, A., et al. (2011). Wild-type HTT modulates the enzymatic activity of the neuronal palmitoyl transferase HIP14. Human Molecular Genetics *20*, 3356–3365.

Huang, K., Sanders, S., Singaraja, R., Orban, P., Cijsouw, T., Arstikaitis, P., Yanai, A., Hayden, M.R., and El-Husseini, A. (2009). Neuronal palmitoyl acyl transferases exhibit distinct substrate specificity. The FASEB Journal *23*, 2605–2615.

Huang, K., and El-Husseini, A. (2005). Modulation of neuronal protein trafficking and function by palmitoylation. Current Opinion in Neurobiology *15*, 527–535.

Huang, K., Kang, M.H., Askew, C., Kang, R., Sanders, S.S., Wan, J., Davis, N.G., and Hayden, M.R. (2010). Palmitoylation and function of glial glutamate transporter-1 is reduced in the YAC128 mouse model of Huntington disease. Neurobiology of Disease *40*, 207–215.

Huang, K., Yanai, A., Kang, R., Arstikaitis, P., Singaraja, R.R., Metzler, M., Mullard, A., Haigh, B., Gauthier-Campbell, C., Gutekunst, C.-A., et al. (2004). Huntingtin-interacting protein HIP14 is a palmitoyl transferase involved in palmitoylation and trafficking of multiple neuronal proteins. Neuron *44*, 977–986.

Humeau, Y., Gambino, F., Chelly, J., and Vitale, N. (2009). X-linked mental retardation: focus on synaptic function and plasticity. J Neurochem *109*, 1–14.

Hunter, P.J., Swanson, B.J., Haendel, M.A., Lyons, G.E., and Cross, J.C. (1999). Mrj encodes a DnaJ-related co-chaperone that is essential for murine placental development. Development *126*, 1247–1258.

Inman, K.E., and Downs, K.M. (2007). The murine allantois: emerging paradigms in development of the mammalian umbilical cord and its relation to the fetus. Genesis *45*, 237–258.

Jacobowitz, D.M., and Kallarakal, A.T. (2004). Flotillin-1 in the substantia nigra of the Parkinson brain and a predominant localization in catecholaminergic nerves in the rat brain. Neurotox Res *6*, 245–257.

Jeffries, O., Tian, L., McClafferty, H., and Shipston, M.J. (2012). An electrostatic switch controls palmitoylation of the large conductance voltage- and calcium-activated potassium (BK) channel. Journal of Biological Chemistry *287*, 1468–1477.

Jennings, B.C., and Linder, M.E. (2012). DHHC protein S-acyltransferases use similar ping-pong kinetic mechanisms but display different acyl-CoA specificities. Journal of Biological Chemistry *287*, 7236–7245.

Jennings, B.C., Nadolski, M.J., Ling, Y., Baker, M.B., Harrison, M.L., Deschenes, R.J., and Linder, M.E. (2009). 2-Bromopalmitate and 2-(2-hydroxy-5-nitro-benzylidene)-benzo[b]thiophen-3-one inhibit DHHC-mediated palmitoylation in vitro. The Journal of Lipid Research *50*, 233–242.

Johnson, D.R., Bhatnagar, R.S., Knoll, L.J., and Gordon, J.I. (1994). Genetic and biochemical studies of protein N-myristoylation. Annu. Rev. Biochem. *63*, 869–914.

Kalchman, M.A., Graham, R.K., Xia, G., Koide, H.B., Hodgson, J.G., Graham, K.C., Goldberg, Y.P., Gietz, R.D., Pickart, C.M., and Hayden, M.R. (1996).

Huntingtin is ubiquitinated and interacts with a specific ubiquitin-conjugating enzyme. J. Biol. Chem. *271*, 19385–19394.

Kanaani, J., Diacovo, M.J., El-Husseini, A.E.-D., Bredt, D.S., and Baekkeskov, S. (2004). Palmitoylation controls trafficking of GAD65 from Golgi membranes to axon-specific endosomes and a Rab5a-dependent pathway to presynaptic clusters. Journal of Cell Science *117*, 2001–2013.

Kanaani, J., El-Husseini, A.E.-D., Aguilera-Moreno, A., Diacovo, J.M., Bredt, D.S., and Baekkeskov, S. (2002). A combination of three distinct trafficking signals mediates axonal targeting and presynaptic clustering of GAD65. The Journal of Cell Biology *158*, 1229–1238.

Kang, K.-H., and Bier, E. (2010). dHIP14-dependent palmitoylation promotes secretion of the BMP antagonist Sog. Developmental Biology *346*, 1–10.

Kang, R. (2004). Presynaptic Trafficking of Synaptotagmin I Is Regulated by Protein Palmitoylation. Journal of Biological Chemistry *279*, 50524–50536.

Kang, R., Wan, J., Arstikaitis, P., Takahashi, H., Huang, K., Bailey, A.O., Thompson, J.X., Roth, A.F., Drisdel, R.C., Mastro, R., et al. (2008). Neural palmitoyl-proteomics reveals dynamic synaptic palmitoylation. Nature *456*, 904–909.

Kato, H., Allen, N.D., Emson, P.C., and Kiyama, H. (2000). GAP-43 N-terminal translocation signal targets beta-galactosidase to developing axons in a pan-neuronal transgenic mouse line. Brain Res. Dev. Brain Res. *121*, 109–112.

Keith, D.J., Sanderson, J.L., Gibson, E.S., Woolfrey, K.M., Robertson, H.R., Olszewski, K., Kang, R., El-Husseini, A., and Dell'acqua, M.L. (2012). Palmitoylation of A-kinase anchoring protein 79/150 regulates dendritic endosomal targeting and synaptic plasticity mechanisms. Journal of Neuroscience *32*, 7119–7136.

Keller, C.A. (2004). The 2 Subunit of GABAA Receptors Is a Substrate for Palmitoylation by GODZ. Journal of Neuroscience *24*, 5881–5891.

Khan, A.A. (2001). Physiological Regulation of the Immunological Synapse by Agrin. Science *292*, 1681–1686.

Kim, E., and Sheng, M. (2004). PDZ domain proteins of synapses. Nat Rev Neurosci *5*, 771–781.

Kirkby, R.J., and Kimble, D.P. (1968). Avoidance and escape behavior following striatal lesions in the rat. Exp. Neurol. *20*, 215–227.

Kolodziejczyk, K., Parsons, M.P., Southwell, A.L., Hayden, M.R., and Raymond, L.A. (2014). Striatal synaptic dysfunction and hippocampal plasticity deficits in

the Hu97/18 mouse model of Huntington disease. PLoS ONE *9*, e94562.

Kong, C., Lange, J.J., Samovski, D., Su, X., Liu, J., Sundaresan, S., and Stahl, P.D. (2013a). Ubiquitination and degradation of the hominoid-specific oncoprotein TBC1D3 is regulated by protein palmitoylation. Biochemical and Biophysical Research Communications *434*, 388–393.

Kong, E., Peng, S., Chandra, G., Sarkar, C., Zhang, Z., Bagh, M.B., and Mukherjee, A.B. (2013b). Dynamic palmitoylation links cytosol-membrane shuttling of acyl-protein thioesterase-1 and acyl-protein thioesterase-2 with that of proto-oncogene H-Ras product and growth associated protein-43. J. Biol. Chem.

Kordasiewicz, H.B., Stanek, L.M., Wancewicz, E.V., Mazur, C., McAlonis, M.M., Pytel, K.A., Artates, J.W., Weiss, A., Cheng, S.H., Shihabuddin, L.S., et al. (2012). Sustained therapeutic reversal of Huntington's disease by transient repression of huntingtin synthesis. Neuron *74*, 1031–1044.

Kostiuk, M.A., Corvi, M.M., Keller, B.O., Plummer, G., Prescher, J.A., Hangauer, M.J., Bertozzi, C.R., Rajaiah, G., Falck, J.R., and Berthiaume, L.G. (2008). Identification of palmitoylated mitochondrial proteins using a bio-orthogonal azido-palmitate analogue. The FASEB Journal *22*, 721–732.

Kotera, J., Sasaki, T., Kobayashi, T., Fujishige, K., Yamashita, Y., and Omori, K. (2004). Subcellular localization of cyclic nucleotide phosphodiesterase type 10A variants, and alteration of the localization by cAMP-dependent protein kinase-dependent phosphorylation. J. Biol. Chem. *279*, 4366–4375.

Kraut, R., Menon, K., and Zinn, K. (2001). A gain-of-function screen for genes controlling motor axon guidance and synaptogenesis in Drosophila. Curr. Biol. *11*, 417–430.

Kreitzer, A.C., and Malenka, R.C. (2008). Striatal Plasticity and Basal Ganglia Circuit Function. Neuron *60*, 543–554.

Kutzleb, C., Sanders, G., Yamamoto, R., Wang, X., Lichte, B., Petrasch-Parwez, E., and Kilimann, M.W. (1998). Paralemmin, a prenyl-palmitoyl-anchored phosphoprotein abundant in neurons and implicated in plasma membrane dynamics and cell process formation. The Journal of Cell Biology *143*, 795–813.

Kwee, L., Baldwin, H.S., Shen, H.M., Stewart, C.L., Buck, C., Buck, C.A., and Labow, M.A. (1995). Defective development of the embryonic and extraembryonic circulatory systems in vascular cell adhesion molecule (VCAM-1) deficient mice. Development *121*, 489–503.

Ladygina, N., Martin, B.R., and Altman, A. (2011). Dynamic palmitoylation and the role of DHHC proteins in T cell activation and anergy. Adv. Immunol. *109*, 1–44.

Lam, K.K.Y., Davey, M., Sun, B., Roth, A.F., Davis, N.G., and Conibear, E. (2006). Palmitoylation by the DHHC protein Pfa4 regulates the ER exit of Chs3. The Journal of Cell Biology *174*, 19–25.

Laux, T., Fukami, K., Thelen, M., Golub, T., Frey, D., and Caroni, P. (2000). GAP43, MARCKS, and CAP23 modulate PI(4,5)P(2) at plasmalemmal rafts, and regulate cell cortex actin dynamics through a common mechanism. The Journal of Cell Biology *149*, 1455–1472.

Lee, Y.-S., and Silva, A.J. (2009). The molecular and cellular biology of enhanced cognition. Nat Rev Neurosci *10*, 126–140.

Lehtovirta, M., Kyttälä, A., Eskelinen, E.L., Hess, M., Heinonen, O., and Jalanko, A. (2001). Palmitoyl protein thioesterase (PPT) localizes into synaptosomes and synaptic vesicles in neurons: implications for infantile neuronal ceroid lipofuscinosis (INCL). Human Molecular Genetics *10*, 69–75.

Levental, I., Grzybek, M., and Simons, K. (2010). Greasing Their Way: Lipid Modifications Determine Protein Association with Membrane Rafts. Biochemistry *49*, 6305–6316.

Li, J., Mahajan, A., and Tsai, M.-D. (2006a). Ankyrin Repeat: A Unique Motif Mediating Protein−Protein Interactions †. Biochemistry *45*, 15168–15178.

Li, W., Serpell, L.C., Carter, W.J., Rubinsztein, D.C., and Huntington, J.A. (2006b). Expression and characterization of full-length human huntingtin, an elongated HEAT repeat protein. J. Biol. Chem. *281*, 15916–15922.

Li, Y., Hu, J., Hofer, K., Wong, A.M.S., Cooper, J.D., Birnbaum, S.G., Hammer, R.E., and Hofmann, S.L. (2010). DHHC5 Interacts with PDZ Domain 3 of Post-synaptic Density-95 (PSD-95) Protein and Plays a Role in Learning and Memory. Journal of Biological Chemistry *285*, 13022–13031.

Linder, M.E., and Deschenes, R.J. (2007). Palmitoylation: policing protein stability and traffic. Nat Rev Mol Cell Biol *8*, 74–84.

Liu, H., Abecasis, G.R., Heath, S.C., Knowles, A., Demars, S., Chen, Y.-J., Roos, J.L., Rapoport, J.L., Gogos, J.A., and Karayiorgou, M. (2002). Genetic variation in the 22q11 locus and susceptibility to schizophrenia. Proc. Natl. Acad. Sci. U.S.A. *99*, 16859–16864.

Lobo, S. (2002). Identification of a Ras Palmitoyltransferase in Saccharomyces cerevisiae. Journal of Biological Chemistry *277*, 41268–41273.

Mangiarini, L., Sathasivam, K., Seller, M., Cozens, B., Harper, A., Hetherington, C., Lawton, M., Trottier, Y., Lehrach, H., Davies, S.W., et al. (1996). Exon 1 of the HD gene with an expanded CAG repeat is sufficient to cause a progressive neurological phenotype in transgenic mice. Cell *87*, 493–506.

Mansilla, F., Birkenkamp-Demtroder, K., Kruhøffer, M., Sørensen, F.B., Andersen, C.L., Laiho, P., Aaltonen, L.A., Verspaget, H.W., and Ørntoft, T.F. (2007). Differential expression of DHHC9 in microsatellite stable and instable human colorectal cancer subgroups. Br J Cancer *96*, 1896–1903.

Mansouri, M.R., Marklund, L., Gustavsson, P., Davey, E., Carlsson, B., Larsson, C., White, I., Gustavson, K.-H., and Dahl, N. (2005). Loss of ZDHHC15 expression in a woman with a balanced translocation t(X;15)(q13.3;cen) and severe mental retardation. European Journal of Human Genetics *13*, 970–977.

Marin, E.P., Derakhshan, B., Lam, T.T., Davalos, A., and Sessa, W.C. (2012). Endothelial cell palmitoylproteomic identifies novel lipid-modified targets and potential substrates for protein acyl transferases. Circ. Res. *110*, 1336–1344.

Martin, B.R., and Cravatt, B.F. (2009). Large-scale profiling of protein palmitoylation in mammalian cells. Nat Meth *6*, 135–138.

Martin, D.D.O., Beauchamp, E., and Berthiaume, L.G. (2011). Post-translational myristoylation: Fat matters in cellular life and death. Biochimie *93*, 18–31.

Mattison, H.A., Hayashi, T., and Barria, A. (2012). Palmitoylation at Two Cysteine Clusters on the C-Terminus of GluN2A and GluN2B Differentially Control Synaptic Targeting of NMDA Receptors. PLoS ONE *7*, e49089.

McKnight, K.D., Hou, J., and Hoodless, P.A. (2007). Dynamic expression of thyrotropin-releasing hormone in the mouse definitive endoderm. Dev. Dyn. *236*, 2909–2917.

Meckler, X., Roseman, J., Das, P., Cheng, H., Pei, S., Keat, M., Kassarjian, B., Golde, T.E., Parent, A.T., and Thinakaran, G. (2010). Reduced Alzheimer's Disease -Amyloid Deposition in Transgenic Mice Expressing S-Palmitoylation-Deficient APH1aL and Nicastrin. Journal of Neuroscience *30*, 16160–16169.

Michaely, P., Tomchick, D.R., Machius, M., and Anderson, R.G.W. (2002). Crystal structure of a 12 ANK repeat stack from human ankyrinR. Embo J. *21*, 6387–6396.

Mill, P., Lee, A.W.S., Fukata, Y., Tsutsumi, R., Fukata, M., Keighren, M., Porter, R.M., McKie, L., Smyth, I., and Jackson, I.J. (2009). Palmitoylation regulates epidermal homeostasis and hair follicle differentiation. PLoS Genet *5*, e1000748.

Milnerwood, A.J., and Raymond, L.A. (2010). Early synaptic pathophysiology in neurodegeneration: insights from Huntington's disease. Trends in Neurosciences *33*, 513–523.

Milnerwood, A.J., Gladding, C.M., Pouladi, M.A., Kaufman, A.M., Hines, R.M., Boyd, J.D., Ko, R.W.Y., Vasuta, O.C., Graham, R.K., Hayden, M.R., et al. (2010). Early increase in extrasynaptic NMDA receptor signaling and expression

contributes to phenotype onset in Huntington's disease mice. Neuron *65*, 178–190.

Milnerwood, A.J., Parsons, M.P., Young, F.B., Singaraja, R.R., Franciosi, S., Volta, M., Bergeron, S., Hayden, M.R., and Raymond, L.A. (2013). Memory and synaptic deficits in Hip14/DHHC17 knockout mice. Proceedings of the National Academy of Sciences *110*, 20296–20301.

Mink, J.W. (1996). The basal ganglia: focused selection and inhibition of competing motor programs. Progress in Neurobiology *50*, 381–425.

Mitchell, D.A., Mitchell, G., Ling, Y., Budde, C., and Deschenes, R.J. (2010). Mutational Analysis of Saccharomyces cerevisiae Erf2 Reveals a Two-step Reaction Mechanism for Protein Palmitoylation by DHHC Enzymes. Journal of Biological Chemistry *285*, 38104–38114.

Mitchell, D.A., Vasudevan, A., Linder, M.E., and Deschenes, R.J. (2006). Protein palmitoylation by a family of DHHC protein S-acyltransferases. The Journal of Lipid Research *47*, 1118–1127.

Mitchison, H.M., Hofmann, S.L., Becerra, C.H., Munroe, P.B., Lake, B.D., Crow, Y.J., Stephenson, J.B., Williams, R.E., Hofman, I.L., Taschner, P.E., et al. (1998). Mutations in the palmitoyl-protein thioesterase gene (PPT; CLN1) causing juvenile neuronal ceroid lipofuscinosis with granular osmiophilic deposits. Human Molecular Genetics *7*, 291–297.

Mizumaru, C., Saito, Y., Ishikawa, T., Yoshida, T., Yamamoto, T., Nakaya, T., and Suzuki, T. (2009). Suppression of APP-containing vesicle trafficking and production of β-amyloid by AID/DHHC-12 protein. J Neurochem *111*, 1213–1224.

Molander-Melin, M., Blennow, K., Bogdanovic, N., Dellheden, B., Mansson, J.-E., and Fredman, P. (2005). Structural membrane alterations in Alzheimer brains found to be associated with regional disease development; increased density of gangliosides GM1 and GM2 and loss of cholesterol in detergent-resistant membrane domains. J Neurochem *92*, 171–182.

Morfini, G.A., You, Y.-M., Pollema, S.L., Kaminska, A., Liu, K., Yoshioka, K., Björkblom, B., Coffey, E.T., Bagnato, C., Han, D., et al. (2009). Pathogenic huntingtin inhibits fast axonal transport by activating JNK3 and phosphorylating kinesin. Nat Neurosci *12*, 864–871.

Motoki, K., Kume, H., Oda, A., Tamaoka, A., Hosaka, A., Kametani, F., and Araki, W. (2012). Neuronal β-amyloid generation is independent of lipid raft association of β-secretase BACE1: analysis with a palmitoylation-deficient mutant. Brain Behav *2*, 270–282.

Mukai, J., Dhilla, A., Drew, L.J., Stark, K.L., Cao, L., MacDermott, A.B., Karayiorgou, M., and Gogos, J.A. (2008). Palmitoylation-dependent

neurodevelopmental deficits in a mouse model of 22q11 microdeletion. Nat Neurosci *11*, 1302–1310.

Mukai, J., Liu, H., Burt, R.A., Swor, D.E., Lai, W.-S., Karayiorgou, M., and Gogos, J.A. (2004). Evidence that the gene encoding ZDHHC8 contributes to the risk of schizophrenia. Nature Genetics *36*, 725–731.

Murphy, K.C., Jones, L.A., and Owen, M.J. (1999). High rates of schizophrenia in adults with velo-cardio-facial syndrome. Arch. Gen. Psychiatry *56*, 940–945.

Nadolski, M.J., and Linder, M.E. (2007). Protein lipidation. FEBS Journal *274*, 5202–5210.

Nasir, J., Floresco, S.B., O'Kusky, J.R., Diewert, V.M., Richman, J.M., Zeisler, J., Borowski, A., Marth, J.D., Phillips, A.G., and Hayden, M.R. (1995). Targeted disruption of the Huntington's disease gene results in embryonic lethality and behavioral and morphological changes in heterozygotes. Cell *81*, 811–823.

Needleman, S.B., and Wunsch, C.D. (1970). A general method applicable to the search for similarities in the amino acid sequence of two proteins. Journal of Molecular Biology *48*, 443–453.

Noritake, J., Fukata, Y., Iwanaga, T., Hosomi, N., Tsutsumi, R., Matsuda, N., Tani, H., Iwanari, H., Mochizuki, Y., Kodama, T., et al. (2009). Mobile DHHC palmitoylating enzyme mediates activity-sensitive synaptic targeting of PSD-95. The Journal of Cell Biology *186*, 147–160.

Nosková, L., Stránecký, V., Hartmannová, H., Přistoupilová, A., Barešová, V., Ivánek, R., Hůlková, H., Jahnová, H., van der Zee, J., Staropoli, J.F., et al. (2011). Mutations in DNAJC5, Encoding Cysteine-String Protein Alpha, Cause Autosomal-Dominant Adult-Onset Neuronal Ceroid Lipofuscinosis. The American Journal of Human Genetics *89*, 241–252.

Ohno, Y., Kashio, A., Ogata, R., Ishitomi, A., Yamazaki, Y., and Kihara, A. (2012). Analysis of substrate specificity of human DHHC protein acyltransferases using a yeast expression system. Mol. Biol. Cell *23*, 4543–4551.

Ohno, Y., Kihara, A., Sano, T., and Igarashi, Y. (2006). Intracellular localization and tissue-specific distribution of human and yeast DHHC cysteine-rich domain-containing proteins. Biochimica Et Biophysica Acta (BBA) - Molecular and Cell Biology of Lipids *1761*, 474–483.

Ohyama, T., Verstreken, P., Ly, C.V., Rosenmund, T., Rajan, A., Tien, A.C., Haueter, C., Schulze, K.L., and Bellen, H.J. (2007). Huntingtin-interacting protein 14, a palmitoyl transferase required for exocytosis and targeting of CSP to synaptic vesicles. The Journal of Cell Biology *179*, 1481–1496.

Otani, K., Ujike, H., Tanaka, Y., Morita, Y., Kishimoto, M., Morio, A., Uchida, N.,

Nomura, A., and Kuroda, S. (2005). The ZDHHC8 gene did not associate with bipolar disorder or schizophrenia. Neuroscience Letters *390*, 166–170.

Oyama, T., Miyoshi, Y., Koyama, K., Nakagawa, H., Yamori, T., Ito, T., Matsuda, H., Arakawa, H., and Nakamura, Y. (2000). Isolation of a novel gene on 8p21.3-22 whose expression is reduced significantly in human colorectal cancers with liver metastasis. Genes Chromosomes Cancer *29*, 9–15.

Palidwor, G.A., Shcherbinin, S., Huska, M.R., Rasko, T., Stelzl, U., Arumughan, A., Foulle, R., Porras, P., Sanchez-Pulido, L., Wanker, E.E., et al. (2009). Detection of alpha-rod protein repeats using a neural network and application to huntingtin. PLoS Comput. Biol. *5*, e1000304.

Parsons, M.P., Kang, R., Buren, C., Dau, A., Southwell, A.L., Doty, C.N., Sanders, S.S., Hayden, M.R., and Raymond, L.A. (2013). Bidirectional control of postsynaptic density-95 (PSD-95) clustering by huntingtin. Journal of Biological Chemistry.

Parsons, R.B., and Austen, B.M. (2007). Protein-protein interactions in the assembly and subcellular trafficking of the BACE (beta-site amyloid precursor protein-cleaving enzyme) complex of Alzheimer's disease. Biochem. Soc. Trans *35*, 974–979.

Planey, S.L., and Zacharias, D.A. (2009). Palmitoyl acyltransferases, their substrates, and novel assays to connect them (Review). Mol Membr Biol *26*, 14–31.

Politis, E.G. (2005). Transmembrane Topology of the Protein Palmitoyl Transferase Akr1. Journal of Biological Chemistry *280*, 10156–10163.

Ponimaskin, E. (2005). Palmitoylation of the 5-Hydroxytryptamine4a Receptor Regulates Receptor Phosphorylation, Desensitization, and -Arrestin-Mediated Endocytosis. Molecular Pharmacology *67*, 1434–1443.

Porsolt, R.D., Bertin, A., and Jalfre, M. (1977a). Behavioral despair in mice: a primary screening test for antidepressants. Arch Int Pharmacodyn Ther *229*, 327–336.

Porsolt, R.D., Le Pichon, M., and Jalfre, M. (1977b). Depression: a new animal model sensitive to antidepressant treatments. Nature *266*, 730–732.

Pouladi, M.A., Graham, R.K., Karasinska, J.M., Xie, Y., Santos, R.D., Petersen, A., and Hayden, M.R. (2008). Prevention of depressive behaviour in the YAC128 mouse model of Huntington disease by mutation at residue 586 of huntingtin. Brain *132*, 919–932.

Pouladi, M.A., Stanek, L.M., Xie, Y., Franciosi, S., Southwell, A.L., Deng, Y., Butland, S., Zhang, W., Cheng, S.H., Shihabuddin, L.S., et al. (2012). Marked

differences in neurochemistry and aggregates despite similar behavioural and neuropathological features of Huntington disease in the full-length BACHD and YAC128 mice. Human Molecular Genetics *21*, 2219–2232.

Prescott, G.R., Gorleku, O.A., Greaves, J., and Chamberlain, L.H. (2009). Palmitoylation of the synaptic vesicle fusion machinery. J Neurochem *110*, 1135–1149.

Pulver, A.E., Nestadt, G., Goldberg, R., Shprintzen, R.J., Lamacz, M., Wolyniec, P.S., Morrow, B., Karayiorgou, M., Antonarakis, S.E., and Housman, D. (1994). Psychotic illness in patients diagnosed with velo-cardio-facial syndrome and their relatives. J. Nerv. Ment. Dis. *182*, 476–478.

Putilina, T., Wong, P., and Gentleman, S. (1999). The DHHC domain: a new highly conserved cysteine-rich motif. Mol. Cell. Biochem. *195*, 219–226.

Raymond, F.L., Tarpey, P.S., Edkins, S., Tofts, C., O'Meara, S., Teague, J., Butler, A., Stevens, C., Barthorpe, S., Buck, G., et al. (2007). Mutations in ZDHHC9, Which Encodes a Palmitoyltransferase of NRAS and HRAS, Cause X-Linked Mental Retardation Associated with a Marfanoid Habitus. The American Journal of Human Genetics *80*, 982–987.

Raymond, L.A., Andre, V.M., Cepeda, C., Gladding, C.M., Milnerwood, A.J., and Levine, M.S. (2011). Pathophysiology of Huntington's disease: time-dependent alterations in synaptic and receptor function. Neuroscience *198*, 252–273.

Ren, J., Wen, L., Gao, X., Jin, C., Xue, Y., and Yao, X. (2008). CSS-Palm 2.0: an updated software for palmitoylation sites prediction. Protein Engineering Design and Selection *21*, 639–644.

Ren, W., Sun, Y., and Du, K. (2013). DHHC17 palmitoylates ClipR-59 and modulates ClipR-59 association with the plasma membrane. Mol. Cell. Biol. *33*, 4255–4265.

Resh, M.D. (2006). Use of analogs and inhibitors to study the functional significance of protein palmitoylation. Methods *40*, 191–197.

Riddell, D.R., Christie, G., Hussain, I., and Dingwall, C. (2001). Compartmentalization of beta-secretase (Asp2) into low-buoyant density, noncaveolar lipid rafts. Curr. Biol. *11*, 1288–1293.

Rocks, O. (2005). An Acylation Cycle Regulates Localization and Activity of Palmitoylated Ras Isoforms. Science *307*, 1746–1752.

Rocks, O., Gerauer, M., Vartak, N., Koch, S., Huang, Z.-P., Pechlivanis, M., Kuhlmann, J., Brunsveld, L., Chandra, A., Ellinger, B., et al. (2010). The Palmitoylation Machinery Is a Spatially Organizing System for Peripheral Membrane Proteins. Cell *141*, 458–471.

Roos, R.A. (2010). Huntington's disease: a clinical review. Orphanet Journal of Rare Diseases *5*, 40.

Rostovtsev, V.V., Green, L.G., Fokin, V.V., and Sharpless, K.B. (2002). A stepwise huisgen cycloaddition process: copper(I)-catalyzed regioselective “ligation” of azides and terminal alkynes. Angew. Chem. Int. Ed. Engl. *41*, 2596–2599.

Roth, A.F. (2002). The yeast DHHC cysteine-rich domain protein Akr1p is a palmitoyl transferase. The Journal of Cell Biology *159*, 23–28.

Roth, A.F., Papanayotou, I., and Davis, N.G. (2011). The yeast kinase Yck2 has a tripartite palmitoylation signal. Mol. Biol. Cell *22*, 2702–2715.

Roth, A.F., Wan, J., Bailey, A.O., Sun, B., Kuchar, J.A., Green, W.N., Phinney, B.S., Yates, J.R., III, and Davis, N.G. (2006). Global Analysis of Protein Palmitoylation in Yeast. Cell *125*, 1003–1013.

Rothstein, J.D. (2009). Current hypotheses for the underlying biology of amyotrophic lateral sclerosis. Ann. Neurol. *65 Suppl 1*, S3–S9.

Rungta, R.L., Choi, H.B., Lin, P.J., Ko, R.W., Ashby, D., Nair, J., Manoharan, M., Cullis, P.R., and Macvicar, B.A. (2013). Lipid Nanoparticle Delivery of siRNA to Silence Neuronal Gene Expression in the Brain. Mol Ther Nucleic Acids *2*, e136.

Rusch, M., Zimmermann, T.J., Bürger, M., Dekker, F.J., Görmer, K., Triola, G., Brockmeyer, A., Janning, P., Böttcher, T., Sieber, S.A., et al. (2011). Identification of Acyl Protein Thioesterases 1 and 2 as the Cellular Targets of the Ras-Signaling Modulators Palmostatin B and M. Angew. Chem. Int. Ed. *50*, 9838–9842.

Rush, D.B., Leon, R.T., McCollum, M.H., Treu, R.W., and Wei, J. (2012). Palmitoylation and trafficking of GAD65 are impaired in a cellular model of Huntington's disease. Biochem. J. *442*, 39–48.

Ruzankina, Y., Pinzon-Guzman, C., Asare, A., Ong, T., Pontano, L., Cotsarelis, G., Zediak, V.P., Velez, M., Bhandoola, A., and Brown, E.J. (2007). Deletion of the Developmentally Essential Gene ATR in Adult Mice Leads to Age-Related Phenotypes and Stem Cell Loss. Cell Stem Cell *1*, 113–126.

Saito, S., Ikeda, M., Iwata, N., Suzuki, T., Kitajima, T., Yamanouchi, Y., Kinoshita, Y., Takahashi, N., Inada, T., and Ozaki, N. (2005). No association was found between a functional SNP in ZDHHC8 and schizophrenia in a Japanese case–control population. Neuroscience Letters *374*, 21–24.

Salaun, C., Greaves, J., and Chamberlain, L.H. (2010). The intracellular dynamic of protein palmitoylation. The Journal of Cell Biology *191*, 1229–1238.

Saleem, A.N., Chen, Y.-H., Baek, H.J., Hsiao, Y.-W., Huang, H.-W., Kao, H.-J., Liu, K.-M., Shen, L.-F., Song, I.-W., Tu, C.-P.D., et al. (2010). Mice with alopecia, osteoporosis, and systemic amyloidosis due to mutation in Zdhhc13, a gene coding for palmitoyl acyltransferase. PLoS Genet *6*, e1000985.

Sanders, S.S., Mui, K.K.N., Sutton, L.M., and Hayden, M.R. (2014). Identification of binding sites in Huntingtin for the Huntingtin Interacting Proteins HIP14 and HIP14L. PLoS ONE *9*, e90669.

Sanderson, J.L., and Dell'Acqua, M.L. (2011). AKAP signaling complexes in regulation of excitatory synaptic plasticity. *17*, 321–336.

Santavuori, P. (1988). Neuronal ceroid-lipofuscinoses in childhood. Brain Dev. *10*, 80–83.

Sayers, E.W., Barrett, T., Benson, D.A., Bolton, E., Bryant, S.H., Canese, K., Chetvernin, V., Church, D.M., DiCuccio, M., Federhen, S., et al. (2011). Database resources of the National Center for Biotechnology Information. Nucleic Acids Research *39*, D38–D51.

Schmidt, M.F., Bracha, M., and Schlesinger, M.J. (1979). Evidence for covalent attachment of fatty acids to Sindbis virus glycoproteins. Proc. Natl. Acad. Sci. U.S.a. *76*, 1687–1691.

Selkoe, D.J. (2001). Alzheimer's disease: genes, proteins, and therapy. Physiol. Rev. *81*, 741–766.

Seong, I.S., Woda, J.M., Song, J.-J., Lloret, A., Abeyrathne, P.D., Woo, C.J., Gregory, G., Lee, J.-M., Wheeler, V.C., Walz, T., et al. (2010). Huntingtin facilitates polycomb repressive complex 2. Human Molecular Genetics *19*, 573–583.

Shahinian, S., and Silvius, J.R. (1995). Doubly-lipid-modified protein sequence motifs exhibit long-lived anchorage to lipid bilayer membranes. Biochemistry *34*, 3813–3822.

Sharma, C., Yang, X.H., and Hemler, M.E. (2008). DHHC2 affects palmitoylation, stability, and functions of tetraspanins CD9 and CD151. Mol. Biol. Cell *19*, 3415–3425.

Shi, S.-P., Sun, X.-Y., Qiu, J.-D., Suo, S.-B., Chen, X., Huang, S.-Y., and Liang, R.-P. (2013). The prediction of palmitoylation site locations using a multiple feature extraction method. J. Mol. Graph. Model. *40*, 125–130.

Shin, H.D., Park, B.L., Bae, J.S., Park, T.J., Chun, J.Y., Park, C.S., Sohn, J.-W., Kim, B.-J., Kang, Y.-H., Kim, J.W., et al. (2010). Association of ZDHHC8 polymorphisms with smooth pursuit eye movement abnormality. Am. J. Med. Genet. B Neuropsychiatr. Genet. *153B*, 1167–1172.

Shiota, C., Woo, J.-T., Lindner, J., Shelton, K.D., and Magnuson, M.A. (2006). Multiallelic disruption of the rictor gene in mice reveals that mTOR complex 2 is essential for fetal growth and viability. Developmental Cell *11*, 583–589.

Sidera, C., Parsons, R., and Austen, B. (2004). Proteolytic cascade in the amyloidogenesis of Alzheimer's disease. Biochem. Soc. Trans *32*, 33–36.

Siegel, G., Obernosterer, G., Fiore, R., Oehmen, M., Bicker, S., Christensen, M., Khudayberdiev, S., Leuschner, P.F., Busch, C.J.L., Kane, C., et al. (2009). A functional screen implicates microRNA-138-dependent regulation of the depalmitoylation enzyme APT1 in dendritic spine morphogenesis. Nat Cell Biol *11*, 705–716.

Singaraja, R.R., Hadano, S., Metzler, M., Givan, S., Wellington, C.L., Warby, S., Yanai, A., Gutekunst, C.-A., Leavitt, B.R., Yi, H., et al. (2002). HIP14, a novel ankyrin domain-containing protein, links huntingtin to intracellular trafficking and endocytosis. Human Molecular Genetics *11*, 2815–2828.

Singaraja, R.R., Huang, K., Sanders, S.S., Milnerwood, A.J., Hines, R., Lerch, J.P., Franciosi, S., Drisdel, R.C., Vaid, K., Young, F.B., et al. (2011). Altered palmitoylation and neuropathological deficits in mice lacking HIP14. Human Molecular Genetics *20*, 3899–3909.

Slow, E.J. (2003). Selective striatal neuronal loss in a YAC128 mouse model of Huntington disease. Human Molecular Genetics *12*, 1555–1567.

Smotrys, J.E., and Linder, M.E. (2004). Palmitoylation of Intracellular Signaling Proteins: Regulation and Function. Annu. Rev. Biochem. *73*, 559–587.

Smotrys, J.E., Schoenfish, M.J., Stutz, M.A., and Linder, M.E. (2005). The vacuolar DHHC-CRD protein Pfa3p is a protein acyltransferase for Vac8p. The Journal of Cell Biology *170*, 1091–1099.

Song, I.-W., Li, W.-R., Chen, L.-Y., Shen, L.-F., Liu, K.-M., Yen, J.J.Y., Chen, Y.-J., Chen, Y.-J., Kraus, V.B., Wu, J.-Y., et al. (2014). Palmitoyl acyltransferase, zdhhc13, facilitates bone mass acquisition by regulating postnatal epiphyseal development and endochondral ossification: a mouse model. PLoS ONE *9*, e92194.

Soskic, V., Nyakatura, E., Roos, M., Müller-Esterl, W., and Godovac-Zimmermann, J. (1999). Correlations in palmitoylation and multiple phosphorylation of rat bradykinin B2 receptor in Chinese hamster ovary cells. J. Biol. Chem. *274*, 8539–8545.

Southwell, A.L., and Patterson, P.H. (2011). Gene therapy in mouse models of huntington disease. Neuroscientist *17*, 153–162.

Southwell, A.L., Ko, J., and Patterson, P.H. (2009). Intrabody gene therapy

ameliorates motor, cognitive, and neuropathological symptoms in multiple mouse models of Huntington's disease. Journal of Neuroscience *29*, 13589–13602.

Southwell, A.L., Warby, S.C., Carroll, J.B., Doty, C.N., Skotte, N.H., Zhang, W., Villanueva, E.B., Kovalik, V., Xie, Y., Pouladi, M.A., et al. (2013). A fully humanized transgenic mouse model of Huntington disease. Human Molecular Genetics *22*, 18–34.

Soyombo, A.A., and Hofmann, S.L. (1997). Molecular cloning and expression of palmitoyl-protein thioesterase 2 (PPT2), a homolog of lysosomal palmitoyl-protein thioesterase with a distinct substrate specificity. J. Biol. Chem. *272*, 27456–27463.

Stack, E.C., Kubilus, J.K., Smith, K., Cormier, K., Del Signore, S.J., Guelin, E., Ryu, H., Hersch, S.M., and Ferrante, R.J. (2005). Chronology of behavioral symptoms and neuropathological sequela in R6/2 Huntington's disease transgenic mice. J. Comp. Neurol. *490*, 354–370.

Stamler, J.S., Simon, D.I., Jaraki, O., Osborne, J.A., Francis, S., Mullins, M., Singel, D., and Loscalzo, J. (1992). S-nitrosylation of tissue-type plasminogen activator confers vasodilatory and antiplatelet properties on the enzyme. Proc. Natl. Acad. Sci. U.S.a. *89*, 8087–8091.

Stowers, R.S., and Isacoff, E.Y. (2007). Drosophila Huntingtin-Interacting Protein 14 Is a Presynaptic Protein Required for Photoreceptor Synaptic Transmission and Expression of the Palmitoylated Proteins Synaptosome-Associated Protein 25 and Cysteine String Protein. Journal of Neuroscience *27*, 12874–12883.

Strekalova, T., Spanagel, R., Bartsch, D., Henn, F.A., and Gass, P. (2004). Stress-induced anhedonia in mice is associated with deficits in forced swimming and exploration. Neuropsychopharmacology *29*, 2007–2017.

Sturrock, A., and Leavitt, B.R. (2010). The Clinical and Genetic Features of Huntington Disease. Journal of Geriatric Psychiatry and Neurology *23*, 243–259.

Sutton, L.M., Sanders, S.S., Butland, S.L., Singaraja, R.R., Franciosi, S., Southwell, A.L., Doty, C.N., Schmidt, M.E., Mui, K.K.N., Kovalik, V., et al. (2013). Hip14l-deficient mice develop neuropathological and behavioural features of Huntington disease. Human Molecular Genetics *22*, 452–465.

Swarthout, J.T. (2005). DHHC9 and GCP16 Constitute a Human Protein Fatty Acyltransferase with Specificity for H- and N-Ras. Journal of Biological Chemistry *280*, 31141–31148.

Swerdlow, N.R., Paulsen, J., Braff, D.L., Butters, N., Geyer, M.A., and Swenson, M.R. (1995). Impaired prepulse inhibition of acoustic and tactile startle response in patients with Huntington's disease. J. Neurol. Neurosurg. Psychiatr. *58*, 192–200.

Takano, H., and Gusella, J.F. (2002). The predominantly HEAT-like motif structure of huntingtin and its association and coincident nuclear entry with dorsal, an NF-kB/Rel/dorsal family transcription factor. BMC Neurosci *3*, 15.

The Huntington's Disease Collaborative Research Group. (1993). A novel gene containing a trinucleotide repeat that is expanded and unstable on Huntington's disease chromosomes. Cell *72*, 971–983.

Thomas, G.M., Hayashi, T., Chiu, S.-L., Chen, C.-M., and Huganir, R.L. (2012). Palmitoylation by DHHC5/8 targets GRIP1 to dendritic endosomes to regulate AMPA-R trafficking. Neuron *73*, 482–496.

Tian, L. (2001). Alternative Splicing Switches Potassium Channel Sensitivity to Protein Phosphorylation. Journal of Biological Chemistry *276*, 7717–7720.

Tian, L., McClafferty, H., Jeffries, O., and Shipston, M.J. (2010). Multiple Palmitoyltransferases Are Required for Palmitoylation-dependent Regulation of Large Conductance Calcium- and Voltage-activated Potassium Channels. Journal of Biological Chemistry *285*, 23954–23962.

Tian, L., Coghill, L.S., McClafferty, H., MacDonald, S.H.-F., Antoni, F.A., Ruth, P., Knaus, H.-G., and Shipston, M.J. (2004). Distinct stoichiometry of BKCa channel tetramer phosphorylation specifies channel activation and inhibition by cAMP-dependent protein kinase. Proc. Natl. Acad. Sci. U.S.a. *101*, 11897–11902.

Tian, L., Jeffries, O., McClafferty, H., Molyvdas, A., Rowe, I.C.M., Saleem, F., Chen, L., Greaves, J., Chamberlain, L.H., Knaus, H.-G., et al. (2008). Palmitoylation gates phosphorylation-dependent regulation of BK potassium channels. Proceedings of the National Academy of Sciences *105*, 21006–21011.

Tian, L., McClafferty, H., Knaus, H.-G., Ruth, P., and Shipston, M.J. (2012). Distinct acyl protein transferases and thioesterases control surface expression of calcium-activated potassium channels. J. Biol. Chem. *287*, 14718–14725.

Tomatis, V.M., Trenchi, A., Gomez, G.A., and Daniotti, J.L. (2010). Acyl-Protein Thioesterase 2 Catalizes the Deacylation of Peripheral Membrane-Associated GAP-43. PLoS ONE *5*, e15045.

Toyoda, T., Sugimoto, H., and Yamashita, S. (1999). Sequence, expression in Escherichia coli, and characterization of lysophospholipase II. Biochim. Biophys. Acta *1437*, 182–193.

Ueno, K. (2000). Involvement of fatty acid synthase in axonal development in mouse embryos. Genes Cells *5*, 859–869.

Valdez Taubas, J., and Pelham, H. (2005). Swf1-dependent palmitoylation of the SNARE Tlg1 prevents its ubiquitination and degradation. Embo J. *24*, 2524–

2532.

Valencia, A., Reeves, P.B., Sapp, E., Li, X., Alexander, J., Kegel, K.B., Chase, K., Aronin, N., and DiFiglia, M. (2010). Mutant huntingtin and glycogen synthase kinase 3-B accumulate in neuronal lipid rafts of a presymptomatic knock-in mouse model of Huntington's disease. J. Neurosci. Res. *88*, 179–190.

Van Raamsdonk, J.M. (2005a). Selective degeneration and nuclear localization of mutant huntingtin in the YAC128 mouse model of Huntington disease. Human Molecular Genetics *14*, 3823–3835.

Van Raamsdonk, J.M. (2005b). Cognitive Dysfunction Precedes Neuropathology and Motor Abnormalities in the YAC128 Mouse Model of Huntington's Disease. Journal of Neuroscience *25*, 4169–4180.

Van Raamsdonk, J.M., Gibson, W.T., Pearson, J., Murphy, Z., Lu, G., Leavitt, B.R., and Hayden, M.R. (2006). Body weight is modulated by levels of full-length huntingtin. Human Molecular Genetics *15*, 1513–1523.

Veit, M. (2000). Palmitoylation of the 25-kDa synaptosomal protein (SNAP-25) in vitro occurs in the absence of an enzyme, but is stimulated by binding to syntaxin. Biochem. J. *345 Pt 1*, 145–151.

Veit, M., and Schmidt, M.F.G. (2006). Palmitoylation of influenza virus proteins. Berl. Munch. Tierarztl. Wochenschr. *119*, 112–122.

Verkruyse, L.A., and Hofmann, S.L. (1996). Lysosomal targeting of palmitoyl-protein thioesterase. J. Biol. Chem. *271*, 15831–15836.

Vesa, J., Hellsten, E., Verkruyse, L.A., Camp, L.A., Rapola, J., Santavuori, P., Hofmann, S.L., and Peltonen, L. (1995). Mutations in the palmitoyl protein thioesterase gene causing infantile neuronal ceroid lipofuscinosis. Nature *376*, 584–587.

Vetrivel, K.S., Meckler, X., Chen, Y., Nguyen, P.D., Seidah, N.G., Vassar, R., Wong, P.C., Fukata, M., Kounnas, M.Z., and Thinakaran, G. (2009). Alzheimer disease Abeta production in the absence of S-palmitoylation-dependent targeting of BACE1 to lipid rafts. J. Biol. Chem. *284*, 3793–3803.

Vonsattel, J.P., and DiFiglia, M. (1998). Huntington disease. J. Neuropathol. Exp. Neurol. *57*, 369–384.

Walker, F.O. (2007). Huntington's disease. Lancet *369*, 218–228.

Wan, J., Roth, A.F., Bailey, A.O., and Davis, N.G. (2007). Palmitoylated proteins: purification and identification. Nat Protoc *2*, 1573–1584.

Wan, J., Savas, J.N., Roth, A.F., Sanders, S.S., Singaraja, R.R., Hayden, M.R.,

Yates, J.R., and Davis, N.G. (2013). Tracking Brain Palmitoylation Change: Predominance of Glial Change in a Mouse Model of Huntington's Disease. Chem. Biol. *20*, 1421–1434.

Warby, S.C., Visscher, H., Collins, J.A., Doty, C.N., Carter, C., Butland, S.L., Hayden, A.R., Kanazawa, I., Ross, C.J., and Hayden, M.R. (2011). HTT haplotypes contribute to differences in Huntington disease prevalence between Europe and East Asia. European Journal of Human Genetics *19*, 561–566.

Wellington, C.L., Ellerby, L.M., Hackam, A.S., Margolis, R.L., Trifiro, M.A., Singaraja, R., McCutcheon, K., Salvesen, G.S., Propp, S.S., Bromm, M., et al. (1998). Caspase cleavage of gene products associated with triplet expansion disorders generates truncated fragments containing the polyglutamine tract. J. Biol. Chem. *273*, 9158–9167.

Willner, P., Towell, A., Sampson, D., Sophokleous, S., and Muscat, R. (1987). Reduction of sucrose preference by chronic unpredictable mild stress, and its restoration by a tricyclic antidepressant. Psychopharmacology (Berl.) *93*, 358–364.

Wilson, J.P., Raghavan, A.S., Yang, Y.-Y., Charron, G., and Hang, H.C. (2011). Proteomic analysis of fatty-acylated proteins in mammalian cells with chemical reporters reveals S-acylation of histone H3 variants. Mol. Cell Proteomics *10*, M110.001198.

Xie, Z., Adamowicz, W.O., Eldred, W.D., Jakowski, A.B., Kleiman, R.J., Morton, D.G., Stephenson, D.T., Strick, C.A., Williams, R.D., and Menniti, F.S. (2006). Cellular and subcellular localization of PDE10A, a striatum-enriched phosphodiesterase. Neuroscience *139*, 597–607.

Xu, M., Clair, D.S., and He, L. (2010). Testing for genetic association between the ZDHHC8 gene locus and susceptibility to schizophrenia: An integrated analysis of multiple datasets. Am. J. Med. Genet. *153B*, 1266–1275.

Xu, X., Weinstein, M., Li, C., Naski, M., Cohen, R.I., Ornitz, D.M., Leder, P., and Deng, C. (1998). Fibroblast growth factor receptor 2 (FGFR2)-mediated reciprocal regulation loop between FGF8 and FGF10 is essential for limb induction. Development *125*, 753–765.

Yamamoto, Y., Chochi, Y., Matsuyama, H., Eguchi, S., Kawauchi, S., Furuya, T., Oga, A., Kang, J.J., Naito, K., and Sasaki, K. (2007). Gain of 5p15.33 is associated with progression of bladder cancer. Oncology *72*, 132–138.

Yanai, A., Huang, K., Kang, R., Singaraja, R.R., Arstikaitis, P., Gan, L., Orban, P.C., Mullard, A., Cowan, C.M., Raymond, L.A., et al. (2006). Palmitoylation of huntingtin by HIP14is essential for its trafficking and function. Nat Neurosci *9*, 824–831.

Yang, G., and Cynader, M.S. (2011). Palmitoyl Acyltransferase zD17 Mediates Neuronal Responses in Acute Ischemic Brain Injury by Regulating JNK Activation in a Signaling Module. Journal of Neuroscience *31*, 11980–11991.

Yang, G., Liu, Y., Yang, K., Liu, R., Zhu, S., Coquinco, A., Wen, W., Kojic, L., Jia, W., and Cynader, M. (2012). Isoform-specific palmitoylation of JNK regulates axonal development. Cell Death Differ. *19*, 553–561.

Yang, G., Zhou, X., Zhu, J., Liu, R., Zhang, S., Coquinco, A., Chen, Y., Wen, Y., Kojic, L., Jia, W., et al. (2013). JNK3 Couples the Neuronal Stress Response to Inhibition of Secretory Trafficking. Sci Signal *6*, ra57.

Yang, J.T., Rayburn, H., and Hynes, R.O. (1995). Cell adhesion events mediated by alpha 4 integrins are essential in placental and cardiac development. Development *121*, 549–560.

Yang, W., Di Vizio, D., Kirchner, M., Steen, H., and Freeman, M.R. (2010). Proteome scale characterization of human S-acylated proteins in lipid raft-enriched and non-raft membranes. Mol. Cell Proteomics *9*, 54–70.

Yap, M.C., Kostiuk, M.A., Martin, D.D.O., Perinpanayagam, M.A., Hak, P.G., Siddam, A., Majjigapu, J.R., Rajaiah, G., Keller, B.O., Prescher, J.A., et al. (2010). Rapid and selective detection of fatty acylated proteins using omega-alkynyl-fatty acids and click chemistry. The Journal of Lipid Research *51*, 1566–1580.

Yeh, D.C., Duncan, J.A., Yamashita, S., and Michel, T. (1999). Depalmitoylation of endothelial nitric-oxide synthase by acyl-protein thioesterase 1 is potentiated by Ca(2+)-calmodulin. J. Biol. Chem. *274*, 33148–33154.

Young, F.B., Butland, S.L., Sanders, S.S., Sutton, L.M., and Hayden, M.R. (2012). Putting proteins in their place: palmitoylation in Huntington disease and other neuropsychiatric diseases. Progress in Neurobiology *97*, 220–238.

Zeidman, R., Jackson, C.S., and Magee, A.I. (2009). Protein acyl thioesterases (Review). Mol Membr Biol *26*, 32–41.

Zeitlin, S., Liu, J.P., Chapman, D.L., Papaioannou, V.E., and Efstratiadis, A. (1995). Increased apoptosis and early embryonic lethality in mice nullizygous for the Huntington's disease gene homologue. Nature Genetics *11*, 155–163.

Zhang, F.L., and Casey, P.J. (1996). Protein prenylation: molecular mechanisms and functional consequences. Annu. Rev. Biochem. *65*, 241–269.

Zhang, J., Planey, S.L., Ceballos, C., Stevens, S.M., Keay, S.K., and Zacharias, D.A. (2008). Identification of CKAP4/p63 as a major substrate of the palmitoyl acyltransferase DHHC2, a putative tumor suppressor, using a novel proteomics method. Mol. Cell Proteomics *7*, 1378–1388.

Zhang, Z., Lee, Y.-C., Kim, S.-J., Choi, M.S., Tsai, P.-C., Xu, Y., Xiao, Y.-J., Zhang, P., Heffer, A., and Mukherjee, A.B. (2006). Palmitoyl-protein thioesterase-1 deficiency mediates the activation of the unfolded protein response and neuronal apoptosis in INCL. Human Molecular Genetics *15*, 337–346.

Zhao, S., Ting, J.T., Atallah, H.E., Qiu, L., Tan, J., Gloss, B., Augustine, G.J., Deisseroth, K., Luo, M., Graybiel, A.M., et al. (2011). Cell type–specific channelrhodopsin-2 transgenic mice for optogenetic dissection of neural circuitry function. Nat Meth *8*, 745–752.

Zhu, Y.-C., Li, D., Wang, L., Lu, B., Zheng, J., Zhao, S.-L., Zeng, R., and Xiong, Z.-Q. (2013). Palmitoylation-dependent CDKL5-PSD-95 interaction regulates synaptic targeting of CDKL5 and dendritic spine development. Proceedings of the National Academy of Sciences *110*, 9118–9123.

(2006). Inhibition of Calcineurin by FK506 Protects against Polyglutamine-Huntingtin Toxicity through an Increase of Huntingtin Phosphorylation at S421. *26*, 1635–1645.